
Electronic Theses and Dissertations, 2004-2019

2015

An Optimization of Thermodynamic Efficiency vs. Capacity for Communications Systems

Gregory Rawlins
University of Central Florida



Part of the [Electrical and Electronics Commons](#)

Find similar works at: <https://stars.library.ucf.edu/etd>

University of Central Florida Libraries <http://library.ucf.edu>

This Doctoral Dissertation (Open Access) is brought to you for free and open access by STARS. It has been accepted for inclusion in Electronic Theses and Dissertations, 2004-2019 by an authorized administrator of STARS. For more information, please contact STARS@ucf.edu.

STARS Citation

Rawlins, Gregory, "An Optimization of Thermodynamic Efficiency vs. Capacity for Communications Systems" (2015). *Electronic Theses and Dissertations, 2004-2019*. 1493.

<https://stars.library.ucf.edu/etd/1493>



AN OPTIMIZATION OF THERMODYNAMIC EFFICIENCY VS. CAPACITY FOR
COMMUNICATIONS SYSTEMS

by

GREGORY S. RAWLINS

B.S. University of Central Florida 1983

M.S. University of Central Florida 1987

A dissertation submitted in partial fulfillment of the requirements
for the degree of Doctor of Philosophy
in the Department of Electrical Engineering and Computer Science
in the College of Engineering and Computer Science
at the University of Central Florida
Orlando, Florida

Spring Term
2015

Major Professor: Pawel M. Wocjan

© 2015 Gregory S. Rawlins

ABSTRACT

This work provides a fundamental view of the mechanisms which affect the power efficiency of communications processes along with a method for efficiency enhancement. Shannon's work is the definitive source for analyzing information capacity of a communications system but his formulation does not predict an efficiency relationship suitable for calculating the power consumption of a system, particularly for practical signals which may only approach the capacity limit. This work leverages Shannon's while providing additional insight through physical models which enable the calculation and improvement of efficiency for the encoding of signals.

The proliferation of Mobile Communications platforms is challenging capacity of networks largely because of the ever increasing data rate at each node. This places significant power management demands on personal computing devices as well as cellular and WLAN terminals. The increased data throughput translates to shorter meantime between battery charging cycles and increased thermal footprint. Solutions are developed herein to counter this trend.

Hardware was constructed to measure the efficiency of a prototypical Gaussian signal prior to efficiency enhancement. After an optimization was performed, the efficiency of the encoding apparatus increased from 3.125% to greater than 86% for a manageable investment of resources. Likewise several telecommunications standards based waveforms were also tested on the same hardware. The results reveal that the developed physical theories extrapolate in a very accurate manner to an electronics application, predicting the efficiency of single ended and differential encoding circuits before and after optimization.

TABLE OF CONTENTS

LIST OF FIGURES	VIII
LIST OF TABLES	XIII
1. INTRODUCTION	1
1.1. Comments Concerning Capacity and Efficiency.....	5
1.2. Additional Background Comments	8
2. REVIEW OF CLASSICAL CAPACITY EQUATION	10
2.1. The Uncertainty Function.....	17
2.2. Physical-Considerations.....	20
3. A PARTICLE THEORY OF COMMUNICATION	21
3.1. Transmitter.....	22
3.1.1. Phase Space Coordinates, and Uncertainty.....	23
3.1.2. Transmitter Phase Space, Boundary Conditions and Metrics.....	24
3.1.3. Momentum Probability	32
3.1.4. Correlation of Motion, and Statistical Independence	45
3.1.5. Autocorrelations and Spectra for Independent Maximum Velocity Pulses.....	51
3.1.6. Characteristic Response	55
3.1.7. Sampling Bound Qualification	65

3.1.8.	Interpolation for Physically Analytic Motion	70
3.1.9.	Statistical Description of the Process.....	92
3.1.10.	Configuration Position Coordinate Time Averages	113
3.1.11.	Summary Comments on the Statistical Behavior of the Particle Based Communications Process Model.....	120
3.2.	Comments Concerning Receiver and Channel	122
4.	UNCERTAINTY AND INFORMATION CAPACITY	129
4.1.	Uncertainty	129
4.2.	Capacity.....	137
4.2.1.	Classical Capacity.....	137
4.3.	Multi-Particle Capacity.....	150
5.	COMMUNICATIONS PROCESS ENERGY EFFICIENCY.....	153
5.1.	Average Thermodynamic Efficiency for a Canonical Model	157
5.1.1.	Comments Concerning Power Source	174
5.1.2.	Momentum Conservation and Efficiency	175
5.1.3.	A Theoretical Limit.....	179
5.2.	Capacity vs. Efficiency Given Encoding Losses.....	181
5.3.	Capacity vs. Efficiency Given Directly Dissipative Losses	194
5.4.	Capacity vs. Total Efficiency	195

5.4.1.	Effective Angle for Momentum Exchange	197
5.5.	Momentum Transfer via an EM Field	199
6.	INCREASING η_{mod} AN OPTIMIZATION APPROACH.....	207
6.1.	Sum of Independent RVs.....	207
6.2.	Composite Processing.....	211
7.	MODULATOR EFFICIENCY AND OPTIMIZATION	214
7.1.	Modulator	214
7.2.	Modulator Efficiency Enhancement for Fixed ζ	220
7.3.	Optimization for Type 1 Modulator , $\zeta = 3$ Case	229
7.4.	Ideal Modulation domains	231
7.5.	Sufficient Number of domains, ζ	234
7.6.	Zero Offset Gaussian Case	237
7.7.	Results for Standards Based Modulations	242
8.	MISCELLANEOUS TOPICS	244
8.1.	Encoding Rate , Some Limits, and Relation to Landauer's Principle	244
8.2.	Time Variant Uncertainty	253
8.3.	A Perspective of Gabor's Uncertainty.....	257
9.	SUMMARY	266
	APPENDIX A: PHASE SPACE UNCERTAINTY AND THE HYPER SPHERE.....	271
	APPENDIX B: DERIVATION FOR MAXIMUM VELOCITY PROFILE.....	281

APPENDIX C: MAXIMUM VELOCITY PULSE AUTO CORRELATION.....	288
APPENDIX D: DIFFERENTIAL ENTROPY CALCULATION.....	295
APPENDIX E MINIMUM MEAN SQUARE ERROR (MMSE) AND CORRELATION FUNCTION FOR VELOCITY BASED ON SAMPLED AND INTERPOLATED VALUES..	300
APPENDIX F: MAX CARDINAL VS. MAX NL. VELOCITY PULSE	306
APPENDIX G: CARDINAL TE RELATION	314
APPENDIX H: RELATION BETWEEN INSTANTANEOUS EFFICIENCY AND THERMODYNAMIC EFFICIENCY	317
APPENDIX I: WAVEFORM, THERMODYNAMIC, AND INSTANTANEOUS EFFICIENCY RELATIONSHIPS.....	328
APPENDIX J: COMPARISON OF GAUSSIAN AND CONTINUOUS UNIFORM DENSITIES	336
APPENDIX K: ENTROPY RATE AND WORK RATE.....	341
APPENDIX L: OPTIMIZED EFFICIENCY FOR AN 802.11A 16 QAM CASE	346
LIST OF REFERENCES	352

LIST OF FIGURES

Figure 1-1 Extended Channel	2
Figure 2-1 Location of Message m_i in Hyperspace	11
Figure 2-2 Sampled Message Signals m_{it} each of Duration T in Seconds and Sampling Interval $T_s = T/N_s = 12B$ where N_s is the Number of Samples over T , $T_s N_s = T$	12
Figure 2-3 Effect of AWGN m_2 with Average Power P_2 Corrupted by AWGN of Power N in a Hyperspace Adjacent to Message Coordinates m_1 and m_3	15
Figure 3-1 3D Phase Space with Particle.....	26
Figure 3-2 Peak Particle Velocity vs. Time	31
Figure 3-3 Peak Particle Velocity vs. Position	31
Figure 3-4 Gaussian Velocity pdf	34
Figure 3-5 Phase Space Boundary	37
Figure 3-6 pdf of Velocity v_α as a Function of Radial Position for a Particle in Motion, Restricted to a Single Dimension and Maximum Instantaneous Power, P_m , Peak to Average Energy Ratio ($PAER = 4$), $P_m = 10 Js$, $v_{max} = 10ms$, $\Delta t = 1$, $R_s = \Delta t v_{max}^3$, $m = 1kg$	38
Figure 3-7 Probability of Velocity	40
Figure 3-8 Probability of Velocity given q (Top View)	40
Figure 3-9 Vector Velocity Deployment	42
Figure 3-10 Normalized Autocorrelation of a Maximum Velocity Pulse	52
Figure 3-11 Normalized Fourier Transform of Maximum Velocity Pulse Autocorrelation	54
Figure 3-12 Normalized Fourier Transform of Maximum Velocity Pulse Autocorrelation	54

Figure 3-13 Fourier Transform of the Rectangular Pulse Autocorrelation.....	56
Figure 3-14 Forming a Rectangular Pulse from the Integration of Delta Functions	56
Figure 3-15 Model for a Force Doublet Generating a Maximum Velocity Pulse	58
Figure 3-16 Max. Velocity Pulse Impulse Response for Transmitter Model with P_{max} Constraint, $m = 1$	58
Figure 3-17 Schematic	75
Figure 3-18 General Interpolated Trajectory	81
Figure 3-19 Autocorrelation for Power limited Gaussian Momentum ($m=1$).....	84
Figure 3-20 Maximum Velocity Pulse Compared to Main Lobe Cardinal Velocity Pulse	85
Figure 3-21 Kinetic Energy vs. Time for Velocity and Cardinal Pulses	86
Figure 3-22 Max Velocity Pulse and Main Lobe Cardinal Velocity Pulse with .4 dB “Backoff”	87
Figure 3-23 Comparison of Max. Nonlinear Velocity Pulse and Max. Cardinal Velocity Pulse.	89
Figure 3-24 Max. Cardinal Vel. Pulse, Associated Force Function and Work Function	91
Figure 3-25 Parallel Observations for Momentum Ensemble	96
Figure 3-26 Three Sample Functions from a Momentum Ensemble.....	97
Figure 3-27 Three sample Functions from a Momentum Ensemble	97
Figure 3-28 Velocity and Position for a Sample Function ($R_s \approx 1$).....	98
Figure 3-29 Three Particle Samples in Phase Space along the α axis.....	100
Figure 3-30 Three Gaussian pdf’s for Three Sample R_v ’s.....	101
Figure 3-31 Three Configuration Ensemble Sample Functions	104
Figure 3-32 Momentum and Position Related by an Integral of Motion.....	113
Figure 3-33 Joint pdf of Momentum and Position 1	117

Figure 3-34 Joint pdf of Momentum and Position 2.....	118
Figure 3-35 Joint pdf of Momentum and Position 3.....	118
Figure 3-36 Extended Channel	123
Figure 3-37 Global Phase Space.....	124
Figure 3-38 Maximum Cardinal Pulse Profile in a Receiver Phase Space along with a Random Particle Trajectory.....	128
Figure 4-1 Capacity in Nats/s vs. SNR for a D dimensional link with a maximum velocity pulse profile, Capacity in nats/s vs. given the following parameters, $PAER=10$, $P_m = 1$ J/s, $m=1$ kg, $f_s = 1$	148
Figure 4-2 Capacity in bits/s vs. $(SNR)^{-1}$ for a D dimensional link given the following parameters, $PAER=10$, $P_m=1$ J/s, $m=1$ kg, $f_s=1$ samp./s , $B=.5$ Hz, $D=1,2,3,4, 8$	149
Figure 5-1 Extended Encoding Phase Space	158
Figure 5-2 Desired Information Bearing Momentum.....	159
Figure 5-3 Actual Momentum of a Target Particle.....	160
Figure 5-4 Encoding Particle Motion on the x_1 axis via Momentum Exchange	160
Figure 5-5 Momentum Exchange Diagram	163
Figure 5-6 Encoding Particle Stream Impulses, $t\varepsilon = 0$	164
Figure 5-7 Encoding Particle Stream Impulses with Timing Skew, $t\varepsilon \neq 0$	164
Figure 5-8 Particle Encoding Simulation Block Diagram for Canonical Offset Model.....	165
Figure 5-9 Simulation Waveforms and Signals	166
Figure 5-10 Simulation Waveforms and Signals	166
Figure 5-11 Simulation Waveforms and Signals	167

Figure 5-12 Encoded Output and Encoded Input	167
Figure 5-13 Momentum Change, Integrated Momentum Exchange, Analytic Filtered Result..	171
Figure 5-14 Zero Offset Open System Canonical Simulation Model.....	172
Figure 5-15 Simulation Results for Open System Zero Offset Model	173
Figure 5-16 Relative Particle Motion Prior to Exchange.....	176
Figure 5-17 Relative Particle Motion after an Exchange.....	176
Figure 5-18 Capacity ratio for truncated Gaussian distributions vs. <i>PAPR</i> for large SNR	188
Figure 5-19 Efficiency vs. Capacity ratio for Truncated Gaussian Distributions & Large SNR	189
Figure 5-20 Canonical Offset Encoding Efficiency.....	190
Figure 5-21 Capacity vs. Dissipative Efficiency	196
Figure 5-22 Momentum Exchange Through Radiated Field	199
Figure 5-23 Conservation Equation for a Radiated Field	202
Figure 5-24 Energy Momentum Tensor	203
Figure 6-1 Summing Random Signals.....	208
Figure 6-2 Gaussian pdf Formed with Composite Sub Densities.....	212
Figure 7-1 Complex RF Modulator	215
Figure 7-2 Complex Signal Constellation for a WCDMA Signal	216
Figure 7-3 Differential and Single Ended Type 1 Series Modulator/Encoder.....	217
Figure 7-4 Measured and Theoretical Efficiency of a Type 1 Modulator	218
Figure 7-5 Gaussian pdf for Output Voltage Voltage, V_L , with $V_s = 2, V_L = V_s4 = 4V$, and $\sigma = .15$	221

Figure 7-6 pdf for η given Gaussian pdf for Output Voltage, V_L , with $V_s = 2, V_L = V_s 4.5V$, and $\sigma = .15, \eta = .34$	223
Figure 7-7 Gaussian pdf for Output Voltage, V_L , with $V_s = 2, V_L = V_s 4.5V$, and $\sigma = .15, 3$ Separate Domains	225
Figure 7-8 Three Domain Type 1 Series Modulator.....	227
Figure 7-9 Relative Efficiency Increase as a Function of the Number of Optimised Domains .	235
Figure 7-10 Relative Frequency of Output Load Voltage Measurements	236
Figure 7-11 Probability density of load voltage for zero offset case	237
Figure 7-12 Type 1 differentially sourced modulator.....	239
Figure 7-13 Thermodynamic efficiency for a given number of optimized domains	241
Figure 7-14 Measured Thermodynamic efficiency for a given number of optimized domains (4, 6, 8).....	241
Figure 7-15 Thermodynamic efficiency for a given number of optimized domains	242
Figure 7-16 Optimized Efficiency Performance vs. ζ for (Standards Cases).....	243
Figure 8-1 Noise Power vs. Frequency.....	247
Figure 8-2 Binary Particle Encoding	249
Figure 8-3 Peak Particle Velocity vs. Position for Motion.....	251
Figure 8-4 Between Sample Uncertainty For a Phase Space Reference Trajectory.....	256
Figure 8-5 Sampling of Two Sine Waves at Different Frequencies	261
Figure 8-6 Sampling of Two Sine Waves at Different Frequencies.....	261

LIST OF TABLES

Table 7-1 Corresponding Power Supply Values Defining optimized Thresholds for a given ζ	236
Table 7-2 Values for Thermodynamic Efficiency vs. Number of Optimized Partitions ($Z_s = 0$), <i>PAPR</i> ~11.8 <i>dB</i>	239
Table 7-3 Calculated thermodynamic efficiency using thresholds from table 7-2.....	240

1. INTRODUCTION

Shannon created the standard by which communications systems are measured. His information capacity theorems are universally recognized and routinely applied by communications systems engineers. Shannon's theorems provide a means for calculating information transfer per unit time for given signal and noise power, yet there is no explicit connection of these concepts to power consumption. This work provides that connection. Power efficiency is an increasingly important topic due to the proliferation of mobile communications and mobile computing. Battery life and heat dissipation vs. the bandwidth and quality of service are driving market concerns for mobile communications. The ultimate goal is to render companion equations which provide joint solutions for calculating and maximizing efficiency while maintaining capacity, based on physical principles complementary to information theory. A method of improving efficiency for physically encoding any signal is also introduced and analyzed in detail.

The preferred power efficiency metric is the thermodynamic efficiency η defined as the effective power output of a system for a given invested input power. P_e is the effective power delivered by the system and P_w is the waste power so that efficiency is given by;

$$\eta = \frac{P_e}{P_e + P_w}$$

In a communications system the effective output power is defined as the power delivered to the communications load or sink and exclusively associated with the information bearing content of a signal. The waste energy is associated with non-information bearing degrees of freedom within

the communications system which siphon some portion of the available input power. Though P_w may take many intermediate forms of expression it is ultimately dissipated as heat in the environment.

The principles presented herein are general in nature and can be applied to any communications process whether it be mechanical, electrical or optical by nature. The classical laws of motion, first two laws of thermodynamics and Shannon’s uncertainty function provide a common means of analysis and foundation for development of important models.

Shannon’s approach is based on a mathematical model rather than physical insight. A particle based model is introduced to emphasize physical principles. At a high level of abstraction the model retains the classical form used by Shannon, consisting of transmitter (Tx), physical transport media and receiver (Rx). Collectively, these elements and supporting functions comprise the extended channel. The extended channel model along with the band width limited additive white Gaussian Noise (AWGN) is illustrated in figure 1-1.

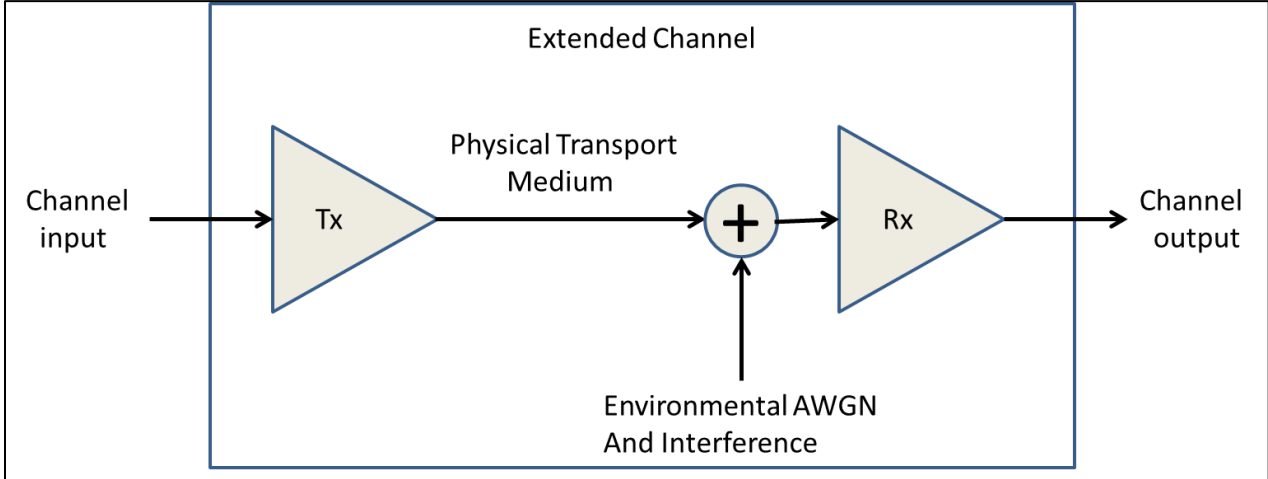


Figure 1-1 Extended Channel

Since this dissertation focuses on thermodynamic efficiency it is necessary to introduce some principles at a fundamental level which reveal the nature of the communications process and are complementary to Shannon's approach. Momentum is a common metric for analyzing the motion of material bodies and particles. It will be shown that the transfer of information using particle based models is accomplished through the exchange of momentum, imprinting the information expressed in the motion of one particle on another. Although not commonly used by electrical engineers, a change in momentum for a charge coupled to a dynamic electromagnetic field is a cornerstone principle of electrodynamics as formulated by Lorentz. The Lorentz force expressed as a rate of change in momentum is reviewed in chapter 5.5.

Momentum transfer principles are presented which can be used to analyze the efficiency of any communications subsystem or extended channel. The principles can be applied to any interface where information is transferred.

The Shannon-Hartley capacity equation 1-1 provides a fulcrum for the evolving discussion [1, 2, 3]. The capacity, C , of an extended communications channel which propagates a signal with average power, \bar{P} , in watts, and bandwidth B , in Hz, in the presence of band limited AWGN with average power \bar{N} , is given by;

$$C = B \log_2 \left(\frac{\bar{P} + \bar{N}}{\bar{N}} \right) \text{ bits/second} \quad (1-1)$$

$B=2f_s$ Hz where f_s is a Shannon-Nyquist sampling frequency required for signal construction [2, 4, 5, 6].

In chapter 3, f_s is derived as the frequency of the forces required to impart momentum to a particle to encode it with information. It is shown that the bandwidth B in a physical system is a direct consequence of the maximum available power P_m , to facilitate particle motion. P_m plays the analogous role in an electronics apparatus when specifying the maximum limit of a power supply with average power P_s .

In chapter 5, the efficiency η is studied in detail to establish the power resource required to generate the average signal power \bar{P} . From the basic definition of efficiency we can state;

$$\eta = \frac{\bar{P}}{P_s}$$

It is shown in chapters 3 and 5 that the average power supplied to a communications apparatus is $f_s \langle \mathcal{E}_{in} \rangle_s$ where $\langle \mathcal{E}_{in} \rangle_s$ is the average energy per sample of a communications process over time. Some of this energy, \mathcal{E}_e , is effectively used to generate and transfer a signal and some is waste, \mathcal{E}_w .

It is clear that for an efficiency of 100 percent that a given non zero and finite capacity in bits per second is attained with the lowest investment of power, $f_s \langle \mathcal{E}_{in} \rangle_s$. Ordinarily, η would be fixed for a given C. However, methods are introduced in chapters 5,6 and 7 to permit improvement of η subject to an optimization procedure.

It is further shown in chapter 5 that the efficiency of an information encoding process can be captured by the following simple equation;

$$\langle \eta \rangle = \frac{1}{k_{mod} PAPR + k_\sigma}$$

k_{mod} and k_{σ} are constants of implementation for the encoding apparatus and $PAPR$ is defined as the peak to average power ratio of the encoded signal. The $PAPR$ is defined for a non-dissipative system as;

$$PAPR = \frac{P_m}{\langle P_e \rangle}$$

The encoding theory also applies for decoding of information in a particle based model since imparted momentum is relative.

The conservation of energy is a necessary but not sufficient principle to account for the efficiencies of interest. Communications processes should conserve information with maximum efficiency as a design goal. The fundamental principles which determine conserved momentum exchanges between particles or virtual particles are necessary and sufficient to satisfy the required information theory constraints and derive efficiency optimization relationships. In this manner the macroscopic observable, η which is regarded as a thermodynamic quantity, may be related to microscopic momentum exchanges. This is the preferred approach for joining the calculation of capacity vs. efficiency in terms of a physical model.

1.1. Comments Concerning Capacity and Efficiency

Shannon proved that the capacity of a system is achieved when the signal possesses a Gaussian statistic. However, this poses a dilemma because such signals are not finite. In the context of a physical model, the power resource P_m would grow infinitely large and the efficiency of

encoding a signal would correspondingly become zero. In addition, the duration of a signal would be infinite as shown in chapter 2. These extremes are avoided by utilizing a prototypical Gaussian signal truncated to a 12 dB PAPR which preserves nearly all of the information encoded in the Gaussian signal.

A capacity equation is derived in chapter 4 using the physical model developed in chapter 3. This capacity equation is called the physical capacity equation and resembles the Shannon-Hartley equation with variations substantiated by physical principles. A notable differentiation is that for a given energy investment the capacity is twice that of the classical capacity equation per encoding dimension because information may be independently encoded in both position and momentum of a particle. Another difference is a modification to avoid an infinite capacity for the condition of zero degrees Kelvin. The quantities f_s , P_m , and PAPR play a prominent role in the equation along with the random variables, momentum and position.

In chapter 5, the efficiency of the capacity based on the prototypical Gaussian signal with a 12 dB PAPR is obtained. This Gaussian signal possesses an entropy defined by Shannon (ref chapter 2) and Appendix J which is given by $-\ln(\sqrt{2\pi e}\sigma)$ where σ is the standard deviation of the Gaussian signal. σ is approximately 1 for the prototypical Gaussian reference signal. The thermodynamic efficiency for encoding this signal is strongly inversely related to the PAPR yet may be improved by using techniques introduced in chapters 6 and 7. It is also shown that PAPR is a nonlinear monotonically increasing parameter of a signal as capacity increases up to the classical Gaussian limit. Thus, efficiency is strongly inversely proportional to capacity. Efficiency enhancement exploits this relationship. The procedures for efficiency enhancement

are accompanied with an optimization procedure which is a numerical calculus of variations approach in chapter 7.

Even though capacity is classically defined using the Gaussian signal, it is well known that designing an extended channel with a calculated theoretical capacity also sets an upper bound for the information throughput for other signal types which are not Gaussian. In high SNR it is easy to estimate the performance bounds of other signals possessing non-Gaussian densities in a comparative manner by defining a normalized entropy ratio H_r which compares the Shannon entropy of a signal of interest to the quantity $\ln(\sqrt{2\pi e}\sigma)$ in such a manner that the ratio $H_r \leq 1$.

It is argued in chapter 5 that as H_r becomes smaller the information transfer of a channel becomes smaller but the efficiency can correspondingly increase. This is because the PAPR for such signals correspondingly decreases.

It is of practical concern to design efficient systems which ever press Shannon's theoretical limit but do not achieve $H_r = 1$. The methods for efficiency enhancement for the Gaussian prototype signal are shown to also apply to all signals. Thus, even if a signal is inherently more efficient than the Gaussian prototype, the efficiency may still be significantly improved. This improvement can be several fold for complexly encoded signals. This is of particular interest to those engaged in designs which use standards based signals deployed by the telecommunications industry as well as wireless local area networks (WLAN).

There is a diminishing rate of return for the investment of resources to improve efficiency. This is evident in the theoretical calculations of chapter 5 and verified with laboratory hardware in chapter 7. Hardware was constructed to measure the efficiency of the prototypical Gaussian

signal prior to efficiency enhancement and after an optimization was performed. Likewise several standards based waveforms were also tested on the same hardware. The results reveal that the particle based theories extrapolate in a very accurate manner to an electronics application. The theory is not restricted to Gaussian waveforms but enables prediction of the efficiency for any signal before and after optimization.

1.2. Additional Background Comments

Communications is the transfer of information through space and time.

It follows, that information transfer is based on physical processes. This approach is consistent with the views of Landauer [7, 8] as well as Karnani, Mahesh, Kimmo Paakkonen, and Arto Annala [9]. This may introduce some ambiguity at a philosophical level concerning Shannon's definition of information. However, the view introduced here is complementary and does not diminish the utility of classical ideas since we shall focus on the nature of information transfer rather than argue the definition of information. The advantage provided, permits the injection of ideas which suggest origins of information transfer derived from laws of nature and therefore are principle rather than constructive theories.

The essential assumptions are; that a transmitter and receiver cannot be collocated in the coordinates of space-time, and that information is transferred between unique coordinates in space-time. Instantaneous action at a distance is not permitted. Also, the discussion is restricted to classical speeds where it is assumed $v/c \ll 1$.

The measure for information is usually defined by Shannon's uncertainty metric $H(\rho(x))$, discussed in detail in the next chapter. Shannon's uncertainty function permits maximum deviation of a constituent random variable x , given its describing probability density $\rho(x)$, on a per sample basis without physical restriction or impact. It is a focus of this work to introduce these restrictions through the joint entropy $H(\rho(q, \rho))$ where q is position and ρ is momentum. It should be noted that a practical form of the Shannon – Hartley capacity equation requires the insertion of the bandwidth B . This insertion was originally justified by a brilliant argument borrowed from the theory of function interpolation developed by E. T. Whittaker and others [6, 10]. The insertion of B limits the rate of change of the random signal $x(t)$ through a Fourier transform. Since $x(t)$ has a limited rate of change, the physical states of encoding must evolve to realize full uncertainty over a specified phase space. It will be shown that the more rapid the evolution, the greater the investment of energy per unit time for a moving particle to access the full uncertainty of a phase space based on physical coordinates, q, ρ .

A signal shall be defined as an information bearing, function of space-time.

It is assumed that continuous signals may be represented by discrete samples vs. time through sampling theorems [3, 11, 12]. The discrete samples shall be associated as the position and momentum coordinates of particles comprising the signals.

2. REVIEW OF CLASSICAL CAPACITY EQUATION

Shannon proved the following capacity limit (Shannon–Hartley Equation) for information transfer through a bandwidth limited continuous AWGN channel based on mathematical reasoning and geometric arguments [3].

$$C = B \log_2 \left(\frac{\bar{P} + \bar{N}}{\bar{N}} \right) \quad (2-1)$$

$C \triangleq$ Channel capacity in bits/second.

$B \triangleq$ Bandwidth of the entire channel in Hz.

$\bar{P} \triangleq$ Average power for the signal of interest in Joules/second (J/s).

$\bar{N} \triangleq$ Average power for additive white Gaussian noise (AWGN) of the channel in Joules/second (J/s).

The definition for capacity is based on;

$$C = \lim_{T \rightarrow \infty} \frac{\log_2 M}{T} \quad (2-2)$$

M is the number of unique signal functions or messages per time interval T which may be distinguished within a hyper geometric message space constraining the signal plus additive white

Gaussian noise (AWGN). The noise does not remain white due to the influence of B yet does retain its Gaussian statistic. Shannon reasoned that each point in the hyperspace represents a single message signal of duration T and that there is no restriction on the number of such distinguishable points except for the influence of uncorrelated noise sharing the hyperspace. Consider figure 2-1.

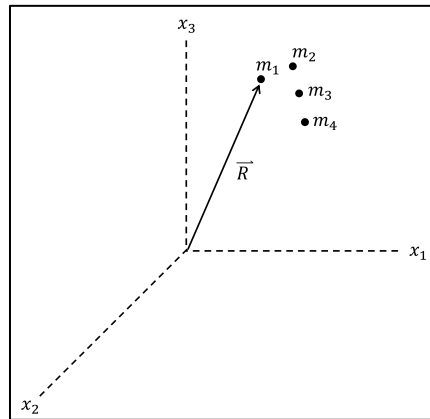


Figure 2-1 Location of Message m_i in Hyperspace

Several points are illustrated in Shannon's hypergeometric space, in this case a simple 3-dimensional view. Shannon permits an infinite number of dimensions in his hyperspace. Time is collapsed at each point. The radial vector \vec{R} is a distance from the origin in this hyperspace and is related to the average power \bar{P}_i of the m_i^{th} message. Consider the following structure of time continuous sampled message signals with time on the horizontal. Each sample ordinate is marked with a vertical line punctuated by a dot.

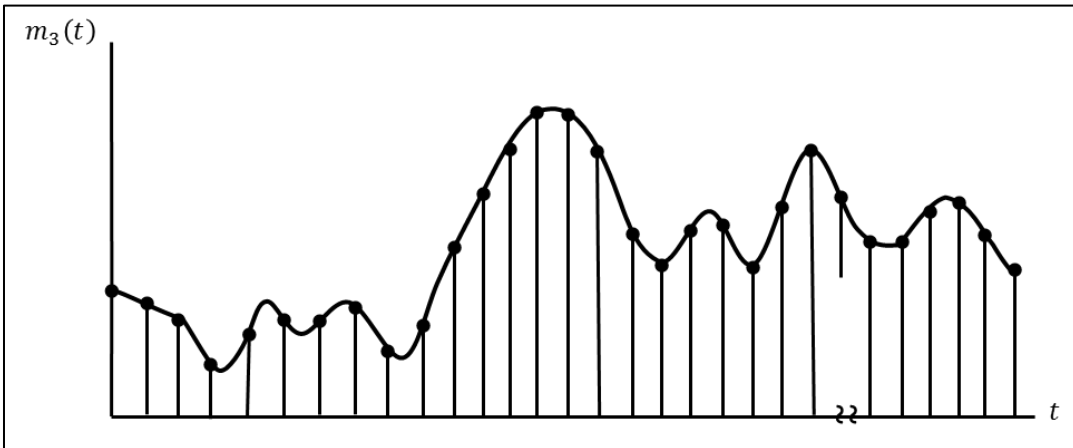
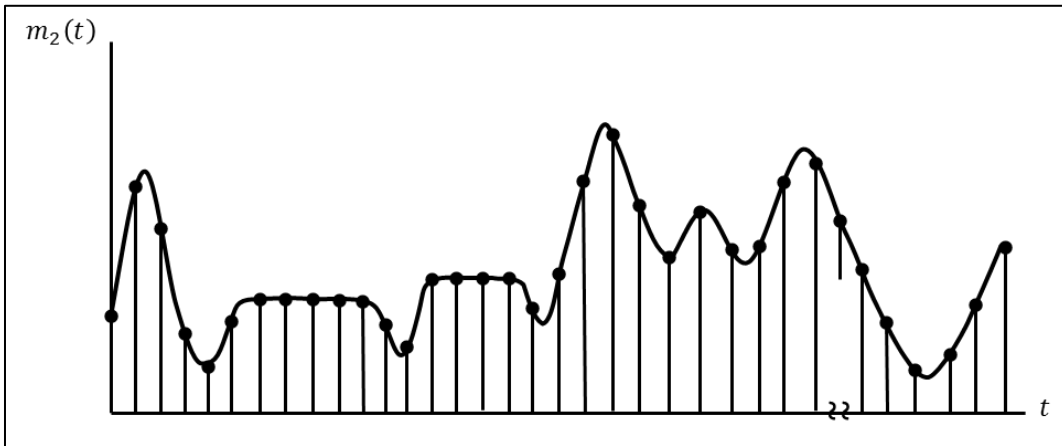
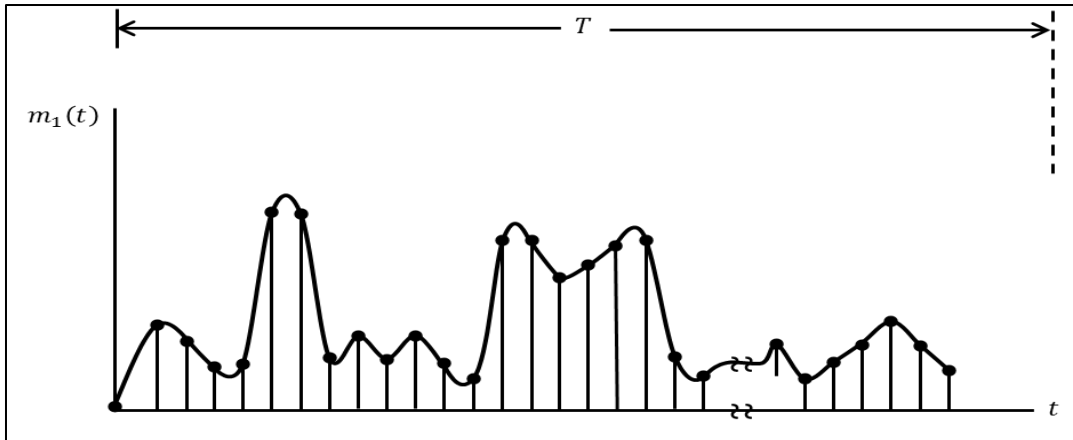


Figure 2-2 Sampled Message Signals $m_i(t)$ each of Duration T in Seconds and Sampling Interval $T_s = (T/N_s) = (1/2B)$ where N_s is the Number of Samples over T , $T_s N_s = T$

It is known that the continuous waveforms can be precisely reproduced by interpolation of the samples using the Cardinal Series originally introduced by Whittaker and adopted by Shannon [6]. The following series forms the basis for Shannon's sampling theorem.

$$m_i(t) = \sum_{n=-\infty}^{\infty} m_{i,n} \frac{\sin \pi(2Bt - n)}{\pi(2Bt - n)} \quad (2-3)$$

If the samples are enumerated according to the principles of Nyquist and Shannon, equation 2-3 becomes;

$$m_i(t) = \sum_{n=1}^{2TN_s} m_{i,n} \frac{\sin \pi(2Bt - n)}{\pi(2Bt - n)} \quad (2-4)$$

For regular sampling, the time between samples, T_s , is given by a constant $1/2B$ in seconds.

This scheme permits faithful reproduction of each $m_i(t)$ message signals with discrete coordinates whose weights are m_n for the n^{th} sample.

Thus, Shannon conceives a hyperspace whose coordinates are message signals, statistically independent, and mutually orthogonal over T . He further proves that the magnitude of coordinate radial \bar{R}_i is given by;

$$|R_i| = \sqrt{2BT\bar{P}_i} \quad (2-5)$$

\bar{P}_i is the average of $2BT$ sample energies per unit time obtained from the expected value of the squared message signals.

$$\bar{P}_i = \frac{1}{2BT} \sum_n m_{i,n}^2 \equiv E\{m_i^2\}$$

(2-6)

Shannon focused on the conditions where $T \rightarrow \infty$. This also implies $N_s \rightarrow \infty$. If all messages permitted in the hyperspace are characterized by statistically independent and identically distributed (*iid*) random variables (*RV*) then the expected values of 2-6 are identical. The independently averaged message signal energies in his representation are compressed to a thin hyper shell at the nominal radius;

$$R = \sqrt{2BT\bar{P}}$$

(2-7)

Having established the geometric view without noise, it is a simple matter to introduce a noise process which possesses a Gaussian statistic. Each of the m_i messages is corrupted by the noise. The noise on each message is also *iid*. It is implied that each of the potential m_i messages, or sub sequence of samples hereafter referred to as symbols, are known a priori and thus distinguishable through correlation methods at a receiver. The symbols are known to be from a standard alphabet. However, the particular transmitted symbol from the alphabet is unknown until detected at the receiver. Hence, each coordinate in the hyper-space possesses an associated

function which must be cross-correlated with the incoming messages and the largest correlation is declared as the message which is most likely communicated. Whenever averaged noise waveform, $\overline{n(t)} = 0$, then the normalized correlation coefficient magnitude, $|\rho| = 1$ for the correct message and zero for all other cross-correlation events. Whenever $\overline{n(t)} \neq 0$ there are partial correlations for all potential messages. Each sample illustrated in Figure 2-2 would become perturbed by the noise process. Reconstruction of the sampled signals plus noise would still faithfully reproduce the original message along with a superposition of the noise samples according to the sampling theorem. The affect that noise induces in the hyper geometric view can be understood by considering adjacent messages in the space when the message of interest is corrupted and the observation interval T is finite.

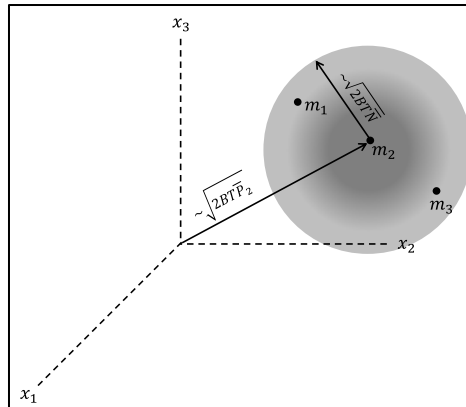


Figure 2-3 Effect of AWGN m_2 with Average Power \overline{P}_2 Corrupted by AWGN of Power \overline{N} in a Hyperspace Adjacent to Message Coordinates m_1 and m_3

Figure 2-3 illustrates the effect of AWGN on the probable coordinate displacement when correlation is performed on m_2 given that m_2 was communicated. The cloud of points surrounding the proper coordinate assigned to m_2 illustrates the possible region for the un-

normalized correlation result. The density of the cloud is proportional to the probability of the correlation output associated with the perturbed coordinate system, with m_2 as the most likely outcome since the multi-dimensional Gaussian noise possesses an unbiased statistic. However, it is important to notice that it is possible to mistake the correlation result as corresponding to messages m_1 or m_3 on occasion for $T < \infty$, because the resolved hyperspace coordinate, after processing, can be closer to a competing (noisy) result with some probability.

Finally, Shannon argues the requirements for capacity C which guarantees that the adjacent messages or any wrong message within the space will not be interpreted during the decoding process even for the case where the signals are corrupted by AWGN. The remarkable but intuitively satisfying result is that even for the case of AWGN, the perturbations may be averaged out over an interval $T \rightarrow \infty$ because the expected value of the noise is zero, yet the magnitude of normalized correlation for the message of interest approaches 1. Thus the correlation output is always correctly distinguishable. This infinite interval of averaging would have the effect of removing the cloud of uncertainty around m_2 in Figure 2-3.

The additional geometrical reasoning to support his result comes from the idea that a hyper volume of radius R which consists of points weighted by signal plus noise energy per unit time $(\bar{P}_i + \bar{N})$, must occupy a larger volume than the case when noise only is present. The ratio of the two volumes must bound the number of possible messages M given in equation 2-8.

$$M \leq \frac{\frac{\pi^{BT}}{\Gamma(BT+1)} \left(\sqrt{2BT(\bar{P} + \bar{N})} \right)^{2BT}}{\frac{\pi^{BT}}{\Gamma(BT+1)} \left(\sqrt{2BT\bar{N}} \right)^{2BT}} = \left(\frac{\bar{P} + \bar{N}}{\bar{N}} \right)^{BT}$$

(2-8)

Hence from 2-8 and 2-2

$$C = \lim_{T \rightarrow \infty} \frac{\log_2 M}{T} \leq B \log_2 \left(\frac{\bar{P} + \bar{N}}{\bar{N}} \right)$$

(2-9)

2.1. The Uncertainty Function

Shannon's uncertainty function is given in both discrete and continuous forms;

$$H(\rho(x)) = - \sum_{\ell} \rho(x)_{\ell} \ell n \rho(x)_{\ell}$$

(2-10)

$$H(\rho(x)) = - \int_{-\infty}^{+\infty} \rho(x) \ell n \rho(x) dx$$

(2-11)

$\rho(x)_{\ell}$ is the ℓ^{th} probability of discrete samples from a message function in the 2-10 and $\rho(x)$ is the probability of a continuous random variable assigned to a message function in 2-11. 2-11 shall also be referred to as the differential entropy. The choice of metric depends on the type of

analysis and message signal. The cumulative metric considers the entire probability space with a normalized measure of 1. The units are given in nats for the natural logarithm kernel and bits whenever the logarithm is base 2. This uncertainty relationship is the same formula as that for thermodynamic entropy from statistical physics though they are not generally equivalent [13, 14, 16].

Jaynes and others have pointed out certain challenges concerning the continuous form which shall be avoided [14, 15]. An adjustment to Shannon's continuous form was proposed by Jaynes and one of the approaches taken in this work. It requires recognition of the limit for discrete probabilities as they become more densely allocated to a particular space [14]. Equations 2-10 and 2-11 are not precisely what is needed moving forward but they provide an essential point of reference for a measure of information. In Shannon's case x is a nondeterministic variable from some normalized probability space which encodes information. For instance, the random values $m_{i,n}$ from the prior section could be represented by x . The nature of $H(\rho(x))$ shall be modified in subsequent discussion to accommodate rules for constraining x according to physical principles. In this context the definition for information is not altered from Shannon's, merely the manner in which the probability space is dynamically derived and defined. Hereafter we will also refer to $H(\rho(x))$ as $H(x)$ on occasion, where the context of the probability density $\rho(x)$ is assumed.

Capacity is defined in terms of maximization of the channel data rate which in turn may be derived from the various uncertainties or Shannon entropies whenever they are assigned a rate in

bits or nats per second. Each sample from the message functions, m_i , possess some uncertainty and therefore information entropy.

Using Shannon's notation, the following relationships illustrate how the capacity is obtained [15].

$$H(x) + H_x(y) = H(y) + H_y(x)$$

$$H(x) - H_y(x) = H(y) - H_x(y)$$

$$R \triangleq H(x) - H_y(x) \text{ per unit time}$$

$$C \triangleq \max\{R\}$$

(2-12)

$H(x)$: Uncertainty metric or information entropy of the source in bits

$H_x(y)$: Uncertainty of the channel output given precise knowledge of the channel input.

$H(y)$: Uncertainty metric for the channel output in bits

$H_y(x)$: Uncertainty of the input given knowledge of the output observable (this quantity is also called equivocation).

R : Rate of the channel in bits/sec.

It is apparent that rates less than C are possible. Shannon's focus was to obtain C .

2.2. Physical-Considerations

The prior sections presented the Shannon formulation based on mathematical and geometrical arguments. However, there are some important observations if one acknowledges physical limitations. These observations fall into the following general categories.

- a) An irreducible message error rate floor of zero is possible for the condition of maximum channel capacity only for the case of $T \rightarrow \infty$.
- b) There is no explicit energy cost for transitioning between samples within a message.
- c) There is no explicit energy cost for transitioning between messages.
- d) Capacities may approach infinity under certain conditions. This is counter to physical limitations since no source can supply infinite rates and no channel can sustain such rates.
- e) The messages m_1, m_2, \dots, m_i , may be arbitrarily close to one another within the hyper geometric signal space.

By collapsing the time variable associated with each message in Shannon's Hyper-space b), c) become obscured. We shall expand the time variable. d) and e) may be addressed by acknowledging physical limits on the resolution of $x(t)$. We introduce this resolution.

3. A PARTICLE THEORY OF COMMUNICATION

In this chapter, a physical model for communications is introduced in which particle dynamics are modeled by encoding information in the position and momentum coordinates of a phase space. The formulation leverages some traditional characteristics of classical phase space inherited from statistical mechanics but also requires the conservation of particle information.

The subsequent discussions suppose that the transmitter, channel, receiver, and environment may be partitioned for analysis purposes and that each may be modeled as occupying some phase space which supports particle motion, as well as exchanged momentum and radiation. The analysis provides a characterization of trajectories of particles and their fluctuations through the phase space. Mean statistics are also necessary to discriminate the fluctuations and calculate average energy requirements. Fortunately, the characteristic intervals of communications processes are typically much shorter than thermal relaxation time constants for the system. This enables the most robust differentiation of information with respect to the environment for a given energy resource. The fundamental nature of communications involves extraction of information through these differentiations.

The primary goals of chapter 3 are to;

- a) Establish a model consisting of a phase space with boundary conditions and a particle which encodes information in discrete samples from a nearly continuous random process.
- b) Obtain equations of motion for a single particle within phase space for item a)

- c) Discover the nature of forces required to move the particle and establish a physical sampling theorem along with the physical description of signal bandwidth.
- d) Derive the interpolation of sampled motion
- e) Describe the statistic of motion consistent with a maximum uncertainty communications process
- f) Discuss the circumstance for physically analytic behavior of the model

The preliminaries of this chapter pave the way for obtaining channel capacity in chapter 4 and deriving efficiency relations of chapter 5. Particular emphasis is applied to items c) and e).

3.1. Transmitter

The transmitter generates sequences of states through a phase space for which a particle possesses a coordinate per state as well as specific trajectory between states. Although more than one particle may be modeled we shall restrict analysis to a single particle since the model may be extended by assuming non-interacting particles. The information entropy of the source is assigned a mathematical definition originated by Shannon, a form similar to the entropy function of statistical mechanics [14, 16]. Shannon's entropy is devoid of physical association and that is its strength as well as limitation. Subsequent models provide a remedy for this omission by assigning a time and energy cost to information encoded by particle motion. Chapter 8 provides a more explicit investigation of a time evolving uncertainty function.

3.1.1. Phase Space Coordinates, and Uncertainty

The model for the transmitter consists of a hyper spherical phase space in which the information encoding process is related to an uncertainty function of the state of the system. That is;

$$H = - \iiint_{-\infty}^{\infty} \rho(\vec{q}, \vec{p}) \ln \rho(\vec{q}, \vec{p}) d\vec{q}d\vec{p}$$

(3-1)

\vec{q}, \vec{p} are the vector position, in terms of generalized coordinates, and conjugate momenta of the particle respectively. In the case of a single particle system we can choose to consider these quantities as an ordinary position and momentum pairing for the majority of subsequent discussion. A specific pair, $\vec{q}(t_\ell), \vec{p}(t_\ell)$ along with time derivatives $\dot{\vec{q}}(t_\ell), \dot{\vec{p}}(t_\ell)$ also defines a state of the system at time t_ℓ . H represents uncertainty or lack of knowledge concerning position of a particle in configuration space and momentum space, or jointly, phase space. Equation 3-1 is the differential form of Shannon's continuous entropy presented in Chapter 2. If all conceivable state transitions are statistically independent then uncertainty is maximized for a given distribution, $\rho(\vec{q}, \vec{p})$.

$\{\dot{\vec{q}}, \dot{\vec{p}}\}$ appear often in the study of mechanics and shall be occasionally referred to as the coordinate derivatives with respect to time, or conjugate derivative field. $\{\dot{\vec{q}}, \dot{\vec{p}}\}$ are random variables.

A transmitter must by practical specification be locally confined to a relatively small space within some reference frame even if that frame is in relative motion to the receiver. The

dynamics of particles within a constrained volume therefore demands that the particles move in trajectories which can reverse course, or execute other randomized curvilinear maneuvers whilst navigating through states, such that the boundary of the transmitter phase space not be violated. This requires acceleration according to Newton's second law of motion [17, 18, 19]. If a particle is aggressively accelerated, its inertia defies the change of its future course according to Newton's first law [17, 18, 19]. A particle with significant momentum will require greater energy per unit time for path modification, compared to a relatively slow particle of the same mass which executes the same maneuver through configuration space. The probability of path modification per unit time is a function of the uncertainty H . *The greater the uncertainty in instantaneous particle velocity and position, the greater the instantaneous energy requirement becomes to sustain its dynamic range.*

3.1.2. Transmitter Phase Space, Boundary Conditions and Metrics

Another important model feature is that particle motion is restricted such that it may not energetically contact the transmitter phase space boundary in a manner changing its momentum. Such contact would alter the uncertainty of the particle in a manner which annihilates information.

An example is that of the Maestro's baton. It moves to and fro rhythmically, with its material points distributing information according to its dynamics. Yet, the motions cannot exist beyond the span of the Maestro's arm or exceed the speeds accommodated by his or her physique and

the mass of the baton. In fact, the motions are contrived with these restrictions inherently enforced by physical laws and resource limitations. A velocity of zero is required at the extreme position (phase space boundary) of the Maestro's stroke and the maximum speed of the baton is limited by the rate of available energy per unit time. The essential features of this analogy apply to all communications processes.

Suppose that it is desirable to calculate the maximum possible rate of information encoding within the transmitter where information is related to the uncertainty of position and momentum of a particle. It is logical that both velocity and acceleration of the transitions between states should be considered in such a maximization. Speed of the transition is dependent on the rate at which the configuration q and momentum p random variables may change.

The following bound for the motions of ordinary matter, where velocity is well below the speed of light, is deduced from physical principles;

$$\lim_{v=v_{max}} (\dot{q}, \dot{p}) = \left(v_{max}, \frac{\max\{\dot{\mathcal{E}}_k\}}{v_{max}} \right) = \left(v_{max}, \frac{P_{max}}{v_{max}} \right) \quad (3-2)$$

v_{max} and P_{max} are the maximum particle velocity and the maximum applied power respectively.

Equation 3-2 naturally provides a regime of most interest for engineering application, where forces and powers are finite for finite space-time transitions. Motions which are spawned by finite powers and forces shall be considered as physically analytic.

It is most general to consider a model analyzing the available phase space of a hyper geometric spherical region around a single particle and the energy requirements to support a limiting case for motion. Appendix A justifies the consideration of the hyper sphere.

The following figure illustrates the geometry for a visually convenient three dimensional case, a relevant model subset of interest. A particle with position and momentum $\{\vec{q}, \vec{p}\}$ is illustrated.

The velocity \vec{v} is also illustrated and the classical linear momentum is given by the particle mass times it's velocity.

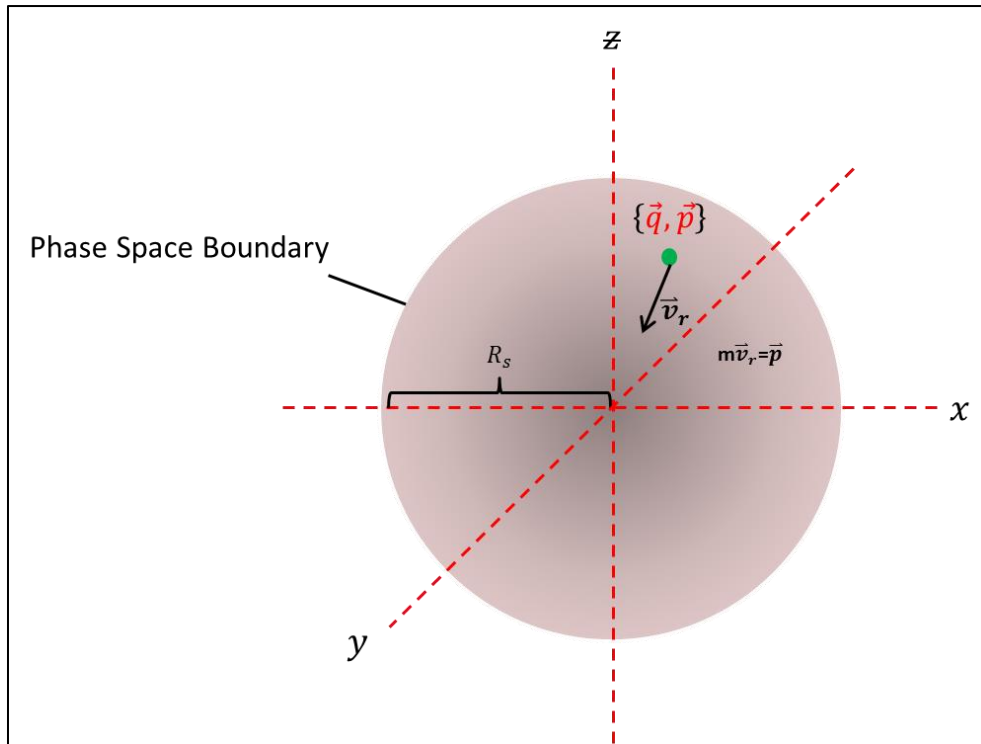


Figure 3-1 3D Phase Space with Particle

The phase space volume accessible to a particle in motion is a function of the maximum acceleration available for the particle to traverse the volume in a specified time, Δt . Maximum acceleration is a function of the available energy resource.

An accessible particle coordinate at some future Δt must always be less than the physical span of the phase space configuration volume. Considering the transmitter boundary for the moment, the greatest length along a straight Euclidian path that a particle may travel under any condition is simply $2R_s$ where R_s is the sphere radius.

At least one force, associated with \vec{p} , is required to move the particle between these limits. However, two forces are necessary and sufficient to comply with the boundary conditions while stimulating motion. It is expedient to assign an interval between observations of particle motion at $t_{\ell+1}, t_{\ell}$ and constrain the energy expenditure over $\Delta t = t_{\ell+1} - t_{\ell}$. Both starting and stopping the motion of the particle contribute to the allocation of energy. If a constraint is placed on $\dot{\mathcal{E}}_k$, the rate of kinetic energy expenditure to accelerate the particle, then the corresponding rate must be considered as the limit for decelerating the particle. The proposition is that the maximum constant rate $\max\{\dot{\mathcal{E}}_k\} = P_{max} = P_m$ bound acceleration and deceleration of the particle over equivalent portions $\Delta t/2$ of the interval Δt , and to be considered as a physical limiting resource for the apparatus. P_m is regarded as a boundary condition.

Given this limiting formulation, the maximum possible particle kinetic energy must occur for a position near the configuration space center. The prior statements imply that $\Delta t/2$ is the shortest time interval possible for an acceleration or deceleration cycle to traverse the sphere.

The total transition energy expenditure may be calculated from adding the contributions of the maximum acceleration and deceleration cycles symmetrically;

$$2 \int_{t_\ell}^{t_\ell + \Delta t/2} \max\{\dot{\mathcal{E}}_k dt\} = 2 \int_{t_\ell}^{t_\ell + \Delta t/2} \max\{\dot{\vec{p}} \cdot \dot{\vec{q}}\} dt = P_{max} \Delta t \quad (3-3)$$

Peak velocity vs. time is calculated from P_{max} .

$$\vec{v}_p = \sqrt{2 \frac{P_{max}(t - t_\ell)}{m}} \hat{a}_R, \quad \text{for } t_\ell < t < \Delta t/2 \quad (3-4)$$

$$\vec{v}_p = \left[\sqrt{\frac{2P_{max}}{m} (\sqrt{(t_\ell + \Delta t) - t})} \right] \hat{a}_R, \quad \text{for } t_\ell + \Delta t/2 < t < t_\ell + \Delta t \quad (3-5)$$

\hat{a}_R is the unit radial vector within the hypersphere.

The range, R_s , traveled by the particle in $\Delta t/2$ seconds from the boundary edge is;

$$R_s = \frac{2}{3} \sqrt{\frac{2P_{max}}{m}} (\Delta t/2)^{\frac{3}{2}} \quad (3-6)$$

The following equation summary and graphics provide the result for the one dimensional case along the x_α axis where the maximum power is applied to move the particle from boundary to boundary, along a maximum radial.

$$\max\{\dot{\mathcal{E}}_k\} = P_m \tag{3-7}$$

$$\mathcal{E}_k = P_m(t - t_\ell) \quad t_\ell \leq t \leq t_\ell + \frac{\Delta t}{2} \tag{3-8}$$

$$\mathcal{E}_k = P_m((t_\ell + \Delta t) - t) \quad t_\ell + \Delta t/2 \leq t \leq (t_\ell + \Delta t) \tag{3-9}$$

Let t_ℓ equal zero for the following equations and graphical illustration of a particular maximum velocity trajectory.

$$\begin{array}{l}
\text{Positive Trajectory} \\
\left\{ \begin{array}{l}
\vec{v}_p = \sqrt{\frac{2P_m t}{m}} \hat{a}_\alpha = \left(\frac{3P_m}{m} (q + R_s) \right)^{\frac{1}{3}} (\hat{a}_\alpha) \quad -R_s \leq q \leq 0; 0 \leq t \leq \frac{\Delta t}{2} \\
\vec{v}_p = \sqrt{\frac{2P_m(\Delta t - t)}{m}} \hat{a}_\alpha = \left(\frac{3P_m}{m} (q - R_s) \right)^{\frac{1}{3}} (\hat{a}_\alpha) \quad 0 \leq q \leq R_s; \frac{\Delta t}{2} \leq t \leq \Delta t
\end{array} \right. \\
\\
\text{Negative Trajectory} \\
\left\{ \begin{array}{l}
\vec{v}_p = -\sqrt{\frac{2P_m t}{m}} \hat{a}_\alpha = \left(\frac{3P_m}{m} (q - R_s) \right)^{\frac{1}{3}} (-\hat{a}_\alpha) \quad 0 \leq q \leq R_s; 0 \leq t \leq \frac{\Delta t}{2} \\
\vec{v}_p = -\sqrt{\frac{2P_m(\Delta t - t)}{m}} \hat{a}_\alpha = \left(\frac{3P_m}{m} (q + R_s) \right)^{\frac{1}{3}} (-\hat{a}_\alpha) \quad -R_s \leq q \leq 0; \frac{\Delta t}{2} \leq t \leq \Delta t
\end{array} \right.
\end{array} \tag{3-10}$$

The characteristic radius and maximum velocity are solved using proper initial conditions applied to integrals of velocity and acceleration.

$$R_s = \frac{v_{max} \Delta t}{3} \tag{3-11}$$

$$v_{max} = \sqrt{\frac{P_m \Delta t}{m}} \tag{3-12}$$

v_{max} Is the greatest velocity magnitude along the trajectory, occurring at $t = \frac{\Delta t}{2}$. More detail is provided for the derivation of equations 3-10, 3-11 and 3-12 in appendix B.

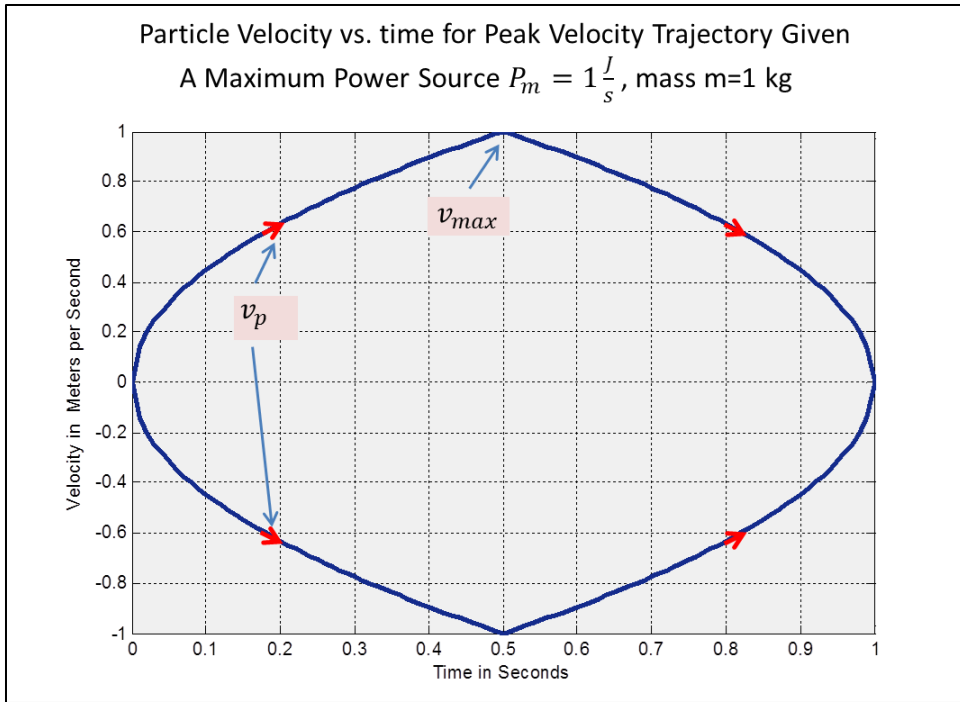


Figure 3-2 Peak Particle Velocity vs. Time

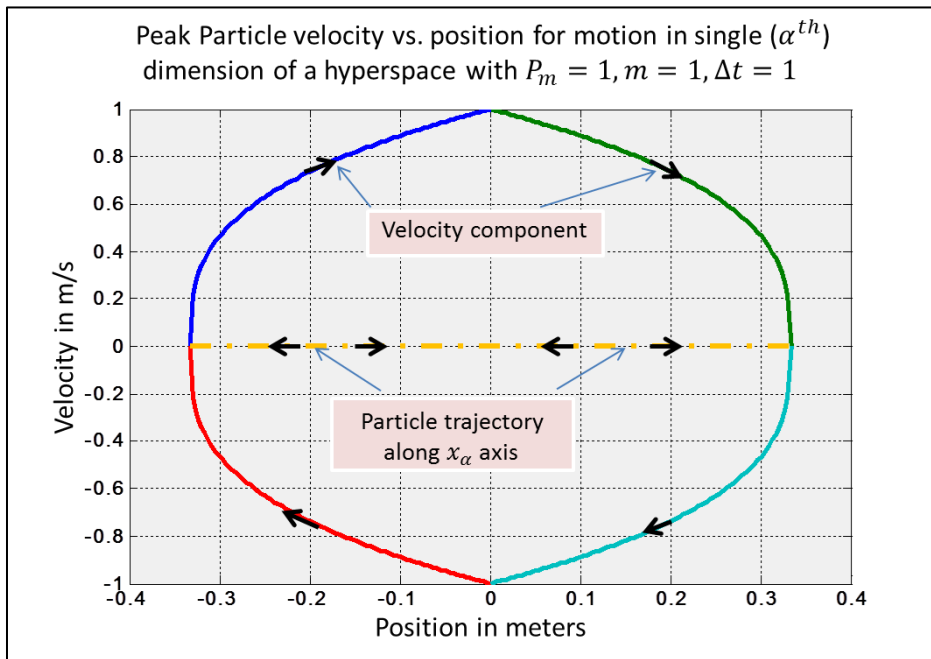


Figure 3-3 Peak Particle Velocity vs. Position

Figure 3-2 depicts peak velocity vs. time where the upper segment of the trajectory in the positive direction is a positive vector velocity. The negative vector velocity is a mirror image. Maximum absolute velocity, v_{max} , occurs at $t = \frac{\Delta t}{2}$. The second graphic transforms the time coordinate to position along the x_α axis, where α is a dimension index from D possible dimensions. Note that the maximum velocity occurs at $q = 0$, the sphere center. This is the coordinate with a maximum distance, R_s , from the boundary. R_s is the maximum configuration span over which positive acceleration occurs. Likewise maximum deceleration is required over the same distance to satisfy proper boundary conditions. These representations are the extremes of velocity profile given R_s , and P_m and shall be referred to as the maximum velocity profile. Slower random velocity trajectories which fall within these boundaries are required to support general random motion.

3.1.3. Momentum Probability

We will now pursue a statistical description for velocity trajectories within the boundaries established in the prior section.

The vector \vec{v} may be given a Gaussian distribution assignment based on a legacy solution obtained from the calculus of variations. An isoperimetric bound is applied to the uncertainty function [20]. H can be maximized, subject to a simultaneous constraint on the variance of the velocity random variable, resulting in the Gaussian pdf [21]. In this case the variance of the velocity distribution is proportional to the average kinetic energy of the particle. It follows that

this optimization extends to the multi-dimensional Gaussian case [15]. This solution justifies replacement of the uniform distribution assumption often applied to maximize the uncertainty of a similar phase space from statistical mechanics [13, 14]. While the uniform distribution does maximize uncertainty, it comes at a greater energy cost compared to the Gaussian assignment. Hence, a Gaussian velocity distribution emphasizes energetic economy compared to the uniform density function. A derivation justifying the Gaussian assumption is provided in appendix A for reference.

The Gaussian assignment is enigmatic because infinite probability tails for velocity invoke relativity considerations, with c (speed of light) as an absolute asymptotic limit. Therefore, the value of the peak statistic shall be limited and approximated on the tail of the pdf to avoid relativistic concerns. The variance or average power is another important statistic. The peak to average power or peak to average energy ratio of a communications signal is an especially significant consideration for transmitter efficiency. The analog of this parameter can also be applied to the multidimensional model for the transmitter particle velocity and shall be subsequently derived for calculating a peak to average power or peak to average kinetic energy ratio, hereafter *PAPR*, *PAER*, respectively. The following figure illustrates the standard zero mean Gaussian velocity v RV with $\sigma^2=1$.

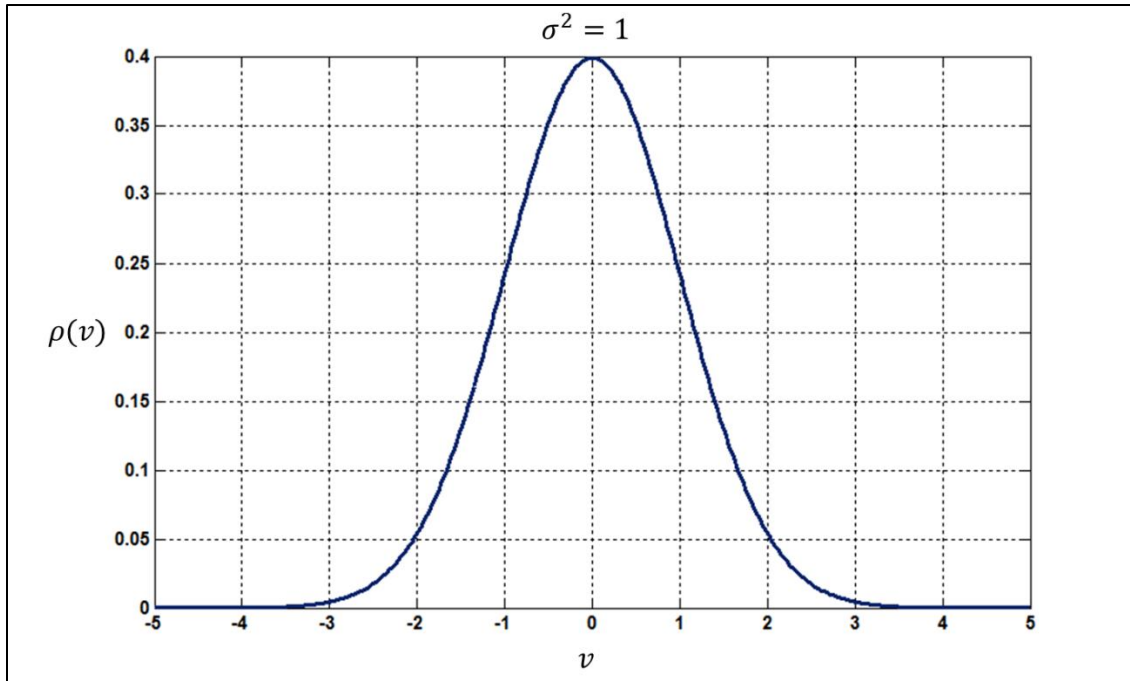


Figure 3-4 Gaussian Velocity pdf

It is apparent that whenever $v = 4$ or greater for the pdf with variance $\sigma^2=1$, the probability values are very small in a relative sense. If $v^2/2$ is directly proportional to the instantaneous kinetic energy then a peak velocity excursion of 4 corresponds to an energy peak of 8. For the case of $\sigma^2=1$, a range of $v = \pm 2\sqrt{2}$ encompasses the majority (97.5 %) of the probability space. Hence, $PAER \geq 4$ is a comprehensive domain for the momentum pdf with a normalized variance. The $PAER$ must always be greater than 1 by design because $\sigma^2 \rightarrow 0$ as $PAER \rightarrow 1$. One may always define a $PAER$ provided $\sigma^2 \neq 0$. This is a fundamental restriction. As $\sigma^2 \rightarrow 0$ the pdf becomes a delta function with area 1 by definition. In the case of a zero mean Gaussian RV the average power becomes zero in the limit along with the peak excursions if the $PAER$ approaches a value of 1.

The probability tails beyond the peak excursion values may simply be ignored (truncated) as insignificant or replaced with delta functions of appropriate weight. This approximation shall be applied for the remainder of the discussion concerning velocities or momenta of particles. *PAER* is an important parameter and may be varied to tailor a design. *PAER* provides a suitable means for estimating the required energy of a communications system over significant dynamic range. It shall be convenient to convert back and forth between power and energy from time to time. In general, *PAPR* is used whenever variance is given in units of Joules per second and *PAER* is used whenever units in joules, are preferred.

Maximum velocity and acceleration along the radial is bounded. At the volume center the probability model for motion is completely independent of θ, ϕ in spherical geometry. However, as the particle position coordinate q varies off volume center, the spread of possible velocities must correspondingly modify. Either the particle must asymptotically halt or move tangential at the boundary or otherwise maneuver away from the boundary avoiding collision. It is apparent that angular distribution of the velocity vector changes as a function of offset radial with respect to the sphere center.

Momentum will be represented using orthogonal velocity distributions. This approach follows similar methods originated by Maxwell and Boltzmann [13, 22]. The subsequent analysis focuses on the statistical motion of a single particle in one configuration dimension. Additional D dimensions are easily accommodated from extension of the 1-D solution. Vibrational, rotational and internal energies of the particle are not presently considered. It is therefore a simple scenario involving a classical particle without additional qualification of its quantum states.

The configuration coordinate may be identified at the tip of the position vector \vec{q} given an orthonormal basis.

$$\vec{q} = q_1 \hat{a}_{x_1} + q_2 \hat{a}_{x_2} + \cdots q_D \hat{a}_{x_D} \quad (3-13)$$

Likewise the velocity is given by;

$$\vec{v} = \dot{q}_1 \hat{a}_{x_1} + \dot{q}_2 \hat{a}_{x_2} + \cdots \dot{q}_D \hat{a}_{x_D} \quad (3-14)$$

Distributions for each orthogonal direction are easily identified from the prior velocity profile calculations, definition of *PAER*, and Gaussian optimization for velocity distribution due to maximization of momentum uncertainty.

The generalized axes of the D dimensional space shall be represented as x_1, x_2, \dots, x_D where D may be assigned for a specific discussion. Similarly, unit vectors in the x_α dimension are assumed a given assignment of \hat{a}_α as the defining unit vector. Velocity and position vectors are given by \vec{v}_α and \vec{q}_α respectively.

The following figure illustrates the particle motion with one linear degree of freedom within a $D = 3$ configuration space of interest.

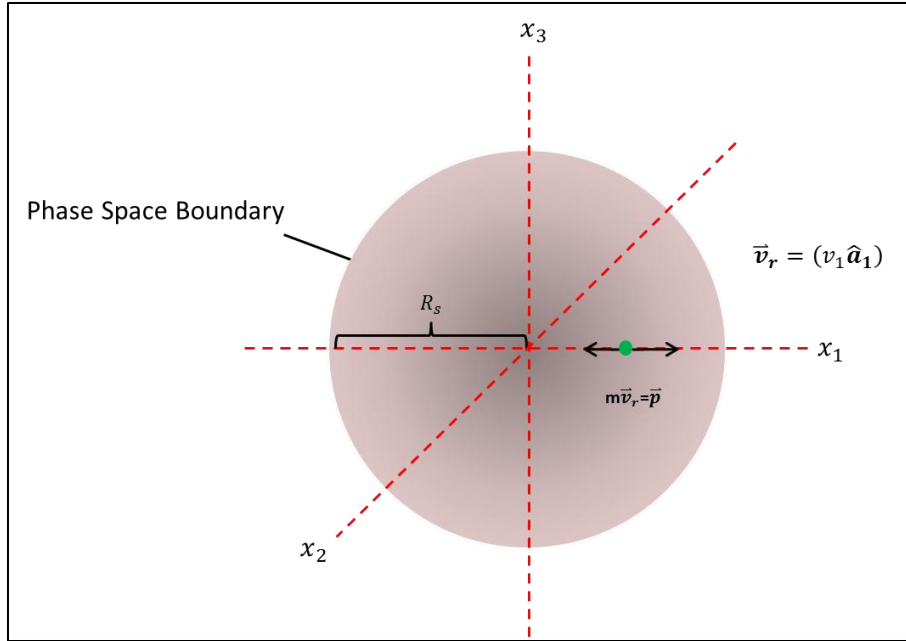


Figure 3-5 Phase Space Boundary

The radial velocity \vec{v}_r as illustrated is defined by $\vec{v}_r = v_\alpha \hat{a}_\alpha$ which is a convenient alignment moving forward. The equations for the peak velocity profile were given previously and are used to calculate the peak velocity vs. radial offset coordinate along the x_α axis. *PAER* may be specified at a desired value such as 4 (6 dB) for example and the pseudo-Gaussian distribution of the velocities obtained as a function of q_α .

The velocity probability density is written in two forms to illustrate the utility of specifying *PAER*.

$$\rho(\vec{v}_r) = \frac{1}{\sqrt{2\pi}\sigma_{v_r}} e^{-\frac{v_r^2}{2(\sigma_{v_r})^2}}, \quad \bar{v}_r = \bar{v}_\alpha = 0, \quad \sigma_{v_r}^2 = \sigma_{v_\alpha}^2$$

(3-15)

$$\rho(\vec{v}_\alpha) \cong \frac{\sqrt{PAER}}{\sqrt{2\pi}v_{\alpha_peak}} e^{-\frac{(PAER)v_\alpha^2}{2(v_{\alpha_peak})^2}}, \quad PAER \equiv \left(\frac{v_{\alpha_peak}}{\sigma_{v_\alpha}}\right)^2 = \frac{\mathcal{E}_{kmax}}{\langle \mathcal{E}_k \rangle}$$

(3-16)

\vec{v}_{α_peak} is the peak velocity profile as a function of q_α which shall occasionally be referred to as \vec{v}_p whenever convenient . $PAER$ is a constant. Therefore σ_{v_α} may be distinctly calculated for each value of q_α as well. The peak velocity bound versus q_α is illustrated in Figure 3-2 as obtained from (3-10)

Each value of q_α along the radial possesses a unique Gaussian random variable for velocity. The graphical illustration of this distribution follows;

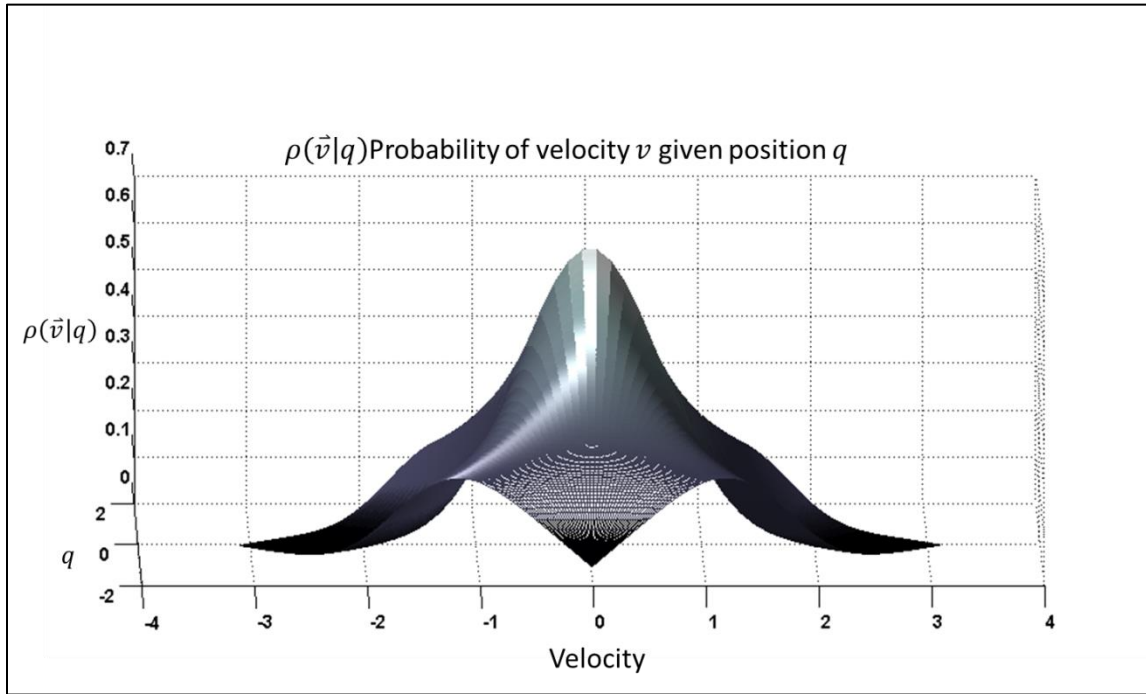


Figure 3-6 pdf of Velocity \vec{v}_α as a Function of Radial Position for a Particle in Motion, Restricted to a Single Dimension and Maximum Instantaneous Power, P_m , Peak to Average Energy Ratio ($PAER = 4$),

$$P_m = 10 \text{ J/s}, v_{max} = \sqrt{10} \text{ m/s}, \Delta t = 1, R_s = (\Delta t(v_{max}/3)), m = 1 \text{ kg}$$

Probability is given on the vertical axis. Notice that the probability of the vector velocity is maximum for zero velocity on the average at the phase space center, with equal probability of positive and negative velocities at a given q . The sign or direction of the trajectory corresponds to positive or negative velocity in the figure. It is also apparent that the velocity probability of zero occurs at the extremes of $+/-R_s$, the phase space boundary. Correspondingly, the variances of the Gaussian profiles are minimum at the boundaries and maximum at the center.

A cross-sectional view from the perspective of the velocity axis is Gaussian with variance that changes according to q_α . In this case a *PAER* of 4 is maintained for all q_α coordinates.

Suppose P_m is decreased from 10 to 5 J/s . The corresponding scaling of phase space is illustrated in the subsequent graphical representations. This trade in phase space access is a fundamental theme illustrating the relationship between phase space volume and rate of energy expenditure.

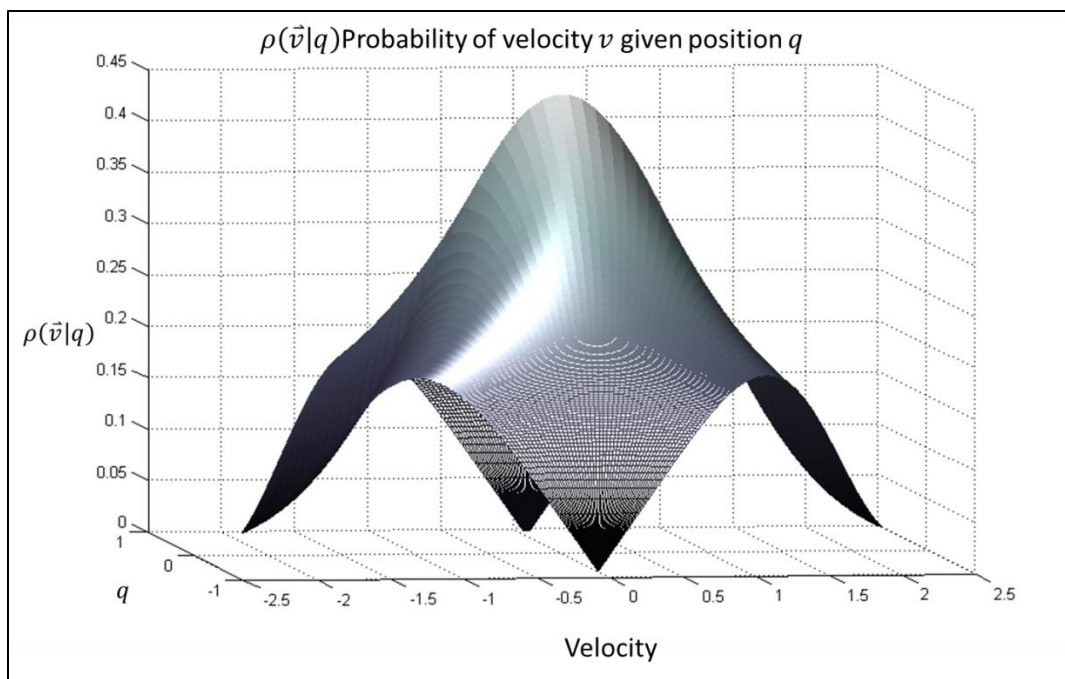


Figure 3-7 Probability of Velocity

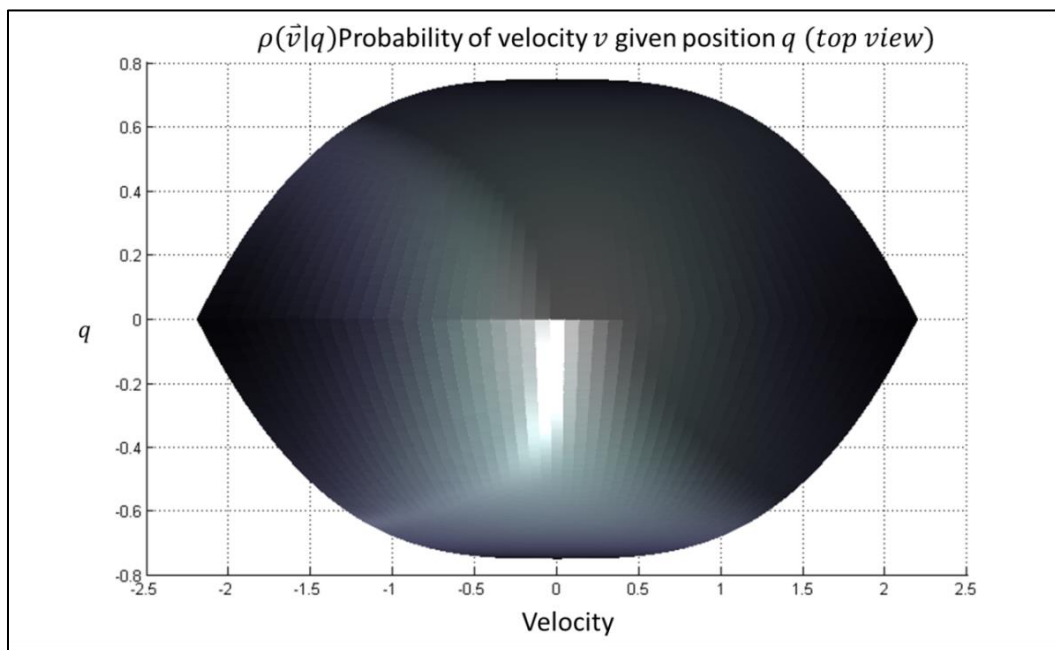


Figure 3-8 Probability of Velocity given q (Top View)

The velocity dynamic range is decreased by the factor $\sqrt{P_{m_new}/P_{m_old}} \cdot R_s$, the characteristic and accessible radius of the sphere, must correspondingly reduce even though the $PAER=4$ is unchanged. Thus, the hyper-sphere volume decreases in both configuration and momentum space.

Now that the momentum conditional pdf is defined for one dimension, the extension to the other dimensions is straight forward given the assumption of orthogonal dimensions and statistically independent distributions. The distribution of interest is 3 dimensional Gaussian. This is similar to the classical Maxwell distribution except for the boundary conditions and the requirement for maintaining vector quantities [22, 23]. The distribution for the multivariate hyper-geometric case may easily be written in terms of the prior single dimensional case.

$$\rho(\vec{v}) = \prod_{\alpha=1}^D \rho(\vec{v}_\alpha)$$

(3-17)

$$\vec{v} = \sum_{\alpha} v_{\alpha} \hat{a}_{\alpha}$$

$$\sigma_{\vec{v}}^2 = \sum_{\alpha} \sigma_{v_{\alpha}}^2$$

$$\bar{\vec{v}} = \sum_{\alpha} \bar{\vec{v}}_{\alpha} = 0$$

The following figure illustrates the vector velocity deployment in terms of the velocity and configuration coordinates.

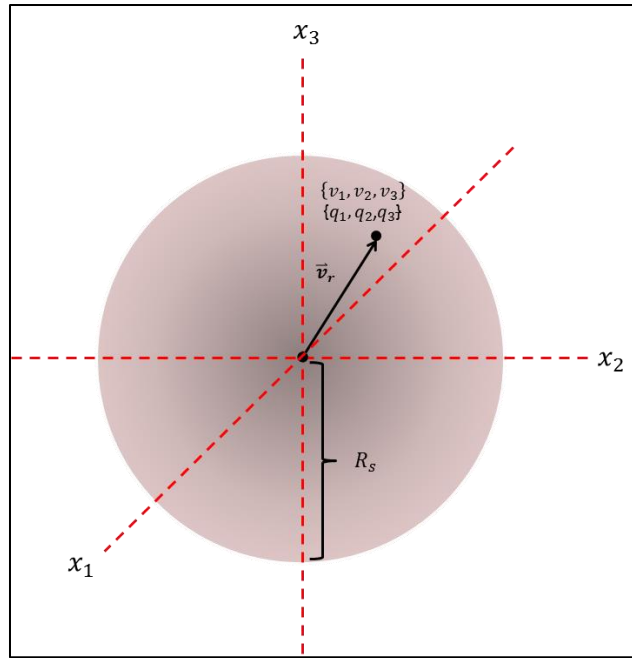


Figure 3-9 Vector Velocity Deployment

The pdf for velocity is easily written in a general form. In this particular representation, the vectors enumerated as α, β through subscripts, are considered to represent orthogonal dimensions for $\alpha \neq \beta$. This is an important distinction of the notation which shall be assumed from this point forward except where otherwise noted.

The multidimensional pdf may be given as;

$$\rho(\vec{v}) = \frac{1}{\sqrt{(2\pi)^D |\Lambda|}} e^{\left[-\frac{1}{2}(v_\alpha - \bar{v}_\alpha)^T \Lambda^{-1} (v_\beta - \bar{v}_\beta)\right]}$$

(3-18)

$$[\Lambda] = \begin{bmatrix} \sigma_{v_1}^2 & \sigma_{12} \dots & \sigma_{1D} \\ \sigma_{21} & \sigma_{v_2}^2 \dots & \sigma_{2D} \\ \sigma_{D1} & \sigma_{D2} \dots & \sigma_{v_D}^2 \end{bmatrix}$$

(3-19)

The covariance and normalized covariance are also given explicitly for reference;

$$\sigma_{\alpha,\beta} = cov\{v_\alpha, v_\beta\} = \iint_{-\infty}^{+\infty} (v_\alpha - \bar{v}_\alpha)(v_\beta - \bar{v}_\beta)\rho(v_\alpha, v_\beta) dv_\alpha dv_\beta$$

(3-20)

$$\Gamma_{norm(\alpha,\beta)} = \frac{\sigma_{\alpha,\beta}}{\sigma_\alpha \sigma_\beta}$$

(3-21)

$\Gamma_{norm(\alpha,\beta)}$ is also known as the normalized statistical covariance coefficient. The diagonal of 3-19 shall be referred to as the dimensional auto covariance and the off diagonals are dimensional cross-covariance terms. These statistical terms are distinguished from the corresponding forms which are intended for the time analysis of sample functions of an ensemble obtained from a random process. However, a correspondence between the statistical form above and the time domain counterpart is anticipated and justified in later sections. Discussions proceed contemplating this correspondence.

[Λ] permits the greatest flexibility for analyzing arbitrarily assigned vectors within the space. Statistically independent vectors are also orthogonal in this particular formulation over suitable intervals of time and space. 3-18 can account for spatial correlations. In the case where state

transitions possesses statistically independent origin and terminus, the off diagonal elements, ($\alpha \neq \beta$), will be zero.

In the Shannon uncertainty view, each statistically independent state is equally probable at a successive infinitesimal instant of time, i.e. $(\Delta t/2) \rightarrow 0$. More directly, time is not an explicit consideration of the uncertainty function. As will be shown in chapter 8, this cannot be true independent of physical constraints such as P_{max} , and R_s . Statistically independent state transitions may only occur more rapidly for greater investments of energy per unit time.

3.1.3.1. Transmitter Configuration Space Statistic

The Configuration space statistic is a probability of a particle occupying coordinates q_α . A general technique for obtaining this statistic is part of an overall strategy outlined in the following brief discussion.

A philosophy which has been applied to this point, and will be subsequently advanced, follows:

First, system resources are determined by the maximum rate of energy per unit time limit. This quantity is P_m . P_m limits $\dot{\vec{p}}$ which requires consideration of acceleration. Secondly, information is encoded in the momentum of particle motion at a particular spatial location. Momentum is approximately a function of the velocity at non-relativistic speeds which in turn is an integral with respect to the acceleration. The momentum is constrained by the joint consideration of P_m and maximum information conservation. Finally, the position is an integral with respect to the velocity which makes it a second integral with respect to the force and in a sense a subordinate variable of the analysis, though a necessary one.

The hierarchy of inter-dependencies is significant. A choice was made to use momentum as an analysis fulcrum because it permits the unambiguous encoding of information in vector quantities. Fortuitously, momentum couples configuration and force through integrals. Since the momentum is Gaussian distributed it is easy to argue that the position is also Gaussian. That is, the integral or the derivative of a Gaussian process remains Gaussian. This is known from the theory of stochastic processes and linear systems [12, 23, 24].

Boundary conditions and laws of motion do provide a basis for obtaining the phase space density of states for a non-uniform configuration. The specific form of the configuration dependency is reserved for section 3.1.10.1 where the joint density $\rho(\vec{q}, \vec{p})$ is fully developed.

3.1.4. Correlation of Motion, and Statistical Independence

Discussions in this section are related to correlation of motion. Since the RV's of interest are statistically independent zero mean Gaussian then they are also uncorrelated over sufficient intervals of time and space.

The mathematical requirement for statistical independence is well known and is repeated here with the appropriate variable representation, preserving space – time indexing [25]. Time indexing t_ℓ and $t_\ell + \tau$ is retained to acknowledge that the pdfs of interest may not evolve from strictly stationary processes.

$$\rho(v_\beta(t_\ell + \tau)|v_\alpha(t_\ell)) = \frac{\rho(v_\alpha(t_\ell), v_\beta(t_\ell + \tau))}{\rho(v_\alpha(t_\ell))} = \rho(v_\beta(t_\ell + \tau)) \quad (3-22)$$

$\rho(v_\beta(t_\ell + \tau)|v_\alpha(t_\ell))$ is the probability of the $(v_\beta, t_\ell + \tau)$ velocity vector given the $v_\alpha(t_\ell)$ velocity vector. It is important to understand the conditions enabling 3-22.

Partial time correlation of Gaussian RVs characterizing physical phenomena is inevitable over relatively short time intervals when the RV's originate from processes subject to regulated energy per unit time. Bandwidth limited AWGN with spectral density N_0 is an excellent example of such a case where the infinite bandwidth process is characterized by a delta function time auto-correlation and the same strictly filtered process is characterized by a harmonic *sinc* auto-correlation function with nulls occurring at intervals $\tau = \pm n (1/2B)$, where B is the filtering bandwidth and $\pm n$ are non-zero integers.

$$\mathfrak{R}_{n,n}(\tau) = N_0 \delta(\tau), \quad B = \infty \quad (3-23)$$

$$\mathfrak{R}_{n,n}(\tau) = 2BN_0 \frac{\sin(2\pi B\tau)}{2\pi B\tau}, \quad B < \infty \quad (3-24)$$

The nature of correlations at specific instants, or over extended intervals, can provide insight into various aspects of particle motions such as the work to implement those motions and the uncertainty of coordinates along the trajectory.

Λ was introduced to account for the inter-dimensional portions of momentum correlations. Whenever v_α and v_β are not simultaneous in time, the desired expressions may be viewed as space and time cross-covariance. This is explicitly written for the ℓ^{th} and $(\ell^{th} + 1)$ time instants in terms of the pdf as;

$$\Lambda_{\alpha,\beta} = \iint_{-\infty}^{+\infty} (v_{\alpha,\ell})(v_{\beta,\ell+1})\rho(v_{\alpha,\ell}, v_{\beta,\ell+1}) dv_{\alpha,\ell} dv_{\beta,\ell+1} = E\{v_{\alpha,\ell}v_{\beta,\ell+1}\} \quad (3-25)$$

This form accommodates a process which defines the random variables of interest yet is not necessarily stationary. This mixed form is a bridge between the statistical and time domain notations of covariance and correlation. It acknowledges probability densities which may vary as a function of time offset and therefore q , as is the current case of interest.

The time cross correlation of the velocity for τ offset is;

$$\Re_{v_\alpha v_\beta} = \langle \vec{v}_\alpha(t - t_\ell) \cdot \vec{v}_\beta(t - (t_\ell + \tau)) \rangle = \lim_{T \rightarrow \infty} \frac{1}{2T} \int_{-T}^T (\vec{v}_{\alpha,(t_\ell)}) \cdot (\vec{v}_{\beta,(t_\ell+\tau)}) dt \quad (3-26)$$

If $\alpha = \beta$ then 3-26 corresponds to a time auto-correlation function. This form is suitable for cases where the velocity samples are obtained from a random process with finite average power [21]. Whenever $\alpha \neq \beta$ then the vector velocities are uncorrelated because they correspond to orthogonal motions. Arbitrary motion is equally distributed amongst one or more dimensions over an interval $2T$, and compared to time shifted trajectories. Then the resulting time based

correlations over sub intervals may range from -1 to 1. In the case of independent Gaussian RV's, equations 3-25 and 3-26 should approach the same result.

In the most general case the momentum, and therefore the velocity, may be decomposed into D orthogonal components. If such vectors are compared at $t = t_\ell$ and $t = t_\ell + \tau$ offsets, then a correlation operation can be decomposed into D kernels of the form given in 3-25 where it is understood that the velocity vectors must permute over all indices of α and β to obtain comprehensive correlation scores. A weighted sum of orthogonal correlation scores determines a final score.

A metric for the velocity function similarity as the correlation space-time offset varies, is found from the normalized correlation coefficient which is the counterpart to the normalized covariance presented earlier. It is evaluated at a time offset .

$$\gamma_{v_\alpha, v_\beta} = \frac{\Re_{v_\alpha, v_\beta}(\tau)}{\langle \vec{v}_{\alpha, t_\ell} \cdot \vec{v}_{\beta, t_\ell + \tau} \rangle} \quad (3-27)$$

It is possible to target the space and time features for analysis by suitably selecting the values α, β, τ .

A finite energy, time autocorrelation is also of some value. Sometimes this is a preferred form in lieu of the form in 3-26. The energy signal auto and cross correlation can be found from [21];

$$\Re_{v_\alpha, v_\beta} = \langle \vec{v}_\alpha(t - t_\ell) \cdot \vec{v}_\beta(t - (t_\ell + \tau)) \rangle = \lim_{T \rightarrow \infty} \int_{-T}^T (\vec{v}_{\alpha, t_\ell}) \cdot (\vec{v}_{\beta, t_\ell + \tau}) dt \quad (3-28)$$

Now we examine the character of the time auto-correlation of the linear momentum over some characteristic time interval, such as $\Delta t = t_\ell - t_{\ell+1}$. The correlation must become zero as the offset time $(t_\ell + \Delta t)$ is approached, to obtain statistical independence outside that window. In that case, time domain de-correlation requires;

$$\langle \vec{p}(t - t_\ell) \cdot \vec{p}(t - (t_\ell + \Delta t)) \rangle = 0; \quad t \geq |(t_\ell + \Delta t)|$$

(3-29)

Similarly, the forces which impart momentum change must also decouple implying that.

$$\langle \dot{\vec{p}}(t - t_\ell) \cdot \dot{\vec{p}}(t - (t_\ell + \Delta t)) \rangle = 0; \quad t \geq |(t_\ell + \Delta t)|$$

(3-30)

Suppose it is required to de-correlate the motions of a rapidly moving particle and this operation is compared to the same particle moving at a diminutive relative velocity over an identical trajectory. Greater energy per unit time is required to generate the same uncorrelated motions for the fast particle over a common configuration coordinate trajectory. The controlling rate of change in momentum must increase corresponding to an increasing inertial force. Likewise, a proportional oppositional momentum variation is required to establish equilibrium, thus arresting a particle's progress along some path. This argument deduces from Newton's laws.

Another consideration is whether or not the particle motion attains and sustains an orthogonal motion or briefly encounters such a circumstance along its path. Both cases are of interest. However, a brief orthogonal transition is sufficient to remove the memory of prior particle momentum altogether if the motions are distributed randomly through space and time.

A basic principle emerges from 3-29 and 3-30 and a consideration of Newton's laws.

Principle: Successive particle momentum and force states must become individually zero, jointly zero or orthogonal, corresponding to the erasure of momentum memory beyond some characteristic interval Δt , assuming no other particle or boundary interactions. This is a requirement for zero mean Gaussian motion of a single particle.

If a particle stops while releasing all of its kinetic energy, or turns in an orthogonal direction, prior information encoded in its motion is lost. This is an important concept because evolving uncertainty is coupled to the particle memory through momentum. Extended single particle de-correlations outside of the interval $\pm\Delta t$, with respect to $\Re_{v_\alpha, v_\beta} @ \tau = 0$, are evidence of increasing statistical independence in those regimes.

Autocorrelations shall be zero outside of the window $(-\Delta t \leq \tau \leq \Delta t)$ for the immediate analysis unless otherwise stated. The reason for this initial analysis restriction is to bound the maximum required energy resource for statistically independent motion beyond a characteristic interval. In other words there is no information concerning the particle motion outside that interval of time.

The derivative $\dot{\mathcal{E}}_k$ is random up to a limit, P_{max} . $\dot{\mathcal{E}}_k$ is a function of the derivative field;

$$\dot{\mathcal{E}}_k = \dot{\vec{p}} \cdot \dot{\vec{q}}$$

(3-31)

This leads to a particular inter-variable cross-correlation expression.

$$\lim_{T \rightarrow \infty} \frac{1}{2T} \int_{-T}^T \dot{\vec{p}}(t - t_\ell) \cdot \dot{\vec{q}}(t - (t_\ell + \tau)) dt = \langle \dot{\vec{p}} \cdot \dot{\vec{q}} \rangle \leq P_{max} @ \tau = 0$$

(3-32)

The kernel is a measure of the rate of work accomplished by the particle. It is useful as an instantaneous value or an accumulated average. This equation is identically zero only for the case where $\dot{\vec{p}}$ or $\dot{\vec{q}}$ are zero or for the case where the vector components of $\dot{\vec{p}}, \dot{\vec{q}}$ are mutually orthogonal. If they are orthogonal for all time then there is no power consumed in the course of the executed motions. Thus, the assumption for statistical independence of momentum and force at relatively the same instant in time can only be possible for the case where the instantaneous rate of work is zero. Whenever there is consumption of energy, force and velocity must share some common nonzero directional component and will be statistically codependent to some extent. This is necessary to bridge between randomly distributed coordinates of the phase space at successively fixed time intervals . *If we restrict motions to an orthogonal maneuver within the derivative field we collapse phase space access and uncertainty of motion goes to zero along with the work performed on the particle.*

3.1.5. Autocorrelations and Spectra for Independent Maximum Velocity Pulses

At this point it is convenient to introduce the concept of the velocity pulse. Particle memory, due to prior momentum, is erased moving beyond time Δt into the future for this analysis.

Conversely, this implies a deterministic component in the momentum during the interval Δt .

Such structure, where the interval is defined as beginning with zero momentum in the direction of interest and terminating with zero momentum in that same direction is referred to as a velocity pulse. For example, the maximum velocity profiles may be distinctly defined as pulses over Δt .

The maximum velocity pulse possesses a time autocorrelation that is analyzed in detail in Appendix C. The corresponding normalized autocorrelation, is plotted in the following graph with $\Delta t = 1$.

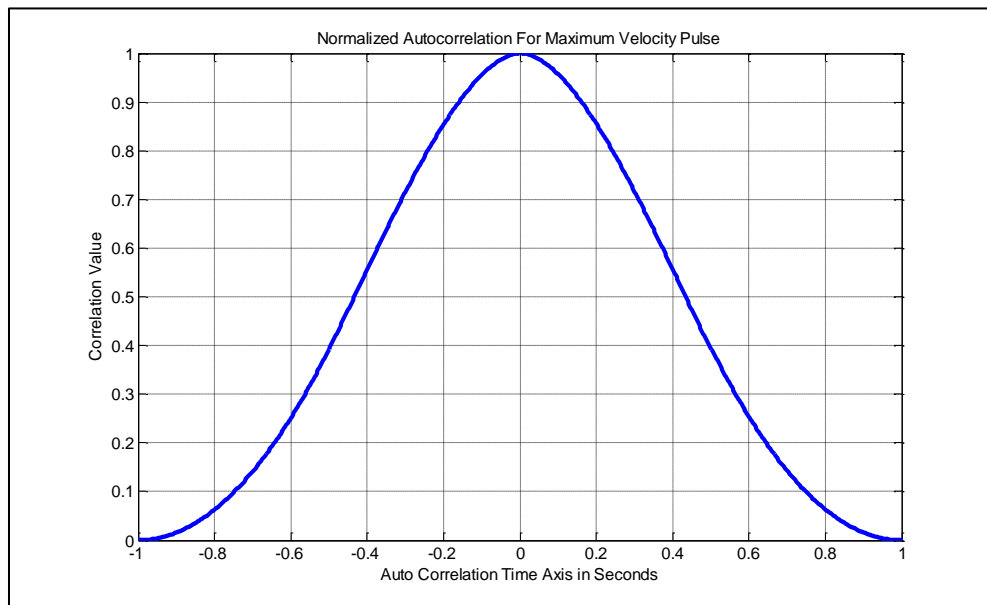


Figure 3-10 Normalized Autocorrelation of a Maximum Velocity Pulse

This is the normalized autocorrelation for the pulse of the maximum velocity which spans the hyper sphere with a single degree of freedom. If it is further assumed that the orthogonal dimensions execute independent motions, it follows that the autocorrelations in the x_1, x_2, \dots, x_D directions are of the same form. One feature of interest here is that the autocorrelation is zero for the extremums, $\pm\Delta t$. This feature significantly influences the Fourier transform response. The

Fourier transform of the autocorrelation may be calculated from the Fourier response of the convolution of two functions by a change of variables. The transform of the convolution is given by;

$$\mathfrak{F}(g_1 * g_2) = \int_{-\infty}^{\infty} \left\{ \int_{-\infty}^{\infty} g_1(t - \lambda) g_2(\lambda) d\lambda \right\} e^{-i\omega t} dt = G_1(\omega)G_2(\omega)$$

(3-33)

The transform of the correlation operation for real functions is given by;

$$\mathfrak{F}\{\langle g_1 g_2 \rangle\} = \int_{-\infty}^{\infty} \left\{ \int_{-\infty}^{\infty} g_1(t' + \tau) g_2(t') dt' \right\} e^{-i\omega t} dt$$

(3-34)

If $(t' + \tau) \rightarrow (t - \lambda)$ then the convolution is identical to the correlation which is precisely the case for symmetric functions of time. Hence, the Fourier transform of the autocorrelation can be obtained from the Fourier transform squared of the velocity pulse in this case.

$$\mathfrak{F}\left\{ \int_{-\infty}^{\infty} v(t' + \tau) v(t') dt' \right\} = \int_{-\infty}^{\infty} \left\{ \int_{-\infty}^{\infty} v(t' + \tau) v(t') dt' \right\} e^{-i\omega t} dt = V(\omega)V(\omega)$$

(3-35)

The following figures illustrate the magnitude response for the transform of the normalized maximum velocity pulse autocorrelation for linear and logarithmic scales.

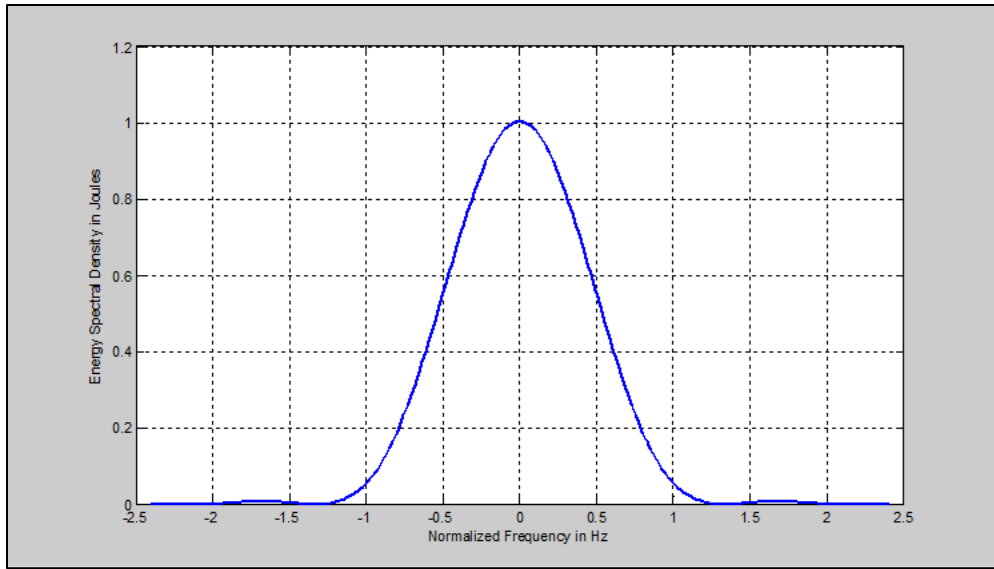


Figure 3-11 Normalized Fourier Transform of Maximum Velocity Pulse Autocorrelation

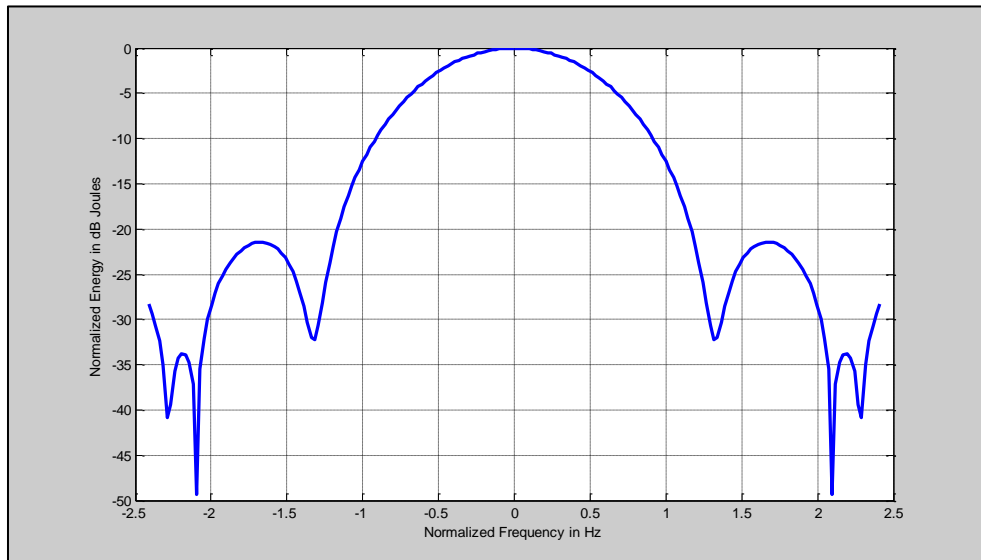


Figure 3-12 Normalized Fourier Transform of Maximum Velocity Pulse Autocorrelation

Figures 3-11 and 3-12 represent the energy spectrum generated by the most radical particle maneuver within the phase space to insure de-correlation of motion beyond a time Δt into the

future. The spectrum possesses infinite frequency content which corresponds to the truncated time boundary conditions requiring zero momentum at those extremes.

The maximum velocity pulse functions given above are not specifically required except at the statistically rare boundary condition extreme. Whenever the transmitter is not pushed to an extreme dynamic range the pulse function can assume a different form.

According to the Gaussian statistic, the maximum velocity pulse, and therefore its associated autocorrelation illustrated above, would be weighted with a low probability asymptotically approaching zero for a large *PAER* parameter. General pulses will consume energy at a rate less than or equal to the maximum velocity pulse and possess spectrums well within the frequency extremes of the derived maximum velocity pulse energy spectrum .

3.1.6. Characteristic Response

Independent pulses of duration Δt possess a characteristic autocorrelation response. All spectral calculations based on this fundamental structure will require a main lobe with a frequency span which is at least on the order of or greater than $2(\Delta t)^{-1}$ according to the Fourier transform of the autocorrelation. This can be verified by Gabor's uncertainty relation [26] .

The Fourier transform of the rectangular pulse autocorrelation follows;

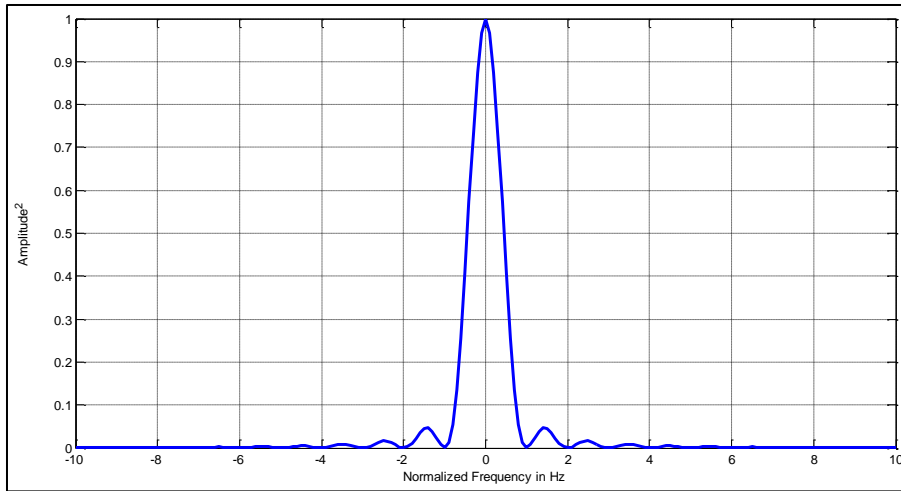


Figure 3-13 Fourier Transform of the Rectangular Pulse Autocorrelation

The pulse, $\Pi\left(\frac{t}{\Delta t}\right)$, can be formed from elementary operations which possess significant intuitive and physical relevance. Any finite rectangular pulse can be modeled with at least two impulses and corresponding integrators. The following figure illustrates schematically the formation of such a pulse.

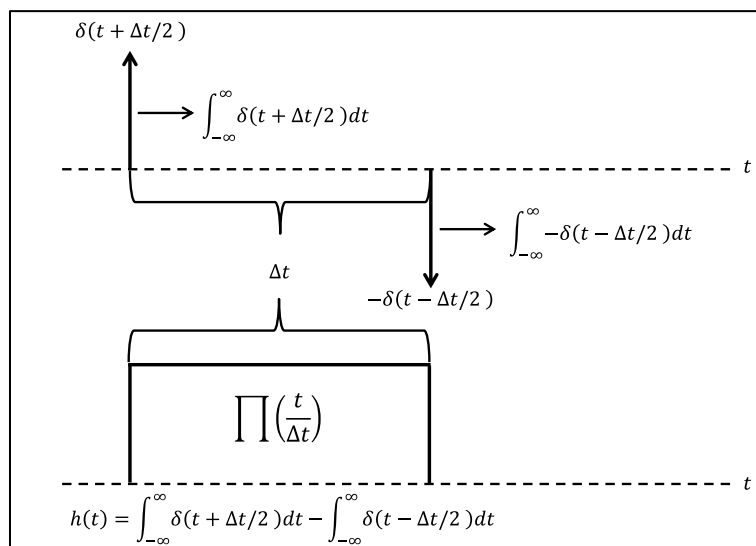


Figure 3-14 Forming a Rectangular Pulse from the Integration of Delta Functions

$h(t)$ is the impulse response of the system which deploys two integrated delta function forces.

Now suppose that the impulse functions are forces applied to a particle of mass $m = 1$. To obtain particle velocity one must integrate the acceleration due to the force. The result of the given integration is the rectangular velocity pulse vs. time. This is a circumstance without practical restrictions on the force functions $\delta(t \mp \Delta t/2)$, i.e. physically non-analytic, yet corresponds mathematically to Newton's laws of motion.

The result is accurate to within a constant of integration. Only the time variant portion of the motion may encode information so the constant of integration is not of immediate interest.

Notice further, that if the first integral were not opposed by the second, motion would be constant and change in momentum would not be possible after $t = -\Delta t/2$. Otherwise uncertainty of motion would be extinguished after the first action. Thus, two forces are required to alter the velocity in a prescribed manner to create a pulse of specific duration.

Recall the original maximum velocity pulse with one degree of freedom previously analyzed in detail. In that case at least two distinct forces are also required to create the velocity profile, which ensures statistical independence of motion outside the interval $\pm\Delta t/2$. The following illustration provides a comparison to the rectangular pulse example. $h_p(t)$ indicates that two distinct forces are required; one to first accelerate then one to decelerate the particle. We may insist that the majority of pulses within the extreme velocity pulse bound can be physically analytic even though the maximum velocity pulse is not. Assume that $h_f(t)$ is the characteristic system impulse response function and $*$ is a convolution operator.

Then;

$$h_p(t) = [\delta(t) * h_f(t)] - [\delta(t - \Delta t/2) * h_f(t)]$$

(3-36)

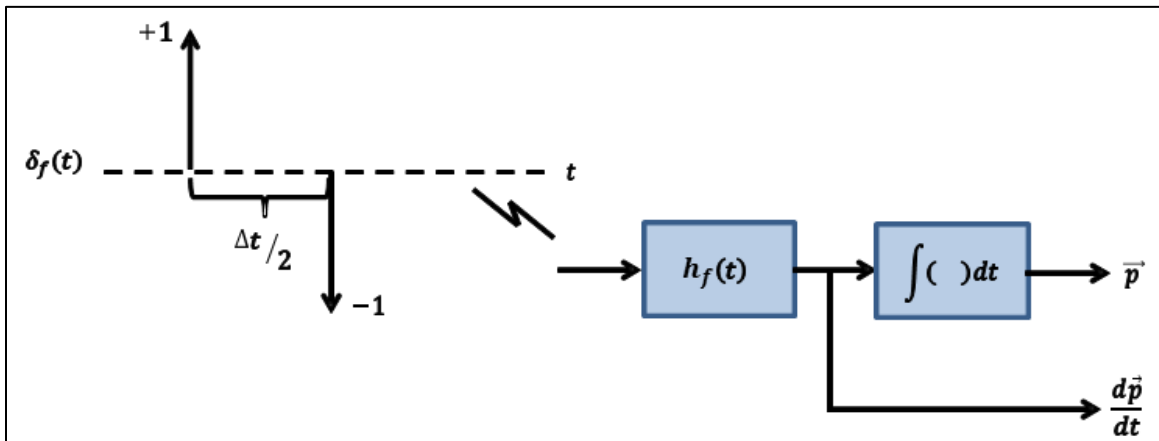


Figure 3-15 Model for a Force Doublet Generating a Maximum Velocity Pulse

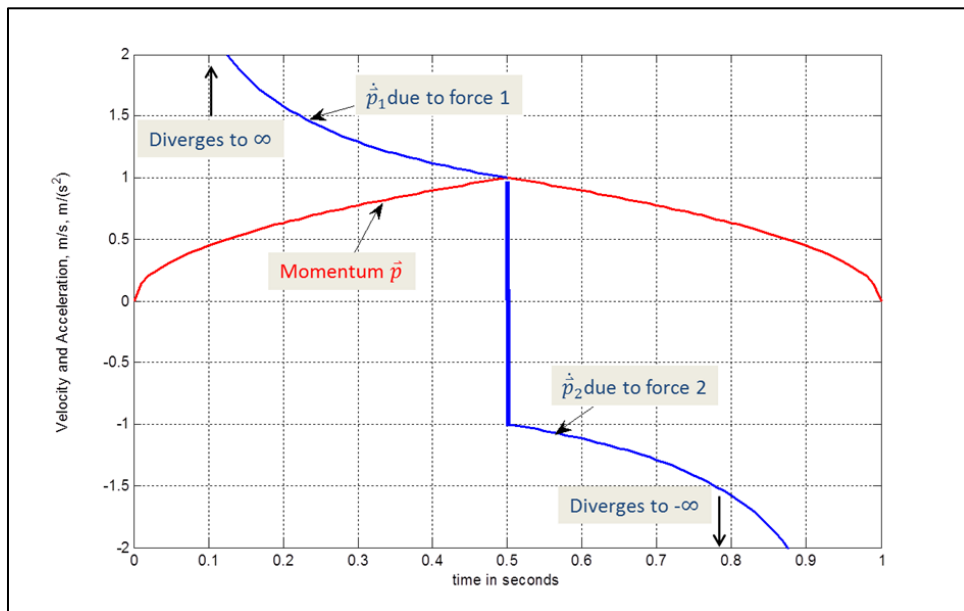


Figure 3-16 Max. Velocity Pulse Impulse Response for Transmitter Model with P_{max} Constraint, $m = 1$

Information is encoded in the pulse amplitude. This level is dependent on the nature of the force over the interval Δt and changes modulo Δt . Regardless of the specific function realized by the velocity pulse, at least two distinct forces are always required to permit independence of motion between succeeding pulse intervals. This property is also evident from energy conservation in the case where work is accomplished on the particle since;

$$\langle \dot{p}_1 \cdot \dot{q}_1 \rangle = \langle \dot{p}_2 \cdot \dot{q}_2 \rangle \quad \Delta t_1 + \Delta t_2 = \Delta t \quad (3-37)$$

$$\mathcal{E}_1 = \mathcal{E}_2 \quad (3-38)$$

The left hand side of the equation is the average energy \mathcal{E}_1 over the interval Δt_1 , the first half of the pulse. The right hand side is the analogous quantity for the second half of the pulse. If the average rate of work by the particle, $\langle \dot{p}_1 \cdot \dot{q}_1 \rangle$, increases, then Δt_1 may decrease in turn reducing Δt , the time to uniquely encode an uncorrelated motion spanning the phase space. The total kinetic energy expended for the first half of the pulse is equivalent to the energy expended in the second half given equivalent initial and final velocities. If the initial and final velocities in a particular direction are zero then the momentum memory for the particle is reset to zero in that direction, and prior encoded information is erased.

This theme is reinforced by $\dot{p}_1(t)$ and $\dot{p}_2(t)$ associated with forces F_1, F_1 illustrating the dynamics of a maximum velocity pulse in figure 3-16 and leads to the following principle;

Principle; At least two unique forces are both necessary and sufficient to encode information in the motion of a particle over an interval Δt . These forces occur at the average rate $f_s \geq 2 \cdot (\Delta t)^{-1}$.

This is a physical form of a sampling theorem. Whether generating such motions or observing them, $f_{s_min} = 2(\Delta t)^{-1}$ is a minimum requirement for the most extreme trajectory possible, which de-correlates particle motion in the shortest time given the limitation of finite energy per unit time. The justification has been provided for generating motions but the analogous circumstance concerning observation of motion logically follows. Acquisition of the information encoded in an existing motion through deployment of forces, requires extracting momentum in the opposite sense according to Newton's 3rd law. Encoding changes particle momentum in one direction and decoding extracts this momentum by an opposite relative action. In both cases the momentum imparted or extracted goes to the heart of information transfer and the efficiency concern to be discussed further in chapter 5.

The well-known heuristic, mathematical, and information theory origins have roots firmly established in the work of Nyquist, Hartley, Gabor, Whittaker, Shannon and others [1, 4, 6, 26]. This current theory addresses questions raised by Nyquist as early as 1924 and Gabor in 1946, concerning physical origins of a sampling theorem [4, 5, 26].

The work of Shannon leveraged the interpolation function derivations of Whittaker as an expedient mathematical solution to a sampling theorem [1]. Because of its importance, Shannon's original statement of the sampling theorem is repeated here, extracted from his 1949 paper;

Shannon's Sampling Theorem; If a function contains no frequencies higher than W cps, it is completely determined by giving its ordinates at a series of points spaced $(2W)^{-1}$ seconds apart [1].

In the same paper, Shannon states, concerning the sample rate; *"This is a fact which is common in the communications art"*. Furthermore, he credits Whittaker, Nyquist and Gabor.

In the limiting case of a maximum velocity pulse, the pulse is symmetrical. The physical sampling theorem does not require this in general as is evident from the equation for averaged kinetic energy from the first half of a pulse over interval Δt_1 vs. the second interval Δt_2 . In the general circumstance, $\langle P_1 \rangle \neq \langle P_2 \rangle$ and $\Delta t_1 \neq \Delta t_2$. Thus, the pulse shape restriction is relaxed for the more general case when $\{P_1, P_2\} < P_m$. Since the sampling forces which occur at the rate f_s are analyzed under the most extreme case, all other momentum exchanges are subordinate.

The fastest pulse, the maximum velocity pulse, possesses just enough power P_m to accomplish a comprehensive maneuver over the interval Δt , and this trajectory possesses only one derivative sign change. Slower velocity trajectories may possess multiple derivative sign changes over the characteristic configuration interval $2 R_s$ but f_s will always be greater than or equal to twice the number of derivative sign changes of the velocity and also always be greater than or equal to twice the transition rate between orthogonal dimensions.

In multiple dimensions the force is a diversely oriented vector but must always possess these specified sampling qualities when decomposed into orthogonal components and the resources spawning forces must support the capability of maximum acceleration and deceleration over the interval Δt , even though these extreme forces are seldom required.

Equations 3-39, 3-40 recall the calculations for the maximum work over the interval $\Delta t/2$ and the average kinetic energy limit of velocity pulses in general, based on the *PAER* metric and practical design constraints. Equation 3-41 is due to the physical sampling theorem.

$$\mathcal{E}_{k_{\Delta t/2}} = \mathcal{E}_{max} = P_m \frac{\Delta t}{2} \quad (3-39)$$

$$\frac{\Delta t}{2} P_m \geq \langle \mathcal{E}_k \rangle (PAER) \quad (3-40)$$

$$f_s \geq 2 \cdot (\Delta t)^{-1} \quad (3-41)$$

Equations 39,40 and 41 may be combined and rearranged, noting that the average kinetic energy must always be less than or equal to the maximum kinetic energy. In other words, P_m is a conservative upper bound and a logical design limit to enable conceivable actions,. Therefore;

$$\frac{P_m}{\langle \mathcal{E}_k \rangle_s (PAER)} \leq f_s \quad (3-42)$$

The averaged energy $\langle \mathcal{E}_k \rangle_s$ is per sample. The total available energy \mathcal{E}_{tot} must be allocated amongst say $2N$ samples or force applications. The average energy per unique force application is therefore just $\mathcal{E}_{tot}/2N = \langle \mathcal{E}_k \rangle_s$. This is the quantity that should be used in the denominator of

3-42 to calculate the proper force frequency f_s . Using 3-42 we may state another form of physical sampling theorem which contemplates extended intervals modulo $T/2N = T_s$.

The physical sampling rate for any communications process must be greater than the maximum available power to invest in the process, divided by the average encoded particle kinetic energy per unique force (sample), times the peak to average energy ratio (PAER) for the particle motions over the duration of a signal.

The prior statement is best understood by considering single particle interactions but can be applied to bulk statistics as well. We shall interpret f_s as the number of *unique* force applications per unit time and f_{s_min} is the number of statistically independent momentum exchanges per unit time. This rate shall also be referred to hereafter, as the sampling frequency. Adjacent samples in time may be correlated. If the correlation is due to the limitation P_m then the system is oversampled whenever more than 2 forces per characteristic interval Δt are deployed.

Conversely, if only two forces are deployed per characteristic interval then it must be possible to make them independent (i.e unique) given an adequate P_m . Therefore, the physical sampling theorem specifies a minimum sampling frequency f_{s_min} as well as an interval of time over which successive samples must be deployed to generate or acquire a signal. By doing so, all frequencies of a signal up to the limit B are contemplated. The lowest frequency of the signal is given by T^{-1} .

More samples are required when they are correlated because they impart or acquire smaller increments of momentum change per sample compared to the circumstance for which a

minimum of two samples must enable particle dynamics which span the entire phase space over the interval Δt .

Shannon's sampling theorem as stated is necessary but not sufficient because it does not require a duration of time over which samples must be deployed to capture both high frequency and low frequency components of a signal over the frequency span B , though his general analysis includes this concept. As Marks points out, Shannon's sampling number is a total of $2BT_s$ samples required to characterize a signal [6].

As a simple example, consider a 1 kg mass which has a peak velocity limit of 1m/s for a motion which is random and the peak to total average energy ratio for a message is limited to 4 to capture much of the statistically relevant motions (97.5 % of the particle velocities for a Gaussian statistic). Let the power source possess a 10 Joule capacity, \mathcal{E}_{tot} . If the apparatus power available to the particle has a maximum energy delivery rate limit of P_m equal to 1 joule per second and we wish to distribute the available energy source over 1 million force exchanges spaced equally in time to encode a message, then the frequency of force application is;

$$f_s = \frac{1}{\frac{10}{10^6}} = 2.5 \times 10^4 \text{ forces per second} \quad (4)$$

If f_s falls below this value, then the necessary maneuvers required to encode information in the particle motion cannot be faithfully executed, thereby eroding access to phase space, which in turn reduces uncertainty of motion and ultimately information loss. If f_s increases above this rate then information encoding rates can be achieved or increased, trading the reduction in transmission time vs. energy expenditure.

Capacity equations can be related to the physical sampling theorem and therefore related to the peak rate of energy expenditure, not just the average. The peak rate is a legitimate design metric, and the ratio of the peak to average is inversely related to efficiency as will be shown. It is even possible to calculate capacity vs. efficiency for non-maximum entropy channels by fairly convenient means, an exercise of considerable challenge according to Shannon [15]. By characterizing sample rate in terms of its physical origin, we gain access to the conceptual utility of other disciplines such as dynamics and thermodynamics and advance toward the goal of trading capacity for efficiency.

3.1.7. Sampling Bound Qualification

Shannon's form of the sampling theorem contains a reference to frequency bandwidth limitation, W . It is of important to establish a connection with the physical sampling theorem. An intuitive connection may be stated simply by comparing two equations (where W is replaced by B);

$$f_s \geq \frac{P_m}{\langle \mathcal{E}_k \rangle_s PAER}, \quad f_s \geq 2B$$

(3-43)

B , shall be justified as the variable symbolizing Nyquist's bandwidth for the remainder of this paper and possesses the same meaning as the variable W used by Shannon. It should be noted that though both the inequalities in equation 3-43 appear different, they possess the same units if one regards a force event (i.e. an exchange of force with a particle) to be defined as a sample.

The bound provided for the sampling rate in equation 3-43 and Shannon's theorem are obtained by two very different strategies. 3-46 is based on physical laws while Shannon's restatement of the sampling rate proposed by Nyquist and Gabor is of mathematical origin and logic. We now examine the conditions under which the inequalities in 3-43 provide the most restrictive interpretation of f_s . This occurs as both equations in 3-43 approach the same value.

$$\frac{P_m}{\langle \mathcal{E}_k \rangle_s (PAER)} \rightarrow 2B \quad (3-44)$$

The arrow in the equation indicates "as the quantity on the left approaches the quantity on the right". We shall investigate the circumstance for this to occur. It will be shown that when signal energy as calculated in a manner consistent with the method employed by Shannon is equated to the kinetic energy of a particle, the implied relation of 3-44 becomes an equality.

The bounding conditions for relating B to f_s , in a traditional information theory context, have been exhaustively established in the literature and will not be rehashed [2, 3, 4, 5, 6, 10, 11, 21, 26].

A direct approach can be illustrated from the Fourier transform pair of a sequence of samples from a message ensemble member. This technique depends on the definition for bandwidth. Shannon's definition requires zero energy outside of the frequency spectrum defined by bandwidth B . A parallel to Shannon's simple proof is provided for reference. In his proof he employs a calculation of the inverse Fourier transform of the band limited spectrum for a sampled function of time, $g(t)$, sampled at discrete instants $\left(t - \frac{n}{2B}\right)$.

$$g\left(\frac{n}{2B}\right) = \frac{1}{2\pi} \int_{-2\pi B}^{2\pi B} G(\omega) e^{-i\omega \frac{n}{2B}} d\omega$$

(3-45)

This results in an infinite series expansion over n, the sample number.

There is a simple way to establish 3-44 as an equality using Rayleigh's and Parseval's theorems.

In this treatment the kinetic energy of individual velocity samples for a dynamic particle are equated to the energy of signal samples so that;

$$\frac{1}{2} m \left(v \left(\frac{n}{2B} \right) \right)^2 = \left(g \left(\frac{n}{2B} \right) \right)^2$$

(3-46)

If 3-46 is true then the right hand side of 3-43 has a kinetic energy form and a signal energy form. We now proceed using Shannon's definition for signal energy.

Consider the signal $g(t)$ to be of finite power in a given Shannon bandwidth B;

$$\mathcal{E}_g = \sum_{n=-\infty}^{\infty} \left(g \left(\frac{n}{2B} \right) \right)^2 = \int_{-B}^B |G(f)|^2 df$$

(3-47)

Shannon requires the frequency span $2B$ to be a constant spectrum over $G(f)$ [2]. Since the approach here is to discover how the particle kinetic energy limitations per unit time correspond to Shannon's bandwidth, a constant is substituted for $G(f)$ in Rayleigh's expression to obtain;

$$\mathcal{E}_g = 2B \langle \mathcal{E}_{g_{Hz}} \rangle = T \langle \tilde{\mathcal{E}}_g \rangle = 2N \langle \mathcal{E}_g \rangle \text{ Joules} \quad (3-48)$$

We have multiplied both sides of 3-47, 3-48 by unit time to obtain energy. $\langle \mathcal{E}_{g_{Hz}} \rangle$ is given in terms of average Joules per Hz where $|G(f)|^2$ is the constant energy spectral density. $T = 2NT_s$ is the duration of the signal $g(t)$, $2N$ is the number of samples, T_s is the time between samples, $\langle \mathcal{E}_g \rangle_s$ is the average energy per sample and $\langle \tilde{\mathcal{E}}_g \rangle$ is the average energy per unit time. Then;

$$\frac{\mathcal{E}_g}{\langle \mathcal{E}_{g_{Hz}} \rangle} = 2B \text{ Hz} \quad (3-49)$$

An alternate form of 3-44 may now be written;

$$\frac{P_m}{\langle \mathcal{E}_k \rangle_s (PAER)} \rightarrow \frac{\mathcal{E}_g}{\langle \mathcal{E}_{g_{Hz}} \rangle} \quad (3-50)$$

$$\frac{\mathcal{E}_g}{\langle \mathcal{E}_{g_{Hz}} \rangle} = \frac{\langle \tilde{\mathcal{E}}_g \rangle T}{\langle \mathcal{E}_{g_{Hz}} \rangle} = \frac{\mathcal{E}_{g_{pk}}}{\frac{\langle \mathcal{E}_{g_{Hz}} \rangle \mathcal{E}_{g_{pk}}}{2NT_s} \frac{\langle \tilde{\mathcal{E}}_g \rangle}}{\frac{\mathcal{E}_g \mathcal{E}_{g_{pk}}}{2N \langle \tilde{\mathcal{E}}_g \rangle}} = \frac{P_{g_{max}}}{\langle \mathcal{E}_g \rangle_s PAER}; \text{ for } 2B = (T_s)^{-1} \quad (3-51)$$

$$\therefore \frac{P_m}{\langle \mathcal{E}_k \rangle (PAER)} = \frac{P_{g_{max}}}{\langle \mathcal{E}_g \rangle PAER}; \text{ for } \langle \mathcal{E}_k \rangle_s = \langle \mathcal{E}_g \rangle_s \quad (3-52)$$

Given equation 3-52 is now an equality, 3-44 may be employed as a suitable measure for bandwidth or sampling rate requirements, in a classical context. Thus, for a communications process modeled by particle motion which is peak power limited;

$$\frac{1}{T_s} \geq \frac{\max\left\{\frac{d\mathcal{E}_k}{dt}\right\}}{k_p\langle\mathcal{E}_k\rangle(PAER)} = \frac{\max\{\dot{\vec{q}} \cdot \dot{\vec{p}}\}}{k_p\langle\mathcal{E}_k\rangle(PAER)}$$

$$f_{s_min} = \frac{\max\left\{\frac{d\mathcal{E}_k}{dt}\right\}}{k_p\langle\mathcal{E}_k\rangle_s(PAER)} = 2B$$

(3-53)

This equation and its variants shall be referred to as the sampled time-energy relationship or simply the TE relation. The TE relation may be applied for uniformly sampled motions of any statistic. If trajectories are conceived to deploy force rates which exceed f_{s_min} , then B may also increase with a corresponding modification in phase space volume. In addition, the factor k_p appears in the denominator. This constant accounts for any adjustment to the maximum velocity profile which is assigned to satisfy the momentum space maximum boundary condition. For the case of the nonlinear maximum velocity pulse studied thus far, in the hyper sphere, $k_p \equiv 1$. This is one design extreme. Another design extreme occurs whenever the boundary velocity profile must also be physically analytic under all conditions. Finally, notice the appearance of the derivatives of the canonical variables, $\dot{\vec{q}}, \dot{\vec{p}}$, in the numerator, illustrating the direct connection between the particle dynamics within phase space to a sampling theorem. In particular, *these variables illustrate the required increased work rate for encoding greater amounts of*

information per unit time. The quantity $\max\{\dot{\vec{q}} \cdot \dot{\vec{p}}\}$ maximizes the rate of change of momentum per unit time over a configuration span.

An example illustrates the utility of eq. 3-53. Suppose a signal of 1 MHz bandwidth must be synthesized. Let the maximum power delivery for the apparatus be set to $\max\left\{\frac{d\mathcal{E}_k}{dt}\right\} = 1 \text{ watt}$. Furthermore, the signal of interest is known to possess a 3dB *PAER* statistic. From these specifications we calculate that the average energy rate per sample is $2.5\text{e-}7$ Joules. If the communications apparatus is battery powered with a voltage of 3.3 V @ 1000 mAh rating, then the signal can sustain for 6.6 hours between recharge cycles of the battery, assuming the communications apparatus is otherwise 100% efficient.

3.1.8. Interpolation for Physically Analytic Motion

This section provides a derivation for the interpolation of sampled particle motion. The Cardinal series is derived from a perspective dependent on the limitations of available kinetic energy per unit time and the assumption of LTI operators for reconstructing a general particle trajectory from its impulse sample representation. A portion of the LTI operator is assumed to be inherent in the integrals of motion. Additional sculpting of motion is due to the impulse response of the apparatus. Together these two effects constitute an aggregate impulse response which determines the form of the characteristic velocity pulse. The cardinal series is considered a sequence of such velocity pulses.

Up to this point the physically analytic requirement for trajectory has not been strictly enforced at the boundary as is evident when reviewing figure 3-16 where the force associated with a maximum nonlinear velocity pulse diverges to infinity.

We now pursue a remedy which insures that all energy rates and forces are finite.

Suppose that there is a reservoir of potential energy \mathcal{E}_ϕ available for constructing a signal. At some phase coordinate $\{q_0, p_0\}$ at time t_{0-} , the infinitesimal instant of time prior to t_0 , the quantity of energy allocated for encoding is;

$$\mathcal{E}_\phi(t - t_{0-}) \tag{3-54}$$

The initial velocity and acceleration are zero and the position is arbitrarily assigned at the center of the configuration space. $\sigma_{k_tot}^2$ is a variance which accounts for the energy to be distributed into all the degrees of freedom forming the signal . The total energy of the particle is;

$$\begin{aligned} \mathcal{E}_{tot} &= \mathcal{E}_\phi(t) + \mathcal{E}_{k_tot}(t) + \mathcal{E}_{dis}(t) \\ \mathcal{E}_k(t - t_{0-}) &= 0 \\ \mathcal{E}_{dis}(t - t_{0-}) &= 0 \end{aligned} \tag{3-55}$$

\mathcal{E}_{tot} remains constant and $\mathcal{E}_{dis}(t)$ accounts for system losses. We shall focus on $\mathcal{E}_{k_tot}(t)$ the evolving kinetic energy of the particle, and ignore dissipation.

Signal evolution begins through dynamic distribution of \mathcal{E}_{tot} which depletes \mathcal{E}_ϕ on a per sample basis when the motion is not conservative. Particle motion is considered to be physically analytic everywhere possessing at least two well behaved derivatives, \dot{q}, \ddot{q} . Such motions may consist of suitably defined impulsive forces smoothed by the particle-apparatus impulse response.

Allocation of the energy proceeds according to a redistribution into multiple dimensions.;

$$\langle \mathcal{E}_{k_tot} \rangle = \sigma_{k_tot}^2 = \sum_{\alpha} \bar{\sigma}_{\alpha}^2 \quad (3-56)$$

All $\alpha = 1, \dots, D$ dimensional degrees of freedom for motion possess the same variance when observed over very long time intervals and thus the over bar is retained to acknowledge a mean variance. In this case $\sigma_{k_tot}^2$ is finite for the process and must be allocated over a duration T for the signal.

The total available energy may be parsed to $2N$ samples of a message signal with normalized particle mass ($m = 1$).

$$\sigma_{k_tot}^2 = \frac{1}{2} E\{v^2\}_{\Sigma\alpha,n} = \frac{1}{2} \sum_{\alpha} \sum_{n=-N}^N v^2_{\alpha,n} \delta(t - nT_s), \quad N = \frac{T}{2T_s} \quad (3-57)$$

The time window $T/2$ is an integral multiple of the sample time T_s . $NT_s, \pm T/2$ may approach $\pm\infty$. The equation illustrates how the kinetic energy \mathcal{E}_k is reassigned to specific instants in time via the delta function representation. The average energy per sample is simply;

$$\frac{1}{2} \left\langle \frac{1}{2N} \sum_n v^2(t - nT_s) \right\rangle = \frac{1}{2} \frac{E\{v^2\}_{\Sigma\alpha,n}}{2N}$$

(3-58)

And the average power per sample is given as;

$$\langle P_{samp} \rangle = \frac{1}{2T} \sum_{\alpha} \sum_{n=-N}^N v_{\alpha,n}^2 \delta(t - nT_s)$$

(3-59)

The delta function weighting has a corresponding sifting notation;

$$v_{\alpha,n}(t - nT_s) = \int_{-\infty}^{+\infty} v_{\alpha,n}(t) \delta(t - nT_s) dt = v_{\alpha}(nT_s)$$

(3-60)

A sampled velocity signal is also represented by a series of convolutions;

$$\tilde{v}_{\alpha}(t) = v_{\alpha}(t - nT_s) * h_t = \sum_{n=-N}^N v_{\alpha}(t) \delta(t - nT_s) * h_t$$

(3-61)

Let $\tilde{v}_{\alpha}(t) = v_{\alpha}(t) \delta(t - nT_s) * h_t$ be a discretely encoded and interpolated approximation of a desired velocity for a dynamic particle. We are mainly concerned with obtaining an interpolation function for reconstitution of $v_{\alpha}(t)$ from the discrete representation. It is logical to

suppose that the interpolation trajectories will spawn from linear time invariant (LTI) operators given that the process is physically analytic. With this basic assumption, a familiar error metric can be minimized to optimize the interpolation. [23, 25];

$$\frac{1}{2} \langle v_{\epsilon}^2 \rangle = \sigma_{\epsilon}^2 = \frac{1}{4N} \left[\sum_n v_{\alpha}(t)(t) - v_{\alpha}(t)(t) \delta(t - nT_s) * h_t \right]^2$$

(3-62)

Minimizing the error variance σ_{ϵ}^2 requires solving;

$$v_{\alpha}(t) - v_{\alpha}(t) \delta(t - nT_s) * h_t = 0$$

(3-63)

h_t may be regarded as a filter impulse response where the associated integral of the time domain convolution operator is inherent in the laws of motion.

A schematic is a convenient way to capture the concept at a high level of abstraction.

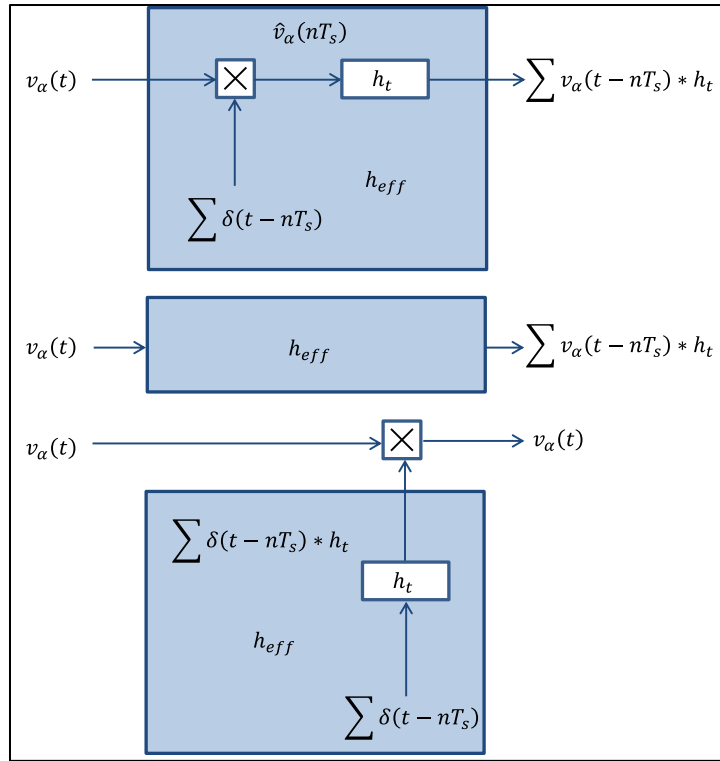


Figure 3-17 Schematic

Figure 3-17 illustrates the α^{th} dimension sampled velocity and its interpolation. Extension to D dimensions is straightforward.

It is evident that an effective LTI impulse response $h_{eff} = 1$ provides the solution which minimizes σ_ϵ^2 . h_t can be obtained from recognition that;

$$\sum_n h_t * \delta(t - nT_s) = h_{eff} = 1$$

(3-64)

$$\therefore h_t * \delta(t - nT_s) = 1, \quad @ t = nT_s$$

(3-65)

Convolution is the flip side of the correlation coin under certain circumstances involving functions which possess symmetry. $h_t * \delta(t - nT_s)$ may be viewed as a particular cross correlation operation when h_t is symmetric.

Correlation functions for the velocity and interpolated reconstructions are constrained by the TE relation. The circumstances for decoupling of velocity samples at the deferred instants $t - nT_s$ are discussed in Appendix E. The cross correlation of a reference velocity function with an ideal reconstruction at zero time shift results in;

$$\Re_{\tau, nT_s}(0) = \langle \mathcal{E}_k \rangle = \sum n \frac{T_s P_m}{k_p \text{PAPR}} \quad (3-66)$$

Therefore;

$$\frac{1}{2} \left\langle \sum_{n=-N}^N (v_\alpha(t - nT_s) * h_t)^2 \right\rangle = \frac{2NT_s P_m}{\text{PAPR} k_p} \quad (3-67)$$

where;

$$T_s = k_p \langle \mathcal{E}_k \rangle_s \frac{\text{PAER}}{P_m} \quad (3-68)$$

As appendix E also shows, the values of a correlation function are zero at offsets,

$$\tau = \bar{\tau} n k_p \langle \mathcal{E}_k \rangle_s \frac{PAER}{P_m} \quad (3-69)$$

Equations 3-66 through 3-69 are necessary but not sufficient to identify the cardinal series because the correlation function parameters as given are not unique. However, 3-66 through 3-69 along with knowledge that the signal is based on a bandwidth limited AWGN process fit the cardinal series profile.

The effective Fourier transform for a sequence of decoupled unit sampled impulse responses may be represented as follows [3, 11];

$$\mathfrak{F} \left\{ \sum_n h_t(t - nT_s) \right\} = \frac{P_m}{k_p \langle \mathcal{E}_k \rangle_s PAER} \sum_n H_t(f - nf_s) e^{-j2\pi f n \frac{k_p \langle \mathcal{E}_k \rangle_s PAER}{P_m}} = \delta(f) = H_{eff} \quad (3-70)$$

The Fourier transform above is thus a series representation for the transform of the constant, unity. The response for $H_t(f)$ is symmetric for positive and negative frequencies. There are $2N$ such spectrums $H_t(f - nf_s)$ due to the recursive phase shifts induced by a multiplicity of delayed samples. The time dependency of the frequency kernel has been supplanted by the preferred TE metric.

Consider the operation;

$$v_\alpha(t) h_{eff} = \tilde{v}_\alpha(t)$$

Then the frequency domain representation is;

$$V(f) * H_{eff} = \tilde{V}(f) \quad (3-71)$$

The series expansion for H_{eff} is now tailored to the target signal $v(t)$. The spectrum of interest is simply;

$$V(f)H_{eff}(f) = V(f) * \frac{P_m}{k_p \langle \mathcal{E}_k \rangle_s PAER} \sum_n H_t(f - nf_s) e^{-j2\pi f n \frac{k_p \langle \mathcal{E}_k \rangle_s PAER}{P_m}} = V(f) \quad (3-72)$$

In this representation $V(f)$ need not be constant over frequency contrary to Shannon's assumption.

It is evident from investigation of the magnitude response of $H_t(f - nf_s) * V(f)$ that $H_t(f)$ must not alter the magnitude response of the velocity spectrum $V(f)$ over the relevant spectral domain, else encoded information is lost and energy not conserved. It is also evident that $H_t(f)$ must possess this quality over the spectral range of $V(f)$ but not necessarily beyond.

The magnitude of the complex exponential function is always one. Also, the phase response is linear and repetitive over all harmonic spectrums according to the frequency of the complex exponential. This is most apparent when examining the spectral components of the original sampled signal.

$$\mathfrak{F}\{v(nT_s)\} = f_s \sum_n V(f - nf_s) \quad (3-73)$$

From the fundamentals of LTI systems and the associated impulse response requirements, $V(f - nf_s)$ possesses even magnitude symmetry and odd phase symmetry and this fundamental spectrum repeats every f_s Hz [3, 11]. Thus only $V_0(f)$ is required to implement any reconstruction strategy because a single correct spectral instantiation contains all encoded information (i.e. $V_0(f) = V_1(f) = V_2(f) = \dots V_n(f)$). Reconstruction of an arbitrary combination of $V_n(f)$, beyond $V_0(f)$ spectrums, requires deployment of increased energy per unit time, violating the P_m constraint of the TE relation. In other words, preservation of an unbounded number of identical spectrums also represents an unsupported and inefficient expansion of phase space (requiring ever increasing power).

From the TE relation, the unambiguous spectral content is limited by $\dot{\mathcal{E}}_k$ such that;

$$\frac{1}{2T_s} \geq \frac{P_m}{2k_p \langle \mathcal{E}_k \rangle_s (PAER)} = B \quad (3-74)$$

This leads to the logical deduction that the optimal filter impulse response requirement can be obtained from;

$$h_t = \frac{P_m}{k_p \langle \mathcal{E}_k \rangle_s (PAER)} \mathfrak{J}^{-1} \left\{ \sum_{n=0} H_t(f - nf_s) e^{-j2\pi f n \frac{k_p \langle \mathcal{E}_k \rangle_s (PAER)}{P_m}} \right\} = h_{eff} |_{n=0} \quad (3-75)$$

where the frequency domain of $H_t(f)$ must correspond to the frequency domain of $V_0(f)$ (the 0^{th} image in the infinite series) , resulting in;

$$h_t = \frac{P_m}{k_p \langle \mathcal{E}_k \rangle_s PAER} \int_{-LL}^{UL} \sum_0 e^{-j2\pi ft} e^{-j2\pi fn \frac{k_p \langle \mathcal{E}_k \rangle_s PAER}{P_m}} df \quad (3-76)$$

$$LL = -\frac{P_m}{2k_p \langle \mathcal{E}_k \rangle_s PAER}, UL = \frac{P_m}{2k_p \langle \mathcal{E}_k \rangle_s PAER} \quad (3-77)$$

LL and UL are necessary limits imposed by the allocation of available energy per unit time, i.e. the TE relation.

Therefore;

$$h_t = \frac{P_m}{k_p \langle \mathcal{E}_k \rangle_s PAER} \left[\frac{\sin[f_s \pi t]}{\pi t} \right] \quad (3-78)$$

h_t is recognized as the unity weighted cardinal series kernel at $n=0$. This is the LTI operator which must be recursively applied at the rate f_s to obtain an optimal reconstruction of the velocity function $v_\alpha(t)$ from the discrete samples $v_\alpha(nT_s)$.

That is;

$$v_\alpha(t) = \sum_n v_\alpha \delta(t - nT_s) * h_t = \sum_n v_\alpha(nT_s) \frac{T_s \sin[f_s \pi(t - nT_s)]}{\pi(t - nT_s)} \quad (3-79)$$

The cardinal series is thus obtained;

In D dimensions the velocity is given by;

$$v(t) = \sum_{\alpha}^D v_{\alpha}(t)$$

(3-80)

Figure 3-18 Illustrates the general interpolated trajectory for D=3 and several adjacent time samples, depicted by vectors coincident with impulsive forces within the phase space. The trajectory is smooth with no derivative sign changes between samples and correspond to the cumulative character of $\delta(t - nT_s) * h_t$ dispersing the forces through time and space.

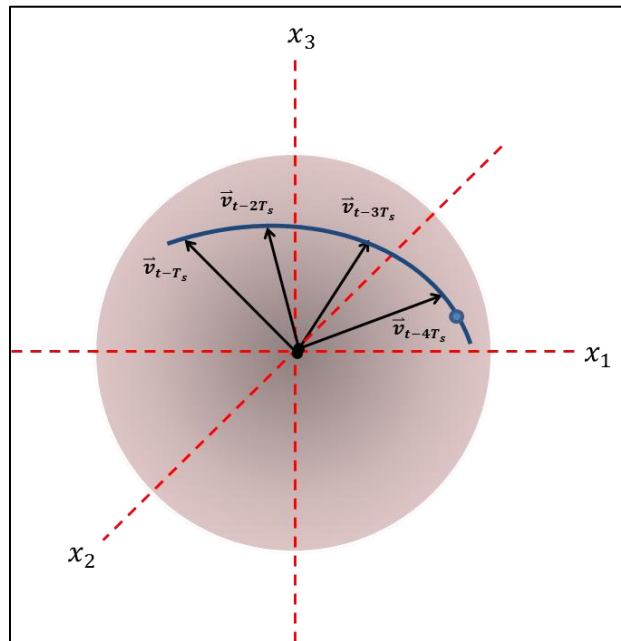


Figure 3-18 General Interpolated Trajectory

The derivation above is different from Shannon’s approach in the following significant way. *In contrast with Shannon’s approach, general excitations of the system are contemplated herein with arbitrary response spectrums automatically accommodated even when the maximum uncertainty requirement for \vec{q}, \vec{p} is waived.* Therefore, the result here is that the cardinal series is substantiated for all physically analytic motions not just those which exhibit maximum uncertainty statistics. Whittaker’s 1915 result is confirmed by this alternate approach based on physical principles without Shannon’s restrictions.

It is apparent by examining multiple derivatives that a cardinal pulse is physically analytic and therefore is a candidate pulse response up to and including phase space boundary conditions. This naturally raises a question concerning preferred maximum velocity pulse type. The next sections provide some additional detail concerning the tradeoff for the boundary condition pulse type.

3.1.8.1. Cardinal Autocorrelation

The autocorrelation of a stationary $v_\alpha(t)$ process can be obtained from the Wiener–Kinchine theorem as the averaged time correlation for velocity;

$$\mathfrak{S}\{\tilde{\mathfrak{R}}_{v_\alpha, v_\alpha}\} = \mathfrak{S}\left\{\lim_{NT_s \rightarrow \infty} \frac{1}{2NT_s} \int_{-NT_s}^{NT_s} v_\alpha(t)v_\alpha(t + \tau) d\tau\right\} = [V(f)]^2 \quad (3-81)$$

Suppose that it is known that v_α has a maximum uncertainty ($\mathfrak{R}_v = 0$) associated with the time domain response at regular intervals, NT_s . The frequency domain representation of the process

must also be of maximum entropy form. The greatest possible uncertainty in its spectral expression, will be due to uniform distribution. This can be verified through the calculus of variations [21]. The result provides further justification for the discussions of 3.1.8 and the required form of autocorrelation in general.

Taking the inverse transform for $[V(f)]^2$ reveals the autocorrelation for the finite power process which has maximum uncertainty in the frequency domain;

$$\tilde{\mathfrak{R}}(\tau)_{v_\alpha, v_\alpha} = \frac{P_m V^2}{k_p \langle \mathcal{E}_k \rangle_s PAER} \frac{\sin \left[\pi \frac{P_m}{k_p \langle \mathcal{E}_k \rangle_s PAER} \tau \right]}{\pi \frac{P_m}{k_p \langle \mathcal{E}_k \rangle_s PAER} \tau} \quad (3-82)$$

$$\tilde{\mathfrak{R}}(0)_{v_\alpha, v_\alpha} = \langle v^2 \rangle = \int_{LL}^{UL} V^2 df = \frac{P_m V^2}{k_p \langle \mathcal{E}_k \rangle_s PAER} \quad (3-83)$$

$$LL = -\frac{P_m}{2k_p \langle \mathcal{E}_k \rangle_s PAER}, UL = \frac{P_m}{2k_p \langle \mathcal{E}_k \rangle_s PAER} \quad (3-84)$$

V^2 is in watts per Hz. Likewise, v^2 is in watts. $\tilde{\mathfrak{R}}(\tau)_{v_\alpha, v_\alpha}$ is the classical result for a bandwidth limited Gaussian process with a TE relation substitution [12, 21].

Integration of any member of the cardinal series squared over the time interval $\pm\infty$ will result in $v_\alpha^2(NT_s)$, a finite energy per sample.

Unique information is obtained by independent observation of random velocity samples at intervals separated by these correlation nulls located at modulo $\pm NT_s$ time offsets. The cardinal series distributes sampled momentum interference for the duration of an entire trajectory throughout phase space. Hence, each member of the cardinal series will constructively or destructively interfere with all other members except at intervals deduced from the correlation nulls. Eventually, at $\pm\infty$ time offset from a reference sample time, all memory of sampled motion dissipates leaving no mutual information between such extremely separated observation points. This is due to the decaying momentum for each member of the cardinal series. Each member function of the cardinal series is instantiated through the allocation of some finite sample energy.

Figure 3-21 illustrates the autocorrelation for a Gaussian distributed velocity. Members of the cardinal series also possess this characteristic *sinc* response so that the unit cardinal series may be regarded as an infinite sum of shifted correlation functions $\sum_N h_t * \delta(t - NT_s)$.

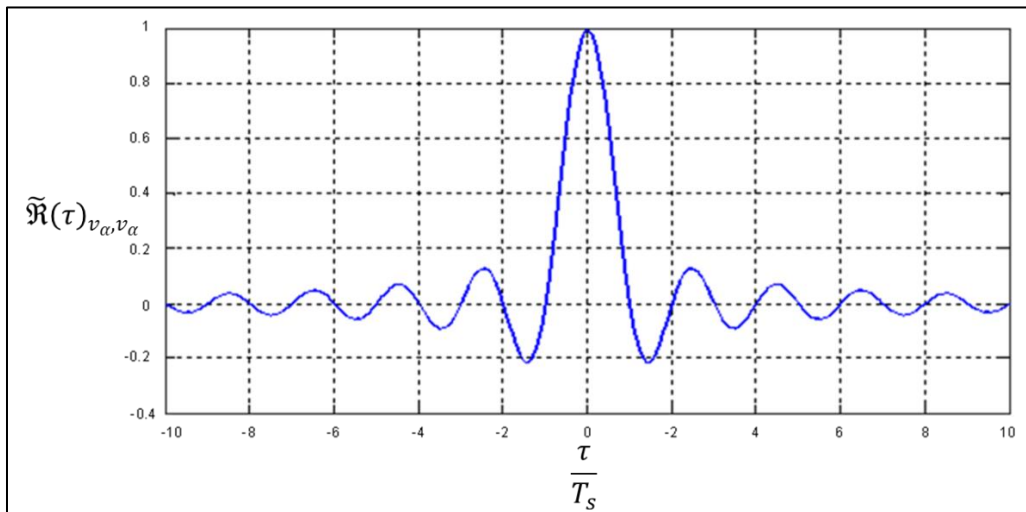


Figure 3-19 Autocorrelation for Power limited Gaussian Momentum (m=1)

3.1.8.2. Max. Nonlinear Velocity Pulse vs. Max Cardinal Pulse

It is now apparent that two pulses can be considered for boundary conditions. The maximum velocity pulse is not physically analytic but does define an extreme for the calculation of energy requirements per unit time to traverse the phase space. A cardinal pulse may also be used for the extreme if the boundary must be physically analytic as well, though P_m has a different limiting value for the cardinal pulse option. This section discusses the tradeoff between the two pulse types in terms of trajectory, P_m , B, etc.

Comparison of both velocity types is provided in the following figure where the peak value is conserved. In this case, $k_p = 1.28$ for the TE relation as can be verified through the equations of appendices F,G.

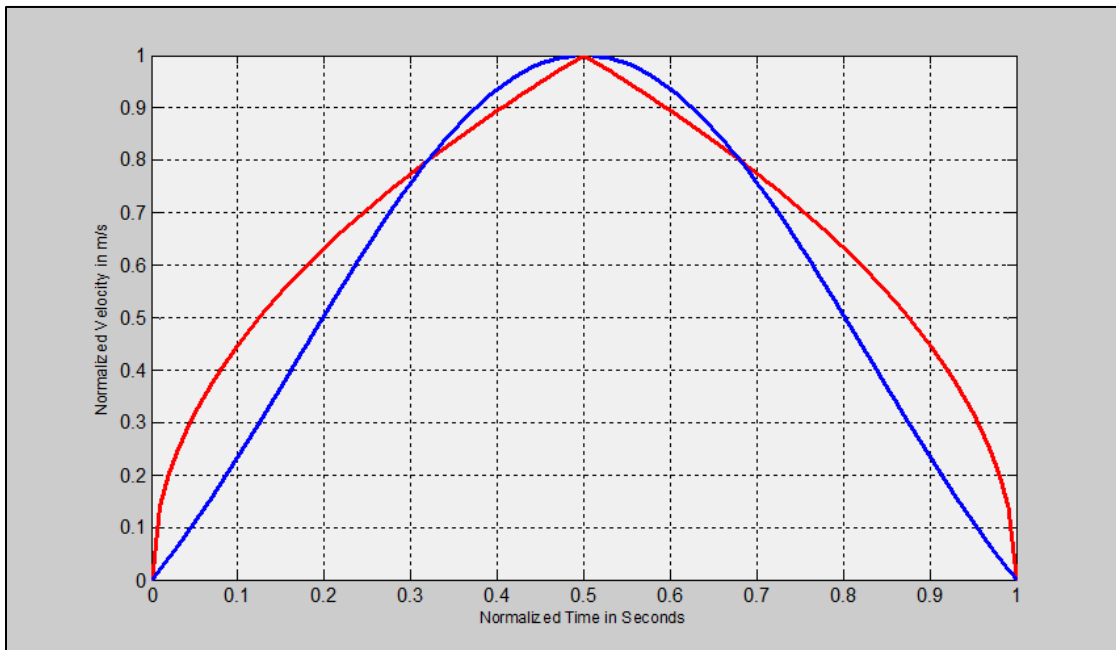


Figure 3-20 Maximum Velocity Pulse Compared to Main Lobe Cardinal Velocity Pulse

The following graphic illustrates the comparison of kinetic energy vs. time and the derivatives for both pulse types with identical amplitudes. It provides an alternate reference for comparing the two pulse types.

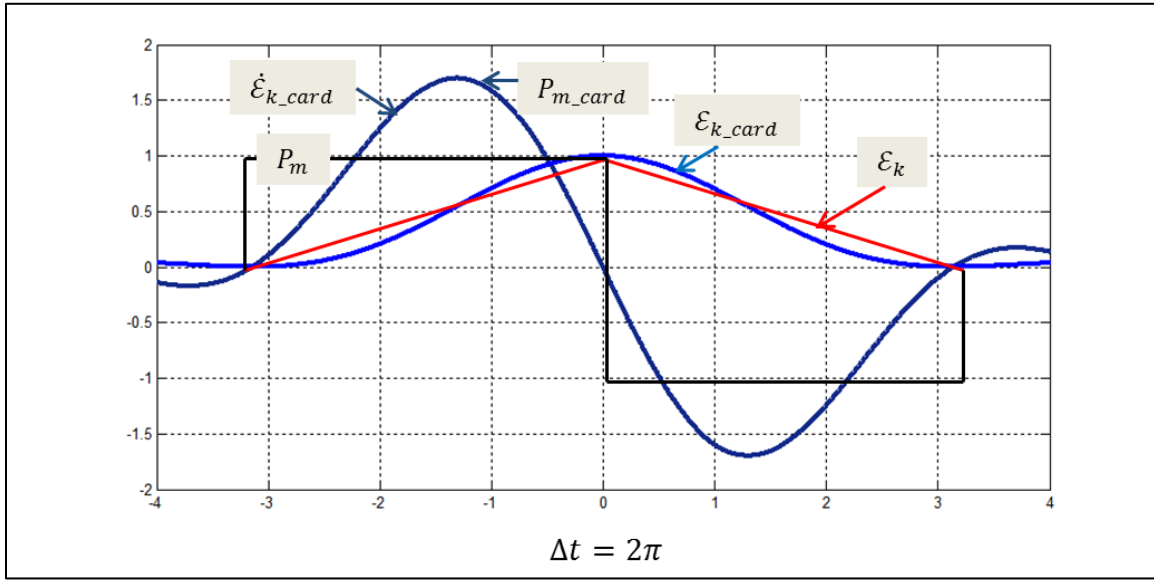


Figure 3-21 Kinetic Energy vs. Time for Velocity and Cardinal Pulses

This analysis suggests that linear operating ranges may easily be established within the domain of the nonlinear maximum velocity pulse or classical cardinal pulse provided appropriate design margins are regarded.

The maximum velocity pulse in the above figure could be exceeded by the generalized cardinal pulse near the time $t = .5 \pm \sim .07$. A design “back off” can be implemented to eliminate this boundary conflict. The following figure illustrates this concept with a modest .4 dB back off for the power associated with the peak pulse amplitude.

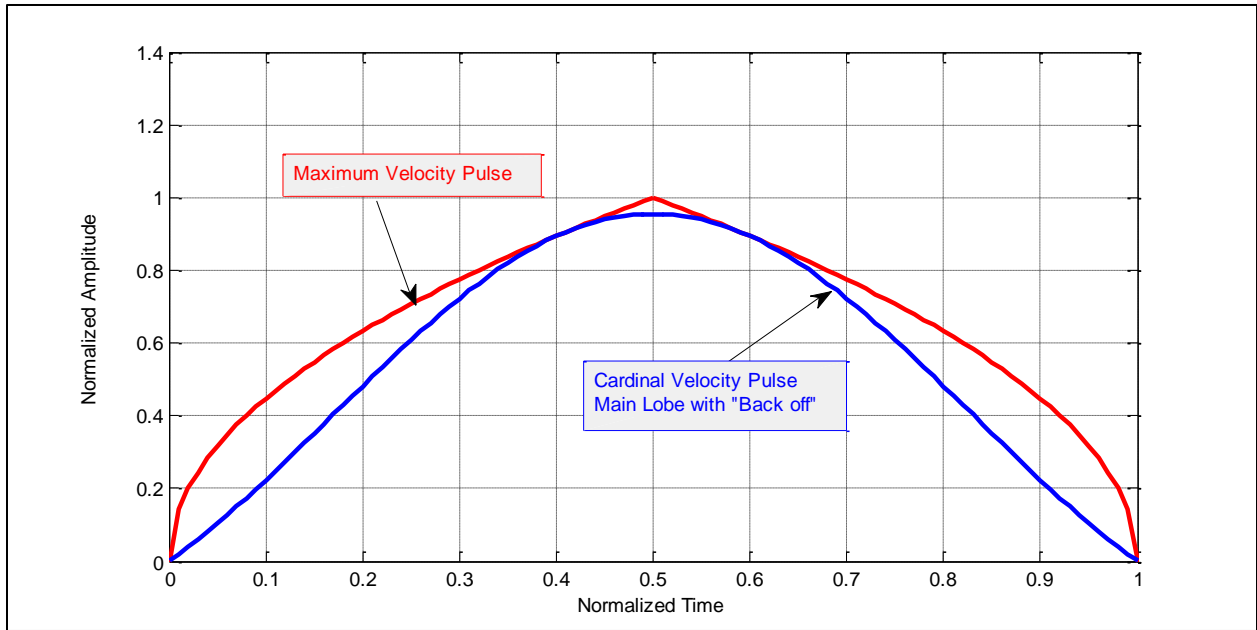


Figure 3-22 Max Velocity Pulse and Main Lobe Cardinal Velocity Pulse with .4 dB “Backoff”

However, this design criteria is not as important to the current theme as the criteria for determining peak power, peak energy, and bandwidth impacts required to maintain a physically analytic profile for the desired boundary condition.

Consider the requirement to sustain identical span of the phase space for both maximum pulse types, given fixed $\Delta t=2T_s$. Solving the position integrals for both pulse types and equating the span covered per characteristic interval results in the following equation (refer to appendix F for additional detail);

$$\int_0^{T_s} v_p dt = \int_0^{T_s} v_{m_card} \frac{\sin\left(t \frac{\pi}{T_s}\right)}{t \frac{\pi}{T_s}} dt$$

$$v_{m_card} = \frac{2\pi}{3} \sqrt{\frac{2P_m T_s}{m}} \left(\frac{1}{\pi} \sum_{n=1}^{\infty} \frac{(2n+1)(2n+1)!}{(-1)^n (T_s)^{2n+1}} \right) \approx 1.6\sqrt{P_m} , \quad \text{for } T_s = 1, m = 1$$

(3-85)

v_{m_card} is the required cardinal pulse amplitude to maintain a specific configuration space span.

The relative velocity increase and peak kinetic energy increase, compared to the nonlinear maximum velocity pulse case, are;

$$\frac{v_{m_card}}{v_m} \cong 1.13$$

$$\frac{\mathcal{E}_{m_card}}{\mathcal{E}_m} \cong 1.28$$

This represents a modest increase in peak kinetic energy of roughly 1.07 dB. The relative increase for the maximum instantaneous power requirement is noticeably larger.

$$\frac{P_{m_card}}{P_m} \cong 2.158$$

Hence, there is a relative requirement to enhance the peak power source specification by 3.34 dB to maintain a physically analytic boundary condition utilizing the maximum cardinal velocity pulse profile. Another way to consider the result is that one may design an apparatus choosing P_m using the nonlinear maximum velocity pulse equations and then expect perfectly linear trajectories up to $\sim .68 v_m$ where v_m is the maximum velocity of the nonlinear maximum velocity pulse. Beyond that point velocity excursions of the cardinal pulse begin to encounter

nonlinearities due to the apparatus power limitations. Alternatively, one may use the appropriate scaling value for k_p in the TE relation to guarantee linearity over the entire dynamic range.

The following figure illustrates velocity vs. position for the circumstance where the two velocities are compared and required to span the same configuration space in the time Δt .

Positive and negative trajectories are illustrated for both types. The precursor and post cursor tails for the maximum cardinal velocity pulse illustrate trajectories outside of the time window $-T_s \leq t \leq T_s$. Though the time span for a maximum cardinal pulse is without bound the position converges to $\pm 0.8459R_s$ within the phase space. The first cardinal pulse nulls occur at the phase space boundaries ($\pm R_s$) and the derivatives of these reflection points are smooth unlike the maximum nonlinear velocity pulse derivatives.

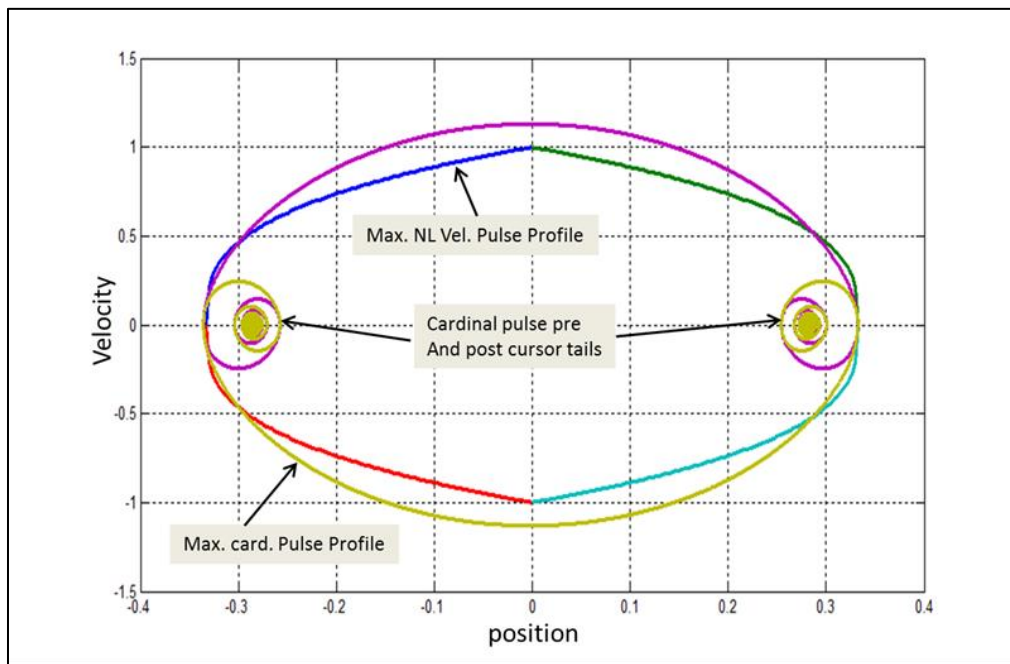


Figure 3-23 Comparison of Max. Nonlinear Velocity Pulse and Max. Cardinal Velocity Pulse

Now consider an alternate case where the value for $P_m = 1$ and is fixed for both pulse types. In this case there are two separate time intervals permitted to span the same physical space. Let the time interval $T_{ref} = 1$ apply to the sampling interval for the nonlinear maximum velocity pulse and T_s apply to the sampling interval for the cardinal maximum velocity pulse. T_s may be calculated from (refer to appendix F for additional detail);

$$T_s \equiv 1.179 T_{ref}$$

(3-86)

The bandwidth is then approximately .848 of the nonlinear maximum velocity case with $T_{ref} = 1$. Another way to consider the result is that for a given P_m in both cases, a physically analytic bandwidth $.848 (T_{ref})^{-1}$ is always guaranteed. As a dynamic particle challenges the boundary through greater peak power excursions, violations of the boundary occur and some information will begin to be lost in concert with undesirable spectral regrowth. In the scenario, where $P_m = P_{max_card}$, instantaneous peak power and configuration span are conserved for both pulse types and $k_p = 1.179$ for the TE relation.

The derivative illustrated in the next figure depicts a time variant force associated with a *sinc* momentum impulse response.

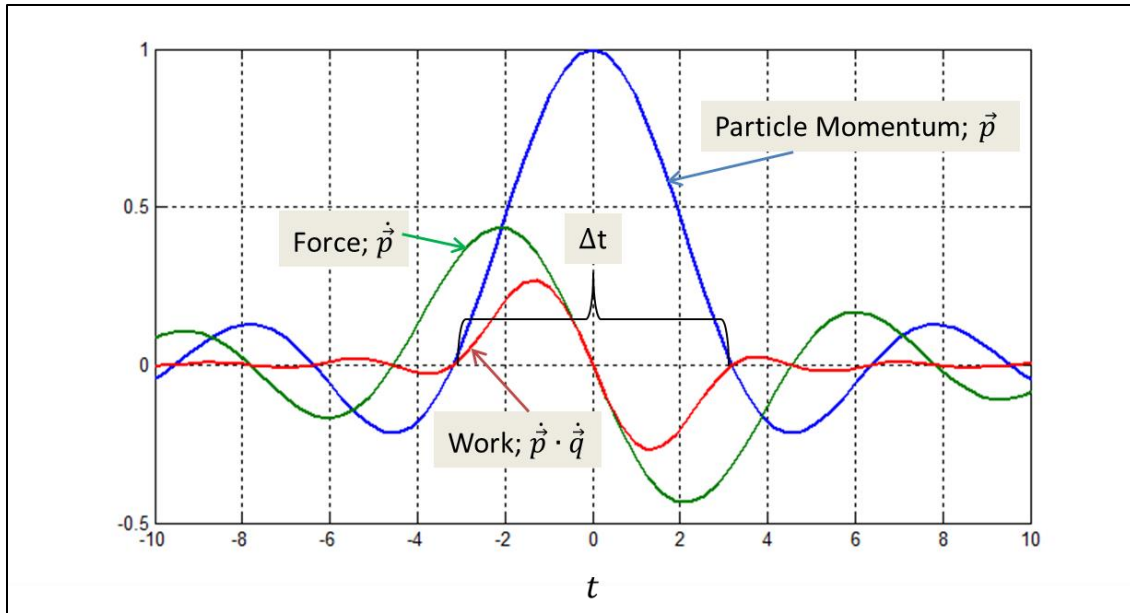


Figure 3-24 Max. Cardinal Vel. Pulse, Associated Force Function and Work Function

Although \dot{p} appears as one continuous function it clearly identifies companion acceleration and deceleration cycles which restrict particle motion to the characteristic phase space radius. The continuous momentum function can be obtained from impulse forces redistributed via h_t . Also, that there are two derivative sign changes in the force over the interval $\pm\Delta t/2 = \pm\pi$. Moreover, the forces are finite. This verifies consistency with the physical sampling theorem and a desire to maintain physically analytic motion. In addition, the instantaneous work function is illustrated for the particle. It is reassuring that the work function is also finite everywhere. The momentum response resembles the impulse response of an infinite Q filter without dissipative loss.

The tails of the *sinc* and its derivative extend in both directions of time to infinity. Fortunately, there are useful classes of impulse responses which avoid this difficulty. For instance, we may opt for a finite length impulse response modification of the *sinc* pulse which performs with

suitable error metrics or resort to other related approximations adapted from a family of impulse responses developed by Harry Nyquist [3, 27]. We will not pursue those discussions as Nyquist pulses are well documented in the literature as are tradeoffs for implementing finite time approximations. Rather, we focus on the *sinc* pulse for the remainder of analysis whenever the physically analytic conditions are desired, confident that suitable finite time duration approximations exist. Therefore, all extended physically analytic trajectories may be considered as a superposition of suitably weighted *sinc* like pulses.

Neither the nonlinear maximum velocity pulse nor the maximum cardinal pulse are absolutely required at the phase space boundary. They represent two logical extremes with constraints such as energy expenditure per unit time for the most expedient trajectory to span a space or this property in concert with physically analytic motion. There can be many logical constructions between these extremes which append other practical design considerations.

3.1.9. Statistical Description of the Process

In this section we establish a framework for describing the characteristics of the model in terms of a stochastic processes. The necessity of this more detailed discussion is to leverage certain conditional stationary properties of the model.

There are physical attributes attached to the random variables of interest with a corresponding timeline due to laws of motion. Each configuration coordinate has assigned to it a corresponding probability density for momentum of a particle, $\rho(\vec{p}|q)$ which is D dimensional Gaussian.

The following discussions assume that the continuous process may be approximated by a sampled process. This assumption is liberally exploited. Middleton provides a thorough justification for this approach [12].

Even though the random variables associated with the process are Gaussian, the variance of momentum is dependent on the coordinate in space which in turn is a function of time. This is true whenever the samples of analysis are organized with an ordered time sequence, which is a desirable feature. On the other hand, statistical characterization may not require such organization. However, any statistical formulation which does not preserve time sequences resists spectral analysis. This is no small impediment.

It is possible to obtain the inverse Fourier transform for the general velocity pulse spectrum justified by the Wiener – Kinchine (W-K) theorem if the underlying process is stationary in the strict or wide sense [3, 11, 21, 24, 25]. Such an analysis can prove valuable since working in both the time and frequency domain affords the greatest flexibility for understanding and specifying communications processes. However, sometimes the underlying process may evade fundamental assumptions which facilitate a routine Fourier analysis of the autocorrelation. Such is the case here.

We now pursue description of the stochastic process with an ensemble of functions possessing random values at regular time intervals separated by T_s .

Several definitions for a random process provides some theoretical and practical insights going forward;

A random process is an uncountable infinite, time ordered continuum of statistically independent random variables [28];

The author's tweak will be adopted for this definition to accommodate physically analytic processes which can adapt to classical or quantum scenarios;

A random physical process is a time ordered set of statistically independent random variables which are maximally dense over their spatial domains.

Middleton's definition provides practical insight [12].

“ ...an ensemble of events in time for which there exists a probability measure, descriptive of the statistical properties, or regularities, that can be exhibited in the real world in a long series of trials under similar conditions”

Thomas provides a flexible interpretation [21].

“A random process (or stochastic process) is an ensemble, or set, of functions of some parameter (usually taken to be time) together with a probability measure by which we can determine that any member, or group of members, has certain statistical properties.”

Thomas's statement is perhaps the most versatile, acknowledging the prominence of a time parameter but not requiring it.

In the following discussions a classical time sampled or momentum ensemble view is discussed as well as a reorganization of the time samples into configuration bins (configuration ensemble).

The configuration bins are defined to collect samples which are maximum uncertainty Gaussian

distributed for momentum, at respective positions q_ℓ . Evolving time samples are required to populate these configuration bins at random time intervals, modulo T_s .

A general statistical treatment of the motions for particles within the phase space can be given when the ensemble members which are functions of time are sampled from the process. This is the usual procedure referred to here as a momentum ensemble. Consider the set of k sample functions extracted from the random process $\mathcal{K}(q, p)$ organized as the following momentum ensemble:

$$\mathcal{K}(q, p) = \{[q(t), p(t)]_1, [q(t), p(t)]_2, [q(t), p(t)]_3, \dots \dots \dots [q(t), p(t)]_k\} \quad (3-87)$$

If each sample function is evaluated (discretely sampled) at a certain time, t_ℓ , then the collection of instantaneous values from the k sample functions, also become random variables. This view implies that a large number of hypothetical experiments or observations could be performed independently and in parallel, given multiple indistinguishable instantiations of the phase space.

Figure 3-25 illustrates the parallel observations characterizing a momentum ensemble with k experiments, where each experiment may be mapped from the I_k information sources through some linear operator J and sampled in time to obtain a record of each sample function. If the time samples occurring at $t_\ell = t - \ell T_s$ are independent for sequential incremental integer values of ℓ then position and momenta appear as samples from a Gaussian RV. If the process is viewed with time ordering then the collection of sampled random variables is non-stationary because the momenta second moments change vs. each unique position to accommodate boundary

conditions. Even though variance of a trajectory's samples changes for each position, the total variance of a collective is bound by the cumulative sum of the independent sample variances, which is a stationary quantity.

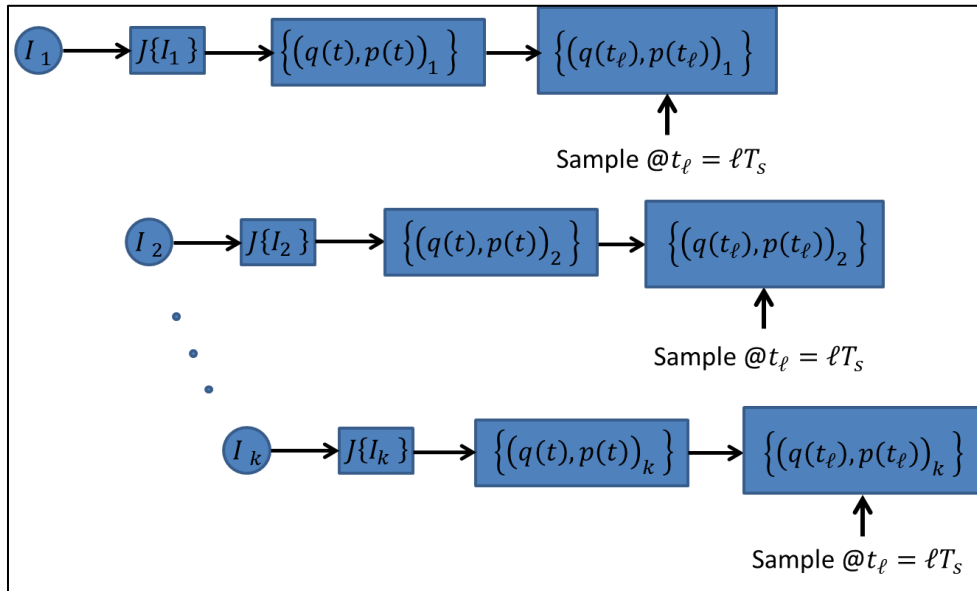


Figure 3-25 Parallel Observations for Momentum Ensemble

The following graphics illustrate three continuous sample functions from the momentum ensemble where the underlying process is of the type discussed here. Two of the members have been provided with an artificially induced offset in the average for utility of inspection (all three sample functions are actually zero mean).

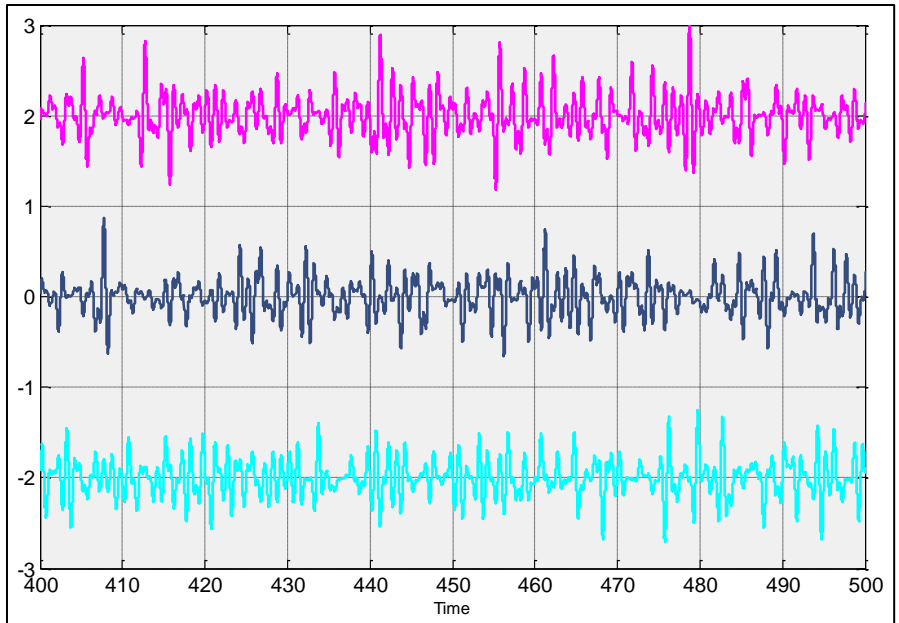


Figure 3-26 Three Sample Functions from a Momentum Ensemble

A closer inspection illustrates the velocity with a bandwidth limit B of approximately 1Hz.

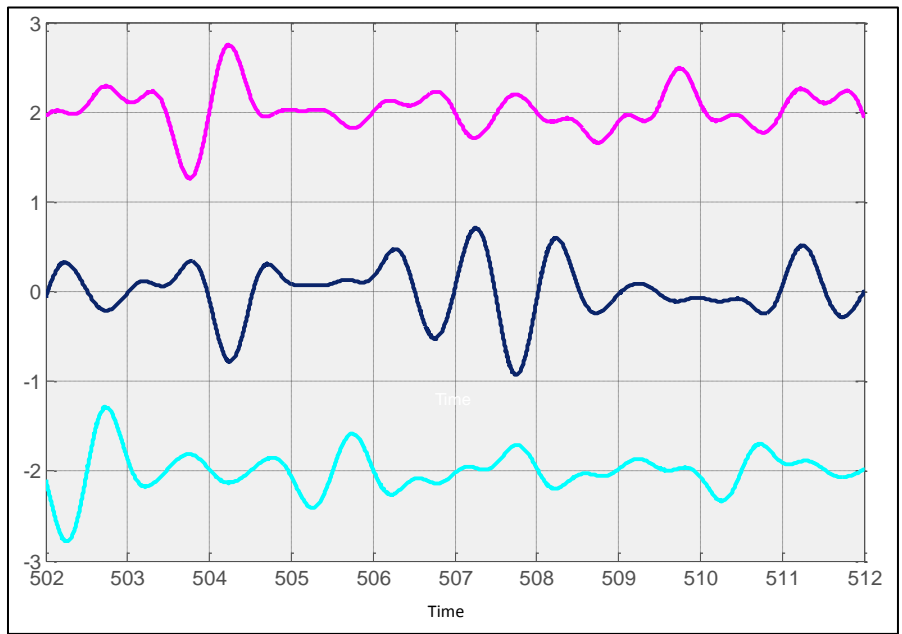


Figure 3-27 Three sample Functions from a Momentum Ensemble

The following plot illustrates how continuous velocity is related to continuous position through an integral of motion for one of the sample functions.

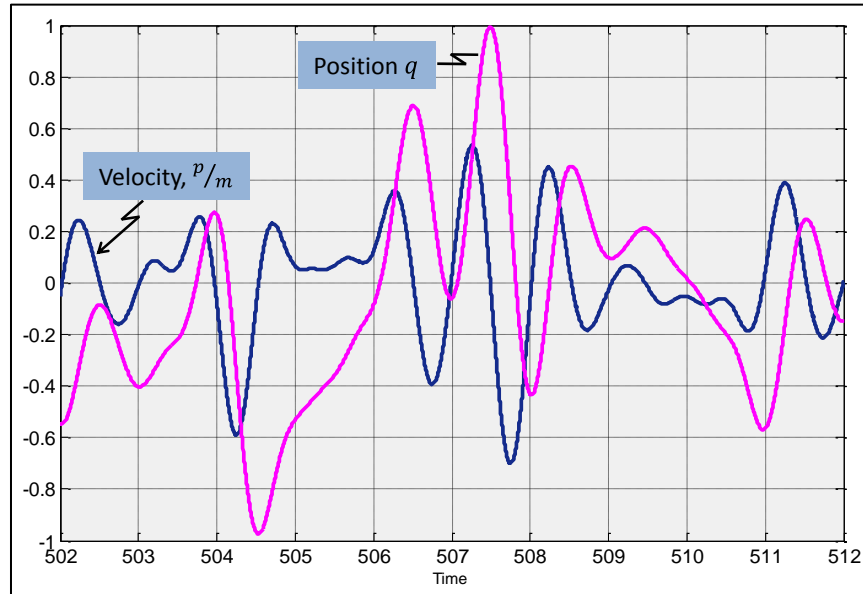


Figure 3-28 Velocity and Position for a Sample Function ($R_s \approx 1$)

These graphics clearly illustrate a limited frequency response. This response however is not the result of a traditional filter but rather the result of the limit for the maximum rate of change of energy (P_m) available to the apparatus. Between samples, physical interpolation such as suggested in section 3.8.1 produces a smoothing effect which incorporates momentum memory between the independent samples. In the case of a maximum velocity pulse the memory is finite while the maximum cardinal pulse distributes momentum over an infinite range of time albeit with a value of zero at multiples of the sampling interval.

At this juncture, the existence of an ergodic process has not been substantiated. Such a characterization provides considerable utility yet demands a process description which is

stationary in the strict sense. The conditional stationary properties assumed by earlier discussions are now in question here. In order to clarify the concern, the ergodic theorem paraphrased by Middleton and attributed to Doob is provided as a reference [12, 29].

For an ergodic ensemble, the average of a function of the random variables over the ensemble is equal with probability unity to the average over all possible time translations of a particular member function of the ensemble, except for a subset of representations of measure zero.

It is clear from this definition that the process cannot be assumed ergodic from inspection.

The apparatus of each unique phase space (ref fig. 3-25) is causally subordinate to its own information source and no other. Each information source maps information i.e. phase space coordinates $\{p, q\}$ to physical function of the apparatus with consideration of boundary conditions.

There is a curiosity in that each of the unique *iid* Gaussian sources possess space-time dependent variances. Each Gaussian RV may not be considered stationary in the usual sense at a specific configuration coordinate q because a particle in motion does not remain at one location. The momentum or velocity samples, at a specific time t_ℓ , come from differing configuration locations $q_{1,2,\dots,k;\ell}$ in the separate experiments. The conditional momentum statistic, $\rho(p|q)$, is determined by the frequency of observed sample values over many subsequent random and independent particle trajectory visits to a specific configuration coordinate. It may not be obvious that statistics of the ensemble collective predict the time averaged moments of ensemble members when considered in this manner or vice-versa. A reorganization of the data will however confirm that this is the case with certain caveats.

The relevance of organizing the RVs in a particular manner can be illustrated by revisiting the peak momentum profile and considering 3 unique configuration coordinates q_1, q_2, q_3 located on the trajectory of a particle moving along the α^{th} axis in a hyper space. This concept is illustrated for both the maximum nonlinear and the maximum cardinal pulse velocity pulses in figure 3-29.

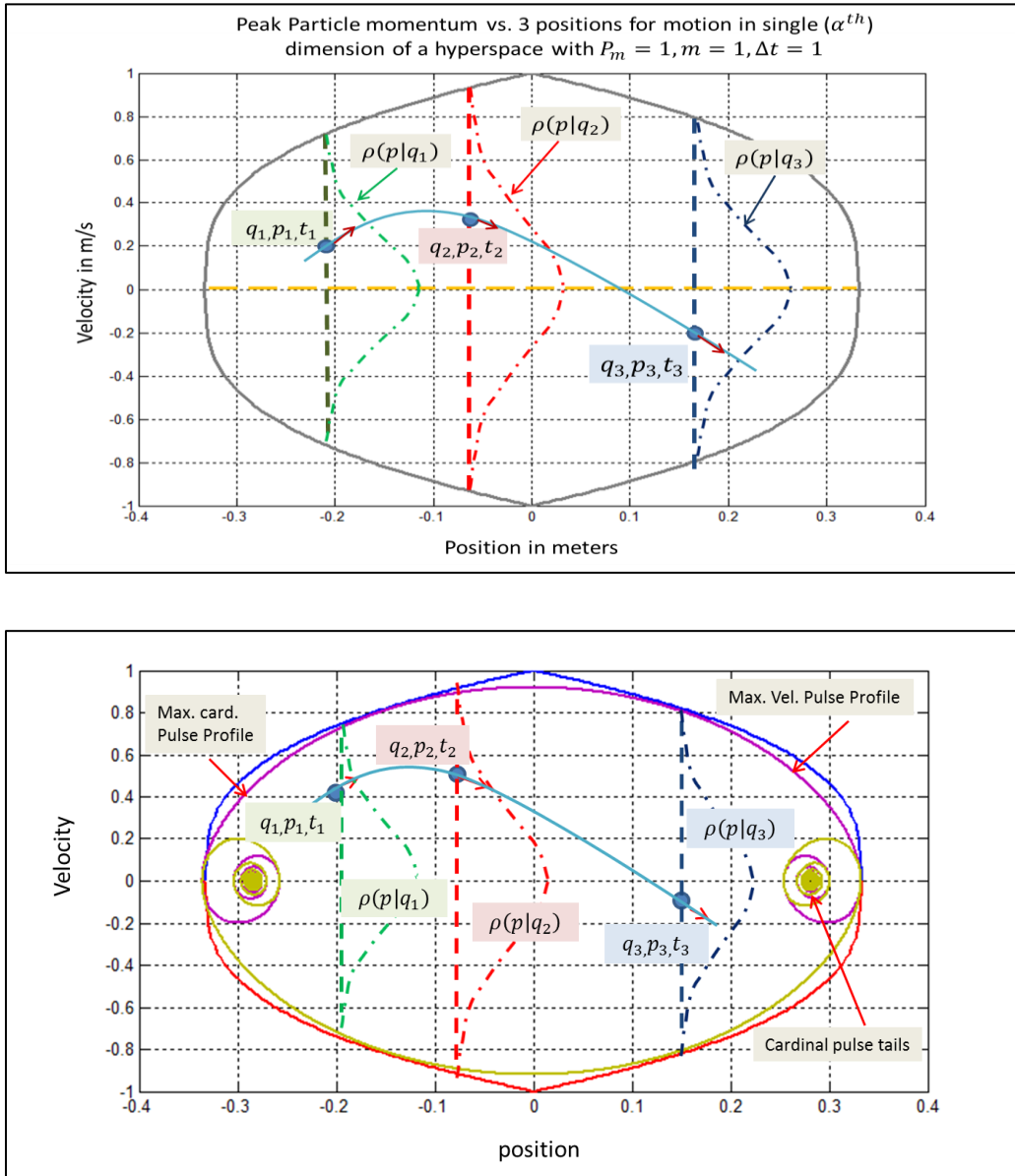


Figure 3-29 Three Particle Samples in Phase Space along the α axis

The extended tail response for the cardinal pulse is also illustrated and reverberates on the α^{th} axis ad infinitum. In contrast, the maximum velocity pulse profile is extinguished at the phase space boundary at relative times $\pm T_s$ corresponding to $\pm R_s$.

Each position q_1, q_2, q_3 has an associated peak momentum on the Gaussian pdf tail illustrated by the associated pdf profiles of figures 3-29 and 3-30. The Gaussian RV at each location has its own variance although the *PAER* is constant and equivalent at each position. Legitimate momentum values of interest lie inside the peak velocity boundaries along the dashed lines and are statistically captured by the following conditional probability densities for the 3 illustrated example configuration points.

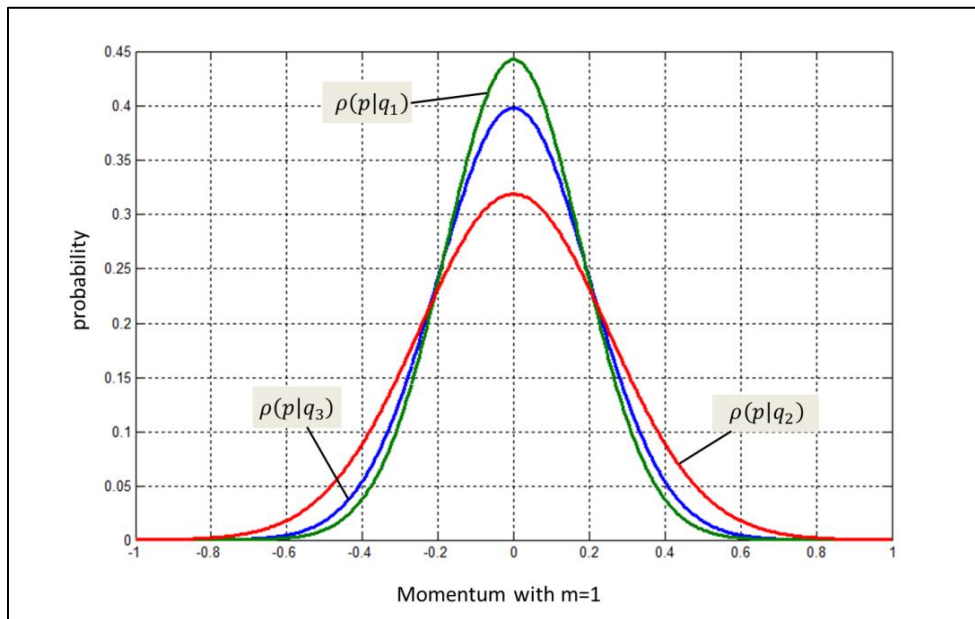


Figure 3-30 Three Gaussian pdf's for Three Sample Rv's

Thus, samples at different times which intersect these position coordinates must be collected and organized to characterize the random variables. The collection of samples at a specific

configuration coordinate would almost never encounter a circumstance where the specific configuration coordinate occupies back to back time samples because this would imply a nearly stationary particle. Rather, the instants at which the coordinates q_ℓ are repeated are separated by random quantities of time samples. Nevertheless, the new collections of samples at each coordinate bin may still be ordered chronologically. These new ensembles possess discontinuous time records though the time records are sequential and each sample is still independent. Such a collection is suitable for obtaining the frequency of occurrence for specific momenta given a particular configuration coordinate, i.e. a statistical counting with dependency. Each pdf at each coordinate possesses a stationary behavior. In contrast, a continuous time record consists of values each from the collection of such differing Gaussian variables at T_s intervals. Each new RV in the time sampled momentum ensemble view is acquired through a time evolution governed by laws of motion. However, time sampled trajectories from the momentum ensemble do not represent a stationary set of samples because each sample comes from a pdf with a different second moment.

A new configuration bin arrangement for the random process can be written with the following representation; (the k -th ensemble member is followed by the set of all k members)

$$\tilde{\mathcal{K}}(q, p)_k = \{(q_1, [p(t_{\ell_1})]); (q_2, [p(t_{\ell_2})]) \dots (q_i, [p(t_{\ell_i})])\}_k$$

$$\tilde{\mathcal{K}}(q, p) = \{\tilde{\mathcal{K}}(q, p)_1, \tilde{\mathcal{K}}(q, p)_2, \dots, \tilde{\mathcal{K}}(q, p)_k\}$$

(3-88)

Each of the k members of a time continuous momentum ensemble is partitioned into sub-ensembles with i configuration centric members. Each sub ensemble is time ordered but also time dis-continuous. The momenta are statistically characterized by pdf's like the examples of figure 3-30.

$(q_i, p(t_{\ell_i}))$ is a sample from the new process at the i^{th} position along the α^{th} dimensional axis where each position is accompanied by a time ordered set of momenta $p(t_{\ell_i})$, with a random but sequential time index t_{ℓ_i} . That is, t_{ℓ_i} is the sample time record for the i^{th} configuration. t_{ℓ_i} is set of numbers extracted from the superset $(t - \ell T_s)$ only when those sample times correspond to an observed configuration bin location q_i for the corresponding particle momentum. The bin can be defined to have a span $q_i \pm \epsilon$, where ϵ is some suitably small increment of distance. In this configuration ensemble view, each configuration coordinate is associated with its own set of "time stamped" momenta, albeit separated by random intervals of ℓT_s . Furthermore, the time index sets for t_{ℓ_A} and t_{ℓ_B} , where $i = A \neq B$, do not permit coincident time samples allocated to two different configuration locations. None of the integer values from the time index ℓ_A can be shared by ℓ_B . This is essentially a statement of an exclusion principle for the case of a single particle. The particle cannot occupy two different locations in space at the same time. This is a classical approximation of a quantum view where the dominant probability for particle location is assigned a single unique particle coordinate, $q_i \pm \epsilon$. In a multiple particle scenario, each particle requires a unique set of indices and also must be subject to Pauli's exclusion principle as well [30].

The following sample plots illustrate how the Gaussian momentum samples are sparsely populated in time for 3 unique coordinates q_1, q_2, q_3 from a configuration sub-ensemble. Even though a particular record is sparse, the full ensemble is comprehensive of all coordinates in time and space (i.e all i, k and ℓ values) and therefore dense in the aggregate.

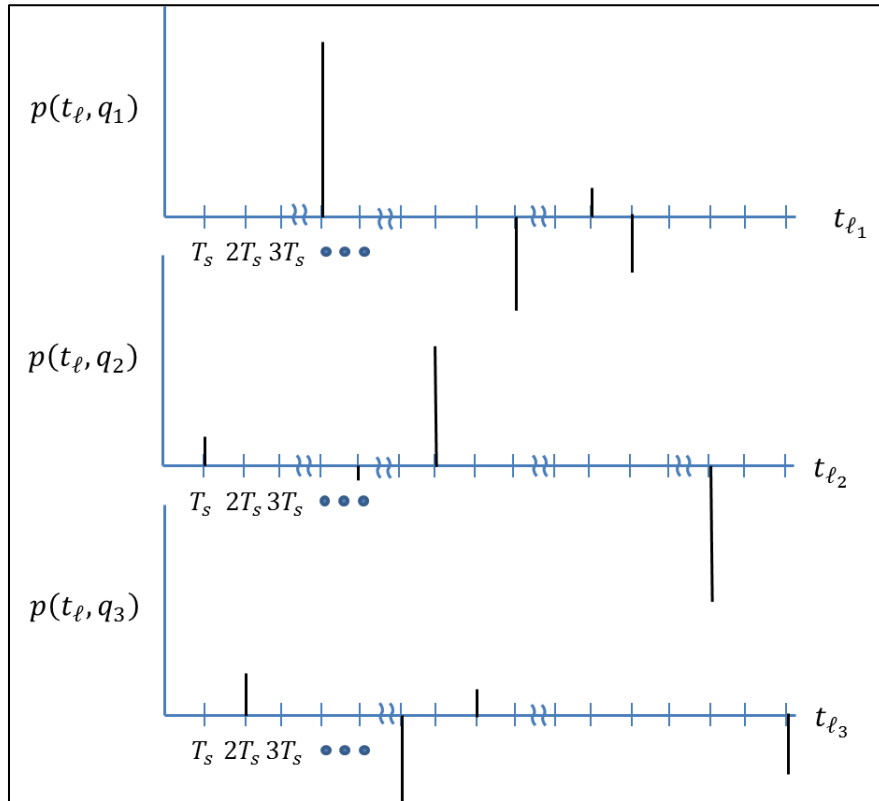


Figure 3-31 Three Configuration Ensemble Sample Functions

There are (i) such sets. While suitable for statistical characterization, it is obvious that such an arrangement is not suitable for time domain analysis of a random process because time continuity is disrupted in this view. Thus, spectral analysis via the W-K theorem is out of the question for these records. The organization illustrated in fig. 3-31 shall be described as a configuration ensemble.

The configuration ensemble representation, $\tilde{\mathcal{K}}(q, p)$ is a very different sample and ensemble organization than the momentum ensemble prescription for the random process given by $\mathcal{K}(q, p)$. In the momentum ensemble arrangement each sample function traces the unique trajectory of a particle sequentially through time and therefore provides an intuitive basis for understanding how one might extract encoded information. It is a continuum of coordinates tracing the particle history in space time. Traditional autocorrelations and spectrums may be calculated in the usual manner via the W-K theorem for the classical momentum ensemble view only if the process is stationary in that view.

A reorganization of time samples into a configuration ensemble for purpose of statistical analysis does not alter the character of the configuration centric RVs. Their moments are constant for each q_i . The justification for this stationary behavior in the configuration ensemble view is due to the boundary conditions, specifically;

$$\frac{dP_m}{dt} = 0$$

$$\frac{d(PAER)}{dt} = 0$$

$$\frac{dR_s}{dt} = 0$$

$$v(\pm R_s) = 0$$

An overall expected momentum variance can be calculated based on the variances at each configuration coordinate. Probabilities for conditional momenta, given position, will blend in some weighted fashion on the average over many trajectories, and time. One may calculate $\sigma_{q_i}^2$

by statistical means or measure the power at each configuration coordinate by averaging over time. Both values will be identical simply due to energy conservation and the conditional stationary behavior. The averages of momenta in both cases remain zero. Since the variable is Gaussian at each position, the higher order moments may also be deduced as well. *Any linear operation on the collection of such random variables cannot alter this conditional stationary behavior.*

3.1.9.1. Momentum Averages

At an arbitrary position, the velocity variance is based on the location of the particle with respect to the phase space boundary. The span of momentum values is determined by the $PAER_c$ and P_m parameters at each position and the span of the configuration domain radius is $\pm R_s$. $PAER_c$ is the peak to average energy ratio of the configuration ensemble. $PAER_p$ is typically specified for a design or analysis not $PAER_c$. Ultimately we shall prefer the $PAER_p$ design parameter.

If each momentum sample function is of sufficiently long duration, consisting of many independent time samples, then particle motions will eventually probe a representative number of states within the space and an appropriate momentum variance could be calculated from a densely populated configuration ensemble with diminishing bias on the alpha axis by averaging all configuration dependent variances. Such a calculation is given by;

$$\langle v_\alpha^2 \rangle = \frac{1}{2R_s} \int_{-R_s}^{R_s} v_q^2 \rho(v|q) dq$$

(3-89)

The time average on the left is then equated with the statistical quantity on the right. This is a correct calculation even if the velocity variance is not stationary. There is an inconvenience with this calculation however. We may only possess the velocity $v_q = v_{\max|q}$ explicitly for trajectories of phase space at boundary conditions. Fortunately there is an alternative.

A time sampled trajectory from the momentum ensemble is composed of independent Gaussian random variables from the configuration ensemble. Hence, we may calculate an average momentum variance over i members of the configuration ensemble where i is a sufficiently large number and λ_i is a relative weighting factor for each configuration ensemble member variance .

$$\langle v_\alpha^2 \rangle = \sum_i \lambda_i v_{q_i}^2 = \sum_i \lambda_i \frac{v_{\max|q}^2}{PAER_c}$$

(3-90)

The variance on the left comes from a Gaussian RV because the variances on the right come from independent Gaussian RV's. Therefore, we can specify the variance we want from the peak to average ratio of energy or power directly in the momentum ensemble, along with P_m , as design or analysis criteria. We need not explicitly calculate λ_i or even specify $PAER_c$ from the configuration ensemble because eq. 3-90 must be true from the properties of Gaussian RV's.

Therefore;

$$\langle v_\alpha^2 \rangle_\zeta = \frac{2P_m}{m f_s PAER_p}$$

(3-91)

This is the velocity variance per sample for the ζ^{th} sample function of the momentum ensemble. Hence, the variables from the configuration ensemble, which are dictated by maximum uncertainty requirements, constrain all samples from continuous time domain trajectories of the momentum ensemble to also be Gaussian distributed. The converse is also true. By simply specifying that the time domain sample functions are composed of Gaussian Random variables we have guaranteed that the uncertainty for any position must be maximum for a given variance. Now 3-90 and 3-91 are verified more deliberately in a derivation where each sample function of the momentum ensemble is treated as a unique message sequence and the time ordered message sequence is reordered to configuration bins. In this analysis, each member of the message sequence is a time sample.

A message is defined by a sequence of $2N$ independent time samples similar to the formulation of chapter 2. The message sequence is then given by;

$$m_{\zeta}(t - \ell T_s) = \{(q, p)_1, (q, p)_2, \dots (q, p)_{2N}\}_{\zeta}$$

(3-92)

The message is jointly Gaussian since it is a collection of independent Gaussian RV's. Position and momentum are related through an integral of motion and therefore q also possesses a Gaussian pdf which may be derived from p .

Now the statistical average is reviewed and compared to message time averages from the perspective of the process first and second moments. The long term time average is nearly

equivalent to the average of the accumulated independent samples, given a suitably large number of samples $2N$ [23, 25, 31, 32, 33].

$$\langle m_{\zeta}(t) \rangle \cong \lim_{N \rightarrow \infty} \frac{1}{2N} \sum_{\ell=-N}^N (q, p)_{\ell} \quad (3-93)$$

The mean square of the message is likewise approximated by;

$$\langle m_{\zeta}(t)^2 \rangle \cong \lim_{N \rightarrow \infty} \frac{1}{2N} \sum_{\ell=-N}^N (q^2, p^2)_{\ell} = \sum_i (\lambda_i \sigma_{q_i}^2, \lambda_i \sigma_{p_i}^2) \quad (3-94)$$

A long term time average is approximated by the sum of independent samples. It is reasonable to assume that the variance of each sample contributes to the mean squared result weighted by some number λ_i where i is a configuration coordinate index. The left hand side of 3-94 is a time average of sample energies over $2N$ samples and the right hand side is the weighted sum of the variances of the same samples organized into configuration bins. Conservation requires the equivalence.

Each time sample may be mapped to a specific configuration coordinate and momentum coordinate at the ℓ^{th} instant. Each position q_i is accompanied by a stationary momentum statistic, $\rho(p|q_i)$. The averaged first and second moments for each q_i are therefore stationary. This insures that any linear functional of a set RVs with these statistics must also be stationary when averaged over long intervals. Thus, long term time averages inherit a global stationary

property as will be shown. The right hand side of the prior equations are a sum of Gaussian RVs and Gamma RVs, respectively. Therefore, the mean and variance of the sum is the sum of the independent means and variances if the samples are statistically independent. The cumulative result remains Gaussian and Gamma distributed respectively. This permits relating the time averages and statistical averages of the messages in the following manner;

$$\lim_{N \rightarrow \infty} \frac{1}{2N} \sum_{\ell=-\infty}^{\infty} (q, p)_{\ell} = \frac{1}{\ell} \sum_i \sqrt{\lambda_i} \sum_{\ell} (q_{\ell}, p_{\ell})_i = (\bar{q}, \bar{p}) \quad (3-95)$$

$$\lim_{N \rightarrow \infty} \frac{1}{2N} \sum_{\ell=-\infty}^{\infty} (q^2, p^2)_{\ell} = \frac{1}{\ell} \sum_i \lambda_i \sum_{\ell} (q_{\ell}^2, p_{\ell}^2)_i = (\bar{\sigma}_q^2, \bar{\sigma}_p^2) \quad (3-96)$$

The right hand sides of these equations is no more than a reordering of the left hand side time samples in a manner which does not alter the overall averages. λ_i are ultimately determined by the characteristic process pdf and boundary conditions and are related to the relative frequency of time samples near a particular coordinate q_i . Whenever the averages are conducted over suitably large i, ℓ the sampled averages are good estimates of a continuum average. Since the right hand side is stationary, then the left hand side is stationary also.

The prior analysis requires that the process appear stationary in the wide sense or [Thomas, Middleton];

$$\langle \{\tilde{p}_\alpha^z\}_\zeta \rangle = \int_{-\infty}^{\infty} \{[\tilde{p}_\alpha(q_\alpha)]^z \rho(\tilde{v}_\alpha|q_\alpha)\}_\zeta d\tilde{v}_\alpha \quad ; z = 1,2$$

(3-97)

The maximum weighting is logically at the configuration origin where it is possible to achieve v_{max} at the apex of the v_p profile. The conditional pdf provides a weighting function for this statistic averaged over all possible positions q_α . Over an arbitrarily long interval of random motion, all coordinates will be statistically visited. The specific order for probing the coordinates vs. time is unimportant because the statistic at each particular configuration coordinate is known to be stationary. The time axis for the momentum ensemble member thus cannot affect the ensemble average or variance per sample.

In summary;

$$\frac{1}{\zeta} \sum_{\zeta=1}^k \langle \{p_\alpha^z\}_\zeta \rangle \cong E\{p_\alpha^z\} \quad ; z = 1,2$$

(3-98)

$$(\bar{\sigma}_{v_\alpha}^2)_s = \frac{P_m \Delta t}{m PAER}$$

(3-99)

$$\langle \mathcal{E}_k \rangle = \frac{m(v_{max})^2}{2 PAER}$$

(3-100)

$$\langle p_{\alpha}^2 \rangle = \frac{(p_{max_a})^2}{PAER}$$

(3-101)

$\langle \tilde{\mathcal{E}}_k \rangle$ may also be calculated for a maximum cardinal pulse boundary condition. We need only consider the primary lobe of the *sinc* function. The average energy for the maximum cardinal velocity pulse main lobe is calculated from (ignoring the tails);

$$\langle \tilde{\mathcal{E}}_{k_card} \rangle = \left\langle \frac{m v_{m_card}^2}{2} \int_{-T_s}^{T_s} \frac{\sin^2(\pi f_s t)}{(\pi f_s t)^2} dt \right\rangle \cong .903 \frac{m v_{m_card}^2}{2}$$

(3-102)

The average energy and momentum of all trajectories subordinate to the maximum cardinal pulse bound is therefore ;

$$\langle \mathcal{E}_{k_car} \rangle = .4515 \frac{m v_{m_card}^2}{(PAER)};$$

$$\langle p_{card}^2 \rangle = .903 \frac{m^2 v_{m_card}^2}{(PAER)};$$

(3-103)

The ratio of the average energy for the trajectories subordinate to the two profiles is approximately 1.1074 when $v_{m_card}^2 = v_m^2$. If the two cases are compared with an equivalent R_s design parameter then the ratio of comparative energies increases to (1.13)(1.1074)~1.25. This was obtained from 3-103 and section 3.1.8.2, as well as appendices F, G.

3.1.10. Configuration Position Coordinate Time Averages

Since the configuration coordinates are related to the momentum by an integral, the position statistic is also zero mean Gaussian with a variance related to the average of the mean square velocity profile. Davenport & Root and Middleton provide extensive discussion and proof of the Linear transformation of a Gaussian random process [12, 24]. Figure 3-32 illustrates the relationship between velocity and position for a particular sample function.

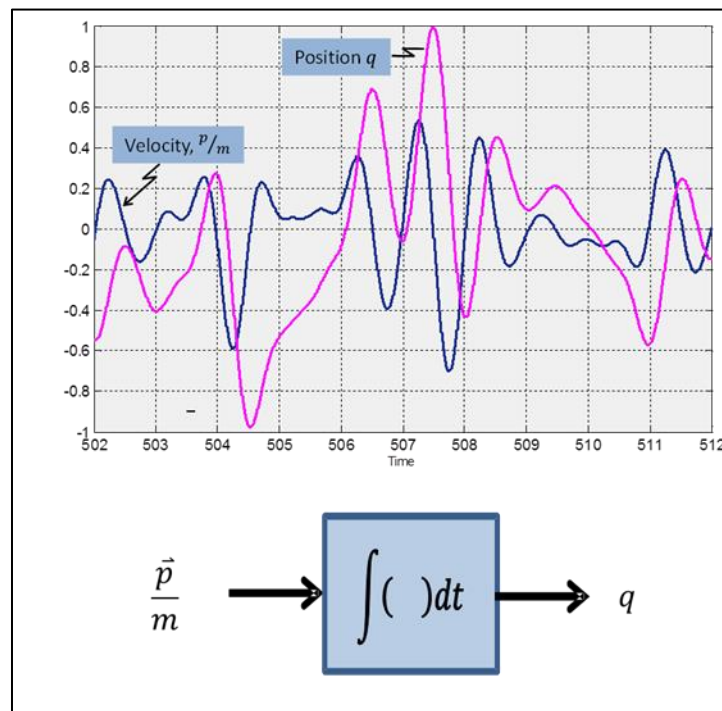


Figure 3-32 Momentum and Position Related by an Integral of Motion

Since the statistics of a position q_i are stationary, the linear function of a particular q_i also possesses a stable statistic.

In the prior sections, the Gaussian nature of momentum was argued from the maximum uncertainty requirement of momentum at each phase space coordinate. The position over an interval of time $t_a - t_b$ is given by;

$$q_{\zeta}(t) = \frac{1}{m} \int_{t_a}^{t_b} \check{p}_{\zeta}(t) dt = \frac{1}{m} \int_{t_a}^{t_b} a_{\zeta}(t) p_{\zeta}(t) dt + q_a \quad (3-104)$$

The momentum $p_{\zeta}(t)$ could be scaled by a continuous function of time $a_{\zeta}(t)$ resulting in an effective momentum, $\check{p}_{\zeta}(t)$. Sample functions of this form produce output RV's which are Gaussian when the kernel $p_{\zeta}(t)$ is Gaussian. Furthermore, if for each ζ this is true it can also be shown that,

$$q_{\zeta}(t) = \frac{1}{m} \int_{t_a}^{t_b} A_{\zeta}(t, \tau) p_{\zeta}(\tau) d\tau + q_a \quad (3-105)$$

and the output process is also Gaussian when $A(t, \tau)$ is a continuous function of both time and τ , an offset time variable [12]. In such cases, the position covariance K_q due to this class of linear transformations can be obtained from;

$$K_q = \frac{1}{m^2} \iint_{t_a}^{t_b} A(t, \tau_1) A(t, \tau_2) K_p(\tau_1, \tau_2) d\tau_1 d\tau_2 \quad (3-106)$$

An alternate form in terms of an effective filter impulse response and input covariance K_p , is given by [12, 24];

$$K_q = \frac{1}{m^2} \iint_{-\infty}^{\infty} h(t - \tau_1)h(t - \tau_2)K_p(\tau_1 - \tau_2) d\tau_1 d\tau_2 \quad (3-107)$$

When the covariance in each sample function is unaffected by time axis offset then $h(t) = u(t - t_a)$ is the impulse response from the integral of motion which leads to;

$$K_q = \frac{1}{m^2} \iint_{t_a}^{\infty} u(t - t_a - \tau_1)u(t - t_a - \tau_2)\tilde{K}_p(\tau_1 - \tau_2) d\tau_1 d\tau_2 = (\sigma_q^2)_s \quad (3-108)$$

\tilde{K}_p includes any time invariant scaling effects due to $A(t)$. $(\sigma_q^2)_s$ is a position variance per sample and T_s is a sample interval. 3-108 is given in meters squared per sample. Alternately, the frequency domain calculation for the covariance is given by;

$$K_q = \frac{1}{m^2} \int_{-\infty}^{\infty} |H_p(j\omega)|^2 S_p(\omega) d\omega \quad (3-109)$$

$S_p(\omega)$ is the double sided power spectral density of the momentum and $H_p(j\omega)$ is the frequency response of the effective filter. We also know that for maximum uncertainty conditions that $S_p(\omega)$ is a constant power spectral density.

Finally, the variance of q is also given in terms of the q_i variables from the prior section (for large i);

$$K_q(\tau = 0) = \sigma_q^2 \cong \sum_i \lambda_i q_i^2 = \frac{1}{m^2} (\sigma_p^2)_s T_s^2 \quad (3-110)$$

Therefore, if we specify σ_p^2 , $PAER_p$, and m we can calculate σ_q^2 . A simulation creating the signals of Figure 3-32 reveals that except for the units, the position and momentum as functions of time seem to possess the same dynamic behavior. This is due to the fact that the momentum is significantly filtered prior to obtaining the position and both are analytic.

3.1.10.1. Joint Probability for Momentum and Position

$\rho(p|q)$ is recalled as a point of reference. The multidimensional pdf may be given as ($m=1$);

$$\rho(\vec{v}_p|q) = \frac{1}{\sqrt{(2\pi)^D |\Lambda|}} e\left[-\frac{1}{2}(\mathbf{v}_\alpha - \bar{v}_\alpha)^T \Lambda^{-1} (\mathbf{v}_\beta - \bar{v}_\beta)\right] \quad (3-111)$$

σ_α^2 , the velocity variance and diagonal of Λ , are averaged over all probable configurations. Each configuration coordinate possesses a characteristic momentum variance which contributes to that average.

A phase space density of states in terms of configuration position must therefore be scaled according to;

$$\rho(q_\alpha) = \frac{1}{\sqrt{2\pi\langle q_\alpha^2 \rangle}} e^{-\frac{(q_\alpha)^2}{2\langle q_\alpha^2 \rangle}}$$

$$\langle q_\alpha^2 \rangle \equiv \sigma_q^2$$

(3-112)

The density along the α^{th} dimension of phase space is obtained from;

$$\rho(v_\alpha, q_\alpha) = \rho(v_\alpha|q_\alpha)\rho(q_\alpha)$$

(3-113)

The following sequence of plots illustrates the joint density of configuration and momentum coordinates in a single dimension for the maximum velocity profile. The probability has been scaled relative to the peak which occurs at the center of the space, at $q_\alpha = 0$. In the following plots, parameters of interest are; $PAER = 4$, $\Delta t = 1s$, $m = 1 kg$, $P_m = 1 J/s$.

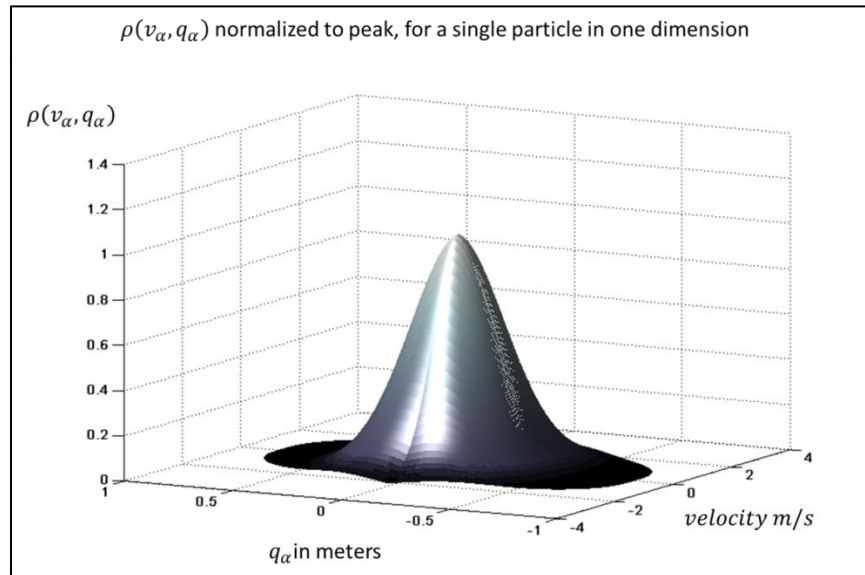


Figure 3-33 Joint pdf of Momentum and Position 1

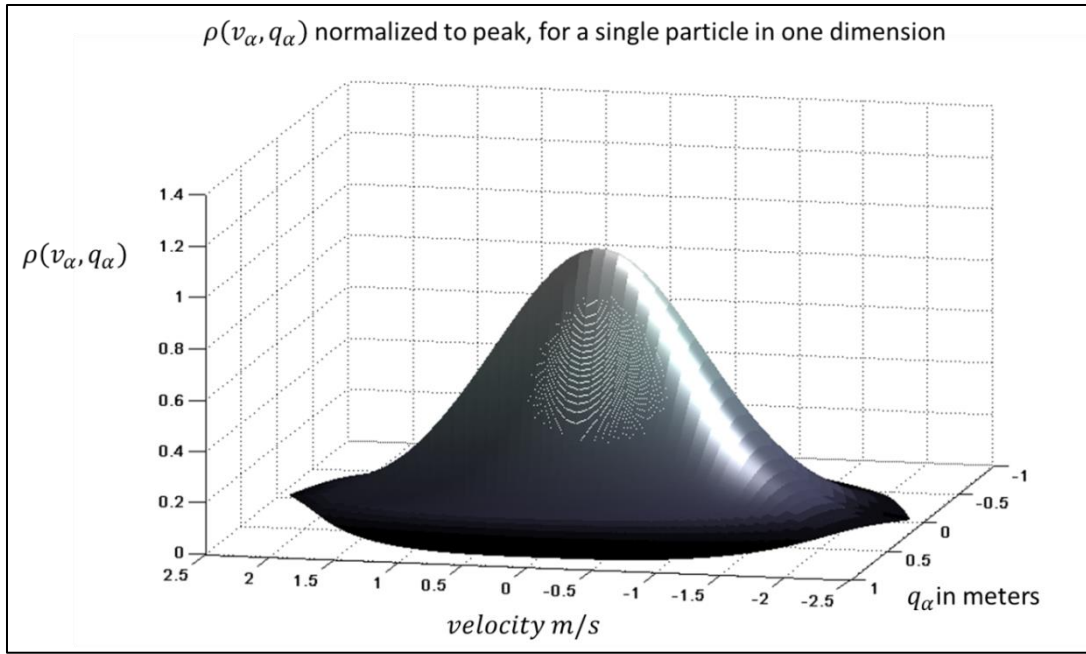


Figure 3-34 Joint pdf of Momentum and Position 2

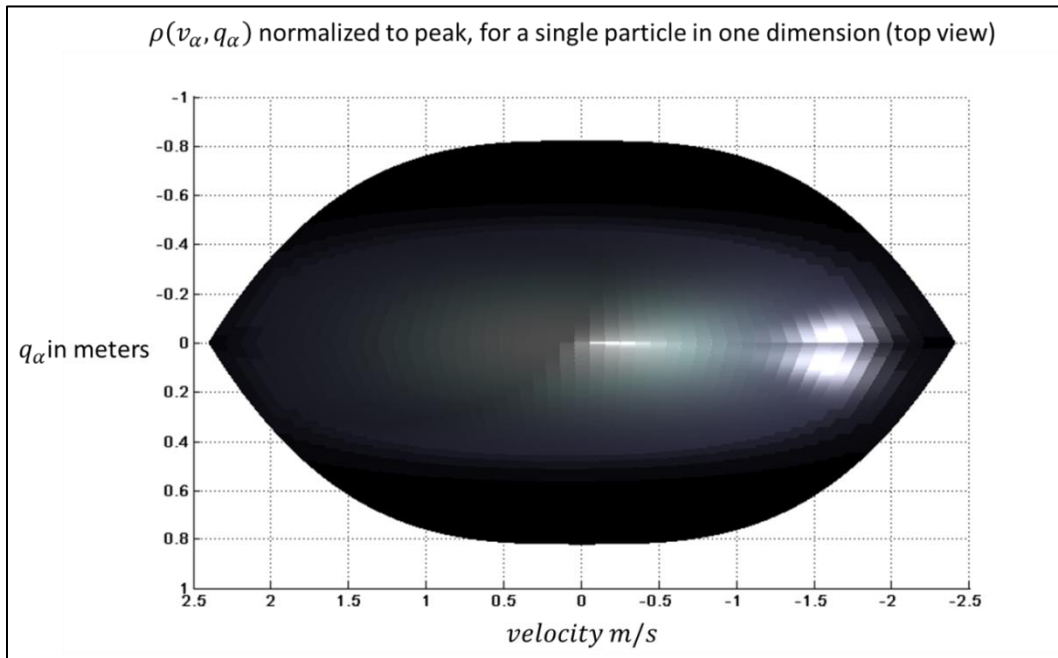


Figure 3-35 Joint pdf of Momentum and Position 3

Whenever, the orthogonal dimensions are also statistically independent then each dimension will have the form illustrated in the figures and there are 2 degrees of freedom per dimension. The 2 degrees of freedom per dimension per particle are fully realized if sample intervals T_s are prescribed.

A joint phase space density representation for the continuous RV's can be specified from the following synopsis of equations whenever momentum and position may be decoupled (case $m = 1$).

$$\rho(v_\alpha, q_\alpha) = \rho(q_\alpha)\rho(v_\alpha|q_\alpha) \tag{3-114}$$

$$\rho(q, p)_\Omega = \left(\frac{1}{\sqrt{2\pi\langle q_\alpha^2 \rangle}} e^{-\frac{q_\alpha^2}{2\langle q_\alpha^2 \rangle}} \left(\frac{\sqrt{PAER}}{\sqrt{2\pi}v_{\alpha_peak}} e^{-\frac{(PAER)v_\alpha^2}{2(v_{\alpha_peak})^2}} \right) \right) \tag{3-115}$$

$$1 = \int_{-v_p}^{v_p} \int_{-R_s}^{R_s} \rho(q, p)_\Omega dq dp; \quad \text{for } m = 1 \tag{3-116}$$

This joint statistic is also zero mean Gaussian.

3.1.11. Summary Comments on the Statistical Behavior of the Particle

Based Communications Process Model

Localized motions in time are correlated over the intervals less than Δt due to the momentum and associated inertia. Eventually, the memory of prior motions is erased by cumulative independent forces as the particle is randomly directed to new coordinates. This erasure requires energy. The evolving coordinates possess both Gaussian momentum and configuration statistics by design and the variance at each configuration coordinate is sculpted to accommodate boundary conditions. The boundary conditions require particle accelerations which may be deduced from the random momenta and finite phase space dimension. If a large number of independent samples are analyzed at a specific configuration coordinate, the momentum variance calculated for that coordinate is stationary for any member of the ensemble. Each configuration coordinate may be analyzed in this manner with its sample values reorganized as a configuration centric ensemble member.

The set of all momentum variances from all configuration coordinates may be averaged. That result is stationary. Yet, the process is not stationary in the strict sense because the momentum statistics are a function of position and therefore fluctuate in time as the history of a single particle evolves sequentially through unique configuration states. The process is technically not stationary in the wide sense because the autocorrelations fluctuate as a function of time origin. The moments of the process are however predictable at each configuration coordinate though the sequence of such coordinates is uncertain.

This process shall be distinguished as an "entropy stable" stationary (ESS) process. The features of such a process are;

- a) Autocorrelations possess the same characteristic form at all-time offsets but differ in some predictable manner; for instance, variance vs. position or parametrically vs. time. The uncertainty of these variances can be removed given knowledge of relative configuration offsets compared to an average, given the boundary conditions of the phase space are known and stationary.
- b) Shannon's entropy over all the configuration ensembles is unchanging even though the momentum random variable is not stationary as each configuration coordinate changes. The momentum does possess a known long term average variance.
- c) The long term time averages are characterized by the corresponding statistical average for a specific RV. The RV statistics (in this case momentum) may change as a function of time but will be constant at a particular configuration coordinate.
- d) Time averages and statistical averages for the ensemble members can be globally related by reorganizing samples from the process to favor either the momentum or configuration ensemble views respectively. The statistics of the process are unaltered by such comparative organizations.
- e) The variance of position may not necessarily be obtained through the momentum autocorrelation and system impulse response without further qualification. That is, the configuration variance may not always be calculated by direct application of the W-K theorem and system impulse response, through knowledge of the momentum variance without detailed consideration of boundary conditions.

Items a) and b) are of specific interest because they illustrate that statistical characterizations which are not classically stationary still may possess an information theoretic stability of sorts.

Stability of the uncertainty metric should be the preoccupation and driving principle rather than the legacy quest to establish an ergodic assumption. This point cannot be overemphasized for if the statistics which encode information change on an instant to instant basis in a stochastic way then the phase space is unstable and may become unbounded or otherwise ill-defined.

Information may be lost or annihilated.

Perhaps the most general view is that the entropy stable stationary communications process is a collection of individually stationary random variables with differing moments determined by physical boundary conditions and a time sequence for accessing the RV's which is randomly manifest whenever the process is sequentially sampled at sufficient intervals.

3.2. Comments Concerning Receiver and Channel

It shall not be necessary to analyze the receiver and channel in detail to obtain an analysis of capacity or efficiency. For the purposes herein, both the channel and receiver are considered to be linear. Therefore, the signal at the receiver is a replica of the transmit signal scaled by some attenuation factor, contaminated by additive white Gaussian noise (AWGN) and perhaps some interference with an arbitrary statistic. The channel conveys motion from the transmitter to the receiver via some momentum exchange whether field or material based.

The extended Channel consists of transmitter, physical transport media, and receiver. The physical transport medium can be modeled as an attenuator without adding other impairments except for AWGN noise. Although, the AWGN contribution may be distributed amongst the transmitter, transport medium and receiver, it is both convenient and sufficient to lump its affect into the receiver since we are concerned with the capacity of a linear system. The following figure illustrates the extended channel.

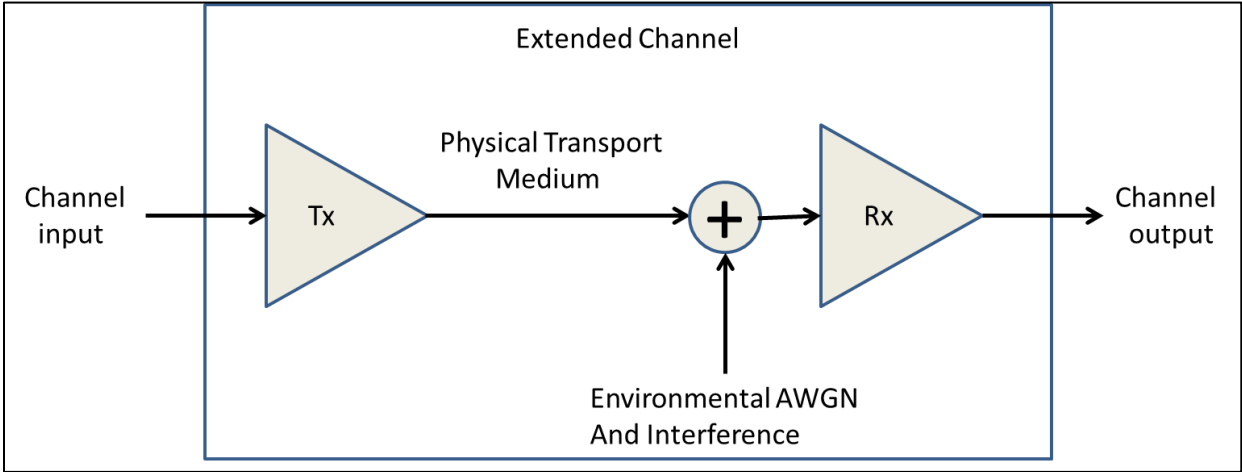


Figure 3-36 Extended Channel

Figure 3-36 represents the continuous bandwidth limited AWGN channel model without physical transport medium memory. Both the transmitter and receiver may possess finite bandwidth restrictions.

It is useful to connect this classical idea to the concepts of phase space. One approach is a global phase space model since it is an extension of the current theme and preserves a familiar analysis context. The following figure indicates the concept.

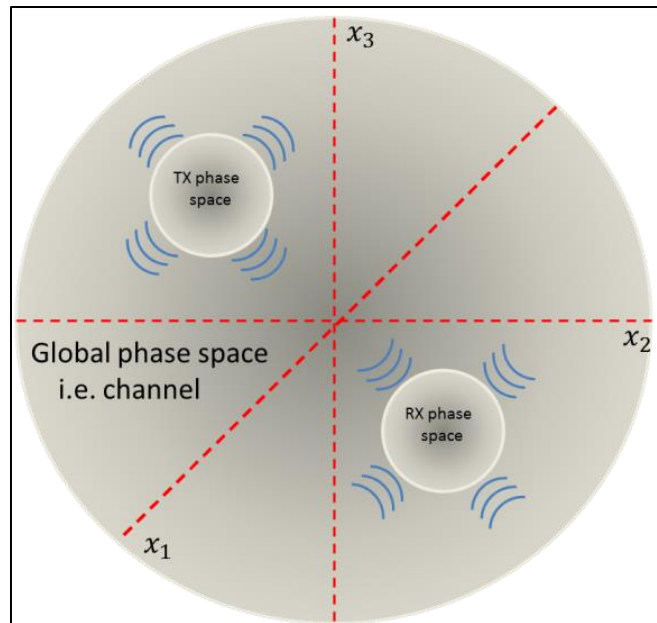


Figure 3-37 Global Phase Space

The coordinate systems for the transmitter, receiver, and channel may be co-referenced. Relative motions between the transmitter and receiver may be accommodated. The implied momentum exchanges between the transmitter, transport medium and receiver indicated by figure 3-37 may be assigned arbitrary direction within the global space. Arbitrary interferences can be simulated by insertion of additional transmitter sources if so desired. Channel distortions may require more detailed consideration and specification of the spatial properties of the transport medium between the transmitter and receiver but such models exist which can be easily adapted [34, 35, 36].

Channel attenuation is a property of the space between the transmitter and receiver. Attenuation is different for mechanical models, electromagnetic models, etc. There is a preferred consideration for the case of free space and an electromagnetic model where the power radiated in fields follows an inverse square law. Likewise, the momentum transferred with the radiated

field is well understood and this momentum reflects corresponding accelerated motions of the charged particles within the transmitter and receiver phase spaces. This will be revisited in section 5.5.

If we assume that transmission times are relatively long term compared to observation intervals then average momentum densities at each point in the global phase space will be relatively stationary if the transmit and receive platforms are fixed in terms of relative position. The momentum density is 3 dimensional Gaussian with a spatial profile sculpted proportional to R^{-2} where R is the radius from the transmitter, excluding the near field zone [40]. This follows the same theme as the analysis for the velocity profiles with the exception of the boundary condition. At large distances, the *PAPR* for the momentum profile is the same as for local fields but the variance converges as R^{-2} . The pdf for the field momentum in the channel transport medium will be of the following form.

$$\rho(\vec{p}_\alpha) \cong \frac{\sqrt{PAER}}{\sqrt{2\pi}p_{\alpha_peak}} e^{-\frac{(PAER)p_{x\alpha}^2}{2(p_{\alpha_peak})^2}}, \quad PAER \equiv \left(\frac{p_{x\alpha_peak}}{\sigma_{p_{x\alpha}}}\right)^2$$

$$\rho(\vec{p}) = \prod_{\alpha=1}^{D=3} \rho(\vec{p}_\alpha)$$

(3-117)

σ_{p_α} is a function of radial offset from the transmitter and the radius vector is a composition of 3 orthogonal position vectors. In the basic model the density is independent of direction. That is, the propagation is omnidirectional. This follows if the receiver position is uncertain. σ_{p_α} could vary as a function of azimuth and elevation for more advanced analysis if the receiver position is

known and the transmitter is equipped to take advantage of this a priori knowledge. The receiver may occupy any region except the transmitter position.

There are two interfaces to consider in the basic model; transmitter-channel and channel-receiver. Maximum power transfer is assumed at both interfaces. Hence, the effect of loading, is that half of the source power is transferred at each interface [41]. Otherwise, the relative statistics for motions of particles and fields through phase space are unaffected except by scale.

Similar analogies can be leveraged for acoustic channels and optical channels. In those cases, momentum may be transferred by material or virtual particles but the same concepts apply.

The receiver model mimics the transmitter model in many respects. The geometry of phase space for the receiver can be hyper-geometric and spherical as well. The significant differences are;

- a) Relative location of information source and phase space
- b) The direction of information flow is from the channel which is reversed from the Tx scenario
- c) The sampling theorem applies in the sense of measuring rather than generating signals
- d) There can be significant competitive interfering signals and contamination of motion beyond thermal agitation, though that is not addressed by this work

With respect to item d); the relative power of the desired signal compared to potential interference power, which may contaminate the channel, can be many orders of magnitude in deficit. The demodulator which decodes the desired signal must discriminate encoded information while removing the effects of the often much larger noise and interference, to the greatest extent possible

Signal strength and therefore capacity is greatly influenced by the separation R of the information source and the information sink (see eq. 3-117). The receiver must redact patterns of motions which can survive transfer through large contaminated regions of space (transport medium) and still recognize the patterns. The sensitivity of this process is remarkable in some cases because the desired signal momenta and associated powers interacting with the particles of the receiver can be on the order of pica watts [35, 42]. This requires very sensitive and linear receiver technology.

The following receiver phase space graphic illustrates a momentum trajectory consisting of the desired signal motions summed with random noise and interference. Notice the collision with the boundary producing a compression event. At that boundary the motions become nonlinear and information is lost. If the signal portion of the motion is much less in magnitude compared to the noise and interference then the nonlinearities will also create competing intermodulation distortions in the preferred motions, unwanted spectrums will grow, etc. . Thus, the P_m and $PAER$ of design are heavily influenced by the levels of permitted interference and noise as well as signal. In chapter 4 it is shown that the particle momenta encoding information must be sufficient to overcome competing momenta from environmental contamination, to achieve a certain capacity. This in turn influences the efficiency of the operating hardware as will be established in chapter 5.

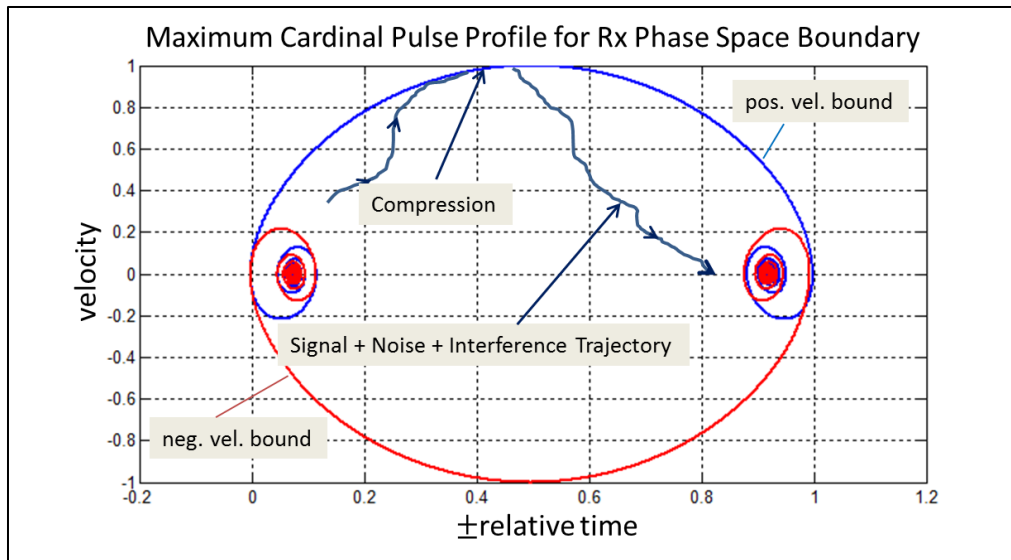


Figure 3-38 Maximum Cardinal Pulse Profile in a Receiver Phase Space along with a Random Particle Trajectory

It will be shown that at the most fundamental level the same concepts for communications efficiency apply throughout the extended channel. Similarly, capacity, while independently affected by receiver performance, transmitter performance and extended channel conditions, finds common expression in certain distributed aspects of the capacity equation such as signal power, noise power, observation time, sampling time, etc. We proceed with a high level analysis of capacity vs. efficiency dependent on these common variables applied to the current particle based model where information is transferred through momentum exchange.

4. UNCERTAINTY AND INFORMATION CAPACITY

This chapter accomplishes two goals;

- a) Refine a suitable uncertainty metric for a communications process of the model described in chapter three.
- b) Derive the physical channel capacity.

What is required is an uncertainty associated with coordinates of phase space. This can be obtained from a density of the phase space states which calculates the probability of particle occupation for position and momentum. Once the uncertainty metric is known, the capacity may be obtained from this metric, the TE relation, and some basic knowledge of the extended channel.

4.1. Uncertainty

Uncertainty is a function of the momentum and configuration coordinates. Thus, formulations from statistical mechanics may be adopted at least in part. However, one of the most powerful assumptions of statistical mechanics is forfeit. A basic postulate of statistical mechanics asserts that all microstates (pairings of $\{q, p\}$) of equal energy for a closed system be equally probable [13, 43]. This postulate provides much utility because particles possess equal energy distribution everywhere within a container or restricted phase space under equilibrium conditions. The communications process of chapter 3 requires that the average kinetic energy for a particle in

motion is a specific function of q due to boundary conditions. Therefore, communications processes require more detailed consideration of the statistics for the particle motion to calculate the uncertainty because they are not in equilibrium.

The uncertainty for a single particle moving in D dimensional continuum is given by;

$$H_{\Omega} = - \iint \dots \rho(\vec{q}, \vec{p})_{\Omega} \ln \rho(\vec{q}, \vec{p})_{\Omega} d^D(q) d^D(p) \quad (4-1)$$

The joint density $\rho(\vec{q}, \vec{p})_{\Omega}$ was obtained in Chapter 3. Some attention must be afforded to Jaynes' scrutiny of Shannon's differential entropy (eq.2-11, 4-1) which was earlier stated by Boltzman in his discussion of statistical mechanics [14]. The discrete form of Shannon's entropy given in eq. 2-10 cannot be readily transformed to the continuous form in 4-1, which may provide some ambiguity for the absolute counting of states. Shannon overcame this ambiguity by calculating a relative entropy metric. In addition to Jaynes' arguments, C. Arndt addresses this concern in significant detail with a conclusion that "...the information of discrete random variables, measured in bits, cannot be transformed to the information of continuous random variables in a simple way" [44]. However, in the same reference Arndt acknowledges the value of continuous differential entropy forms and indeed engages the classical maximum entropy solutions based on the continuous Gaussian distribution. He points out that the infinite offset which plagues the differential entropy "...is neglected in all practical applications of this entropy measure" [44]. In addition to infinite offsets precluding absolute measure, the differential entropy may assume negative values. Shannon was aware of these limitations and

used ratios of pdfs in his uncertainty functions which eliminates ambiguities [15]. The ratio of probabilities in the argument of the natural logarithm results in difference terms for uncertainty which neutralizes the effect of the probability continuum resolution.

It is the difference in entropy measures which is at the heart of capacity. This is because capacity is a property of the communication system's ability to both convey and differentiate variations in states rather than evaluate absolute states.

If the mechanisms which encode and decode information possess baseline uncertainties prior to information transfer, then such pre-existing ambiguity cannot contribute to the capacity. Thus, a change in state referred to a baseline state is necessary and sufficient as a metric to calculate capacity. This is a kind of information relativity principle in that only relative differences of some physical quantity may convey information.

In this chapter, we promote a lower limit resolution for the momentum and configuration, based on quantum uncertainty. A discrete resolution is introduced to limit the number of states per trajectory which may be unambiguously observed.

That is, even though a continuum of states may exist mathematically they cannot be resolved due to physical limitations. Hence, we may only count what we can resolve.

Middleton also forwarded a similar suggestion though he did not pursue the details of a probability density function [12]. He stated that uncertainty functions based on pdf ratios, result in forms of mutual information metrics which eliminate the concerns for cell resolution of the phase space. He states “ Cell size no longer appears in these expressions for information gain, since they represent the difference between two states of ignorance or uncertainty” [12]. This

statement is based on his assessment of the insertion of quantum uncertainty into the analysis and thus the reference to “cell size”. However, discarding an explicit quantum uncertainty in the numerator and denominator terms of the mutual information kernel of the uncertainty function ignores certain physical aspects for limiting conditions in a capacity equation. Therefore this quantum uncertainty will be addressed in the subsequent analysis.

One may be tempted to simply write down a proposed discrete form of a pdf without a physical measure. This is unnecessary and potentially problematic as Arndt points out. Arndt provides the logical motivation to begin with a continuous rather than discrete entropy form. He asserts, “Discrete entropies are based on probabilities of the events and do not have any reference to the concrete observations” [44]. Continuous entropies originate from observables connected to the phase space proper. In this connection the Gaussian distribution explicitly includes the variance of the observable as well as the character of its time evolution. If the discrete random variable is derived by sampling a continuous process then it may logically inherit attributes of the continuous physical process, if it is properly sampled. Conversely if it is merely a probability measure of events without connection to physics it may provide an incomplete characterization. The approach moving forward, adopts the statistical mechanics formulation . The applicable probability density is normalized to a measure of unity while accommodating the quantum uncertainty by setting the granularity of phase space cells for each observable coordinate [13, 43].

$$\frac{1}{h^D} \int \dots \int \rho(\vec{q}, \vec{p})_{\Omega} d^D(q) d^D(p) = 1$$

(4-2)

h^D provides a scale according to a phase cell possessing a D dimension span on the order of h , Planck's constant.

The total uncertainty may be calculated from a weighted accumulation of Gaussian random variables. Each variable is associated with a position coordinate q_{α} and each coordinate possesses a corresponding probability weighting.

The inclusion of the factor $\frac{1}{h^{D\nu}}$ (where the number of particles $\nu=1$) addresses Jaynes' concern since he suggested its use in the absence of an explicit statistical quantum theoretical treatment.

Quoting Jaynes [14];

“Before we can set up the information measure for this case, we must decide on a basic measure for phase space. In classical statistical mechanics, one has always taken uniform measure largely because one couldn't think of anything else to do.....In other words, the well-known proposition that each discrete quantum state corresponds to a volume $\frac{1}{h^{3\nu}}$ of classical phase space, will determine our uniform measure....”

Landau had a complementary perspective with respect to Gibbs' entropy [43];

“It is not difficult to establish the relation between $\Delta\Gamma$ (number of relevant quantum states within a phase space) in quantum theory and $\Delta p\Delta q$ in the limit of classical theory. ...we can say that a

“cell” of volume $(2\pi\hbar)^s$ (where s is the number of degrees of freedom of the system)

“corresponds” in phase space to each quantum state...the number of states $\Delta\Gamma$ may be written

$$\Delta\Gamma = \frac{\Delta p \Delta q}{(2\pi\hbar)^s}$$

He further points out that the logarithm of $\Delta\Gamma$ is dimensionless when scaled by the denominator and that

“changes of entropy in a given process, are definite quantities independent of the choice of units...Only the concept of the number of discrete quantum states, which necessarily involves a non-zero quantum constant, enables us to define a dimensionless statistical weight and so to give an un-ambiguous definition of the entropy”

This phase space measure normalization is generally regarded as a cornerstone for classical statistical mechanics [13]. This theme is carried forward to derive uncertainty and capacity. However, we must add an important note to distinguish the classical entropy of statistical mechanics and the uncertainty function we seek here. Classical statistical mechanics is largely preoccupied with conditions of equilibrium. Thermodynamic equilibrium entropy may be defined by the condition $(dS/dt) = 0$ [43]. Also, typically a large number of particles on the order of Avagadro’s number are statistically examined for a closed system. Here we begin with the analysis of a single particle where the fluctuations of the particle momentum are governed by Gaussian not uniform distributions. We ignore rotational, vibrational and other degrees of freedom and retain only the translation motions since the other modes are extensible [13]. The statistics of many non-interacting particles may then be implied. Nevertheless, in both

circumstances the distribution of momentum and position are at the heart of uncertainty, only the boundary conditions of the system differ between the two paradigms.

The single particle uncertainty with finite phase cell, in 3 dimensions is;

$$H = -\frac{1}{\hbar^3} \int_{-p_{max}}^{p_{max}} \dots \int_{-R_s}^{R_s} \dots \rho(q, p)_\Omega \ln[\rho(q, p)_\Omega] dq_1 dp_1 \dots dq_3 dp_3 \quad (4-3)$$

It is apparent that this entropy is that of a scaled Gaussian multivariate and;

$$H = H_q + H_p \quad (4-4)$$

H_q, H_p are the uncertainties due to position and momentum respectively which are statistically independent Gaussian RV's. The momentum and position may be encoded independent of one another subject to the boundary conditions.

$$H_q + H_p = \ln(\sqrt{2\pi e})^{2D} + \ln(|\Lambda|^D) = \ln(2\pi e \sigma_q)^D + \ln(2\pi e \sigma_p)^D \quad (4-5)$$

Λ is the joint covariance matrix.

The lower limit of this entropy can be calculated by allowing the classical quantity $(\sigma_q \sigma_p)$, to approach the quantum value $(\sigma_{q_{\hbar}} \sigma_{p_{\hbar}})$, and assuming that the quantum variance may be

approximated as Gaussian. $\tilde{\hbar}$ is the rationalized form of Plank's constant and $\tilde{\hbar}/2 \leq \sigma_{q_{\tilde{\hbar}}} \sigma_{p_{\tilde{\hbar}}}$, according to the quantum uncertainty relation [45].

$$\tilde{\hbar} = \frac{\hbar}{2\pi}$$

The number of single particle degrees of freedom D may be set to one since the entropy is extensible. Our limit is achieved for $\sigma_q \sigma_p \rightarrow \sigma_{q_{\tilde{\hbar}}} \sigma_{p_{\tilde{\hbar}}}$, $D=1$ case,

$$H_{min} \geq \lim_{\sigma_q \sigma_p \rightarrow \sigma_{q_{\tilde{\hbar}}} \sigma_{p_{\tilde{\hbar}}}} \{ \ln(2\pi e) + \ln(\sigma_q \sigma_p) \} \quad (4-6)$$

$$H_{min} \geq \left\{ \ln(2\pi e) + \ln\left(\frac{\hbar}{4\pi}\right) \right\} \quad (4-7)$$

Therefore, the minimum entropy is non negative and fixed by a physical constant, assuming the resolution of the phase space cell is subject to the uncertainty principle. This limit is approached whenever the joint particle position and momentum recedes to the quantum “noise floor”.

Positive differences from this limit correspond to the uncertainty in motions available to encode information. The limit is also independent of temperature. An equivalent form of the entropy limit is revisited subsequently as derived by Hirschman and Beckner [45, 46, 47].

4.2. Capacity

Capacity is defined as the maximum transmission rate possible for error free reception. Error free will be defined as the ability to resolve position and momentum of a particle. We shall direct the following analysis to the continuous bandwidth limited AWGN channel without memory.

“Without memory” refers to the circumstance where samples of momentum and position from the random communications process may be decoupled and treated as independent quantities at proper sampling time intervals.

The capacity of a system is determined by the ability to generate and discriminate sequences of particle phase space states, and their associated connective motions through an extended channel. Each sequence can be regarded as a unique message similar to the discussion of chapter 2. The ability to discriminate one sequence from all others necessarily must contemplate environmental contamination which can alter the intended momentum, and position of the particle.

4.2.1. Classical Capacity

In this section Shannon’s definition of capacity is extended to encompass the desired physical models. In doing so, the difficulties associated with continuous probability densities for describing communications processes have been avoided so that entropy expressions do not diverge as pointed out by Jaynes and others.

A summary of Shannon’s solution follows [15];

$$C = \max_{\rho(x)} \{H(\rho(x)) - H_y(\rho(x))\}$$

$$C = \lim_{T \rightarrow \infty} \max \left\{ \frac{1}{T} \left[- \int \rho(x) \ln(\rho(x)) dx + \iint \rho(x, y) \ln \left(\frac{\rho(x, y)}{\rho(y)} \right) dx dy \right] \right\}$$

$$C = \lim_{T \rightarrow \infty} \max \left\{ \frac{1}{T} \left[\iint \rho(x, y) \ln \left(\frac{\rho(x, y)}{\rho(x)\rho(y)} \right) dx dy \right] \right\}$$

(4-8)

Maximization is with respect to the Gaussian pdf $\rho(x)$ given a fixed variance. The channel input and output variables are given by x, y respectively, where y is a contaminated version of x . Now the scale within the argument of the logarithm is ratio-metric and therefore the concerns of infinities are dispensed, but only in the case where thermal noise variance is greater than zero, as will be shown. This form can also be applied to the continuous approximation of the quantized space or even the quantized space if each volume element is suitably weighted with a Dirac delta function. Thomas, Mackay and Middleton have similar treatments and provide thorough derivations based on principles of mutual information [12, 21, 48]. In the following derivation we use differential entropy forms and take ratios. Ultimately, the quantum uncertainty shall also be accounted for through distinct terms to emphasize its limiting impact on capacity.

The mutual information can be defined as;

$$I(x; y) = \ln \left(\frac{\rho(x|y)}{\rho(x)} \right)$$

$\rho(x|y)$ is the probability of x entering the channel given the observation of y at the receiver load. This is the probability kernel of the equivocation $H_y(x)$. Thomas derives the capacity for the discretely sampled continuous AWGN channel as;

$$C = \max\{E[I(x; y)]\} = \max\left\{E\left[\ln\left(\frac{\rho(x|y)}{\rho(x)}\right)\right]\right\} = \max\left\{E\left[\ln\left(\frac{\rho(y|x)}{\rho(y)}\right)\right]\right\} \quad (4-9)$$

E is the expectation operator. Mackay shows the equivalence of Shannon's solution and this mutual information form [48].

Finding the capacity requires, weighting all possible mutual information conditions, resulting in an uncertainty relationship. The averaged mutual information of interest may be written as;

$$E[I(x; y)] = \overline{[I(x; y)]} = H(y) - H_x(y)$$

$$\overline{[I(x; y)]} = H(x) - H_y(x)$$

$$\overline{[I(x; y)]} = +H(x, y) - H(x) - H(y)$$

(4-10)

The joint density $\rho(q, p)_\Omega$ developed in the previous sections accounts for this through detailed expansion of covariance as a function of time where all off diagonal terms of the covariance matrix are zero. The pdf for the channel output is given by;

$$\rho(y) = \rho(\tilde{q}, \tilde{p})_\Omega$$

The tilde represents the corrupted observation of the joint position and momentum. The variances introduced by a noise process can be represented by $\sigma_{q_n}^2, \sigma_{p_n}^2$. The joint pdf $\rho(x, y)$ is easily obtained for the Gaussian case where time samples are elements of the Gaussian vector (see Appendix D). Using a shorthand notation, which simultaneously contemplates position and momentum, the expected value for the mutual information for a single dimension can be calculated from;

$$\overline{I(x; y)} = \ln((2\pi e)^{N/2} |\Lambda_x|^{1/2}) + \ln((2\pi e)^{N/2} |\Lambda_y|^{1/2}) - \ln((2\pi e)^N |\Lambda_{x,y}|^{1/2}) \quad (4-11)$$

Λ_x, Λ_y , are the input, output covariance matrices respectively for the samples. Λ_x, Λ_y are N square in dimension while $\Lambda_{x,y}$ is a 2N by 2N composite covariance of the N input and output samples [21]. The approach for the single configuration dimension thus mimics Shannon's where the independent time samples are arranged as a Gaussian multivariate vector of sample dimension $N=2BT$, sometimes referred to as Shannon's number [6]. The extension of capacity for D configuration dimensions may then be calculated simply by using a multiplicative constant if all D dimensions are independent. The variance terms for the input and output samples are;

$$\sigma_x^2 = \left\{ \langle q_\alpha^2 \rangle, \frac{(p_{\alpha_max})^2}{2 PAER} \right\}$$

$$\sigma_y^2 = \left\{ [k_g \langle q_\alpha^2 \rangle + \sigma_{q_n}^2], \left[k_g \frac{(p_{\alpha_max})^2}{2 PAER} + \sigma_{p_n}^2 \right] \right\} \quad (4-12)$$

The variance terms are segregated because they have different units. Each sample has a unique position and momentum variance. Thus, position and momentum are treated as independent data types. Subsequently the units will be removed through ratios. k_g is a gain constant for the extended channel and may be set to 1 provided the channel noise power terms are accounted for relative to signal power. The elements of the covariance matrices are therefore obtained from the enumeration of (i, j) over N for $\sigma_{xi}\sigma_{xj}$ and $\sigma_{yi}\sigma_{yj}$. The elements for the joint covariance Λ are derived from the composite input-output vector samples. The compact representation for the averaged mutual information from 4-11 then becomes;

$$\overline{I(x; y)} = \frac{1}{2} \ln \left[\frac{|\Lambda_x| |\Lambda_y|}{|\Lambda|} \right] \quad (4-13)$$

Maximization of this quantity yields capacity.

In the case where the process interfering with the input variable x is Gaussian and independent from x, the capacity can be obtained from the alternate version of $\overline{I(x; y)}$ by inspection;

$$C = \max\{\overline{I(x; y)}\} = \max\{H(y) - H_x(y)\} \quad (4-14)$$

$H_x(y)$ is the uncertainty in the output sample given the desired variable x entered the channel.

This is simply the uncertainty due to the corrupting noise or;

$$H_x(y) = \frac{1}{2} \ln[(2\pi e)^N |\Lambda_n|] \quad ; D = 1 \quad (4-15)$$

Likewise,

$$H(y) = \frac{1}{2} \ln[(2\pi e)^N |\Lambda_y|] \quad ; D = 1 \quad (4-16)$$

Since the corruption consists of N independent samples from the same process, samples possess a statistic with noise variance σ_n^2 and the capacity becomes;

$$C = \frac{1}{2} \left(\ln \left[\frac{(\sigma_x^2 + \sigma_n^2)}{\sigma_n^2} \right] \right) \frac{nats}{sample} \quad (4-17)$$

N is not present in the normalized capacity because of the ratio of 4-13 and 4-14. Furthermore, it is assumed that the required variances are calculated over representative time intervals for the process.

The capacity of 4-17 is per unit sample for a one particle system. Capacity rate must consider the minimum sample rate f_{s_min} which sets the information rate. This is known from the TE relationship as the minimum number of forces per unit time to encode information.

$$C = \frac{f_{s_min}}{2} \left(\ln \left[\frac{(\sigma_x^2 + \sigma_n^2)}{\sigma_n^2} \right] \right) = \frac{P_m}{2 \langle \mathcal{E}_k \rangle_s PAER} \left(\ln \left[\frac{(\sigma_x^2 + \sigma_n^2)}{\sigma_n^2} \right] \right) = B \left(\ln \left[\frac{(\sigma_x^2 + \sigma_n^2)}{\sigma_n^2} \right] \right) \quad (4-18)$$

Now an appropriate substitution using the results of chapter 3 can be made for σ_x^2 and σ_n^2 to realize the capacity for the case of a particle in motion with information determined from independent momentum and position in the α^{th} dimension. Capacity can be organized into configuration and momentum terms.

$$C_\alpha = C_{q_\alpha} + C_{p_\alpha}$$

$$C_\alpha = \frac{P_{m_\alpha}}{2\langle \mathcal{E}_{k_\alpha} \rangle_s PAER_\alpha} \left(\ln \left[\frac{([\langle q_{x_\alpha}^2 \rangle + \tilde{\sigma}_{q_{n\alpha}}^2])}{\tilde{\sigma}_{q_{n\alpha}}^2} \right] + \ln \left[\frac{([\langle (p_{x_\alpha})^2 \rangle + \tilde{\sigma}_{p_{n\alpha}}^2])}{\tilde{\sigma}_{p_{n\alpha}}^2} \right] \right) \quad (4-19)$$

It is presumed that there will always be some variance due to quantum uncertainty. The variances $\sigma_{q_{\hbar}}^2, \sigma_{p_{\hbar}}^2$ prevent the capacity equation from diverging because their minimums reflect this quantum uncertainty. One way of expressing this is;

$$\tilde{\sigma}_{q_n}^2 = \sigma_{q_n}^2 + \sigma_{q_{\hbar}}^2$$

$$\tilde{\sigma}_{p_n}^2 = \sigma_{p_n}^2 + \sigma_{p_{\hbar}}^2$$

(4-20)

This formulation estimates the maximum entropy of the quantum uncertainty to be based on a Gaussian RV. Therefore the variance of quantum uncertainty may add to the noise variance $\sigma_{q_n}^2$ and $\sigma_{p_n}^2$ in a simple way. Hirschman and Beckner studied this form of entropy with a bound given by [45, 46, 47];

$$H_q + H_p \geq \ln\left(\frac{\pi e \tilde{h}}{2}\right)$$

$$\left[\ln(\sigma_{q_{\tilde{h}}}) + \ln(\sqrt{2\pi e}) \right] + \left[\ln(\sigma_{p_{\tilde{h}}}) + \ln(\sqrt{2\pi e}) \right] \geq \ln(\pi e \tilde{h})$$

$$\sigma_{q_{\tilde{h}}} \sigma_{p_{\tilde{h}}} \geq \frac{\tilde{h}}{2} e^{(H_q + H_p - \ln(e\pi))} \geq \frac{\tilde{h}}{2}$$

(4-21)

Hirschman exploited the property that if $|f(q)|^2$ and $|g(p)|^2$ are both probability frequency functions and $g(p)$ is the Fourier transform of $f(q)$ then the entropies of $|f(q)|^2$ and $|g(p)|^2$ cannot be simultaneously concentrated in q and p . Beckner proved Hirschman's entropy conjecture for the case where q and p are the position and momentum conjugates. This agrees with Weyl's result for quantum mechanics and the uncertainty of position and momentum [47]. Hirschman's bound was derived using Shannon's entropy metric for the quantum uncertainty based on continuous Gaussian probability densities. The usual maximum entropy Gaussian assumption applies to derive the bound. The Hirschman-Beckner result is considered as a robust bound with a lower limit consistent with Heisenberg's uncertainty principle [45]. Even if the temperature of the communications system reaches absolute zero, this uncertainty is retained. Figure 8-1 illustrates the impact of the quantum uncertainty compared to the thermal noise floor.

The implication is that; *It is impossible to attain a capacity of infinity for the band limited AWGN channel with finite signal power.*

This is a logical and physically correct conclusion, unsupported by the Shannon-Hartley capacity equation.

For the case of information transfer via D independent dimensions, the available energy and information may be distributed amongst these dimensions. When all dimensions have parity, the capacity with a maximum velocity pulse boundary condition ($k_p = 1$), is given by;

$$C \leq \sum_{\alpha=1}^D \frac{P_{m_\alpha}}{2\langle \mathcal{E}_{k_\alpha} \rangle_s PAER_\alpha} \left(\ln \left[\frac{\left(\left[\frac{1}{m^2} (\sigma_{p_\alpha}^2)_s T_{s_\alpha}^2 f_{s_\alpha} + \tilde{\sigma}_{q_{n_\alpha}}^2 \right] \right)}{\tilde{\sigma}_{q_{n_\alpha}}^2} \right] + \ln \left[\frac{\left(\left[(\sigma_{p_\alpha}^2)_s f_{s_\alpha} + \tilde{\sigma}_{p_{n_\alpha}}^2 \right] \right)}{\tilde{\sigma}_{p_{n_\alpha}}^2} \right] \right) \quad (4-22)$$

, where variances from chapter 3 have been substituted and are also normalized per unit time.

A multidimensional channel can behave like D independent channels which share the capacity of the composite. Given a fixed amount of energy, the bandwidth per dimension scales as

$B/D = \frac{P_{m_\alpha}}{2D\langle \mathcal{E}_{k_\alpha} \rangle_s PAER_\alpha}$ and the overall capacity remains constant for the case of independently modulated dimensions. Capacity as given, is in units of nats/second but can be converted to bits/second if the logarithm is taken in base 2.

The capacity equation may also be written in terms of the original set of hyperspace design parameters ($m = 1$).

$$C \leq \sum_{\alpha=1}^D \frac{P_{m_\alpha}}{2\langle \mathcal{E}_{k_\alpha} \rangle_s PAER_\alpha} \left(\ln \left[\frac{\left(\left[\frac{2P_{m_\alpha} T_{s_\alpha}^2}{PAER_\alpha} + \tilde{\sigma}_{q_{n_\alpha}}^2 \right] \right)}{\tilde{\sigma}_{q_{n_\alpha}}^2} \right] + \ln \left[\frac{\left(\left[\frac{2P_{m_\alpha}}{PAER_\alpha} + \tilde{\sigma}_{p_{n_\alpha}}^2 \right] \right)}{\tilde{\sigma}_{p_{n_\alpha}}^2} \right] \right) \quad (4-23)$$

$$C \leq \sum_{\alpha=1}^D \frac{P_{m,\alpha}}{2\langle \mathcal{E}_{k,\alpha} \rangle_s PAER_{\alpha}} (\ln[\overline{SNR}_{q,\alpha} + 1] + \ln[\overline{SNR}_{p,\alpha} + 1])$$

(4-24)

This form assumes that D dimensions from the original hyper sphere transmitter are linearly translated through the extended channel. The signal is sampled at an effective rate of f_s , though each dimension is sampled at the rate $f_{s,\alpha} = f_s/D$. It should be noted that a reference coordinate system at the receiver may be ambiguous and the aggregate sample rate of f_s may in general be required to resolve this ambiguity in the absence of additional extended channel knowledge.

$\tilde{\sigma}_{q_{n,\alpha}}^2$ may be replaced by the filtered variance of a noisy process with input variance $\tilde{\sigma}_{p_{n,\alpha}}^2$. This was calculated in chapter 3 and results in the substitution (for $m=1$);

$$\tilde{\sigma}_{q_{n,\alpha}}^2 = \tilde{\sigma}_{p_{n,\alpha}}^2 T_{s,\alpha}^2$$

After substitution into 4-23 and cancelling the $T_{s,\alpha}^2$ terms, the capacity equation becomes;

$$C \leq \sum_{\alpha=1}^D \frac{P_{m,\alpha}}{\langle \mathcal{E}_{k,\alpha} \rangle_s PAER_{\alpha}} \left(\ln \left[\frac{\left(\frac{2 P_{m,\alpha}}{PAER_{\alpha}} \right)}{\tilde{\sigma}_{p_{n,\alpha}}^2} + 1 \right] \right); \quad PAER > 1$$

$$C \leq \sum_{\alpha=1}^D \frac{P_{m,\alpha}}{\langle \mathcal{E}_{k,\alpha} \rangle_s PAER_{\alpha}} (\ln[\overline{SNR}_{eq} + 1])$$

(4-25)

The influence of The TE relation in 4-25 indicates that greater energy rates correspond to larger capacities. The scaling coefficient is the number of statistically independent forces per unit time

encoding particle information while the logarithm kernel reflects the allocated signal momentum squared relative to competing environmental momentum squared.

A similar result can be written for the case with a cardinal velocity pulse boundary condition by appropriate substitutions for the variance in equation 4-23. The proper substitutions from chapter 3 are ($m = 1$);

$$\langle (p_{x_\alpha})^2 \rangle_{card} = .903 \frac{m^2 v_{m_{card}}^2}{(PAER)}; \quad (4-26)$$

$$\langle q_{card}^2 \rangle \cong \langle p_{card}^2 \rangle T_s^2 \quad (4-27)$$

$$R_s = 1.85 (v_{m_{card}}) \quad (\text{see Appendix F}) \quad (4-28)$$

Both position and momentum are regarded as statistically independent and equally important in this capacity formula. This is an intuitively satisfying result since the coordinate pairings (q, p) are equally uncertain, at least to lower bound values just above the quantum noise floor.

Although not contemplated by these equations, an upper relativistic bound would also limit the momentum accordingly. The implication of this model is that physical capacity summarized by equation 4-25 is twice that given in the Shannon-Hartley formula.

Quantum uncertainty prevents the argument of the logarithm in equation 4-23 from diverging when environmental thermal agitation is zero, unlike the classical forms of the Shannon-Hartley

capacity equation . When the absolute temperature of the system is zero, the capacity is quite large but finite for finite P_m . \overline{SNR}_{eq} applies to any one dimension or all dimensions collectively for this capacity formula since energy is equally partitioned for signal and noise processes alike.

Capacity in nats per second and bits per second are plotted in the following graphics.

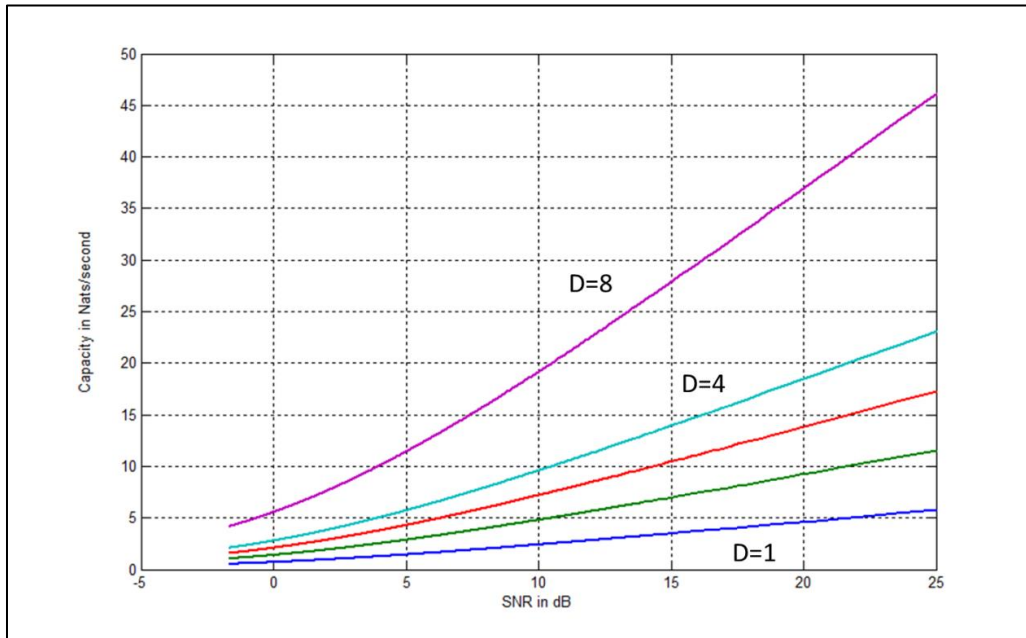


Figure 4-1 Capacity in Nats/s vs. \overline{SNR} for a D dimensional link with a maximum velocity pulse profile, Capacity in nats/s vs. given the following parameters, $PAER=10$, $P_m = 1$ J/s, $m=1$ kg, $f_s = 1$

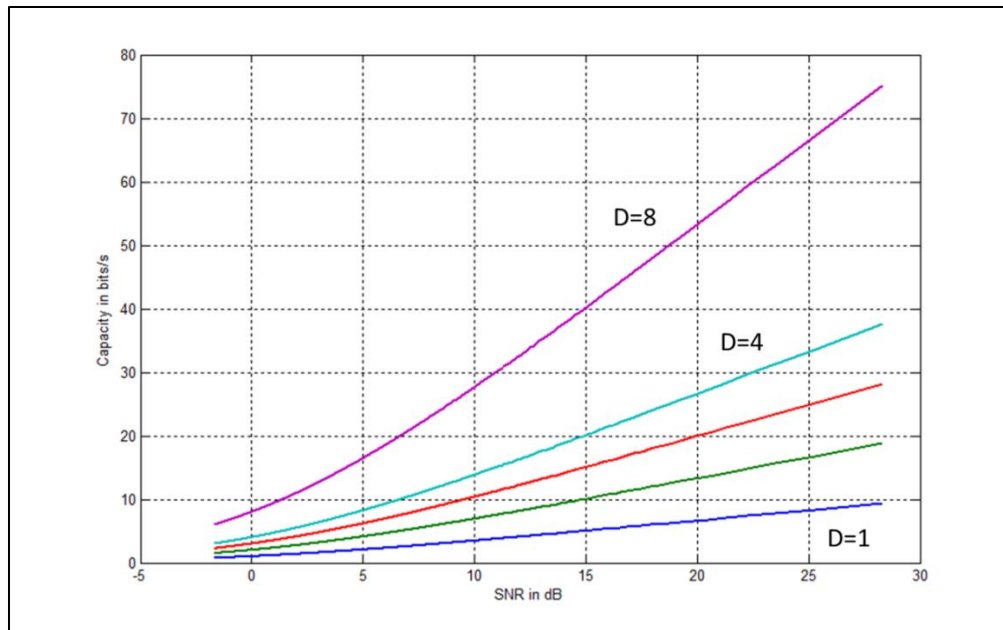


Figure 4-2 Capacity in bits/s vs. $(\text{SNR})^{-1}$ for a D dimensional link given the following parameters, PAER=10, $P_m=1$ J/s, $m=1$ kg, $f_s=1$ samp./s, $B=.5$ Hz, $D=1,2,3,4, 8$

The capacity for the case of a cardinal velocity pulse boundary condition follows the same form but the SNR for a given P_{m_card} must necessarily adjust according to the relationships provided in 4-26, 4-27, 4-28. There it was illustrated that the energy increase on the average for the cardinal case is approx. 1.967 times that of a maximum nonlinear velocity pulse boundary condition. This factor ignores the precursor and post cursor tails of the maximum cardinal pulse profile. If the tails are considered then the factor is approximately equal to the peak power increase requirement. The peak power increase ratio for the cardinal profile is 2.158. This corresponds to the circumstance where the same R_s must be spanned in an equivalent time while comparing the impact of the two prototype pulse profiles. Thus, roughly 3 dB more power is required by the cardinal profile to maintain a standard configuration span for a given time interval and capacity comparison.

4.3. Multi-Particle Capacity

Capacity for the multi-particle system is extensible from the single particle case. We now expand comments to non-interacting species of particles under the influence of independent forces with multiple internal degrees of freedom.

The form for the uncertainty function is given as a reference for μ species of particle, where the particle clusters might exhibit dynamics governed by μ Gaussian pdfs. Each cluster would consist of one or more particles. A general uncertainty function considers coordinates from all the particle clusters which can contain ν_μ particles per cluster and ℓ_μ states per particle and spatial dimensionality = $1, 2 \dots D$. Within each cluster domain, particles may swarm subject to a few constraints. One constraint is that particle collisions are forbidden. The total number of degrees of freedom, \aleph , can generally be considered as the product $\aleph = D\nu\mu\ell$ and for a single particle type with one internal state per sample, $\aleph = D$.

$$H_\Omega(q, p) = - \sum_1^D \sum_1^\mu \sum_1^{\ell_\mu} \sum_1^{\nu_\mu} \int \dots \int \rho_\mu(q_{\nu,\ell}, p_{\nu,\ell}) \ell n \rho_\mu(q_{\nu,\ell}, p_{\nu,\ell}) d^{D\nu_\mu}(q_{\nu,\ell}) d^{D\nu_\mu}(p_{\nu,\ell})$$

(4-29)

The pdf for this form of uncertainty can be adjusted using the procedures previously justified.

The normalization integral is integrated over all states within the D dimensional hyper-sphere where the lower and upper limits (ll, ul) are set according to the techniques presented in chapter 3.

The capacity for a system with \aleph equivalent degrees of freedom is simply

$$C \leq \sum_{i=1}^{\aleph} \frac{P_{m_{\aleph}}}{\langle \mathcal{E}_{k_{\aleph}} \rangle_s PAER_{\aleph}} (\ln[\overline{SNR}_{eq} + 1])$$

(4-30)

Energy is equally dispersed amongst all the degrees of freedom in equation 4-30.

Whenever \aleph is not composed of homogeneous degrees of freedom then the form of 4-30 may be adjusted by calculating an \overline{SNR}_{eq} from the amalgamation of particle diversities.

The multi-particle impact is an additional consideration which is important to mention at this point. The effect of particle number ν on the momentum and energy of a signal is as important as velocity. Energy and energy rate of signals is a central theme of legacy theories as well as the theories presented here. Classical formulations are somewhat deficient in this respect.

Modulation of momentum through velocity is emphasized for the present discussion. However, this presents the obvious challenge in the classical case because of the uncertainty $\Delta q \Delta p \geq \hbar$. At the least, two factors which may accommodate this concern when particles are indistinguishable, are, $(\nu! \hbar^{D\nu})^{-1}$ and m , where $\nu!$ is the Gibb's correction factor for counting states of indistinguishable particles [13]. Mass m is extensive and therefore may represent a bulk of particles. Such a bulk at a particular velocity will have a greater momentum and kinetic energy as the mass (*number of particles*) increases. The same is true of charge. A multiplicity of charges in motion will proportionally increase momentum and the energies of interest both in terms of material and electromagnetic quantities. *Hence, velocity is not the only means of controlling*

signal energy. The number of particles can also fluctuate whilst maintaining a particular velocity of the bulk. Such is the case for instance where current flow in an electronic circuit is modulated. The fundamental motions of electrons and associated fields may possess characteristic wave speeds in certain media yet the square of the number of wave packets per interval of time traversing a cross section of the media is a measure of the power in the signal. This logically means that counting particles and possibly additional particle states is every bit as important as acknowledging their individual momentums. Indeed, the probability density of numbers of particles possessing particular kinetic energies distributed in various degrees of freedom is the comprehensive approach. This requires specific detail of the physical phenomena involved, accompanied by greater analytic complexity.

5. COMMUNICATIONS PROCESS

ENERGY EFFICIENCY

In this chapter we discuss the efficiency of target particle motion within the phase space introduced in chapter 3. Though we have a primary interest in Gaussian motion, the derived relationships for efficiency can be applied to any statistic given knowledge of the *PAPR* for the particle motions. This is a remarkable inherent characteristic of the TE relation.

The 1st Law of thermodynamics accounts for all types of energy conversions as well as exchanges and requires that energy is conserved in processes restricted to some boundary such as a closed system. We can account for energy at a specific time using simple equations such as;

$$\begin{aligned}\mathcal{E}_{tot} &= \sum \mathcal{E}_{kin} + \sum \mathcal{E}_{\varphi} + \sum \mathcal{E}_{elec.} + \sum \mathcal{E}_{mag.} + \dots + U \\ \mathcal{E}_{tot} &= \sum \mathcal{E}_e + \sum \mathcal{E}_w + \sum \mathcal{E}_{\varphi} + U\end{aligned}$$

(5-1)

In this representation, energy is effectively utilized, \mathcal{E}_e , wasted, \mathcal{E}_w , or potential, \mathcal{E}_{φ} . U is defined as the internal system energy. From the work of Mayer, it is known that all forms of energy may be included in this accumulation, such as chemical, mechanical, electrical, magnetic, thermal, etc. [13, 49].

Alternatively, consider a classical formulation of the first law. δQ is an incremental amount of energy acquired from some source to power an apparatus and δW is an incremental quantity of

work accomplished by an apparatus. A change in the total internal energy of a closed system can be given in terms of heat and work as [50];

$$\Delta U = Q - W$$

$$dU = \delta Q - \delta W$$

(5-2)

Although originally formulated for heat engines, this equation is useful for general purpose. dU is an exact differential and is therefore independent of the procedure required for exchange of heat and work between the apparatus and environment [50].

For a system in isolation, the total energy and internal energy are equivalent [13, 51]. Using this definition enables several interchangeable representations which will be employed from time to time depending on circumstance.

$$Q - W = \sum \Delta \mathcal{E}_e + \sum \Delta \mathcal{E}_w + \sum \Delta \mathcal{E}_\varphi$$

$$\Delta \mathcal{E}_{tot} = Q - (W_{effective} + W_{waste})$$

$$\mathcal{E}_{tot} = \mathcal{E}_e + \mathcal{E}_w + \mathcal{E}_\varphi = \mathcal{E}_\varphi + \mathcal{E}_k$$

(5-3)

\mathcal{E}_k and \mathcal{E}_φ are kinetic and potential energies respectively. One may account for the various quantities using the most convenient formulation to fit the circumstance and a suitable sign convention for the directional flow of work when the energy varies with time. Negative work shall mean that the apparatus accomplishes work on its environment. Positive work means that

the environment accomplishes work on the apparatus. Work forms of energy exchange such as kinetic for example or a charge accelerated by an electric field may be effective or waste. Thus the change in total energy of a system can be found from, Q , the energy supplied and, W , the work accomplished with sign conventions determined by the direction of energy and work flow. The forms of energy exchanged for work in equation 5-3 is a form of the work energy theorem [52].

It is also desirable to define energy efficiency consistent with the second law of thermodynamics. In the streamlined view needed here we simply state that the consequence of the second law is that efficiency $\eta \leq 1$ where the equality is never observed in practice. The tendency for waste energy to be translated to heat, with an increase of environmental entropy, is also a consequence of the second law [51]. \mathcal{E}_w reduces to heat by various direct and indirect dissipative mechanisms. Directly dissipative refers to the portion of waste originating from particle motion and described by such phenomena including, drag, viscous forces, friction, electrical resistance etc.. Indirectly dissipative or ancillary dissipative phenomena, in a communications process, are defined as those inefficiencies which arise from the necessary time variant potentials synthesizing forces to encode information.

As will be illustrated, momentum exchange between particles of an information encoding mechanism possess overhead as uncertainty of motion increases. The overhead cannot be efficiently recycled and significant momentum must be discarded as a byproduct of encoding. \mathcal{E}_e is the deliverable portion of energy to a load which evolves through the process of encoding. \mathcal{E}_w is generated by the absorption of overhead momentum into various degrees of freedom for the

system, including modes which increase the molecular kinetic energy of the apparatus constituents. This latter form is generally lost to the environment, eventually as heat.

The equation for energy efficiency can be written as;

$$\langle \eta \rangle = \frac{\langle \mathcal{E}_e \rangle}{\langle \mathcal{E}_e + \mathcal{E}_w \rangle} = \frac{\langle \mathcal{E}_e \rangle}{\langle \mathcal{E}_{in} \rangle} \leq \frac{P_{out}}{P_{in}}$$

(5-4)

$\frac{P_{out}}{P_{in}}$ represents a familiar definition for efficiency often utilized by engineers. In this definition, the output power from an apparatus is compared to the total input power consumed to enable the apparatus function [51]. The proper or effective output power, P_e , is the portion of the output power which is consistent with the defined function of the apparatus and delivered to the load. Usually, we are concerned with the case where $P_{out} = P_e$. This definition is important so that waste power is not incidentally included in P_{out} .

In subsequent discussion the phase space target particle is considered as a load. Its energy consists of \mathcal{E}_e and \mathcal{E}_w corresponding to desired and unwanted kinetic energies, respectively. Not only are there imperfections in the target particle motion, but there will be waste associated with the conversion of a potential energy to a dynamic form. This conversion inefficiency may be modeled by delivery particles which carry specified momentum between a power source and the load. Thus the inefficiencies of encoding particle motion are distributed within the encoding apparatus where ever there is a possibility of momentum exchange between particles.

5.1. Average Thermodynamic Efficiency for a Canonical Model

Consider the basic efficiency definition using several useful forms including the sampled TE relation from chapter 3 (eq. 3-42);

$$\langle \eta \rangle = \frac{\langle \mathcal{E}_e \rangle}{\langle \mathcal{E}_e \rangle + \langle \mathcal{E}_w \rangle} = 1 - \frac{\langle P_w \rangle}{\langle P_{in} \rangle} = \frac{\langle P_e \rangle}{\langle P_{in} \rangle} = \frac{P_{m_e}}{f_s \langle \mathcal{E}_{in} \rangle_s P A P R_e} \quad (5-5)$$

In terms of apparatus power transfer from input to output;

$$\begin{aligned} \langle P_{in} \rangle \langle \eta \rangle &= \langle P_e \rangle \\ f_s \langle \mathcal{E}_{in} \rangle_s \langle \eta \rangle &= \frac{P_{m_e}}{P A P R_e} = \langle P_e \rangle \end{aligned} \quad (5-6)$$

$\langle \mathcal{E}_{in} \rangle_s$ is defined as the average system input energy per sample, given the force sample frequency f_s obtained in chapter 3. In systems which are 100 percent efficient, the effective maximum power associated with the signal, P_{m_e} , and maximum power required by the apparatus, P_m , are equivalent. In general though, $P_m \geq P_{m_e}$, when dissipation exists where, $P_m = \max \left\{ \frac{d}{dt} \mathcal{E}_{in} \right\}$. In both 5-5 and 5-6 we recognize that $P A P R_e$ is inversely proportional to efficiency. Whenever directly dissipative phenomena are not present we may assume $P_m = P_{m_e}$, unless otherwise specified.

The phase space model of chapter 3 is now extended to facilitate a discussion concerning the nature of momentum exchange which stimulates target particle motion. The following figure illustrates the relationship between the several functions; information encoding/modulation, power source and target particle phase space. As a whole, this could be considered as a significant portion of a transmitter phase space for an analogous communications system.

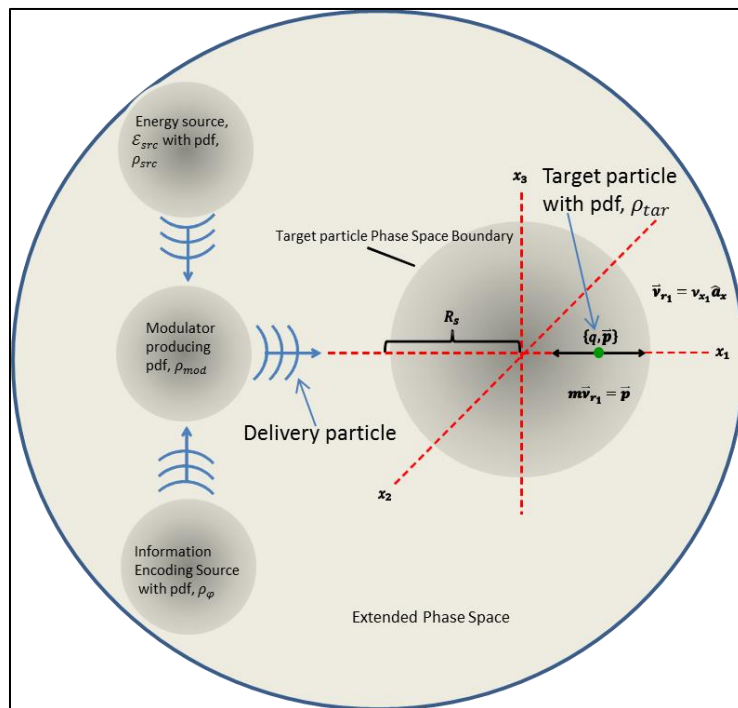


Figure 5-1 Extended Encoding Phase Space

The information source possesses a Gaussian statistic of the form introduced in chapter 3. It provides instruction to internal mechanisms which convert potential energy to a form suitable to encode the motion of particles in the target phase space. The interaction between the various apparatus segments may be through fields or virtual particles which convey the necessary forces. The energy source for accomplishing this task, illustrated in a separate sub phase space, is

characterized by its specific probability density for particle motions within its distinct boundaries. \mathcal{E}_{src} is used as the resource to power motions of particles comprising the apparatus. A modulator is required which encodes these particles with a specific information bearing momentum profile. As a consequence, delivery particles or fields recursively interact with the target particle imparting impulsive forces at an average rate greater than or equal to $f_{s,min}$. The sculpting rate of the impulse forces may be much greater than the effective sample rate $f_{s,min}$ for detailed models. However, when f_s is used to characterize the signal samples it is understood that a single equivalent impulse force per sample at the f_s frequency may be used, provided the TE relation is regarded.

The following figures illustrates the desired target particle momentum statistic $\rho_\phi = \rho_e$ and an actual target particle statistic ρ_{tar} for an example.

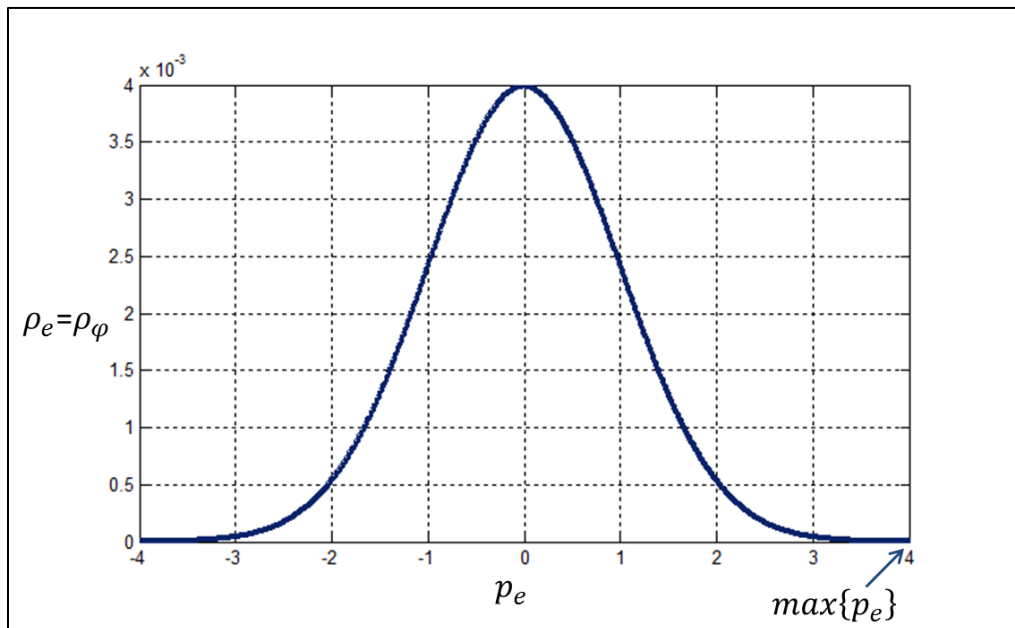


Figure 5-2 Desired Information Bearing Momentum

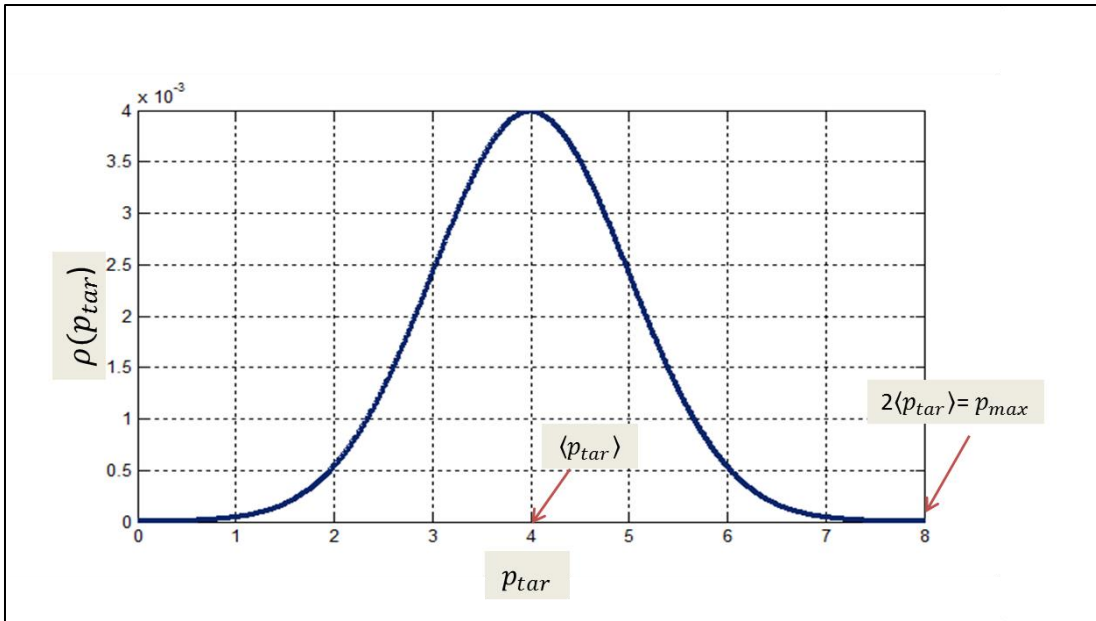


Figure 5-3 Actual Momentum of a Target Particle

One hypothetical method for encoding the particle motion is illustrated in apparatus graphic, figure 5-4. All particles of this hypothetical model are ballistic and possess the same mass.

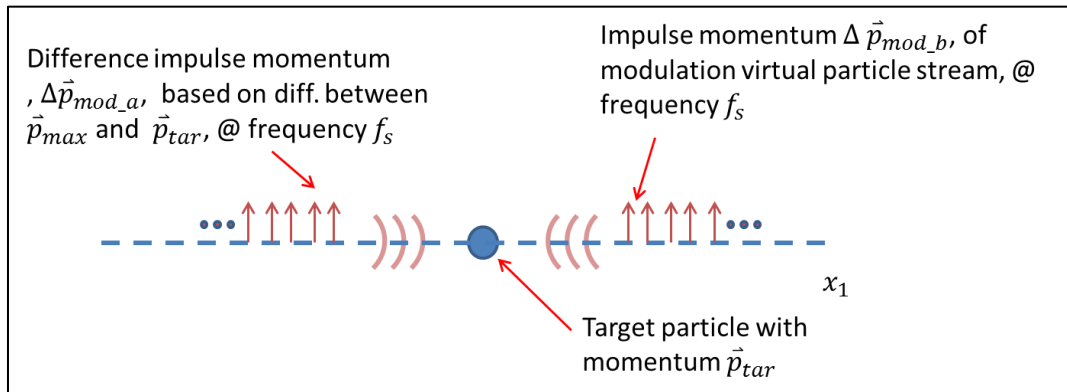


Figure 5-4 Encoding Particle Motion on the x_1 axis via Momentum Exchange

There are two delivery particle streams illustrated, oriented along the x_1 axis. Such an arrangement could be deployed for generating motion along the x_2 and x_3 axes as well. The

l^{th} momentum impulse $(\Delta\vec{p}_{mod_a})_l$ from a successive non-interacting stream of delivery particles accelerates the target particle to the right (positive x_1 direction). The modulation impulse stream $\Delta\vec{p}_{mod_b}$ decelerates the target particle through application of forces in the negative direction. These two opposing streams interact with the target particle at regular intervals, $\sim\Delta T_s$, though their relative interactions may not be perfectly synchronized. That is, the opposing particle streams can possess some relative small time offset $\Delta t_\epsilon \ll \Delta T_s$. The domains for the impulse momenta are;

$$0 \leq \Delta p_{mod_a} \leq \Delta p_{max}$$

$$0 \geq \Delta p_{mod_b} \geq \Delta p_{max}$$

In the absence of $\Delta\vec{p}_{mod_b}$ the particle accelerates up to a terminal velocity \vec{v}_{max} and can no longer be accelerated whenever $\vec{p}_{tar} \geq \vec{p}_{max}$. \vec{p}_{max} is a boundary condition inherited from the phase space model of chapter 3. The finite power resource P_m limits the maximum available momentum, system wide. The finite limit of the velocity due to forward acceleration can be deduced through the difference equation;

$$\Delta\vec{p}_{(mod_a)_l} = (\vec{p}_{max} - \Delta\vec{p}_{tar_{l-1}})_l$$

$$\Delta\vec{p}_{(mod_a)_l} = \left(\vec{p}_{max} \left[1 - \frac{\Delta\vec{p}_{tar_{l-1}}}{\vec{p}_{max}} \right] \right)_l$$

(5-7)

,where $\vec{p}_{tar_{l-1}} \geq 0$. Thus, the impulse momentum of the delivery particle at the l^{th} sample is a function of the maximum available momentum and the prior target particle momentum. The output differential momentum is given by;

$$\Delta\vec{p}_{tar_l} = \Delta\vec{p}_{(mod_a)_l} + \Delta\vec{p}_{(mod_b)_l} \quad (5-8)$$

The output momentum at the l^{th} sample is obtained by;

$$\vec{p}_{tar_l} = \int_{T_s(l-1)}^{T_s(l)} \Delta\vec{p}_{tar_l} \delta(t - T_s(l-1)) dt + \vec{p}_{tar_{l-1}} \quad (5-9)$$

5-9 indicates that an impulse momentum weighted by $\Delta\vec{p}_{tar_l}$ is imparted during the sampling interval to generate a new momentum value \vec{p}_{tar_l} when summed to the initial condition $\vec{p}_{tar_{l-1}}$. The target particle momentum samples at the l^{th} and $(l-1)^{th}$ are Gaussian and statistically independent by definition. Therefore, $\Delta\vec{p}_{(mod_a)_l}$ and $\Delta\vec{p}_{(mod_b)_l}$ are also independent in this case. However, careful review of figures 5-6,5-7 and 5-10 in the following simulation records, illustrate that these waveforms are inverted with respect to one another and delayed by one sample. The inversion follows since one waveform is associated with acceleration and one with deceleration. If not for the delay of one cycle, these signals would be anti-correlated, a consequence of Newton's third law and momentum conservation.

A momentum exchange diagram (figure 5-5) illustrates the successive interaction of modulation delivery and target particles.

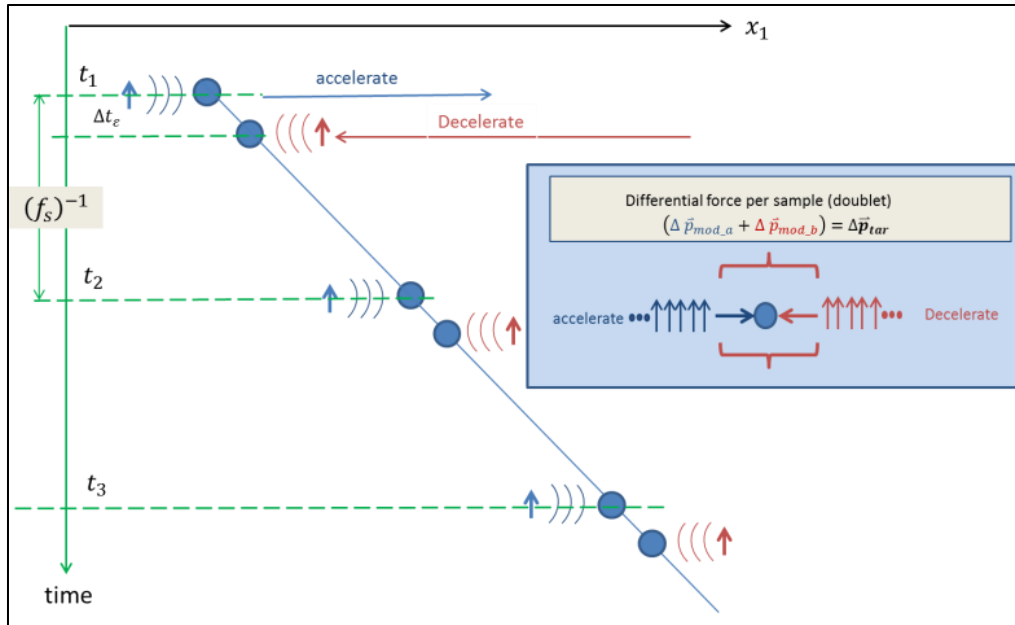


Figure 5-5 Momentum Exchange Diagram

Interactions are realized via impulse doublets. Impulses forming the doublets may be slightly skewed in time by Δt_ε seconds and the doublets are separated by a nominal $t_s = \Delta t/2$ seconds corresponding to a sampling interval. The target particle may possess a nonzero average drift velocity along x_1 . Figure 5-6 and 5-7 illustrate the input and output impulses related to the interactions for the cases where $\Delta t_\varepsilon = 0$ and $\Delta t_\varepsilon \neq 0$ respectively. The error in timing alignment does not affect motion appreciably at the time scale of interest because Δt_ε is much less than the nominal sampling time interval separating doublets. The integral of eq. 5-8 suppresses the effect of a Δt_ε offset.

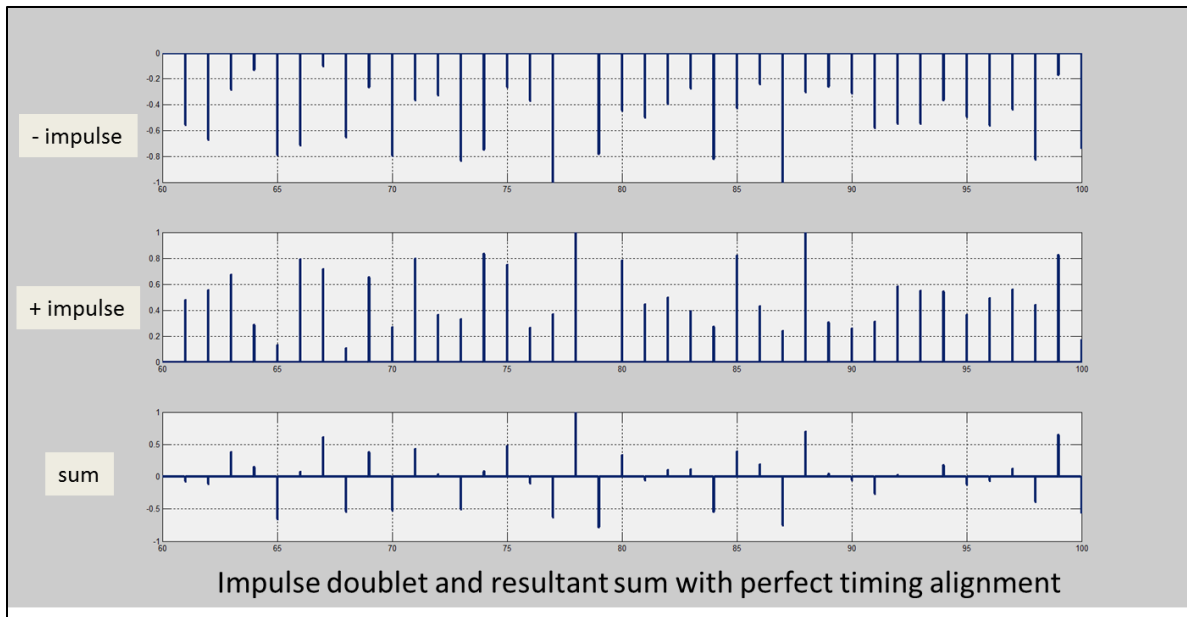


Figure 5-6 Encoding Particle Stream Impulses, $t_{\varepsilon} = 0$

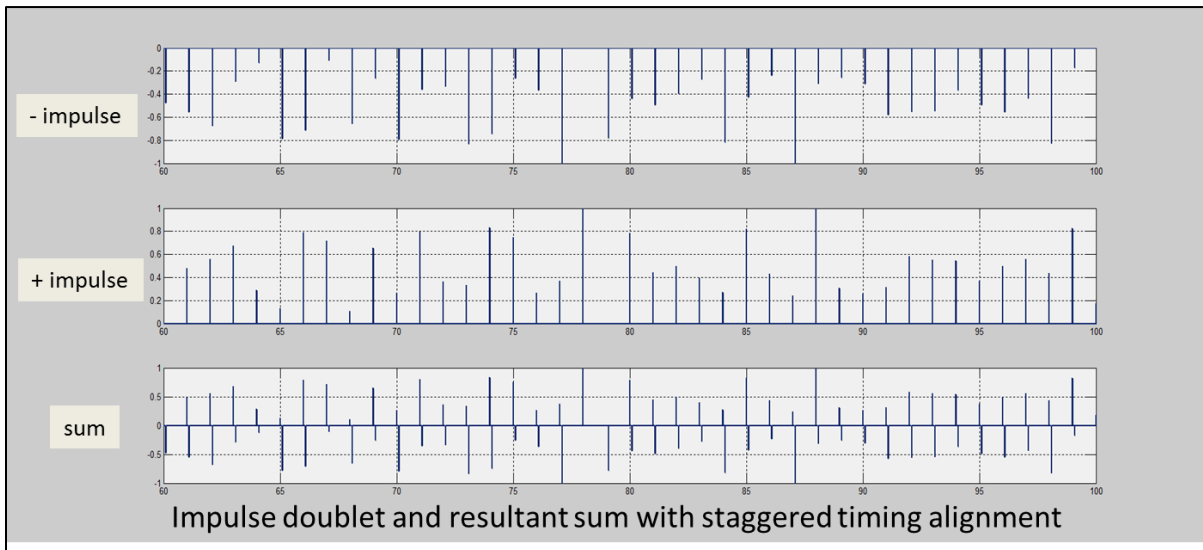


Figure 5-7 Encoding Particle Stream Impulses with Timing Skew, $t_{\varepsilon} \neq 0$

A block diagram suitable for simulating the particle motion follows;

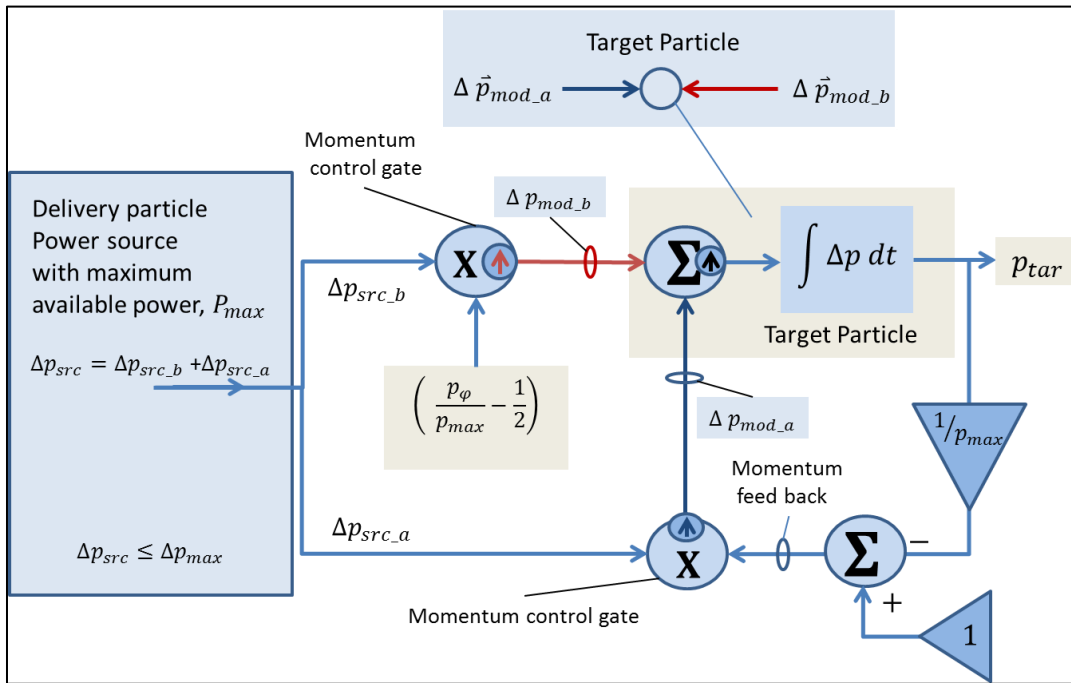


Figure 5-8 Particle Encoding Simulation Block Diagram for Canonical Offset Model

The following sequence of graphics illustrate various signals and waveforms associated with the simulation model of figure 5-8. T_s equals 1 in these simulations.

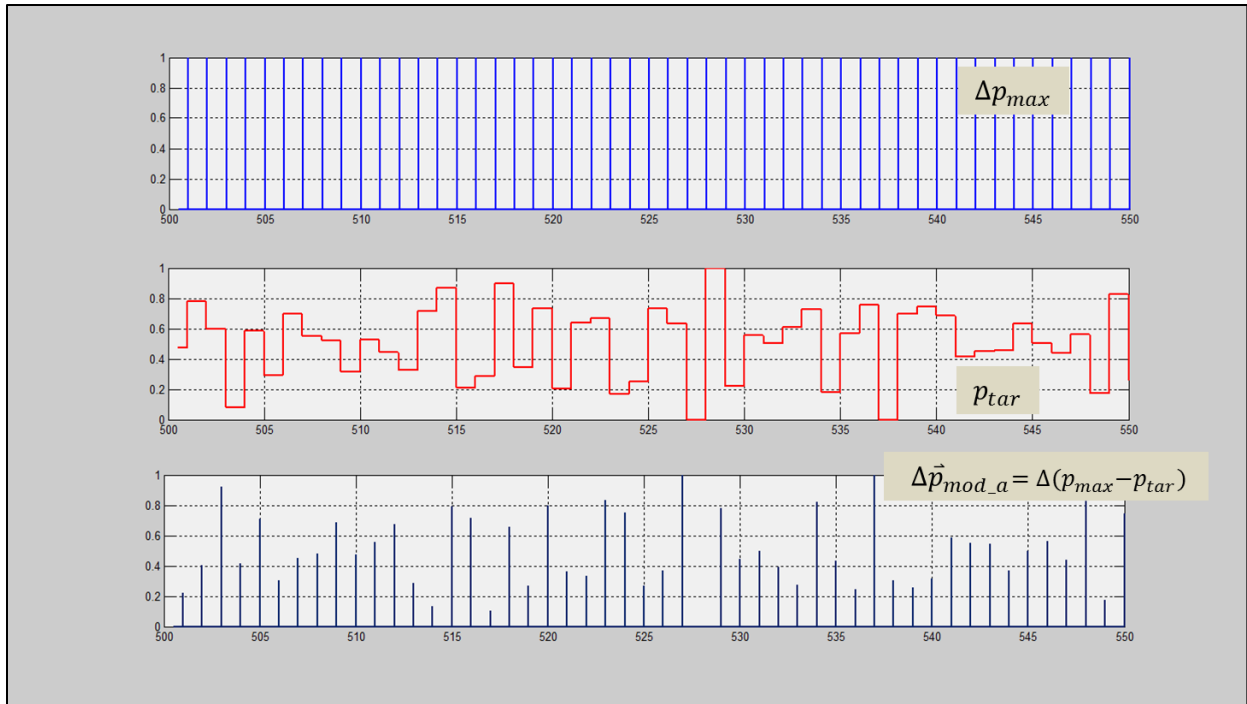


Figure 5-9 Simulation Waveforms and Signals

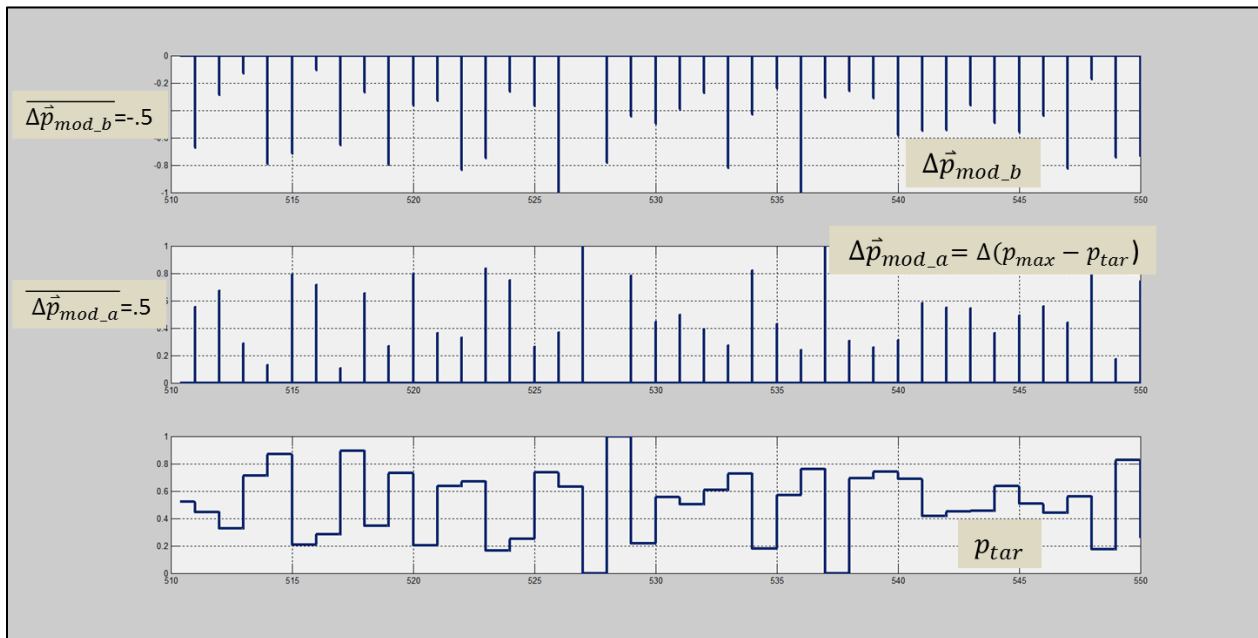


Figure 5-10 Simulation Waveforms and Signals

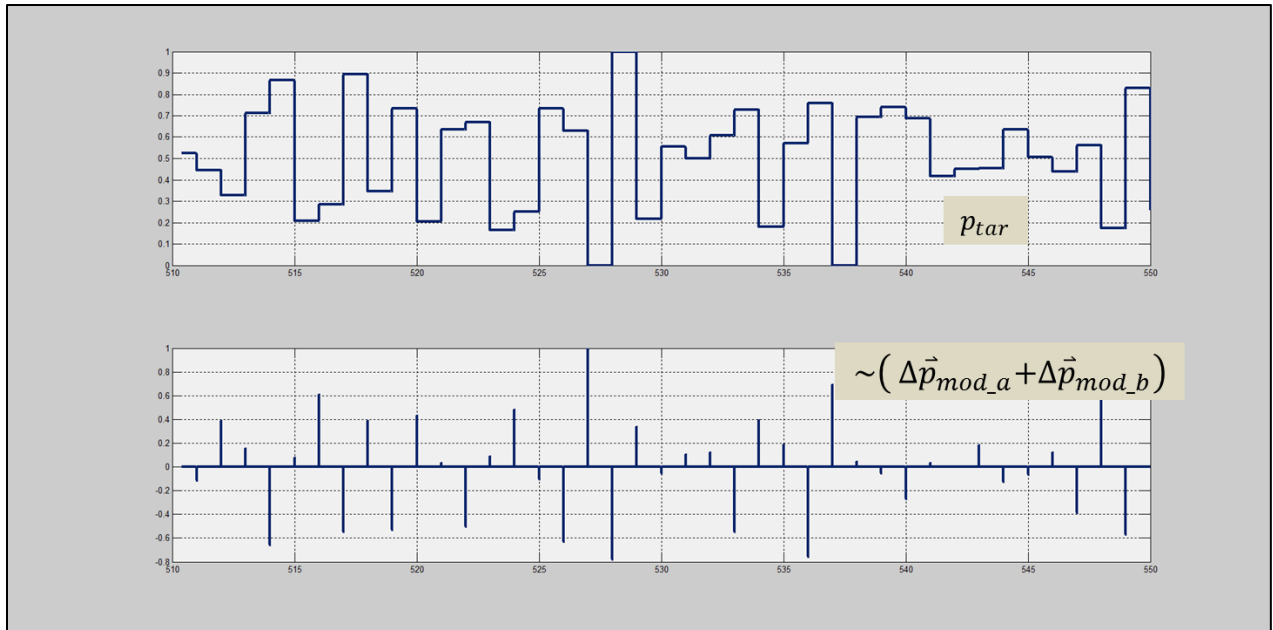


Figure 5-11 Simulation Waveforms and Signals

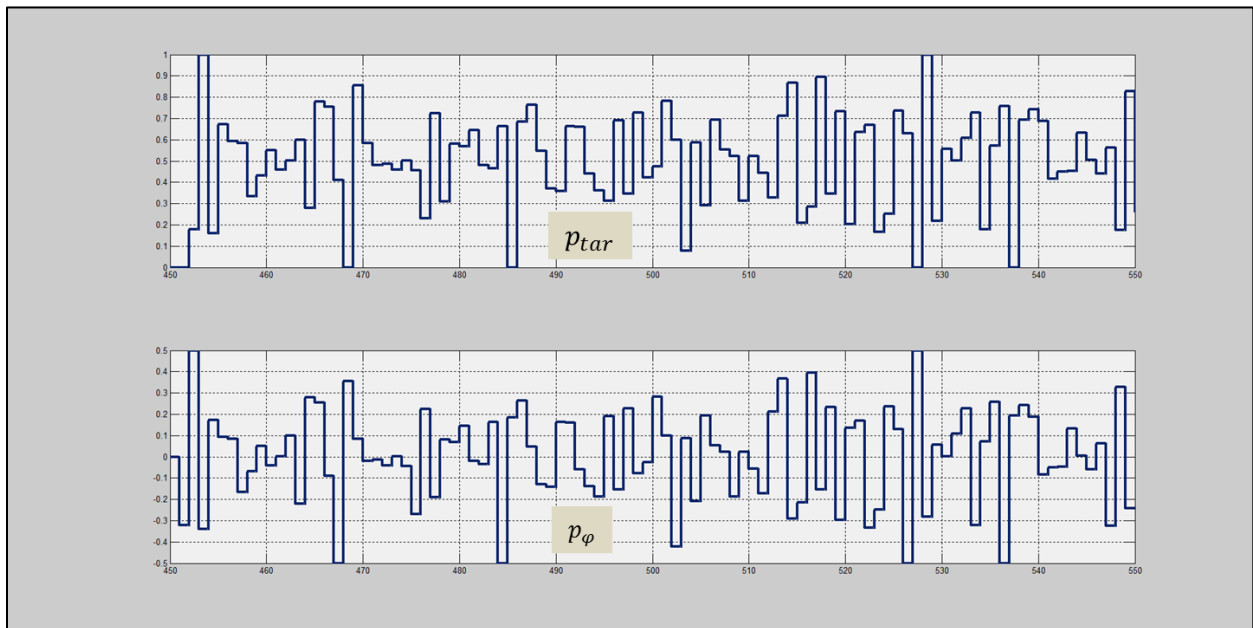


Figure 5-12 Encoded Output and Encoded Input

Figure 5-12 confirms the reproduction of the input signal p_ϕ in the form p_{tar} at the target particle, albeit with an offset. The startup transient near time sample 450 confirms the nature of the feedback convergence of the model. In addition, there is a one sample delay.

The momentum transfers from the power source through two branches labeled p_{src_a} and p_{src_b} . The maximum power transfer from the power source is less than or equal to P_{max} . The momentum flows through these supply paths metered by the illustrated control functions. Due to symmetry, each input supply branch possesses the same average momentum transfer and energy consumption statistics though the instantaneous values fluctuate. In the Δp_{src_b} path, momentum is controlled by an input labeled $\left(\frac{p_\phi}{p_{max}} - \frac{1}{2}\right)$. This unit-less control, gates effective impulse momentum weighting Δp_{src_b} through to the branch segment labeled Δp_{mod_b} such that $\Delta p_{src_b} \sim \Delta p_{mod_b} = \Delta \left(p_\phi - \frac{p_{max}}{2}\right)$, causing deceleration. It is a virtually lossless gating operation analogous to a sluice gate metering water flow supplied by a gravity driven reservoir. Impulse momentum weighting Δp_{src_a} is formed from the difference of the maximum available momentum p_{max} and target particle momentum p_{tar} as indicated by equation 5-7, 5-8. This is a feedback mechanism built into nature through the laws of motion. This feedback control meters the gating function channeling the resource Δp_{src_a} to generate Δp_{mod_a} , which in turn causes forward acceleration. The gating process in the feedback path is also virtually 100 percent efficient so that $\Delta p_{src_a} \sim \Delta p_{mod_a}$.

Given this background, we proceed to calculate the work associated with the two input/delivery particle streams from corresponding cumulative kinetic energy differentials over n exchanges.

$$\begin{aligned}
\langle \Delta \mathcal{E}_k \rangle_{in} &= \langle \Delta \mathcal{E}_k \rangle_{mod_a} + \langle \Delta \mathcal{E}_k \rangle_{mod_b} \\
\langle \Delta \mathcal{E}_k \rangle_{in} &\cong \frac{1}{(2m)n} \sum_{l=1}^n \Delta \vec{p}_{(mod_a)_l}^2 + \frac{1}{(2m)n} \sum_{l=1}^n \Delta \vec{p}_{(mod_b)_l}^2 \\
\langle \Delta \mathcal{E}_k \rangle_{in} &\cong \frac{1}{(2m)n} \sum_{l=1}^n (\Delta [p_{max} - p_{tar_{l-1}}])^2 + \frac{1}{(2m)n} \sum_{l=1}^n \left(\Delta \left[\frac{p_{max}}{2} - p_{\phi_l} \right] \right)^2 \\
\langle \Delta \mathcal{E}_k \rangle_{in} &\cong \frac{1}{(2m)n} \sum_{l=1}^n \left(\Delta \left[\frac{p_{max}}{2} - p_{\phi_l} \right] \right)^2 + \frac{1}{(2m)n} \sum_{l=1}^n \left(\Delta \left[\frac{p_{max}}{2} - p_{\phi_l} \right] \right)^2 \\
&\sim 2 \left\langle \left(\left[\frac{p_{max}}{2} - p_{\phi_l} \right] \right)^2 \right\rangle
\end{aligned}$$

(5-10)

The time average and statistical average are approximately equal for a sufficiently large n , the number of sample intervals observed for computing the average. The final two lines of eq. 5-10 were obtained by substitution of the relevant pdf definitions for p_{ϕ} and p_{tar} (see figures 5-2 and 5-3). Each average can be obtained from the sum of the variance and mean squared, recognizing that the relevant power statistic for both input impulse streams is also given by a non-central Gamma probability density [25,32, and appendix H]. Hence,

$$\langle \Delta \mathcal{E}_k \rangle_{in} = 2 \left(P_{m_e} + \frac{\sigma_{\phi}^2}{2m} \right)$$

$$\sigma_e^2 = \frac{1}{2m} \sigma_\varphi^2$$

$$P_{m_e} = \frac{1}{2m} \left(\frac{p_{max}}{2} \right)^2$$

(5-11)

The effective output power is by definition σ_e^2 and σ_φ^2 is the information momentum pdf of interest. The maximum waveform momentum p_{max} , in 5-11 is twice that of the effective signal momentum. Therefore the efficiency is given by;

$$\eta = \frac{P_e}{P_{in}} = \frac{\sigma_e^2}{2(P_{m_e} + \sigma_e^2)} = \frac{1}{2(PAPR_e + 1)}$$

(5-12)

For large information capacity signals the efficiency is approximately $(2PAPR_e)^{-1}$. This result may also be deduced by noticing that the total input power to the encoding process is split between delivery particles and the target particle. This power may be calculated by inspecting figures 5-2 and 5-3. The target particle power in this process may be calculated from a non-central Gamma RV applied to figure 5-3 or simply obtained from inspection as $P_{tar} = P_e + P_w = \sigma_e^2 + P_{m_e}$. In the example provided, the delivery particles recoil, which is evidence of a form of overhead. The statistic of this recoil momentum is identical to the statistic of figure 5-3 which can be reasoned from the principle of momentum conservation and Newton's laws. Hence, the input power due to conveyed momentum in the exchange and the recoil momentum,

is simply $P_{in} = 2(\sigma_e^2 + P_{m,e})$. The effective output power of the target particle is defined as σ_e^2 and so equations 5-11, 5-12 are justified by inspection.

Figure 5-13 illustrates a physically analytic version of p_{tar} without offset. $\tilde{p}_{tar} = \Delta p_{tar} * h_t$ is a filtered version of Δp_{tar} which corresponds with the result discussed in section 3.1.8. h_t is an effective impulse response for the system created by integrating acceleration and additional non dissipative mechanisms which smooth the particle motion. An analytic boundary condition is obtained by complying with the TE relation and using the methods disclosed in chapter 3. The effective impulse response could be due to some apparatus network of mass, springs and shock absorbers operating on the impulses. The analog for an electronic communications system is obvious where a preferred form of h_t could be implemented by capacitors and inductors organized to enable a “raised cosine” or other suitable filtered impulse response. In addition, the effect of P_m via the TE relation could be used to smooth the delivery particle forces.

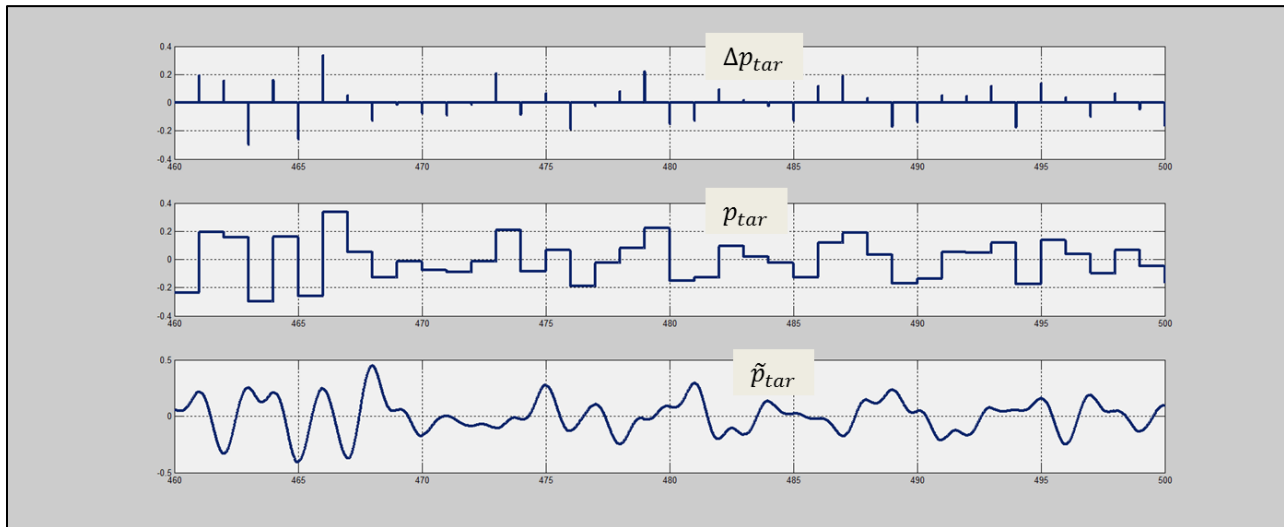


Figure 5-13 Momentum Change, Integrated Momentum Exchange, Analytic Filtered Result

Figure 5-8 is considered to be the offset canonical model because of the offset in p_{tar} of the output waveform of figure 5-12. It is a closed system model because the target particle momentum is not transferred beyond the boundary of the target phase space. However, in a communications scenario, this momentum must also transfer beyond the target particle phase space by some means. In electronic applications, the momentum is primarily transferred through the additional interaction of electromagnetic fields.

Suppose that the model of figure 5-8 is adjusted to reflect the transfer of momentum from the target particle sample by sample to some load outside of the original target particle phase space. In this circumstance, the feedback is no longer active because p_{tar} is effectively regulated sample to sample by transfer of momentum to another load, ensuring a peak target particle velocity which resets to some average value just prior to subsequent input momentum exchanges from delivery particles. This model variation is referred to as an open system canonical model and illustrated in figure 5-14.

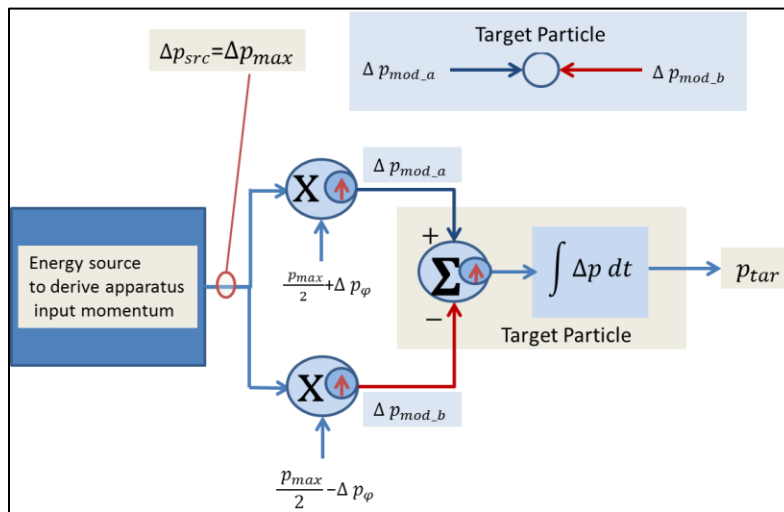


Figure 5-14 Zero Offset Open System Canonical Simulation Model

The following graphic illustrates the waveforms associated with a simulation of fig. 5-14.

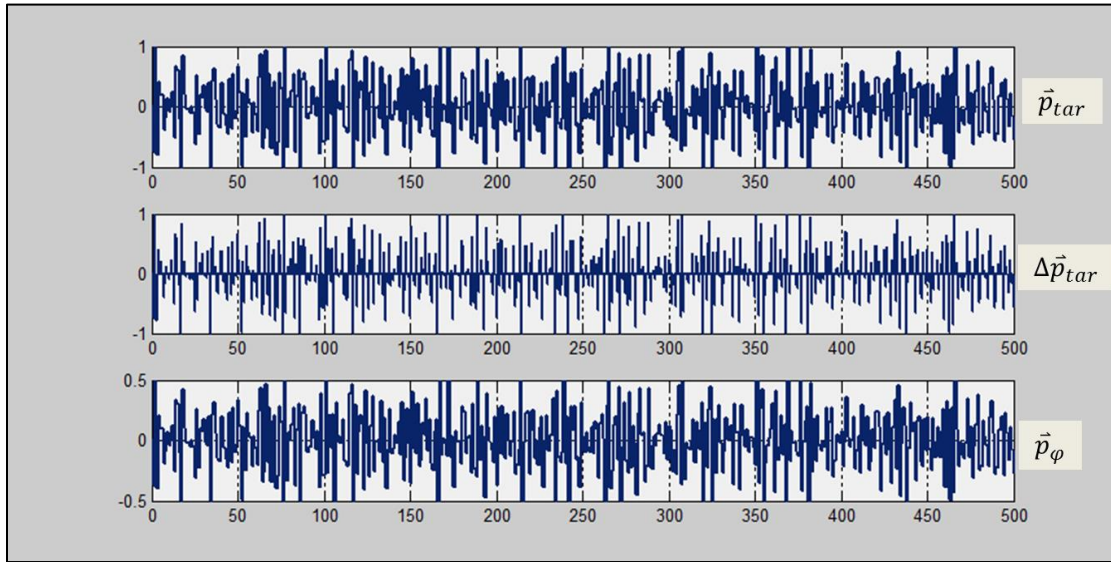


Figure 5-15 Simulation Results for Open System Zero Offset Model

There is an offset for each branch of the apparatus of $p_{max}/2$. The offsets cancel while the random variables $\pm\Delta p_\varphi$ add in a correlated manner to double the dynamic range of the particle momentum peak to peak. The energy source must contemplate this requirement. An efficiency calculation follows the procedures introduced earlier, taking into account the symmetry of the apparatus, offsets, as well as the correlated acceleration and deceleration components.

$$\eta = \frac{P_e}{P_{in}} = \frac{\sigma_e^2}{(P_{m_e} + \sigma_e^2)} = \frac{1}{(PAPR_e + 1)}$$

(5-13)

This model reflects an increase in efficiency over the apparatus of figure 5-8. If the $PAPR_e$ approaches 1 then the efficiency approaches 50%.

5.1.1. Comments Concerning Power Source

The particle motions within the information source are statistically independent from the relative motions of particles in the power source. There is no a priori anticipation of information betwixt the various apparatus functions. A joint pdf captures the basic statistical relationship between the energy source and encoding segment.

$$\rho_{\varphi\varepsilon} = \rho_{\varphi}\rho_{src}$$

(5-14)

$\rho_{\varphi\varepsilon}$ is the joint probability where the covariance of relative motions are zero in the most logical maximum capacity case. The maximum available power resource may or may not be static, although the static case was considered as canonical for analytical purposes in the prior examples. In those examples the instantaneous maximum available resource is always P_{max} , a constant. This is not a requirement, merely a convenience. If the power source is derived from some time variant potential then an additional processing consideration is required in the apparatus. Either the time variant potential must be rectified and averaged prior to consumption or the apparatus must otherwise ensure that a peak energy demand does not exceed the peak available power supply resource at a sampling instant. Given the nature of the likely statistical independence between the particle motions in the various apparatus functions, the most practical solution is to utilize an averaged power supply resource. An alternative is to regulate and coordinate the $PAPR_e$ and hence the information throughput of the apparatus as the instantaneous available power from a power source fluctuates.

5.1.2. Momentum Conservation and Efficiency

Section 5.1 provided a derivation of average thermodynamic efficiency based on momentum exchange sampled from continuous random variables. This section verifies that idea with a more detailed discussion concerning the nature of a conserved momentum exchange. The quantities here are also regarded as recursive changes in momentum at sampling intervals $f_s^{-1} = T_s$, where samples are obtained from a continuous process. The model is based on the exchange of momentum between delivery particles and a target particle to be encoded with information. The encoding pdf is given by $\rho(p_\varphi)$, a Gaussian random variable.

The current momentum of a target particle is a sum of prior momentum and some necessary change to encode information. Successive samples are de-correlated according to the principles presented in chapter 3. The momentum conservation equation is;

$$\sum_i \vec{p}_i^- = \sum_i \vec{p}_i^+ = C$$

(5-15)

C is a constant. \vec{p}_i^- is the i^{th} particle momentum t_ϵ seconds just prior to the n^{th} momentum exchange. \vec{p}_i^+ is the i^{th} particle momentum just after the n^{th} momentum exchange.

$$\vec{p}_i^- = \vec{p}_i(t - nT_s + t_\epsilon)$$

$$\vec{p}_i^+ = \vec{p}_i(t - nT_s - t_\epsilon)$$

In the following example only two particles are deployed per exchange. In concept, many particles could be involved.

Figure 5-16 illustrates the possible single axis relative motions of the delivery and target particles prior to exchange.

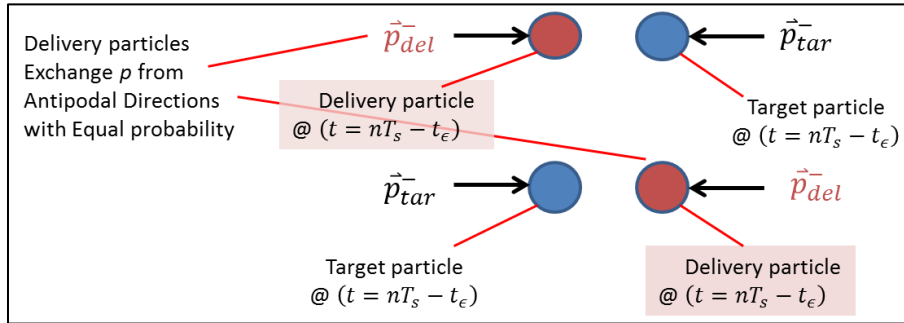


Figure 5-16 Relative Particle Motion Prior to Exchange

After the sample instant, i.e. the momentum exchange, the particles recoil as illustrated in figure 5-17 for the first of the cases illustrated in 5-16.

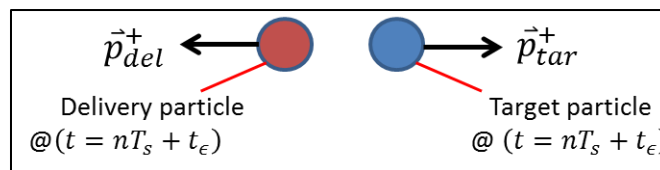


Figure 5-17 Relative Particle Motion after an Exchange

More explicitly we write the conservation equation over n exchanges;

$$\sum_n [\vec{p}_{del}^- + \vec{p}_{tar}^-]_n = \sum_n [\vec{p}_{del}^+ + \vec{p}_{tar}^+]_n$$

(5-16)

First we examine the case of differential information encoding. The information is encoded in momentum differentials of the target particle rather than absolute quantities.

$$\vec{p}_{tar}^+ - \vec{p}_{tar}^- = \Delta\vec{p}_{tar}$$

Also it follows that;

$$\langle \vec{p}_{del}^- \rangle = \langle \vec{p}_{tar}^+ - \vec{p}_{tar}^- \rangle = \langle \Delta\vec{p}_{tar} \rangle$$

This comes from the fact that particle motions are relative and random with respect to one another, and the exchanging particles possess the same mass. $\vec{p}_{del}^- = \vec{p}_\phi + \langle \vec{p}_{del}^- \rangle$ is exchanged in a set of impulses at the delivery and target particle interface at the sample instants, $t = nT_s$.

$\langle \vec{p}_{del}^- \rangle$ is an average overhead momentum for the encoding process. Using the various definitions the conservation equation may be restated as;

$$\sum_n [\vec{p}_\phi + \langle \vec{p}_{del}^- \rangle]_n = \sum_n [\vec{p}_{del}^+ + \Delta\vec{p}_{tar}]_n$$

(5-17)

\vec{p}_{del}^+ on the right side of 5-17 can be discarded in efficiency calculations since it is a delivery particle recoil momentum and therefore output waste. Now we proceed with the efficiency calculation which utilizes the average energies from the momentum exchanges.

$$\eta \left(\frac{1}{n} \sum_n [\vec{p}_\phi + \langle \vec{p}_{del}^- \rangle]_n^2 \right) = \frac{1}{n} \sum_n [\Delta\vec{p}_{tar}]_n^2$$

The left hand side of the above equation represents the input energy of delivery particles prior to exchange multiplied by efficiency. The right hand side represents the desired output signal

energy associated with a differential encoded target particle. For large n we approximate the sample averages with the time averages so that;

$$\eta \left(\langle (\vec{p}_\varphi)^2 \rangle + \langle 2\vec{p}_\varphi \langle \vec{p}_{del}^- \rangle \rangle + \langle (\vec{p}_{del}^-)^2 \rangle \right) = \langle (\Delta \vec{p}_{tar})^2 \rangle \quad (5-18)$$

We can calculate the efficiency along the α^{th} axis from;

$$\eta_\alpha = \left[\frac{P_{out}}{P_{in}} \right]_\alpha = \frac{\langle (\Delta p_{tar})^2 \rangle_\alpha}{\langle (p_\varphi)^2 \rangle_\alpha + \langle p_{del}^- \rangle_\alpha^2} \quad (5-19)$$

We now specify an encoding pdf such that $\max\{p_\varphi\} = \langle p_{del}^- \rangle$ (ref. figures 5-2, 5-3) Also, in the differential encoding case, $\langle (\Delta p_{tar})^2 \rangle \equiv \langle (p_\varphi)^2 \rangle$, with a zero mean Δp_{tar} .

Now the averaged efficiency over all dimensions may be rewritten as;

$$\eta = \sum_\alpha \frac{\lambda_\alpha \langle (p_\varphi)^2 \rangle_\alpha}{\langle (p_\varphi)^2 \rangle_\alpha + (\max\{p_\varphi\})_\alpha^2} = \frac{\langle (p_\varphi)^2 \rangle}{\langle (p_\varphi)^2 \rangle + (\max\{p_\varphi\})^2} = \frac{1}{1 + PAPR} \quad (5-20)$$

λ_α is a probability weighting of the efficiency in the α^{th} dimension. Equation 5-20 is the efficiency of the differentially encoded case. When the $PAPR$ is very large the efficiency may be approximated by $(PAPR)^{-1}$.

Now suppose that we define the encoding to be in terms of absolute momentum values where the target particle momentum average is zero as a result of the symmetry of the delivery particle motions. The momentum exchanges per sample are independent Gaussian RV's so that the two sample variance forming $\langle(\Delta p_{tar})^2\rangle$ is twice that of the absolute quantity $\langle(p_{tar}^+)^2\rangle$. That is, $\langle(p_{tar}^+)^2\rangle = \frac{1}{2}\langle(p_\phi)^2\rangle$. If the same *PAPR* is stipulated for the comparison of the differential and absolute encoding techniques then the average of the delivery particle momentum must scale as $\frac{1}{\sqrt{2}}$, and we obtain;

$$\eta = \frac{\frac{1}{2}\langle(p_\phi)^2\rangle}{\langle(p_\phi)^2\rangle + \left(\frac{1}{\sqrt{2}}\max\{p_\phi\}\right)^2} = \frac{1}{2(PAPR + 1)}$$

(5-21)

In the most general encoding cases the efficiency may be written as;

$$\langle\eta\rangle = \frac{\sigma^2}{k_{mod}P_m + k_\sigma\sigma^2}$$

σ^2 is desired output signal power and k_{mod} , k_σ are constants which absorb the variation of potential apparatus implementations and contemplate other imperfections as well.

5.1.3. A Theoretical Limit

Figures 5-16 and 5-17 illustrate the case for particles where each exchange possesses a random recoil momentum because the motions of delivery and target particles are not synchronized and a

material particle possesses a finite speed. If we posit a circumstance where the momentum of each delivery particle is 100% absorbed in an exchange then the efficiency can approach a theoretical limit of 1 given a fully differential zero offset scenario. In this hypothetical case

$$\eta = \frac{P_{out}}{P_{in}} = \frac{\sum_{\alpha} \lambda_{\alpha} \langle (\Delta p_{tar})^2 \rangle_{\alpha}}{\sum_{\alpha} \lambda_{\alpha} \langle (p_{\phi})^2 \rangle_{\alpha}}$$

Suppose that a stream of virtual delivery particles, such as photons, acts upon a target particle. Each delivery particle possesses a constant momentum used to accelerate or decelerate the target particle and the desired target particle statistic \vec{p}_{ϕ} is created by the accumulation of n impulse exchanges over time interval T_s . The motion of the target particle with statistic \vec{p}_{ϕ} is verified by sampling at intervals of time $t - \ell T_s$ where ℓ is a sample index for the target particle signal.

Also, we identify the time averages $\langle (\vec{p}_{\phi})^2 \rangle \leq \langle (\vec{p}_{del})^2 \rangle$ and $\langle (\vec{p}_{del})^2 \rangle \leq \langle [max\{\vec{p}_{del}\}]^2 \rangle$. We further assume that the statistics in each dimension are *iid* so that efficiency is a constant with respect to α .

Time averages may be defined by the following momentum quantities imparted to the target particle by the delivery particles over n impulses exchanges per sample interval and N samples where N is a suitably large number;

$$\langle (p_{\phi})^2 \rangle \equiv \frac{1}{NT_s} \sum_{\ell=1}^N \sum_n [(p_{del})^2]_n$$

$$max\{(p_{\phi})^2\} \equiv \frac{1}{T_s} \sum_{\ell=1}^N \sum_n [max\{(p_{del})^2\}]_n$$

And finally;

$$\eta \leq \frac{\frac{1}{NT_s} \sum_{\ell=1}^N \sum_n [(p_{del})^2]_n}{\frac{1}{T_s} \sum_{\ell=1}^N \sum_n [\max\{(p_{del})^2\}]_n} = \frac{1}{PAPR}$$

(5-22)

Equation 5-22 presumes that n the number of delivery particle impulses over the material particle sample time T_s can be much greater than 1.

When $PAPR \rightarrow 1$ the efficiency approaches 1. An example of this circumstance is binary antipodal encoding where the momentum encoded for two possible discrete states or the momentum required to transition between two possible states is equal and opposite in direction and $\dot{p} \rightarrow \infty$.

This would be a physically non-analytic case.

5.2. Capacity vs. Efficiency Given Encoding Losses

Encoding losses are losses incurred for particle momentum modulation where the encoding waveform is an information bearing function of time. This may be viewed as a necessary but inefficient activity. If the momentum is perfectly Gaussian then the efficiency tends to zero since the $PAPR$ for the corresponding motion is infinite. However, practical scenarios preclude this extreme case since P_m is limited. Therefore, in practice, some reasonable $PAPR$ can be assigned such that efficiency is moderated yet capacity not significantly impacted.

A direct relationship between *PAPR* and capacity can be established from the capacity definition of equation 4-14.

$$C = \max\{\overline{I(x; y)}\} = \max\{H(y) - H_x(y)\}$$

As before we shall assume an AWGN which is band limited but we relax the requirement for the nature of $\rho(p)$ such that a Gaussian density for momentum is not required. Also the following capacity discussion is restricted to a consideration of continuous momentum since the capacity obtained from position is extensible. Technically we are considering a qualified capacity or pseudo capacity \tilde{C} whenever $\rho(p)$ is not Gaussian, yet $\rho(p)$ is still descriptive of continuous encoding.

$$\tilde{C} = \max \left\{ - \int_{p_{ul}}^{p_{ul}} \rho(p_y) \ln[\rho(p_y)] dp_y - \frac{1}{2} \ln(\sqrt{2\pi}e\sigma_n) \right\} \quad (5-23)$$

We can rewrite equation 5-22 with a change of variables $z = p_y/\sigma_{p_y}$ as follows;

$$\tilde{C} = \max \left\{ -\sigma_{p_y} \int_{z_{ul}}^{(\sqrt{PAER})_y} \rho(z) \ln[\rho(z)] dz - \frac{1}{2} \ln(\sqrt{2\pi}e\sigma_n) \right\} \quad (5-24)$$

For a given value of momentum variance $\sigma_{p_y}^2$ with a fixed SNR ratio $\frac{(\sigma_{p_x})^2}{(\sigma_{p_n})^2}$, an increase

in $(\sqrt{PAER})_y$ always increases the integral of 5-23 and therefore increases pseudo capacity \tilde{C} .

This can also be confirmed by finding the derivative of \tilde{C} with respect to $(\sqrt{PAER})_y$ with the lower limit in eq. 5-23 held constant.

$$\frac{d\tilde{C}}{d(\sqrt{PAER})_y} = \rho(\sqrt{PAER}) \ln[\rho(\sqrt{PAER})]$$

(5-25)

Equation 25 confirms that capacity is a monotonically increasing function of $PAER$ without bound.

$(\sqrt{PAER})_y$ includes the consideration of noise as well as signal. When the noise is AWGN and statistically independent from the signal;

$$\sigma_{p_y} = \sqrt{(\sigma_{p_x})^2 + (\sigma_{p_n})^2} \quad , \quad \sigma_y = \sqrt{(\sigma_x)^2 + (\sigma_n)^2}$$

Thus $PAPR_y = P_m / \sigma_y^2$ is the output peak to average power ratio for a corrupted signal.

$PAPR_y$ may be obtained in terms of the effective peak to average ratio for the signal as;

$$PAPR_y = \frac{\sigma_e^2}{\sigma_y^2} PAPR_e + \frac{\sigma_n^2}{\sigma_y^2} PAPR_n + \frac{\sqrt{P_{m-e}}\sqrt{P_{m-n}}}{\sigma_y^2}$$

$PAPR_n$ is the peak to average power ratio for the noise. $PAPR_y$ is of concern for a receiver analysis since the contamination of the desired signal plays a role. In the receiver analysis where the noise or interference is significant, a power source specification P_m must contemplate the extreme fluctuation due to $p_x + p_n$. The efficiency of the receiver is impacted since the phase space must be expanded to accommodate signal plus noise and interference so that information is not lost as discussed in chapter 3.

Most often, the efficiency of a communications link is dominated by the transmitter operation. That is, the dominant noise is due to some environmental perturbation added after the target particle has been modulated. We thus proceed with a focus on the transmitter portion of the link.

Whenever the signal density is Gaussian we then have the classical result;

$$\lim_{PAER \rightarrow \infty} \tilde{C} = \max \left\{ -\sigma_{p_y} \int_{-\infty}^{\infty} \rho(z) \ln[\rho(z)] dz + \frac{1}{2} \ln(\sqrt{2\pi e} \sigma_n) \right\} = \ln(\overline{SNR}_{eq} + 1) = C \quad (5-26)$$

It is possible to compare the pseudo-capacity or information rate of some signaling case to a reference case like the standard Gaussian to obtain an idea of relative performance with respect to throughput for continuously encoded signals.

We now define the relative continuous capacity ratio figure of merit from;

$$C_r = \frac{\tilde{C}_{\rho_x}}{C_G} = \frac{\max \left\{ -\int_{p_{ul}}^{p_{ul}} \rho(p_y) \ln[\rho(p_y)] dp_y - \frac{1}{2} \ln(\sqrt{2\pi e} \sigma_n) \right\}}{\ln \left(\frac{\sigma_G^2}{\sigma_n^2} + 1 \right)} = \frac{H_y - H_x(y)}{[\ln(\overline{SNR}_{eq} + 1)]} \quad (5-27)$$

The uncertainty H_y is due to a random signal plus noise. C_G is a reference AWGN channel capacity found in chapter 4 and \tilde{C}_{ρ_x} is a pseudo-capacity calculated with the pdf describing the signal random variable of interest. The noise is band limited AWGN with entropy $H_x(y) = H_n$. There are several choices for the constituents of C_r such as the SNR's of numerator and denominator as well as the form of the probability densities involved. A preferred method specifies the denominator as the maximum entropy case for a given variance. Nevertheless, the relative choice of numerator and denominator terms can tailor the nature of comparison.

A precise calculation of C_r first involves finding the numerator pdf for the sum of signal plus noise RV's. When the signal and noise are completely independent then the separate pdf's may be convolved to obtain the pdf, ρ_y , of their sum. A generalization of C_r is possible whenever the numerator and denominator noise entropy are identical and when the signal of interest is statistically independent from the noise. In this circumstance a capacity ratio bound can be obtained from;

$$C_r \leq \log_{\left\{\frac{\sigma_G^2}{\sigma_n^2} + 1\right\}} \left[\frac{k\sigma_G^2}{\sigma_n^2} + 1 \right]; \quad 0 \leq k \leq 1$$

(5-28)

k is a constant and σ_x^2 is the variance of a signal which is to be compared to the Gaussian standard. k is determined from the entropy ratio H_r of the signal to be compared to the standard entropy, $\ln(\sqrt{2\pi e}\sigma_G)$. Most generally, the value for C_{ρ_x} must be explicitly obtained from the

integral in 5-26. However, C_{ρ_x} may also be known for some common distributions like for instance a continuous uniform distribution.

H_r is the relative entropy ratio for an arbitrary random variable compared to the Gaussian case with a fixed variance. A bounded value for H_r can be estimated by assuming that the noise and signal are statistically independent and uncorrelated. It has been established that the reference maximum entropy process is Gaussian so that for a given variance all other random variables will possess lower relative differential entropies. This means that $H_r \leq 1$ for all cases since $H_{\rho_x} \leq H_{G_x}$. Thus;

$$H_r \equiv \frac{H_{\rho_x}}{H_{G_x}} = \frac{H_{\rho_x}}{\ln(\sqrt{2\pi e}\sigma_x)}$$

An example illustrates the utility of H_r . We find H_r for the case when the signal is characterized by a continuous uniform pdf over $\{-v_{max}, v_{max}\}$ ($m = 1$). In that case ;

$$H_r = \frac{\ln(2 p_{max})}{\ln(\sqrt{2\pi e}\sigma)} = \frac{\ln(2\sqrt{3})}{\ln(\sqrt{2\pi e})} \approx .876$$

The variance of the Gaussian reference signal and the uniformly distributed signal are equated in this example ($\sigma_G^2 = \sigma_U^2 = 1$) to obtain a relative result. At large SNR, the capacity ratio can be approximated;

$$C_r = \frac{H_{\rho_y} - H_{p_n}}{H_G - H_n} \approx \frac{H_{\rho_x}}{H_G} = H_r \quad ; \quad \text{for } \overline{SNR}_{eq} \gg 1$$

(5-29)

Therefore, the capacity for the band limited AWGN channel when the signal is uniformly distributed and power limited, is approximately .876 that of the maximum capacity case whenever the AWGN of the numerator and denominator are not dominant. Appendix J provides additional detail concerning the comparison of the Gaussian and continuous uniform density cases.

In general, the relative entropy is calculated from;

$$H_r = \frac{\int_{-v_{max}}^{+v_{max}} \rho(v) \ln \rho(v) dv}{\int_{-\infty}^{+\infty} \rho_G(v) \ln \rho_G(v) dv}$$

(5-30)

$\rho(v)$ is the pdf for the signal of analysis and $\rho_G(v)$ is the Gaussian pdf. v_{max} is a peak velocity excursion. The denominator term is the familiar Gaussian entropy, $\ln(\sqrt{2\pi e}\sigma_G)$.

This formula may be applied to the case where $\rho(v)$ for the numerator distribution of a $C_r \approx H_r$ calculation is based on a family of clipped or truncated Gaussian velocity distributions. η is inversely related to $PAPR$ by some function as indicated by two prior examples using particle based models, summarized in equations 5-11 and 5-12. $PAPR$ can be found where $\pm v_{max}$ indicates the maximum or clipped velocities of each distribution.

$$PAPR = \frac{v_{max}^2}{\int_{-v_{max}}^{+v_{max}} v^2 \rho(v) dv}$$

(5-31)

The following graphics illustrate the relationship between the relative capacity ratio, $PAPR$, and η for a single degree of freedom at high SNR where $\rho(v)$ is a truncated Gaussian density function. Both variance and $PAPR$ may vary in the numerator function compared to the reference Gaussian case of the denominator, though the variance must never be greater than unity when the denominator is based on the classical Gaussian case. Notice in figure 5-18 that the relative entropy and therefore potential capacity reduces significantly as a function of $PAPR$. The lowest $PAPR = 1$ of the graph approximates the case of a constant (the mean value of the Gaussian density) and therefore results in an entropy of zero for the numerator of the H_r calculation.

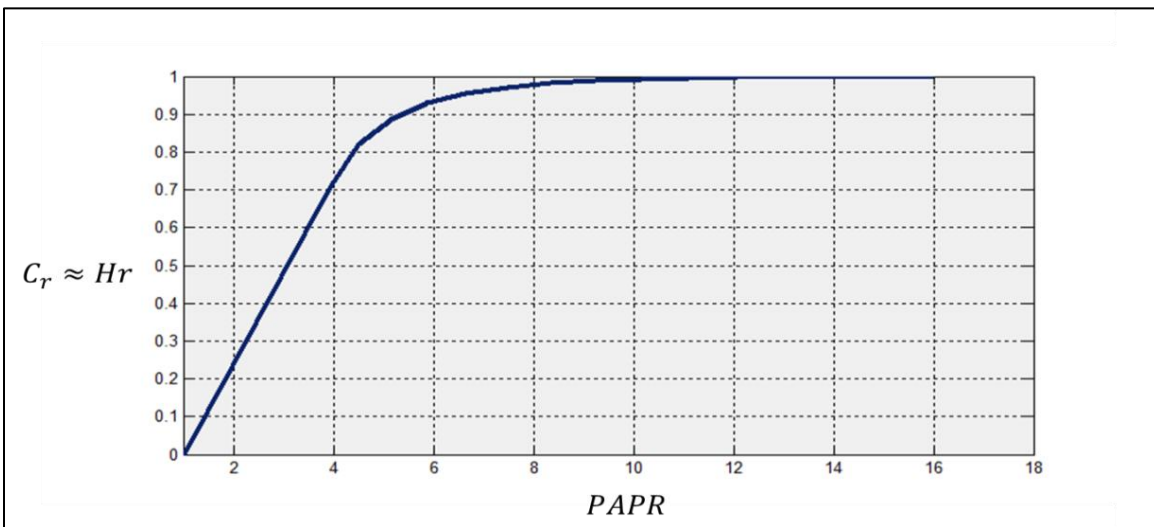


Figure 5-18 Capacity ratio for truncated Gaussian distributions vs. $PAPR$ for large SNR

Figure 5-19 assumes an efficiency due to a particle based encoding model illustrated in 5-14 with efficiency given by equation 5-12.

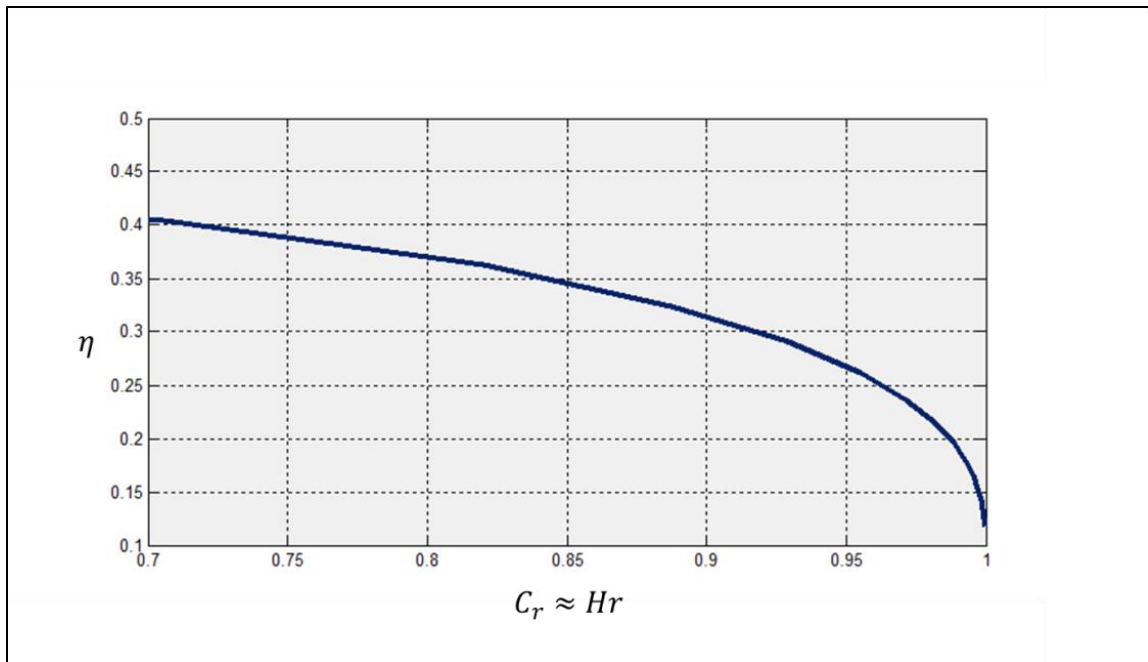


Figure 5-19 Efficiency vs. Capacity ratio for Truncated Gaussian Distributions & Large SNR

The results indicate that preserving greater than 99% of the capacity results in efficiencies lower than 15 percent for these particular truncated distribution comparisons. In the cases where the Gaussian distribution is significantly truncated, the momentum variable extremes are not as great and efficiency correspondingly increases. However, the corresponding phase space is eroded for the clipped signal cases thereby reducing uncertainty and thus capacity. A *PAPR* of 16 (12 dB) preserves nearly all the capacity for the Gaussian case while an efficiency of 40% can be obtained by giving up approximately 30 % of the relative capacity.

As another comparison of efficiency, consider figure 5-20 which illustrates the number of encoded Joules per nat (JPN) for the truncated Gaussian densities vs. *PAPR* given 1 kg mass of encoding .

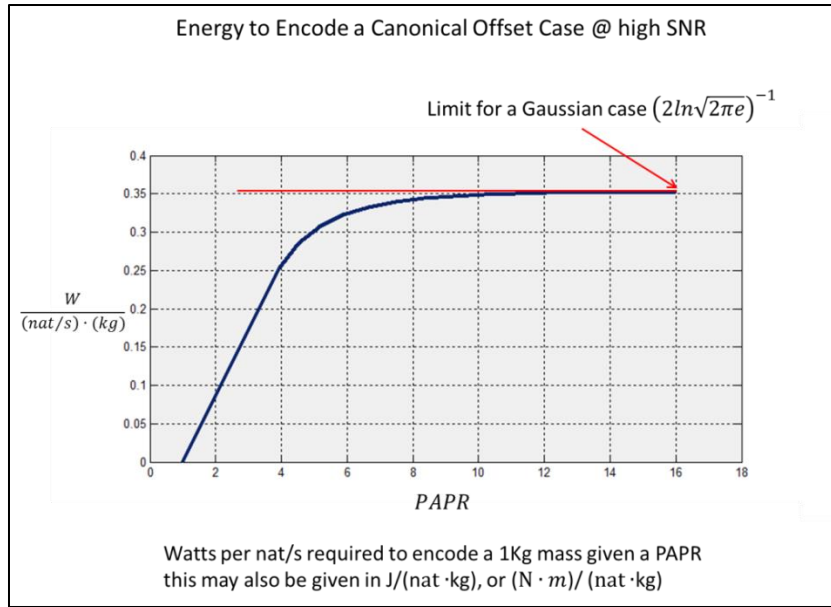


Figure 5-20 Canonical Offset Encoding Efficiency

For relatively low *PAPR*, an investment of energy is more efficiently utilized to generate 1 nat/s of information (i.e. *PAPR* is inversely proportional to efficiency). However, the total number of nats instantly accessible and associated with the physical encoding of phase space, is also lower for the low *PAPR* case compared to the circumstance of high *PAPR* maximum entropy encoding. Another way to state this is; there are fewer nats imparted per momentum exchange for a phase space when the *PAPR* of particle motion is relatively low. Even though a low *PAPR* favors efficiency, more particle maneuvers are required to generate the same total information entropy compared to a higher *PAPR* scenario when the comparison occurs over an equivalent time interval. Message time intervals, efficiency, and information entropy are interdependent.

The TE relation illustrates the energy investment associated with this process as given by eq. 5-5 and modified to include a consideration of capacity. In this case $\mathfrak{F}\{\tilde{C}\}$ is some function of

capacity. The prior analysis indicates the nonlinearly proportional increase of $\mathfrak{J}\{\tilde{\mathcal{C}}\}$ for an increasing $PAPR_e$. The following TE relation equivalent combines elements of time, energy, and information where information capacity $\tilde{\mathcal{C}}$ is a function of $PAPR_e$ and vice versa. We shall refer to this or substantially similar form (eq. 5-32) as a TEC relation, or time-energy-capacity.

$$\langle \eta \rangle = \frac{P_{m,e}}{f_s \langle \mathcal{E}_{in} \rangle_s PAPR_e} \leq \frac{P_{m,e}}{f_s \langle \mathcal{E}_{in} \rangle_s \mathfrak{J}\{\tilde{\mathcal{C}}\}} \quad (5-32)$$

If the power resource, sample rate and average energy per momentum exchange for the process are fixed then;

$$\langle \eta \rangle \leq \frac{k}{\mathfrak{J}\{\tilde{\mathcal{C}}\}} \quad (5-33)$$

k is a constant. As $\mathfrak{J}\{\tilde{\mathcal{C}}\}$ increases $\langle \eta \rangle$ decreases. This trend is always true. The exact form of $\mathfrak{J}\{\tilde{\mathcal{C}}\}$ depends on the realization of the encoding mechanisms. The \leq operator accounts for the fact that an implementation may always be made less efficient if the signal of interest is not required to be of maximum entropy character over its span $\{-p_{max}, p_{max}\}$.

Since $\mathfrak{J}\{\tilde{\mathcal{C}}\}$ is not usually a convenient function, it is often expedient to use one of several techniques for calculating efficiency in terms of capacity. The alternate related metric $PAPR_e$ may be used then related back to capacity. Numerical techniques may be exploited such as those used to produce the graphics of figures 5-18,5-19, and 5-20. A suitable convenient

approximation of the function depicted by graphic 5-18 is sometimes available. For instance, $PAPR_e$ can be approximated as follows;

$$PAPR_e \approx \left(3.1 \tanh^{-1} \left[\frac{\tilde{c}}{1.4189385} \right] \right) + 1$$

(5-34)

The numerical constant in the denominator of the inverse hyperbolic tangent argument is the entropy for a Gaussian distribution with variance of unity. When C_r tends to a value of 1 then $PAPR_e$ tends to infinity. Figures 5-18 and 5-19 illustrate that efficiency tends to zero for the truncated Gaussian example and $PAPR_e \rightarrow \infty$. When $C_r = .7$ the corresponding calculations using eq.5-35 and figure 5-18 predict a $PAPR_e \approx 3.886$ and an efficiency of approximately 40 % is likewise deduced. This result is also apparent by comparing the graphs from figures 5-18 and 5-19.

This approximation is now re-examined using the general result extrapolated from equation 5-32, a TEC relation, and some numbers from an example given in section 3.1.6. For our truncated Gaussian case then;

$$\langle \eta \rangle \approx \frac{P_{m_e}}{f_s \langle \mathcal{E}_{in} \rangle_s \left[\left(3.1 \tanh^{-1} \left[\frac{\tilde{c}}{1.4189385} \right] \right) + 1 \right]} = \frac{k}{\left[\left(3.1 \tanh^{-1} \left[\frac{\tilde{c}}{1.4189385} \right] \right) + 1 \right]}$$

(5-35)

$f_s, \langle \mathcal{E}_{in} \rangle_s$ and P_{m_e} are easily specified or measured system values in practice. We use the following values from the example of section 3.1.6 to illustrate the application of this approximation and the consistency of the various expressions for efficiency developed thus far.

$P_{m_e} = 1$ Joule, $\langle \mathcal{E}_k \rangle_s = 10 \times 10^{-6}$ Joules, $f_s = 2.5 \times 10^4$ momentum exchanges per second

If we wish a maximum capacity solution then the efficiency tends to zero in equation 5-35 verifying prior calculations. If we would like to preserve 70 % of the maximum capacity solution then the efficiency should tend to 40% confirming the prior calculation. This would require that $k \cong 1.554$ for consistency between the formulations of 5-35 and numerical techniques related to the transcendental graphic procedure leveraging figures 5-18 and 5-19. Using the values for P_{m_e} , f_s and the fact that $\langle \mathcal{E}_k \rangle_s = \langle \mathcal{E}_{in} \rangle_s \eta$ we can easily verify that;

$$k = \frac{P_{m_e}}{f_s \langle \mathcal{E}_{in} \rangle_s} = \frac{1}{.625} = 1.6$$

Alternately, if we insist that $k = 1.554$ then the efficiency calculates to 39.98 %. This is a good approximation and a verification of consistency between the various theories and techniques developed to this point.

It is apparent from the prior examples, that we may choose a variety of ratios and metrics to compare how arbitrary distributions reduce capacity in exchange for efficiency compared to some reference like the Gaussian norm. The curves of 5-18, 5-19 and 5-20 will change depending on the distributions to be compared and encoding mechanisms but the trend is always the same. Lower *PAPR* increases efficiency but decreases capacity compared to a canonical case.

5.3. Capacity vs. Efficiency Given Directly Dissipative Losses

Directly dissipative losses refer to additional energy expenditures due to drag, viscosity, resistance, etc. These time variant scavenging affects impact the numerator component of the \overline{SNR}_{eq} term in the capacity equations of chapter 4 by reducing the available signal power. As direct dissipation increases, the available \overline{SNR}_{eq} also decreases thereby reducing capacity.

The relationship between channel capacity and efficiency η_{diss_alpha} can be analyzed by recalling the capacity equations of chapter 4 and substituting the total available energy for supporting particle motion into the numerator portion of \overline{SNR}_{eq} .

$$C \leq \sum_{\alpha=1}^D f_{s_\alpha} (\ln[\overline{SNR}_{eq} + 1])$$

$$C \leq \sum_{\alpha=1}^D f_{s_\alpha} \left(\ln \left[m^2 \frac{(\langle P_e \rangle \langle \eta_{diss_alpha} \rangle)}{\tilde{\sigma}_{p_{n_alpha}}^2} + 1 \right] \right); \quad 0 \leq \eta_{diss_alpha} \leq 1$$

(5-36)

As the average efficiency $\langle \eta_{diss_alpha} \rangle$ reduces, the average signal power $\langle P_e \rangle$ must increase to maintain capacity.

5.4. Capacity vs. Total Efficiency

In this section both direct and modulation efficiency (η_{diss}, η_{mod}) impacts are combined to express a total efficiency. The total efficiency is then $\eta = \eta_{diss}\eta_{mod}$ where η_{mod} is the efficiency due to modulation loss described in sections 5.1 and 5.2.

We may use the procedure and equations developed in section 5.2 to obtain a modified TEC relation;

$$\langle \eta \rangle = \eta_{diss}\eta_{mod} \leq \frac{P_{m,e}}{f_s \langle \mathcal{E}_{in} \rangle_s \mathfrak{S}\{\tilde{C}\}}$$

$$\langle \mathcal{E}_k \rangle_s = \langle \mathcal{E}_{in} \rangle_s \eta_{diss}\eta_{mod}$$

(5-37)

The capacity equation 5-36 may be modified to include overall efficiency $\eta = \eta_{diss}\eta_{mod}$. The following equation applies only for the case where the signal is nearly Gaussian. As indicated before, this requires maintaining a *PAPR* of nearly 12 dB with only the extremes of the distribution truncated.

$$C \leq \sum_{\alpha=1}^D f_{s\alpha} \left(\ln \left[m^2 \frac{(\langle P_{src} \rangle \eta_{diss_alpha} \eta_{mod_alpha})}{\tilde{\sigma}_{p_{n\alpha}}^2} + 1 \right] \right);$$

(5-38)

η has a direct influence on the effective signal power, $P_e = \langle P_{src} \rangle \eta_{diss_alpha} \eta_{mod_alpha}$. When the average signal power output decreases, then the channel noise power becomes more significant in the logarithm argument, thereby reducing capacity. For a given noise power the average power

$\langle P_e \rangle$ for a signal must increase to improve capacity. In order to attain an adequate value for

$$\langle P_e \rangle = \langle P_{src} \rangle \eta_{diss} \eta_{mod}, \langle P_{src} \rangle \text{ must increase.}$$

The capacity of 5-38 applies only to the maximum entropy process. Arbitrary processes may possess a lower *PAPR* and therefore higher efficiency but the capacity equation must be modified by using the approximate relative capacity method of section 5.2 or the explicit calculation of pseudo-capacity for a particular information and noise distribution through extension of the principles from chapter 4.

Efficiency vs. capacity in nats/second for the 10 dB SNR Gaussian signal case is illustrated in the following graphic. η_{mod} possesses a small but finite value associated with some standardized norm for an approximate Gaussian case and assumed encoder mechanism, such as for instance a *PAPR* of 12 dB and the encoder model of figure 5-14. Since η_{mod} is fixed in such an analysis, capacity performance is further determined by η_{diss} .

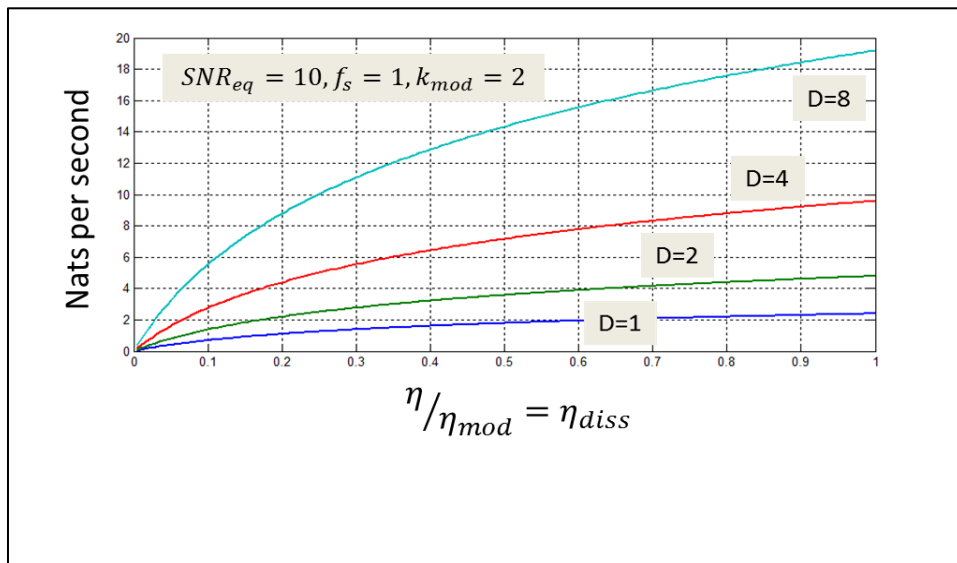


Figure 5-21 Capacity vs. Dissipative Efficiency

All members of the capacity curve family can be made identical to the $D = 1$ case if the sample rate $f_{s_α}$, per sub channel is reduced by the multiplicative factor D^{-1} . That is, Dimensionality may be traded for sample rate to attain a particular value of C , and a given η .

5.4.1. Effective Angle for Momentum Exchange

Information can be lost in the process of waveform encoding or decoding unless momentum is conserved during momentum exchange. The capacity equation may be altered to emphasize the effective work based on the angle of time variant linear momentum exchanges.

$$C \leq \sum_{\alpha=1}^D f_{s_α} \left(\ln \left[\frac{(m^2 \langle \dot{\vec{p}}_{\alpha} \cdot \dot{\vec{q}}_{\alpha} \rangle_{eff_α})}{\tilde{\sigma}_{p_{n_α}}^2} + 1 \right] \right) = \sum_{\alpha=1}^D f_{s_α} \left(\ln \left[\frac{(m^2 \langle (|\dot{\vec{p}}_{\alpha}| |\dot{\vec{q}}_{\alpha}|)_{in_α} \cos(\theta_{eff_α}) \rangle)}{\tilde{\sigma}_{p_{n_α}}^2} + 1 \right] \right) \quad (5-39)$$

The subscript “in” refers to input work rate. $\cos \theta_{eff_α}$ controls the efficiency relationship in the second equation. $\langle (|\dot{\vec{p}}_{\alpha}| |\dot{\vec{q}}_{\alpha}|)_{in_α} \cos(\theta_{eff_α}) \rangle$ is the effective work rendered at the target particle. Therefore, $\langle \eta_{\alpha} \rangle = \langle \cos \theta_{eff_α} \rangle$.

$\cos \theta_{eff_α}$ must be unity for every momentum exchange to reflect perfect motion and render a maximum efficiency of 1. $\theta_{eff_α} = (\theta_{mod_α} - \theta_{diss_α})$ is composed of a dissipative angle and a modulation angle, relating to the discussion of the prior section. θ provides a means for investigation of the inefficiencies at a most fundamental scale in multiple dimensions, where angular values may also be decomposed into orthogonal quantities.

For an increasing number of degrees of freedom and dimensionality, the relative angle of particle encoding and interaction is important and provides more opportunity for inefficient momentum exchange. For example, the probability of perfect angular recoil of the encoding process is on the order of $(2\pi)^{-D}$ in systems whenever the angular error is uniformly distributed. Even when the error is not uniformly distributed it tends to be a significant exponential function of the available dimensional degrees of freedom.

Whenever $D > 1$, the angle θ_{eff_a} may be treated as a scattering angle. This concept is well understood in various disciplines of physics where momentum exchanges may be modeled as the interaction of particles or waves [53, 54]. The variation of this scattering angle due to vibrating particles or perturbed waves goes to the heart of efficiency at a fundamental scale. Thermal state of the apparatus is one way to increase θ_{diss_a} , the unwanted angular uncertainty in θ_{eff_a} .

Interaction between the particles of the apparatus, environment and the encoded particles exacerbates inefficiency evidenced as an inaccurate particle trajectory. Energy is bilaterally transferred at the point of particle interface as we have noted from examining recoil momentum. Thus during every targeted non-adiabatic momentum exchange in which some energy is dissipated to the local environments there is also some tendency to expose the target particle momentum to environmental contamination.

5.5. Momentum Transfer via an EM Field

The focus of prior discussions has been at the subsystem level, examining the dynamics of particles constrained to a local phase space. However, the discussion of section 3.3 and the implication of chapter 4 is that such a model may be expanded across subsystem interfaces. It is not necessary to resolve all of the particulars of the interfaces enabling the extended channel to understand the fundamental mechanisms of efficiency. Where ever momentum is exchanged the principles previously developed can apply. It is valuable to understand how the momentum may extend beyond boundaries of a particular modeled phase space, particularly for the case of charge-electromagnetic field interaction. Here we shall restrict the discussion to the case where particles are conserved charges. Specifically, charges in the transmitter phase space do not cross the ether to the receiver, or vice-versa, yet momentum is transferred by EM fields. This is the case for a radio communications link.

The following figure provides a reference point for the discussion.

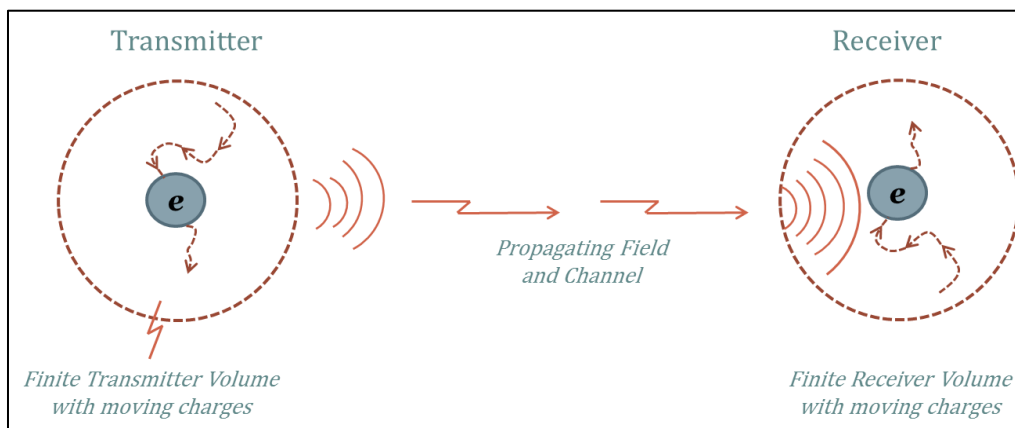


Figure 5-22 Momentum Exchange Through Radiated Field

The figure illustrates a charge in a restricted transmitter phase space which moves according to accelerations from applied forces. The accelerating transmitter charge radiates energy and momentum contained in the fields which transport through a physical medium to the receiver. The transmitter charge does not leave the transmitter phase space, complying with the boundary conditions of chapter 3. In electronic communications applications, we can obtain the momentum of the transmitter charge from the Lorentz force [38, 39, 55, 56, 57].

$$\frac{d}{dt}\vec{p}_{tx} = e\vec{E} + \frac{e}{c}\vec{v} \times \vec{H}$$

(5-40)

\vec{E} is the stimulating electric field and \vec{H} is the stimulating magnetic field. Often electronic communications application will stimulate charge motion using a time variant scalar potential $\varphi(t)$ alone so that the magnetic field is zero. In those common cases;

$$\frac{d}{dt}\vec{p}_{tx} = e\vec{E} = -e\nabla\varphi(t)$$

(5-41)

The momentum of the transmitter charge is imparted by a time variant circuit voltage in this circumstance. Since the charge motions involve accelerations, encoded fields radiate with momentum. Radiated fields transfer time variant momentum to charges in the receiver, likewise transferring the information originally encoded in the motion of transmitter charges.

The receiver charge mimics the motion of the transmitter charge at some deferred time.

The equations of motion for the receiver charge are given by;

$$\frac{d}{dt} \vec{p}_{rx} = e\vec{E} + \frac{e}{c} \vec{v} \times \vec{H}$$

$$\frac{d}{dt} \mathcal{E} = e(\vec{v} \cdot \vec{E})$$

(5-42)

The Lorentz force, which moves the receiver particle, is a function of the dynamic electric (\vec{E}) and magnetic (\vec{H}) field components of the field bridging the channel. These fields can be derived from the Lienard-Wiechert potentials which in turn reflect variations associated with the transmitter charge motion [58]. The so called radiation field of the transmitter charge is based on accelerations i.e. $\frac{d}{dt} \vec{p}_{tx}$ [56]. Literature is replete with the relevant derivations which connect $\dot{\vec{p}}_{tx}$ with $\dot{\vec{p}}_{rx}$ via the components of the retarded scalar and vector potentials which give rise to the EM fields according to Maxwell's equations [39].

A comprehensive treatment developed from the equations of motion for a charge in a field is provided by Landau and Liftshitz and summarized here [39]. In addition, complementary analysis is provided by Jackson, Goldstein, and Griffiths [37, 38, 59].

The following integral equation in figure 5-23, for a D=3 hyper sphere illustrates the various components of energy and momentum flux through the surface of a transmit phase space volume. The integral equation is deduced using the techniques of Landau and Liftshitz as well as Jackson. It is written in a conservation form with particle terms on the left and field terms on the right accounting for momentum within the space and moving through the surface of the space.

The components with super scripts labeled (\rightsquigarrow) and ($\textcircled{\text{R}}$) in the integral equation refer to particle and field components respectively.

$$\underbrace{\frac{1}{c^2} \frac{\partial}{\partial t} \int_{\text{volume}} \mathbf{s}_\alpha^{(\rightsquigarrow)} dV}_{\text{forces on particles in specified volume}} + \underbrace{\oint_{\text{surface}} -\mathfrak{S}_{\alpha\beta}^{(\rightsquigarrow)} df}_{\text{particle flux through surface bounding volume}} = \underbrace{-\frac{1}{c^2} \frac{\partial}{\partial t} \int_{\text{volume}} \mathbf{s}_\alpha^{(\textcircled{\text{R}})} dV}_{\text{rate of change of field momentum in specified volume}} - \underbrace{\oint_{\text{surface}} -\mathfrak{S}_{\alpha\beta}^{(\textcircled{\text{R}})} df}_{\text{flux of field momentum through surface bounding specified volume}}$$

Figure 5-23 Conservation Equation for a Radiated Field

The energy-momentum tensor provides a compact summary of the quantities of interest associated with the momentum flux of the phase space based on the calculations of the conservation equation [38, 39]. The tensor is related to the space-time momentum \mathcal{P} by;

$$\mathcal{P}^\alpha = \frac{1}{c} \int T^{\alpha\beta} df_\beta$$

(5-43)

α, β are the spatial indices of the tensor in three space and the 0^{th} index is reserved for the time components in the first row and column.

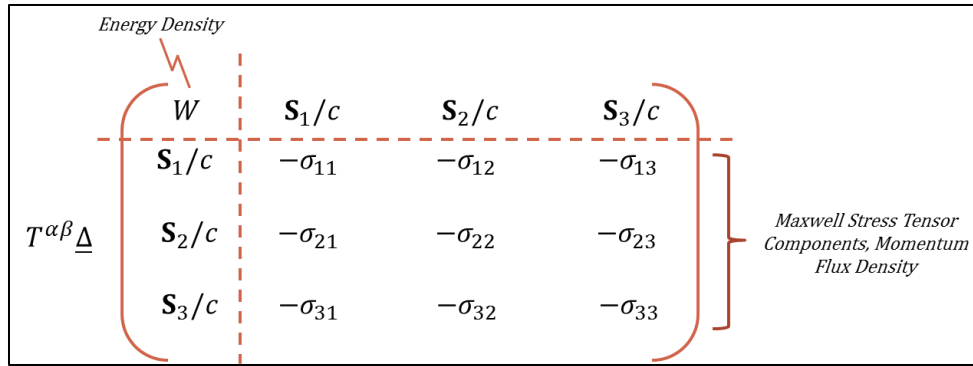


Figure 5-24 Energy Momentum Tensor

The energy density associated with the phase space in joules per unit volume is given by;

$$T^{00} = \frac{1}{8\pi} (E^2 + H^2) \equiv W$$

(5-44)

The energy flux density per unit time crossing the differential surface element df (chosen perpendicular to the field flux) is given by the tensor elements $T^{0\beta}$ multiplied by c , where ;

$$T^{01} = \frac{S_1}{c}, T^{02} = \frac{S_2}{c}, T^{03} = \frac{S_3}{c}$$

(5-45)

And Poynting's Vector is obtained from ;

$$\vec{S} = \frac{c}{4\pi} (\vec{E} \times \vec{H})$$

(5-46)

Maxwell's stress tensor expresses the components of the momentum flux density per unit time passing from the transmitter volume through a surface element of the hyper-sphere;

$$T^{\alpha\beta} = -\mathfrak{S}_{\alpha\beta} = -\frac{1}{4\pi} \left\{ E_{\alpha} E_{\beta} + H_{\alpha} H_{\beta} - \frac{1}{2} \delta_{\alpha\beta} (E^2 + H^2) \right\}; \alpha, \beta = 1, 2, 3$$

(5-47)

The second term in the integral equation of figure 5-23 is zero in our case, $\left\{ \sigma_{\alpha,\beta}^{(\infty)} = 0 \right\}$, since transmit charges are confined by boundary conditions. The right hand side of the integral equation is the momentum change within the transmit volume along with the momentum flux transported through the phase space volume surface. The momentum flux carries information from the transmitter to the receiver through a time variant modulated field. Poynting's vector may also be used to calculate the average energy in that field.

We now comment on extended results by application of modulation to encode information in the fields.

One classic case involves modulated harmonic motion of the electron which corresponds to a modulated RF carrier. This case is addressed in detail by Schott [55]. He develops the field components from the retarded potentials in several coordinate systems. It can be shown that the modulated harmonic motion produces an approximate transverse electromagnetic plane wave in the far field given by [60, 61];

$$E_y(t) = E_0(a(t))e^{j(\omega t - \phi(t))}$$

(5-48)

$$H_z(t) = \frac{1}{-j\omega\mu} \frac{\partial}{\partial x} E_y(t) = \frac{2\pi}{\lambda(t)} \frac{1}{j\omega\mu} E_0(a(t)) e^{j(\omega t - \phi(t))}$$

(5-49)

$a(t)$ and $\phi(t)$ are random variables encoded with information in this view corresponding to the amplitude and phase of the harmonic field. The momentum of the field changes according to $a(t)$ and $\phi(t)$ in a correlated manner. Therefore the E_y and H_z field components are also random variables possessing encoded information from which we may calculate time variant momentum using the integral conservation equation above.

Accelerating charges radiate fields which carry energy away from the charge. This radiating energy depletes the kinetic energy of the charge in motion, a distinct difference compared to the circumstance of matter without charge. The prior comments do not explicitly contemplate the impact of the radiation reaction on efficiency which may become significant at relativistic speeds. Schott exhaustively investigates the radiation reaction of the electron and its impact on the kinetic energy [55, 56]. We shall not require a separate calculation of the radiation reaction for subsequent examples but the reader is cautioned that under certain conditions it may be significant. Simple examples involving radiation from circular or other periodic orbits may be found in the literature [38]. The simple examples typically involve the use of Larmor's formula or the Abraham-Lorentz formula [37]. In the case of routine circuit analysis it is usually not a concern since conduction rather than radiation is a primary method of moving the charge and its momentum and drift velocities of the constrained charges are typically far below the speed of light [62].

The field energies calculated by Poynting's vector at the receiver are attenuated by the spherical expansion of the transmitted flux densities as the EM field propagates through space. This attenuation is in proportion to the square of the distance between the transmitter and receiver for free space conditions according to Friis' equation when the separation is on the order of 10 times the wavelength of the RF carrier or greater [42]. Ultimately, the effect of this attenuation is accounted for in the capacity calculations by a reduction in SNR at the receiver.

Finally, it is posited that the principles of section 5.5 are extensible to the general electronics application moving forward. Variable momentum is due to the modulation of charge densities and their associated fields, whether it is viewed as simply a bulk phenomena or the ensemble of individual scattering events which average to the bulk result. A circuit composed of conductors and semiconductors can be characterized by voltage and current. Voltage is the work per unit charge to convey the charge through a potential field. When multiplied by the charge per unit time conveyed, we may calculate the total work required to move the charge. This is analogous to the prior discussions involving the conjugate derivative field quantities of particles in a model phase space used to calculate the trajectory work rate $(\dot{\vec{p}} \cdot \dot{\vec{q}})$ which can be integrated over some characteristic time interval Δt , to obtain the total work over that interval.

6. INCREASING η_{mod} AN OPTIMIZATION APPROACH

Chapter 5 establishes the total efficiency for processing as $\eta = \eta_{diss}\eta_{mod}$. η_{mod} applies for the modulation process wherever there is an associated efficiency for any interface where the momentum of particles must deliberately be altered to support a communications function. For communications this could include encoding, decoding, modulation, demodulation, increasing the power of a signal, etc.. In this chapter we introduce a method for increasing η_{mod} whilst maintaining capacity. The method can apply to cases for which distributions of particle momentum are not necessarily Gaussian. Nevertheless, we focus on the Gaussian case, since modern communications signals and standards are ever marching toward this limit.

6.1. Sum of Independent RVs

Consider the comparative case where $\zeta=1$ vs. some greater integer number where ζ is the number of summed signal inputs x_i to a channel. Suppose that it is desirable to conserve energy in the comparison. The total energy is allocated amongst ζ distributions with an i^{th} branch efficiency inversely related to the $PAPR_i$ of the i^{th} signal.

$$\eta_i = (k_i PAPR_i + a_i)^{-1}$$

(6-1)

Equation 6-1 is a general form suitable for handling all information encoding circumstances given a suitable choice of k_i and a_i .

The following diagram assists with ongoing discussion;

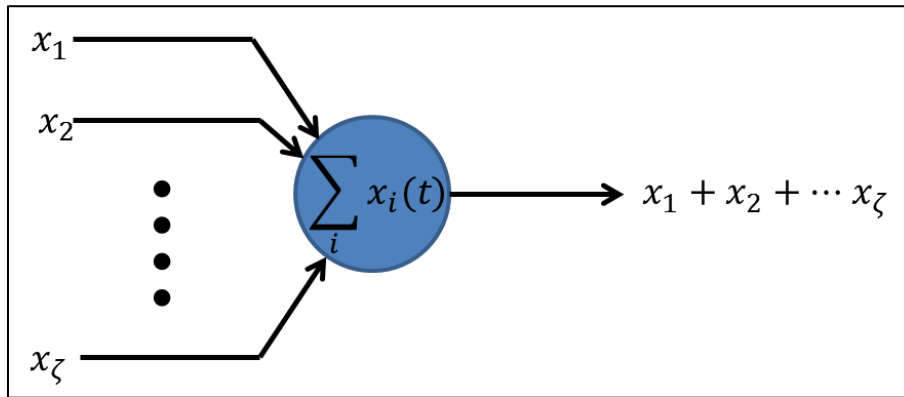


Figure 6-1 Summing Random Signals

It is possible to calculate an effective total efficiency from the input efficiencies when the densities of x_i are independent, beginning from the general form developed in chapter 5 where k_{mod} and k_σ are constants based on encoder implementation.

$$\langle \eta \rangle = \frac{\sigma^2}{k_{mod} P_m + k_\sigma \sigma^2} \tag{6-2}$$

$$P_m = \max \sum_i x_i^2 \tag{6-3}$$

Then, eq. 6-2 may be written for the i^{th} branch as;

$$\eta_i = \frac{\sigma_i^2}{k_{mod_i}' P_{m_i} + k_{\sigma_i}' \sigma_i^2} \quad (6-4)$$

Now we define $k_{mod_i}' = \lambda_i k_{mod}$ and $k_{\sigma_i}' = \lambda_i k_{\sigma}$

6-4 becomes;

$$\lambda_i \eta_i = \frac{\sigma_i^2}{k_{mod_i} P_{m_i} + k_{\sigma_i} \sigma_i^2} \quad (6-5)$$

Now we form a time average of 6-5;

$$\langle \eta \rangle = \left\langle \sum_i \lambda_i \eta_i \right\rangle = \left\langle \sum_i \frac{\sigma_i^2}{k_{mod_i} P_{m_i} + k_{\sigma_i} \sigma_i^2} \right\rangle \quad (6-6)$$

We further stipulate that;

$$\sum_i \lambda_i = 1 \quad (6-7)$$

Equation 6-7 defines λ_i as a suitable probability measure for the i^{th} branch. Comparing 6-2 and 6-6, yields;

$$\langle \eta \rangle = \sum_i \lambda_i \eta_i$$

(6-8)

Equation 6-8 requires that the weighting coefficients associated with the i^{th} branch be specified to yield the corresponding composite time average. Equations 6-1 through 6-6 suggest that a particular design $PAPR$ may be achieved using a composite of signals and the individual branch $PAPR_i$ may be lower than the final output which implies that overall efficiency may be improved.

Examination of figure 6-1 and equation 6-6 carries an additional burden of ensuring that each input branch not adversely interact or alternately that η_i not be a function of more than 1 input. This is no small challenge for linear continuous processing technologies. In a particle based model it is possible for all particles of the input delivery streams to interact at a common target particle (i.e. summing node). Energy from a delivery particle in one branch may be redistributed amongst the ζ branches as well as the output target particle. A preferred strategy would allocate as much momentum from an input branch to the output target particle, without other branch interaction.

In electronics, the analogy is that all the input branches can interact via a circuit summing node through the branch impedances, thus distributing energy from the inputs to all circuit branches not just the intended output load. Fortunately, there are methods for avoiding these kinds of redistributions.

6.2. Composite Processing

A sampled system provides one means of controlling the signal interactions at the summing node of figure 6-1. A solution addressing the Gaussian case, which is also suitable for application using any pdf, follows. Figure 6-2 illustrates composite sub densities which fit the continuous Gaussian curve precisely. An appealing feature of this approach is that even with a few sub distributions the composite is Gaussian and capacity is preserved. Each sub density, ρ_1 through ρ_6 ($\zeta = 6$), possesses an enhanced efficiency due to a reduced $PAPR_i$. In addition, it is interesting to note that as more sub densities of this ilk are deployed with narrower spans, they resemble uniform densities. In the extreme limit $\zeta \rightarrow \infty$, they become discrete densities with the momenta probabilities equal to λ_i and overall efficiency asymptotically approaches a maximum since each $PAPR_i \rightarrow 1$. Just as argued in chapter 4 a quantum resolution can be assigned to avoid ill-behaved interpretations of entropy for the theoretical case $\zeta \rightarrow \infty$.

For a single dimension $D=1$ it is easy to understand that samples for each sub density ρ_i , occur at noninterfering sampling intervals. Thus, if this scheme is applied to the system illustrated in figure 6-1 each input x_i possesses a unique pdf $\rho_i = \rho(x_i)$ and unique sets of signal samples are assigned to populate the sub densities ρ_i whenever the composite signal $\sum x_i(t - NT_s)$ crosses the respective sub density domain thresholds. The thresholds are defined as the boundaries between each sub density.

We may extend this approach to each orthogonal dimension for $D > 1$ since orthogonal samples are also physically decoupled. The intersection of the thresholds in multiple dimensions form

hyper geometric surfaces defining subordinate regions of phase space. In the most general cases these thresholds can be regarded as the surfaces of manifolds.

Figure 6-2 illustrates each sub distribution as occupying a similar span. However, this is not optimal. In fact, the spans only approach parity for a large number of sub densities. For a few sub densities the spans must be specifically defined to optimize efficiency. Each unique value of ζ will require a corresponding unique set of density domains and corresponding thresholds.

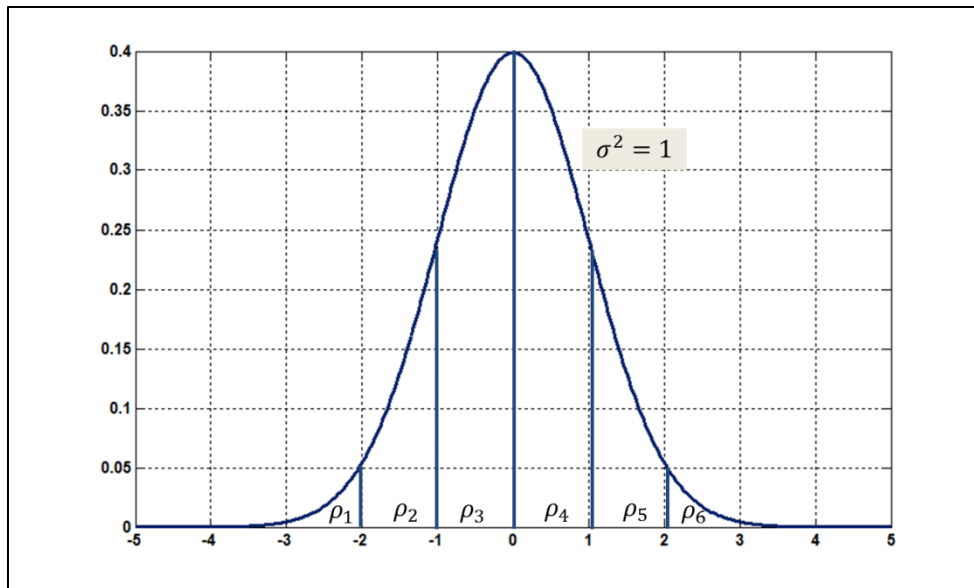


Figure 6-2 Gaussian pdf Formed with Composite Sub Densities

Figure 6-2 and equation 6-6 suggests that the optimal efficiency can be calculated from;

$$\eta_{opt} = \max_{\tilde{\eta}_{\zeta}} \left\{ \sum_{i=1}^{\tilde{\zeta}} \lambda_i \eta_i \right\}$$

(6-9)

The coefficients, λ_i are variables dependent on the total number of domains ζ . The thresholds, $\tilde{\eta}_\zeta$, for the domains of each sub-density are varied for the optimization, requiring specific λ_i . η increases as ζ increases though there is a diminishing rate of return for practical application. Therefore a significant design activity is to trade η vs. ζ vs. cost, size, etc. . The trade between efficiency and ζ is addressed in chapter 7 along with examples of optimization.

7. MODULATOR EFFICIENCY AND OPTIMIZATION

In this chapter, some modulator examples are presented to illustrate optimization consistent with the theory presented in prior chapters. Modulators encode information onto an RF signal carrier.

This chapter focuses on encoding efficiency. Thus we are primarily concerned with the efficiency of processing the amplitude of the complex envelope, though the phase modulated carrier case may also be obtained from the analysis.

7.1. Modulator

RF modulation is the process of imparting information uncertainty $H(\rho(x))$ to the complex envelope of an RF carrier. An RF modulated signal takes the form,

$$x(t) = a(t)e^{j\omega_c t + \varphi(t)} = a_I(t) \cos(\omega_c t + \varphi(t)) - a_Q(t) \sin(\omega_c t + \varphi(t))$$

$$a(t) \triangleq \text{Magnitude of complex envelope} \quad a(t) = \sqrt{(a_I(t))^2 + (a_Q(t))^2}$$

$$a_I(t) \triangleq \text{Time variant In Phase (real) component of the RF Envelope}$$

$$a_Q(t) \triangleq \text{Time variant Quadrature (Imaginary) Phase component}$$

$$\omega_c \triangleq \text{RF Carrier Frequency}$$

$$\varphi(t) \triangleq \text{Instantaneous RF carrier phase} \quad \varphi(t) = \tan^{-1} \frac{a_Q(t)}{a_I(t)}$$

(7-1)

Any point in the complex signaling plane can be traversed by the appropriate orthogonal mapping of $a_I(t)$ and $a_Q(t)$. Alternatively, magnitude and phase of the complex carrier envelope can be specified provided the angle $\varphi(t)$ is resolved modulo $\pi/2$. As pointed out in section 5.5, information modulated onto an RF carrier can propagate through the extended channel via an associated EM field.

An example top level RF modulator diagram is shown in figure 7-1.

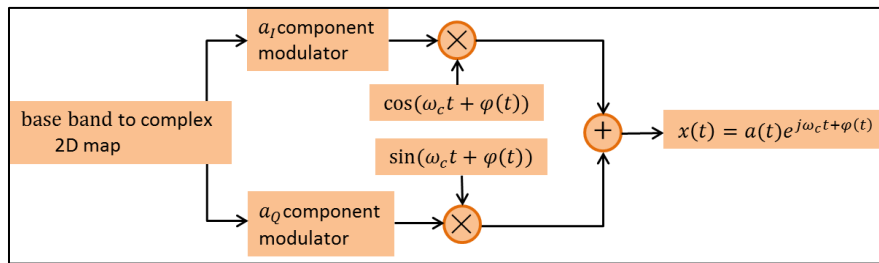


Figure 7-1 Complex RF Modulator

A complex modulator consists of orthogonal carrier sources ($\sin(\omega_c t + \varphi(t))$) and ($\cos(\omega_c t + \varphi(t))$), multipliers, in-phase as well as quadrature phase baseband modulators/encoders and an output summing node.

An example of a measured output from an RF modulator mapped into the complex signal plane results in a 2D signal constellation as illustrated in figure 7-2. The constellation corresponds to the case of a wideband code division multiple access signal. Specific sampling points are illustrated at the connecting nodes of trajectories which collectively define the constellation. The 2D time variant voltage trajectories of figure 7-2 are analogous to phase space particle

trajectories presented in the prior chapters, restricted to 2 dimensions. Section 5.5 makes the connection to $\dot{\rho}$ through the Lorentz Equation.

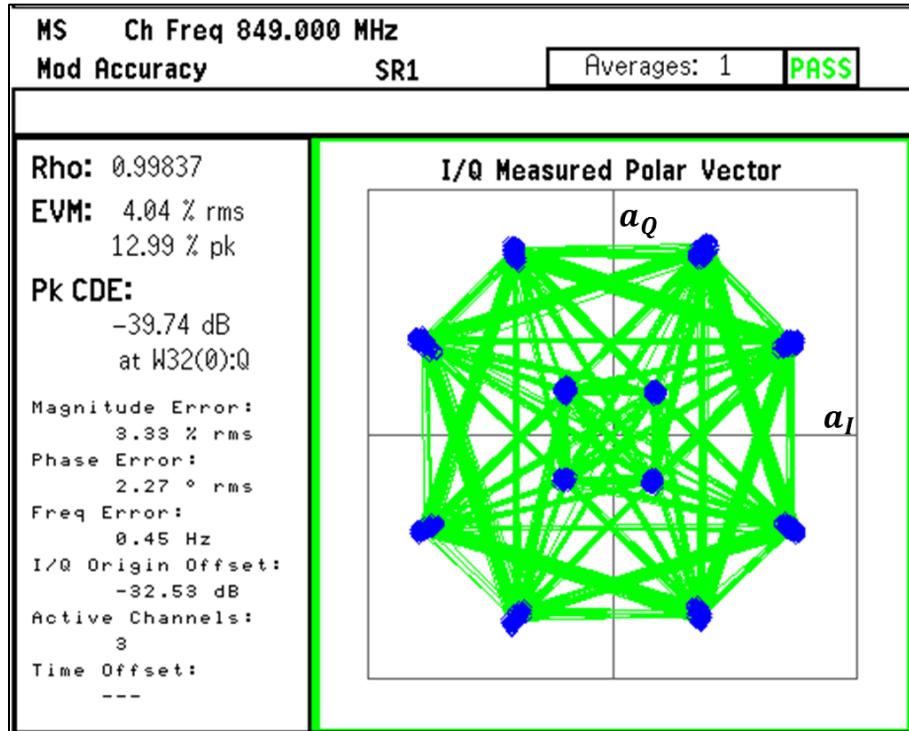


Figure 7-2 Complex Signal Constellation for a WCDMA Signal

Battery operated mobile communications platforms typically possess unipolar energy sources. In such cases, the random variables defining $a_I(t)$, $a_Q(t)$ are usually characterized by non-central parameters within the modulator segment. We shall focus efficiency optimization examples on circuits which encode $a_I(t)$ and $a_Q(t)$ since extension to carrier modulation is straightforward. We need only understand the optimization of in phase $a_I(t)$ voltage or quadrature phase $a_Q(t)$ voltage encoding, then treat each result as independent parts of a 2D solution.

The following discussion advances efficiency performance for a generic series modulator/encoder configuration. Efficiency analysis of the generic model also enjoys common principles applicable to other classes of more complicated modulators.

The series impedance model for a baseband modulator in phase or quadrature phase segment of the general complex modulator is provided in the following two schematics which illustrate differential and single ended topologies;

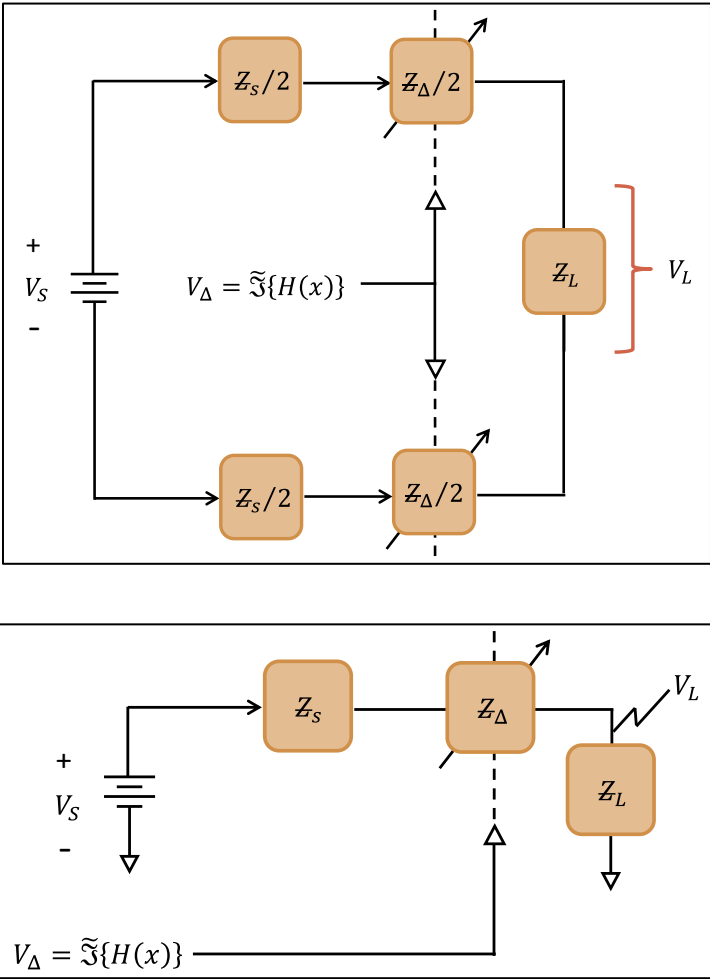


Figure 7-3 Differential and Single Ended Type 1 Series Modulator/Encoder

Figure 7-3 is referred to as a type 1 modulator. V_{Δ} is some encoding function of the information uncertainty $H(x)$ to be mapped using controlled voltage changes which modify a variable impedance Z_{Δ} . Impedance Z_{Δ} is variable from $(0 + 0_j)\Omega$ to $(\infty + \infty_j)\Omega$. Alternative configurations may be Thevinized, consisting of current sources rather than voltage sources, working in conjunction with finite Z_s .

Appendices H and I derive the thermodynamic efficiency for the type 1 modulator which results in a familiar form for symmetric densities without dissipation;

$$\eta = \frac{1}{2PAPR_{sig}}$$

(7-2)

This formula was verified experimentally through the testing of a type one modulator. The following graphic provides a synopsis of the results.

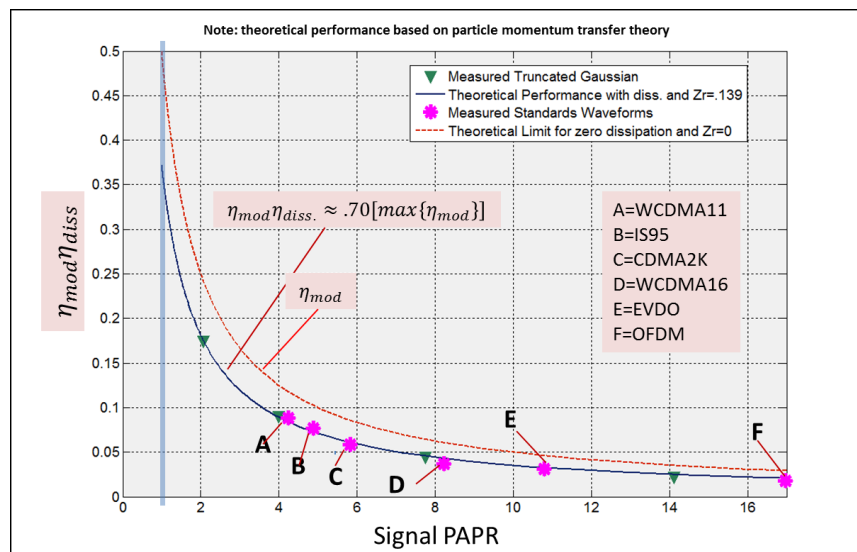


Figure 7-4 Measured and Theoretical Efficiency of a Type 1 Modulator

Several waveforms were tested, including truncated Gaussian waveforms studied in chapter 5 as well as 3G and 4G+ standards based waveforms used by the mobile telecommunications industry. The maximum theoretical bound for η_{mod} (i.e. $\eta_{diss} = 1$) represented by the upper curve is based on the theories of this work, for the ideal circumstance. The efficiency of the apparatus due to directly dissipative losses was found to be approximately 70 %. The locus of test points depicted by the various markers falls nearly exactly on the predicted performance when directly dissipative results are accounted for. For instance, a truncated Gaussian signal (inverted triangle) with a *PAPR* of 2 (3dB) was tested with a measured result of $\eta_{mod}\eta_{diss}=.175$. Dividing .175 by the inherent test fixture efficiency of .7 equates to an $\eta_{mod} = .25$ in agreement with theoretical prediction of $(2PAPR)^{-1}$. At the other extreme an IEEE802.11a standard waveform based on orthogonal frequency division multiplexed modulation was tested, with a result recorded by data point F. Data point E is representative of the Enhanced Voice Data Only services typical of most code division multiplexed (CDMA) based cell phone technology currently deployed. B and C represent the legacy CDMA cell phone standards. Data points A and D are representative of the modulator efficiency for emerging (WCDMA) wideband code division multiplexed standards. A key point of the results is that the theory of chapters 3 through 5 applies to Gaussian and standards waveforms alike with great accuracy.

7.2. Modulator Efficiency Enhancement for Fixed ζ

An analysis proceeds for a type 1 series modulator with some numerical computations to illustrate the application of principles from chapter 5 and a particular example where efficiency is improved.

Voltage domains are related to energy or power domains through a suitable transformation. $\rho(\check{\eta}(a(t)))$ or simply $\rho(\check{\eta})$, may be obtained from the appropriate Jacobian to transform a probability density for a voltage at the modulator load to an efficiency (refer to appendix H). $\check{\eta}$ is defined as the instantaneous efficiency of the modulator and is directly related to the proper thermodynamic efficiency (refer to appendix I).

Let the baseband modulator output voltage probability density, $\rho(V_L)$, be given by;

$$\rho(V_L) \approx \frac{1}{\sqrt{2\pi}\sigma_{V_L}} e^{-\frac{(V_L - \langle V_L \rangle)^2}{2\sigma_{V_L}^2}} ; \quad 0 \leq V_L \leq 1$$

(7-3)

Equation 7-3 depicts an example pdf which is truncated non-zero mean Gaussian. V_L corresponds to the statistic of a hypothetical in-phase amplitude or quadrature phase amplitude of the complex modulation at an output load. The voltage ranges are selected for ease of illustration but may be scaled to any convenient values by renormalizing the random variable.

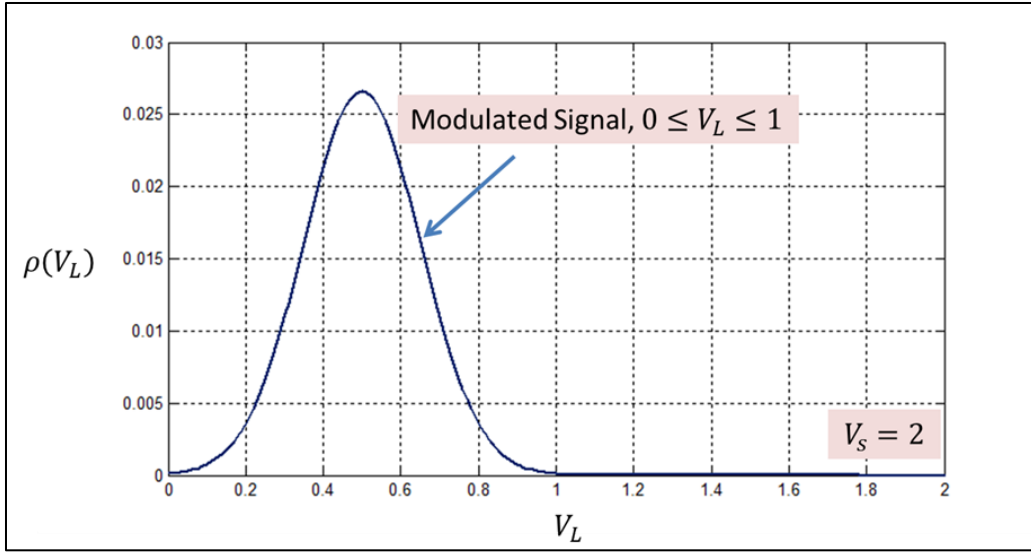


Figure 7-5 Gaussian pdf for Output Voltage Voltage, V_L , with $V_s = 2$, $\langle V_L \rangle = V_s/4 = (4V)$, and $\sigma = .15$

Average instantaneous waveform efficiency is obtained from;

$$\langle \tilde{\eta} \rangle = \left\langle \frac{P_{out}}{P_{in}} \right\rangle = \left\langle \frac{V_L^2}{(V_L V_s) - \text{Re} \left\{ \frac{Z_s^*}{Z_L} (V_L^2) \right\}} \right\rangle \quad (7-4)$$

Appendix H and I provide a discussion concerning the use of instantaneous efficiency in lieu of thermodynamic efficiency. In this example we utilize the instantaneous efficiency to illustrate a particular streamlined procedure to be applied for optimization in section 7.3.

η_{WF} is the total waveform efficiency where the output power consists of signal power $\langle \tilde{V}_L^2 \rangle$ plus modulator overhead. That is, the RV of interest is $V_L = \tilde{V}_L + \langle V_L \rangle$. This differs from the preferred definition of output efficiency given in chapter 5. We are ultimately interested in $\tilde{\eta}$, the thermodynamic efficiency, based on the signal output. $\tilde{\eta}$ is based on the proper output power,

due exclusively to the information bearing amplitude envelope signal. Optimization of $\langle \eta_{WF} \rangle$ and $\langle \tilde{\eta} \rangle$ also optimizes thermodynamic efficiency (reference Appendix H).

$$\tilde{\eta} = \langle \eta_{WF} \rangle - \frac{\langle V_L \rangle}{V_s}; \quad Z_r = \frac{Z_s^*}{Z_L} = 1$$

Sometimes the optimization procedure favors manipulation of one form of the efficiency over the other depending on the statistic of the output signal.

We also note the supplemental relationships for an example case where the ratio of the conjugate power source impedance to load impedance, $Z_r = 1$.

$$Z_L = Z_s^*$$

$$Z_r = \frac{Z_s^*}{Z_L}$$

$$V_{Lmax} = \frac{V_s}{2}$$

$$\langle V_L \rangle = \frac{V_s}{4}$$

$$V_L = \frac{\eta V_s}{(1 + Z_r \eta)} = \frac{\eta V_s}{(1 + \eta)}$$

More general cases can also consider any value for the ratio Z_r other than 1. Z_s has been defined as the power source impedance. The given efficiency calculation adjusts the definition of available input power to the modulator and load by excluding consideration of the dissipative power loss internal to the source. V_s therefore is an open circuit voltage in this analysis.

Ultimately then, Z_s limits the maximum available power P_{max} from the modulator.

Now we write the waveform efficiency pdf.

The Jacobian, $\rho_\eta = \rho(V_L) \frac{d(V_L)}{d(\eta)}$, yields;

$$\rho(\eta_{WF}) = \frac{V_s}{(1 + \eta)^2} \frac{1}{\sqrt{2\pi\sigma^2}} e^{-\frac{\left(\eta \frac{V_s}{(1+\eta)} - \frac{V_s}{4}\right)^2}{2\sigma^2}}$$

(7-5)

A plot of this pdf follows:

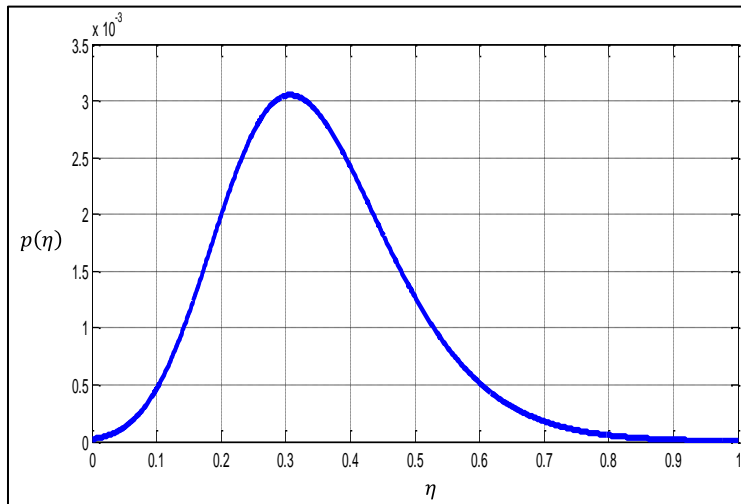


Figure 7-6 pdf for η given Gaussian pdf for Output Voltage, V_L , with $V_s = 2$, $\langle V_L \rangle = V_s/4 (.5V)$, and $\sigma = .15$, $\langle \eta \rangle = .34$

This efficiency characteristic possesses an $\langle \eta_{wf} \rangle$ of approximately .347. The $PAPR_{wf}$ is equal to $\langle \eta_{wf} \rangle^{-1}$ or $\sim 4.68 \text{ dB}$. Just as the waveform and signal efficiency are related, the associated peak to average power ratios, $PAPR_{wf}$ and $PAPR_e$, are also related by;

$$PAPR_{wf} = \frac{4PAPR_e}{1 + PAPR_e}$$

The signal peak to average power ratio $PAPR_e = 11.11$ for this example.

Now we apply 2 waveform voltage thresholds which correspond to 3 momentum domains, using a modified type 1 modulator architecture illustrated in fig. 7-7 and 7-8.

In this example the baseband modulation apparatus possesses 3 separate voltage sources

V_{s1}, V_{s2}, V_{s3} . These sources are multiplexed at the interface between the corresponding potential

boundaries, V_1, V_2 , as the signal requires. An upper potential boundary $V_3 = V_{max}$ represents the maximum voltage swing across the load. There is no attempt to optimally determine values for

signal threshold voltages V_1, V_2 at this point. The significant voltage ranges defined by

$\{0, V_1\}, \{V_1, V_2\}, \{V_2, V_3\}$, correspond to signal domains within phase space. We regard these domains as momentum domains with corresponding energy domains.

Domains are associated to voltage ranges according to;

Domain 1 if; $V_L < V_1$

Domain 2 if; $V_1 \leq V_L \leq V_2$

Domain 3 if; $V_2 < V_L < V_3$

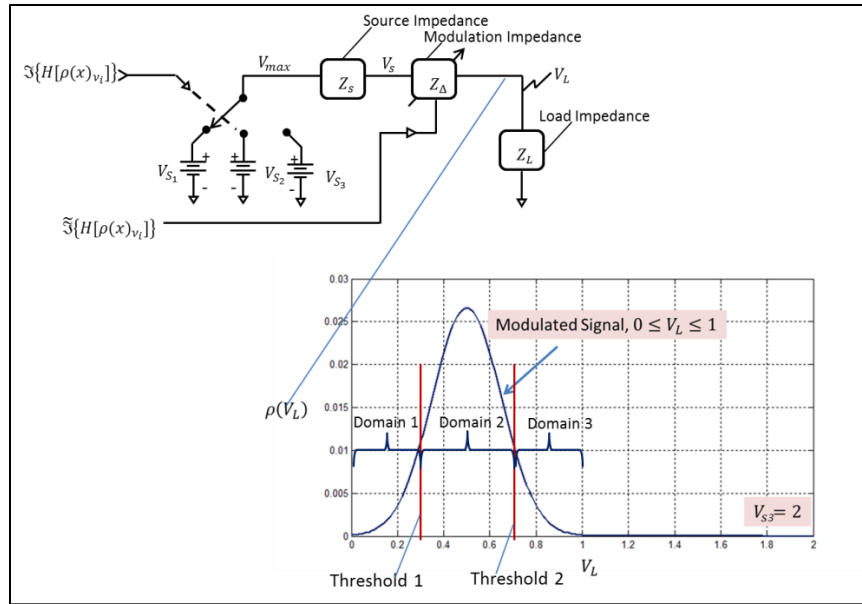


Figure 7-7 Gaussian pdf for Output Voltage, V_L , with $V_s = 2$, $\langle V_L \rangle = V_s/4$ (.5V), and $\sigma = .15$, 3 Separate Domains

Average efficiency for each domain may be obtained from subordinate pdfs parsed from the waveform efficiency of figure 7-6.

The calculations of $\langle \check{\eta}_{1,2,3} \rangle$ are obtained from;

$$\langle \check{\eta}_\zeta \rangle = k_{\zeta_norm} \int_{\check{\eta}_{\zeta-1}}^{\check{\eta}_\zeta} \check{\eta} \rho_\zeta(\check{\eta}) d(\check{\eta}) ; \zeta = 1, 2, 3$$

(7-6)

ζ is a domain increment for the calculations and k_{ζ_norm} provides a normalization of each partition domain such that each separate sub pdf possesses a proper probability measure. Thus, the averages of eq. 7-6 are proper averages from three unique pdfs. First we calculate the peak

efficiency in domain 1, using a 2V power supply as an illustrative reference for a subsequent comparison.

$$\check{\eta}_{1peak} \triangleq \frac{\langle V_L^2 \rangle}{\langle V_L V_S \rangle - V_L^2}; \quad V_L = .3V, \quad V_S = 2V, \quad \therefore \check{\eta}_{1peak} \approx .176$$

$\check{\eta}_{1peak}$ is the instantaneous peak waveform efficiency possible for the modulator output voltage of .3V when the modulator supply is at 2V. $\langle \check{\eta}_1 \rangle$ according to eq. 7-6, calculates to $\approx .131$ in the domain where $0 \leq V_L \leq .3V$.

Now suppose that this region is operated from a new power source with voltage $V_{S_1} = .6V$ instead of 2 volts. The calculations above are renormalized so that

$$\check{\eta}_{1peak_norm} \triangleq 1, \quad \{V_{S_1} = .6V, \quad V_{L1_max} = V_S/2 = .3V\}$$

$$\langle \check{\eta}_{1_norm} \rangle = .131/.176 \cong .744, \quad PAPR_{wf1} \approx 1.344$$

$\langle \check{\eta}_{1_norm} \rangle$ is substantially enhanced because the original peak efficiency of .176 is transformed to 100 percent available peak waveform efficiency through the selection of a new voltage source, V_{S_1} . Another way to consider the enhancement is that Z_Δ becomes zero for the series modulator when .3 volts is desired at the load. There is therefore zero dissipation in Z_Δ , for that particular operating point. Hence, just as $\check{\eta}_{1peak}$ is transformed from .176 to 1, $\langle \check{\eta}_1 \rangle$ is transformed from .131 to .744.

In domain 2 we perform similar calculations

$$\check{\eta}_{2peak} = .538 ; \{V_S = 2V, V_{L2} = .7V\}$$

Again we use the modified CDF to obtain the un-normalized $\langle \check{\eta}_2 \rangle \approx .338$ first, followed by $\langle \check{\eta}_{2_norm} \rangle$.

$$\langle \check{\eta}_{2_norm} \rangle \approx .629, \quad \check{\eta}_{2_peak_norm} \triangleq 1, \quad \{V_{s_2} = 1.4V, V_{L2_max} = .7V\}, \quad PAPR_{wf2} \approx 1.589$$

Likewise we apply the same procedure for domain 3 and obtain;

$$\langle \check{\eta}_{3_norm} \rangle \approx .626, \quad \check{\eta}_{3p_norm} \triangleq 1, \quad \{V_s = 2V, V_{L3_max} = 1V\}, \quad PAPR_{wf3} \approx 1.597$$

The corresponding block diagram for an instantiation of this solution becomes;

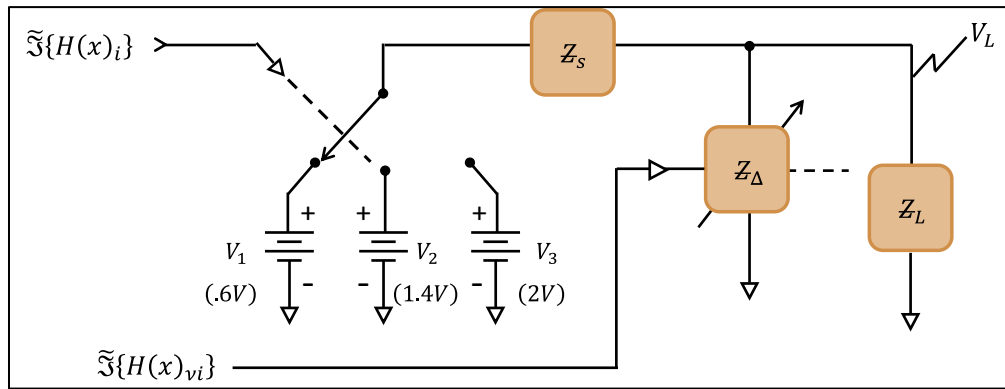


Figure 7-8 Three Domain Type 1 Series Modulator

The switch transitions as each threshold associated with a statistical boundary is traversed, selecting a new domain according to $\tilde{\mathfrak{S}}\{H(x)_1, H(x)_2, H(x)_3\}$ ($\zeta = 3$). The index i in the figure 7-8 is a domain index which is a degree of freedom for the modulator. The v, i subscript refers to v degrees of modulator freedom associated with the i^{th} domain. In a practical implementation, the entropy $H(x)$ of the information source is parsed between the various modulator degrees of freedom. In this example 2 bits of information can be assigned to select the i^{th} domain. Using this method we obtain efficiency improvements above the single domain average which is

calculated as $\langle \eta \rangle \approx .347$. In comparison, the new efficiencies and probability weightings per domain are;

$$\langle \check{\eta}_1 \rangle = .744; \quad 9.1\% \text{ probability weighting}$$

$$\langle \check{\eta}_2 \rangle = .629; \quad 81.8\% \text{ probability weighting}$$

$$\langle \check{\eta}_3 \rangle = .626; \quad 9.1\% \text{ probability weighting}$$

The final weighted average of this solution, which has not yet been optimized, is given by;

$$\langle \check{\eta}_{tot} \rangle = \eta_{sx} \cdot [(.091 \times .744) + (.818 \times .629) + (.091 \times .626)] \cong \eta_{sx} \cdot .64$$

As we shall show in the next section, the optimal choice of values for V_1, V_2 , can improve on the results of this example, which is already a noticeable improvement over the single domain solution of $\langle \check{\eta}_{mod} \rangle = .347$.

η_{sx} is the efficiency associated with the switching mechanism which is a cascade efficiency.

Typical switch efficiencies of moderate to low complexity can attain efficiencies of .9.

However, as switch complexity increases, η_{sx} may become a design liability. η_{sx} is considered a directly dissipative loss and a design tradeoff.

Voltage is the fundamental quantity from which the energy domains are derived. Preserving the information to voltage encoding is equivalent to properly accounting for momentum. This is important because $\rho(\check{\eta})$ is otherwise not unique. We could also choose to represent efficiency as an explicit function of momentum as in chapter 5, thereby emphasizing a more fundamental view. However, there is no apparent advantage for this simple modulator example. More

complex encoder mappings involving large degrees of freedom and dimensionality may benefit from explicitly manipulating the density ($\check{\eta}(p)$) at a more fundamental level.

7.3. Optimization for Type 1 Modulator , $\zeta = 3$ Case

From the prior example we can obtain an optimization of the form

$$\max\{\langle\check{\eta}_{tot}\rangle\} = \max\{\lambda_1\langle\check{\eta}_1\rangle + \lambda_2\langle\check{\eta}_2\rangle + \lambda_3\langle\check{\eta}_3\rangle\} \quad (7-7)$$

$$\sum \lambda_i = 1$$

It is also noted that

$$\langle\check{\eta}_1\rangle = \mathfrak{F}\{V_{s_1}\}, \quad \langle\check{\eta}_2\rangle = \mathfrak{F}\{V_{s_1}, V_{s_2}\}, \quad \langle\check{\eta}_3\rangle = \mathfrak{F}\{V_{s_2}, V_{s_3}\}$$

The goal is to solve for the best domains by selecting optimum voltages $V_{s_1}, V_{s_2}, V_{s_3}$. V_{s_3} is selected as the maximum available supply by definition and was set to 2V for the prior example. The minimum available voltage is set to $V_{s_0} = 0$. Therefore only V_{s_1} and V_{s_2} must be calculated for the optimization of a three domain example, which also simultaneously determines λ_1, λ_2 and λ_3 . We proceed with substitutions for thresholds, domains, and efficiencies in terms of appropriate variables and supplementary relations;

$$\max\{\check{\eta}_{tot}\} = \max\left\{\lambda_1 k_{1norm} \int_0^{\eta_1} \check{\eta}_1 \rho_1(\check{\eta}_1) d\check{\eta}_1 + \lambda_2 k_{2norm} \int_{\eta_{12}}^{\eta_2} \check{\eta}_2 \rho_2(\check{\eta}_2) d\check{\eta}_2 + \lambda_3 k_{3norm} \int_{\eta_{23}}^{\eta_3} \check{\eta}_3 \rho_3(\check{\eta}_3) d\check{\eta}_3\right\} \quad (7-8)$$

$$\eta_1 = \frac{V_{L_1}^2}{V_{L_1}V_{S_1} - V_{L_1}^2}, \quad \eta_2 = \frac{V_{L_2}^2}{V_{L_2}V_{S_2} - V_{L_2}^2}, \quad \eta_3 = \frac{V_{L_3}^2}{V_{L_3}V_{S_3} - V_{L_3}^2}$$

$$\eta_{12} = \frac{V_{L_1}^2}{V_{L_1}V_{S_2} - V_{L_1}^2}, \quad \eta_{23} = \frac{V_{L_2}^2}{V_{L_2}V_{S_3} - V_{L_2}^2},$$

$$\check{\eta}_1 = \frac{V_L^2}{V_LV_{S_1} - V_L^2}, \quad \check{\eta}_2 = \frac{V_L^2}{V_LV_{S_2} - V_L^2}, \quad \check{\eta}_3 = \frac{V_L^2}{V_LV_{S_3} - V_L^2}$$

$$d\check{\eta}_\zeta = \left(\frac{V_{S_\zeta}}{(V_{S_\zeta} - V_L)^2} \right) dV_L, \quad \zeta = 1, 2, 3$$

$$\lambda_1, \lambda_2, \lambda_3 \geq 0 \quad \lambda_1 + \lambda_2 + \lambda_3 = 1$$

$$\begin{cases} \lambda_1 = \int_0^{V_{L_1}} \rho_1(V_L) dV_L \\ \lambda_2 = \int_{V_{L_1}}^{V_{L_2}} \rho_2(V_L) dV_L \\ \lambda_3 = \int_{V_{L_2}}^1 \rho_3(V_L) dV_L \end{cases}$$

$$V_{L_\zeta} \triangleq \frac{V_{S_\zeta}}{2}, \quad \zeta = 1, 2, 3$$

$k_{\zeta_{norm}}$ are determined such that each sub distribution max{CDF} equal 1, transforming them into separate pdfs with proper probability measures. $\lambda_{1,2,3}$ are simply the following probabilities with respect to the original composited Gaussian pdf $\rho(V_L)$;

$$\lambda_1 = \{P(0 \leq V_L \leq V_{L_1})\}$$

$$\lambda_2 = \{P(V_{L_1} < V_L \leq V_{L_2})\}$$

$$\lambda_3 = \{P(V_{L_2} < V_L \leq 1)\}$$

What must be obtained from the prior equations are V_{L_1} and V_{L_2} . Varying V_{L_1} and V_{L_2} provides an optimization for $\langle \check{\eta}_{tot} \rangle$. The optimization performed according to the domains calculation equations yields an optimal set of fixed sources, $V_{s_1} \cong .976$ and $V_{s_2} \cong 1.328$, which enable the overall averaged efficiency $\langle \check{\eta}_{tot} \rangle \cong .736$. This is significantly better than the original single domain partition result of .347 and 9.6 % better than the guess used to demonstrate calculation mechanics in the previous section. If the signal amplitude statistic changes then so do the numbers. However, the methodology for optimization remains essentially the same. What is also significant is the fact that partitioning the original pdf has simultaneously lowered the dynamic range requirement in each partitioned domain. This dynamic range reduction can figure heavily into strategies for optimization of architectures which use switched power supplies.

7.4. Ideal Modulation domains

Suppose we wish to ascertain an optimal theoretical solution for both number of domains and their respective threshold potentials for the case where amplitude is exclusively considered as a function of any statistical distribution $p(V_L)$. We begin in the familiar way using $PAPR$ and $\langle \check{\eta} \rangle$ definitions from chapter 6.

$$\langle \check{\eta}_i \rangle = \frac{1}{(k_i PAPR_i + a_i)}$$

This defines instantaneous $\langle \check{\eta} \rangle$ for a single domain. For multiple energy domains and the 1st Law of Thermodynamics we may write;

$$\langle \check{\eta} \rangle = \sum_i \langle \check{\eta}_i \lambda_i \rangle = \sum_i \lambda_i \left\langle \frac{P_{out_i}}{P_{in_i}} \right\rangle$$

(7-9)

From the 2nd Laws of Thermodynamics we know

$$\left\langle \frac{P_{out_i}}{P_{in_i}} \right\rangle \leq 1$$

$$\langle \check{\eta}_i \rangle \leq 1$$

λ_i is the statistical weighting for $\check{\eta}_i$ over the i^{th} domain so that;

$$\sum_i \lambda_i = 1$$

It is apparent that each and every $\check{\eta}_i \rightarrow 1$ for $\langle \check{\eta} \rangle$ to become one. That is, it is impossible to achieve an overall efficiency of $\langle \check{\eta} \rangle \rightarrow 1$ unless each and every i^{th} partition is also 100% efficient. Hence,

$$\max \langle \check{\eta} \rangle = \sum_i \lambda_i = 1$$

λ_i are calculated as the weights for each i^{th} partition such that;

$$\lambda_i = \int_{V_{L_{i-1}}}^{V_{L_i}} \rho(V_L) dV_L$$

It follows for the continuous analytical density function $\rho(V_L)$ that

$$\sum_i \lambda_i = \int \rho(V_L) dV_L$$

In order for the prior statements to be consistent we recognize the following for infinitesimal domains;

$$\Delta V_{L_i} \triangleq (V_{L_i} - V_{L_{i-1}}) \rightarrow dV_L$$

$$\Delta \lambda_i \rightarrow \lambda_i - \lambda_{i-1} \rightarrow d\lambda$$

$$\zeta \rightarrow \infty$$

This means that in order for the Riemannian sum to approximately converge to the integral,

$$\lambda_i \approx \rho(V_{L_i})$$

The increments of potentials in the domains must become infinitesimally small such that ζ grows large even though the sum of all probabilities is bounded by the CDF. Since there are an infinite number of points on a continuous distribution and we are approximating it with a limit of discrete quantities, some care must be exercised to insure convergence. This is not considered a significant distraction if we assign a resolution to phase space according to the arguments of chapter 4.

This analysis implies an architecture consisting of a bank of power sources which in the limit become infinite in number with the potentials separated by $\Delta V_{S_i} \rightarrow dV_S$. A switch may be used to select this large number of separate operating potentials “on the fly”. Such a switch cannot be easily constructed. Also, its dissipative efficiency η_{sx} , would approach zero, thus defeating a

practical optimization. Such an architecture can be emulated by a continuously variable power supply with bandwidth calculated from the TE relation of chapter 3. Such a power supply poses a number of competing challenges as well. Fortunately, a continuously variable power source is not required to obtain excellent efficiency increases as we have shown with a 3 domain solution and will presently revisit for domains of variable number.

7.5. Sufficient Number of domains, ζ

A finite number of domains will suffice for practical applications. A generalized optimization procedure may then be prescribed for setting domain thresholds.

$$\max\{\check{\eta}_{tot}\} = \max\left\{\sum_i \lambda_i k_{i_{norm}} \int_{\eta_{\{i-1,i\}}}^{\eta_i} \check{\eta}_i p_i(\check{\eta}_i) d\check{\eta}_i\right\}$$

(7-10)

$$\eta_i \triangleq \frac{V_{L_i}^2}{V_{L_i} V_{S_i} - V_{L_i}^2}, \quad \eta_{\{i-1,i\}} \triangleq \frac{V_{L_{i-1}}^2}{V_{L_{i-1}} V_{S_i} - V_{L_{i-1}}^2}$$

$$\check{\eta}_i \triangleq \frac{V_L^2}{V_L V_{S_i} - V_L^2}$$

$$d\check{\eta}_i = \left(\frac{V_{S_i}}{(V_{S_i} - V_L)^2}\right) dV_L$$

$$\lambda_i = \int_{V_{L_{i-1}}}^{V_{L_i}} p(V_L) dV_L$$

$$\sum_i \lambda_i \triangleq 1$$

$$V_{L_i} \triangleq \frac{V_{S_i} Z_L}{(Z_s + Z_L)}$$

Figure 7-8 illustrates the thermodynamic efficiency improvement as a function of the number of optimized domains in the case where the signal $PAPR \sim 10.5 \text{ dB}$. Figure 7-9 was verified with theoretical calculation and experimentation using a laboratory apparatus. In all cases the deviation between calculation and measurement was less than .7%, attributed to test fixture imperfections, resolution in generating the test signal distribution and measurement accuracies. Figure 7-10 illustrates the relative frequencies of voltages measured across the load for the experiment with a circuit source impedance of zero. Table 7-1 lists the optimized voltage thresholds or alternately, the power supplies required for implementation.

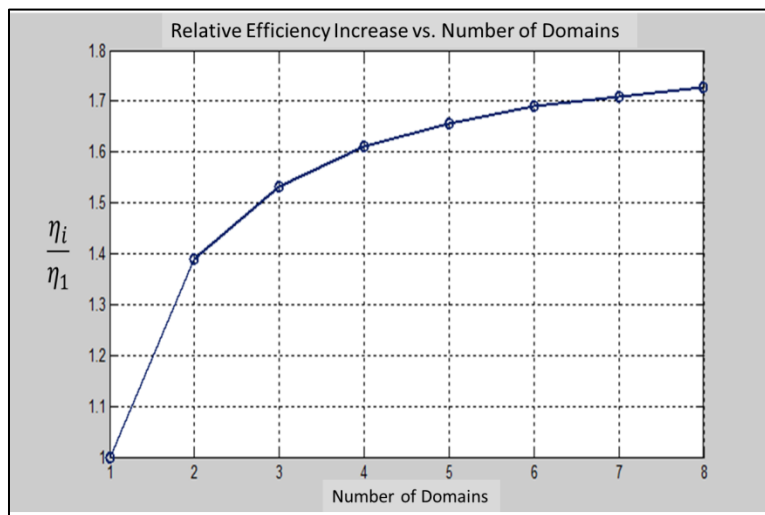


Figure 7-9 Relative Efficiency Increase as a Function of the Number of Optimised Domains

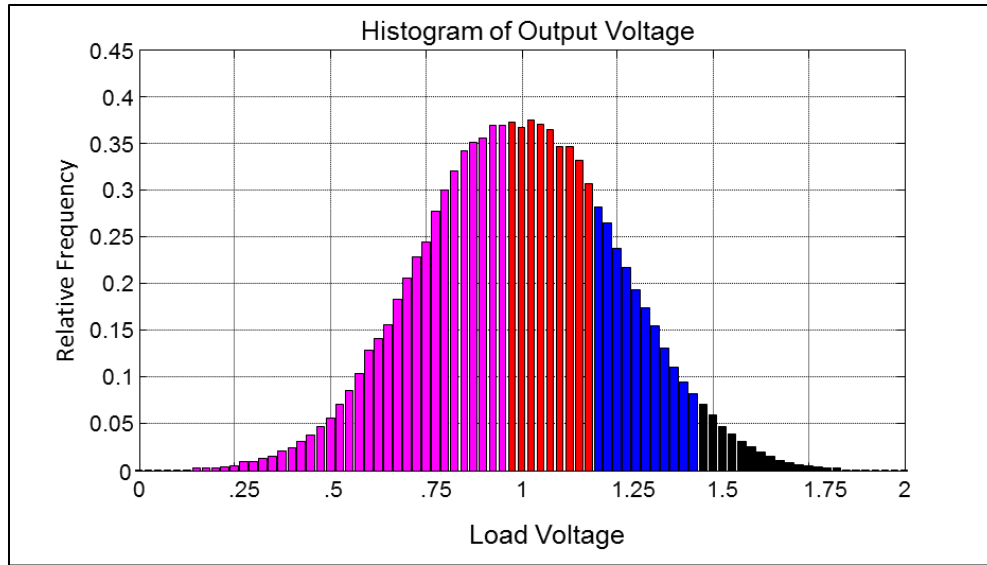


Figure 7-10 Relative Frequency of Output Load Voltage Measurements

Table 7-1 Corresponding Power Supply Values Defining optimized Thresholds for a given ζ

	1 Domain	2 Domains	3 Domains	4 Domains	5 Domains	6 Domains	7 Domains	8 Domains
Supply1	2.0V	2.0V	2.0V	2.0V	2.0V	2.0V	2.0V	2.0V
Supply2		1.28V	1.41V	1.46V	1.53V	1.55V	1.57V	1.59V
Supply3			1.07V	1.19V	1.28V	1.34V	1.37V	1.39V
Supply4				0.95V	1.09V	1.18V	1.22V	1.26V
Supply5					0.89V	1.02V	1.07V	1.12V
Supply6						0.85V	0.92V	0.99V
Supply7							0.81V	0.88V
Supply8								0.79V

This optimization procedure is applicable for all forms of $\rho(V_L)$ even those with discrete RVs, provided care is exercised in defining the thresholds and domains for the RV. Optimization is best suited to numerical techniques for arbitrary $\rho(V_L)$.

7.6. Zero Offset Gaussian Case

A zero offset Gaussian case is reviewed in this section using a direct optimization method to illustrate the contrast compared to the instantaneous efficiency approach. The applicable probability density for the load voltage is illustrated in figure 7-11.

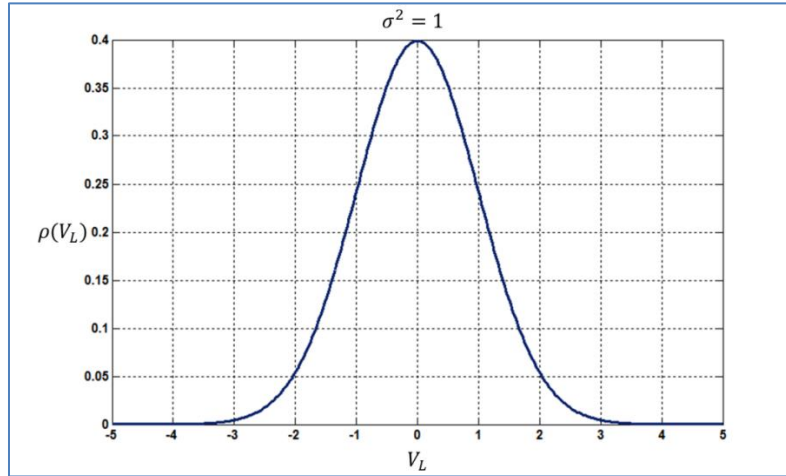


Figure 7-11 Probability density of load voltage for zero offset case

The optimization procedure in this case uses the proper thermodynamic efficiency as the kernel of optimization so that;

$$\max\{\eta\} = \max\left\{\frac{\langle P_e \rangle}{\langle P_{in} \rangle}\right\}$$

The more explicit form with domain enumeration is given by;

$$\max\{\eta\} = \max\left\{\sum_i \lambda_i k_{i_{norm}} \frac{\langle P_e \rangle_i}{\langle P_{in} \rangle_i}\right\}$$

$\langle P_e \rangle_i$ and $\langle P_{in} \rangle_i$ are the average effective and input powers respectively. Appendix H provides the detailed form in terms of the numerator RV and denominator RV which are in the most general case non-central gamma distributed with domain spans defined as functions $f\{V_T\}_i$, $f\{V_T\}_{i-1}$ of the threshold voltages.

$$\eta = \max \left\{ \frac{\sum_i \lambda_i k_{inorm} \int_{f\{V_T\}_{i-1}}^{f\{V_T\}_i} x_e \rho(x_e) dx_e}{\sum_i \lambda_i k_{inorm} \int_{f\{V_T\}_{i-1}}^{f\{V_T\}_i} x_{in} \rho(x_{in}) dx_{in}} \right\} \quad (7-11)$$

The general form of the gamma distributed RV in terms of the average i^{th} domain load voltage is [25, 32];

$$\rho(x) = \frac{1}{2} \left(\frac{x}{\sum_i \langle V_{L_i} \rangle} \right)^{[(N-2)/4]} e^{-\frac{(x - \sum_i \langle V_{L_i} \rangle)}{2\sigma^2}} I_{[(N-2)/2]} \left(\frac{1}{2\sigma^2} \sqrt{x \sum_i \langle V_{L_i} \rangle} \right); \quad x \geq 0 \quad (7-12)$$

Since a single subordinate density corresponds to figure 7-11, $N=1$ for the current example .

$I_{[(N-2)/2]}$ is a modified Bessel function. The i^{th} domain load voltage in the numerator of eq. 7-11

is due to signal only while the denominator must contemplate signal plus any overhead terms. It

is apparent that this direct form of efficiency optimization may be more tedious under certain

circumstances compared to an optimization based on the instantaneous efficiency metric. The

optimized thresholds can be calculated by varying the domains similar to the method illustrated

in Equation 7-10 . This is a numerical calculus of variations approach where the ratio of 7-11 is

tested to obtain a converging gradient . Optimized thresholds are provided in table 7-2 for up to $\zeta = 16$ and normalized maximum Load Voltage of 1 . In this case symmetry reduces the number of optimizations by half. The corresponding circuit architecture is illustrated in figure 7-12.

Table 7-2 Values for Thermodynamic Efficiency vs. Number of Optimized Partitions ($Z_s = 0$), $PAPR \sim 11.8dB$

Num. of Domains $\zeta = \max\{i\}$	Supply Voltages (V_{si})	Thermodynamic Efficiency
2	± 1	32.0%
4	$\pm 1, \pm 0.45$	56.6%
6	$\pm 1, \pm 0.55, \pm 0.32$	68.26%
8	$\pm 1, \pm 0.6, \pm 0.4, \pm 0.24$	75.0%
10	$\pm 1, \pm 0.65, \pm 0.47, \pm 0.33, \pm 0.21$	79.45%
12	$\pm 1, \pm 0.67, \pm 0.51, \pm 0.39, \pm 0.29, \pm 0.19$	82.5%
14	$\pm 1, \pm 0.68, \pm 0.53, \pm 0.42, \pm 0.33, \pm 0.25, \pm 0.16$	84.8%
16	$\pm 1, \pm 0.70, \pm 0.56, \pm 0.46, \pm 0.38, \pm 0.3, \pm 0.23, \pm 0.15$	86.5%

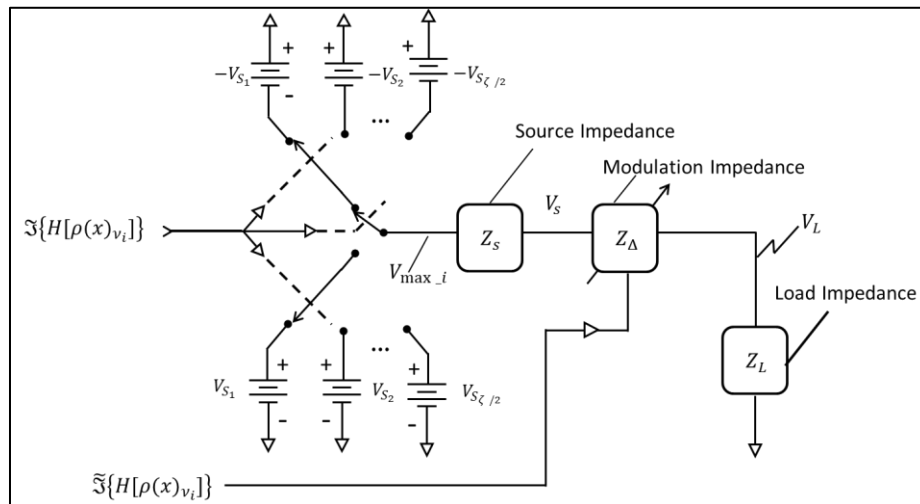


Figure 7-12 Type 1 differentially sourced modulator

Table 7-3 and figure 7-13 illustrate the important performance metrics.

Table 7-3 Calculated thermodynamic efficiency using thresholds from table 7-2

	$\zeta = 2$	$\zeta = 4$	$\zeta = 6$	$\zeta = 8$	$\zeta = 10$
Domain Pair 1	$2\lambda_1 = 1$ $\eta_1 = 32.0\%$	$2\lambda_1 = 0.627$ $\eta_1 = 56.6\%$	$2\lambda_1 = 0.368$ $\eta_1 = 61.6\%$	$2\lambda_1 = 0.199$ $\eta_1 = 64.1\%$	$2\lambda_1 = 0.147$ $\eta_1 = 64.8\%$
Domain Pair 2		$2\lambda_2 = 0.373$ $\eta_2 = 56.5\%$	$2\lambda_2 = 0.424$ $\eta_2 = 75.7\%$	$2\lambda_2 = 0.329$ $\eta_2 = 79.1\%$	$2\lambda_2 = 0.229$ $\eta_2 = 81.7\%$
Domain Pair 3			$2\lambda_3 = 0.201$ $\eta_3 = 64.7\%$	$2\lambda_3 = 0.325$ $\eta_3 = 80.2\%$	$2\lambda_3 = 0.295$ $\eta_3 = 83.4\%$
Domain Pair 4				$2\lambda_4 = 0.146$ $\eta_4 = 68.8\%$	$2\lambda_4 = 0.234$ $\eta_4 = 83.5\%$
Domain Pair 5					$2\lambda_5 = 0.093$ $\eta_5 = 73.1\%$
Final Efficiency	32.0%	56.6%	68.26%	75.0%	79.45%

	$\zeta = 12$	$\zeta = 14$	$\zeta = 16$
Domain Pair 1	$2\lambda_1 = 0.117$ $\eta_{11} = 65.3\%$	$2\lambda_1 = 0.074$ $\eta_{11} = 66.0\%$	$2\lambda_1 = 0.063$ $\eta_{11} = 66.1\%$
Domain Pair 2	$2\lambda_2 = 0.174$ $\eta_2 = 82.9\%$	$2\lambda_2 = 0.134$ $\eta_2 = 82.4\%$	$2\lambda_2 = 0.110$ $\eta_2 = 83.14\%$
Domain Pair 3	$2\lambda_3 = 0.216$ $\eta_3 = 86.7\%$	$2\lambda_3 = 0.163$ $\eta_3 = 87.7\%$	$2\lambda_3 = 0.133$ $\eta_3 = 88.3\%$
Domain Pair 4	$2\lambda_4 = 0.233$ $\eta_4 = 87.1\%$	$2\lambda_4 = 0.197$ $\eta_4 = 88.8\%$	$2\lambda_4 = 0.177$ $\eta_4 = 89.1\%$
Domain Pair 5	$2\lambda_5 = 0.18$ $\eta_5 = 85.9\%$	$2\lambda_5 = 0.202$ $\eta_5 = 88.6\%$	$2\lambda_5 = 0.168$ $\eta_5 = 90.7\%$
Domain Pair 6	$2\lambda_6 = 0.078$ $\eta_6 = 74.75\%$	$2\lambda_6 = 0.158$ $\eta_6 = 87.05\%$	$2\lambda_6 = 0.162$ $\eta_6 = 90.2\%$
Domain Pair 7		$2\lambda_7 = 0.072$ $\eta_7 = 75.6\%$	$2\lambda_7 = 0.127$ $\eta_7 = 88.2\%$
Domain Pair 8			$2\lambda_8 = 0.059$ $\eta_8 = 77.2\%$
Final Efficiency	82.5%	84.8%	86.5%

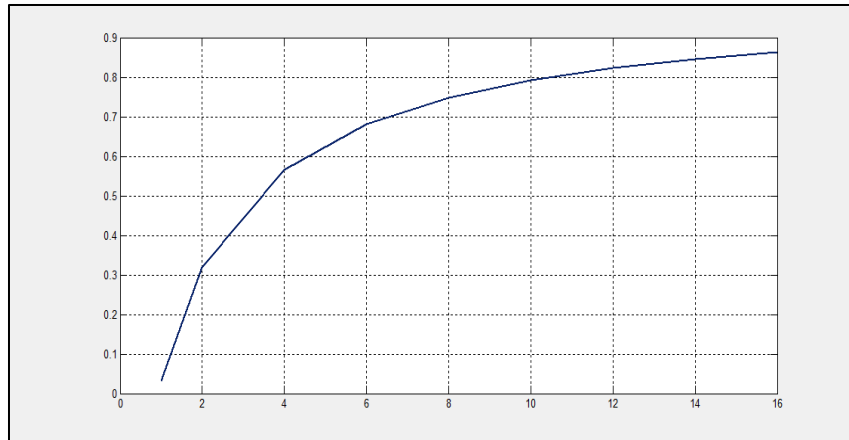


Figure 7-13 Thermodynamic efficiency for a given number of optimized domains

Experiments were conducted with modulator hardware 4,6, and 8 domains with a signal $PAPR \sim 11.8 \text{ dB}$. Figure 7-14 shows the measured results for thermodynamic efficiency compared to theoretical. The differences were studied and found to be due to fixture losses (i.e. $\eta_{diss} \neq 1$) and the resolutions associated with signal generation as well as measurement. The $\zeta=1$ case in figure 7-13 is based on the single supply solution.

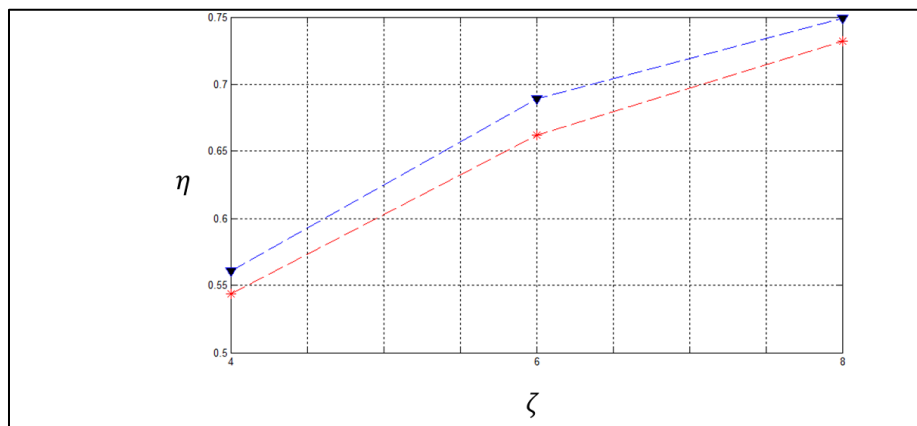


Figure 7-14 Measured Thermodynamic efficiency for a given number of optimized domains (4, 6, 8)

Experiments agree well with the theoretical optimization.

7.7. Results for Standards Based Modulations

The standards based modulation schemes, used to obtain the efficiency curve of figure 7-4 for the canonical non-zero offset case, were tested after optimization using a differential based zero offset implementation of figure 7-12 . The results are given for 4, 6, 8 domains illustrated in figure 7-15.

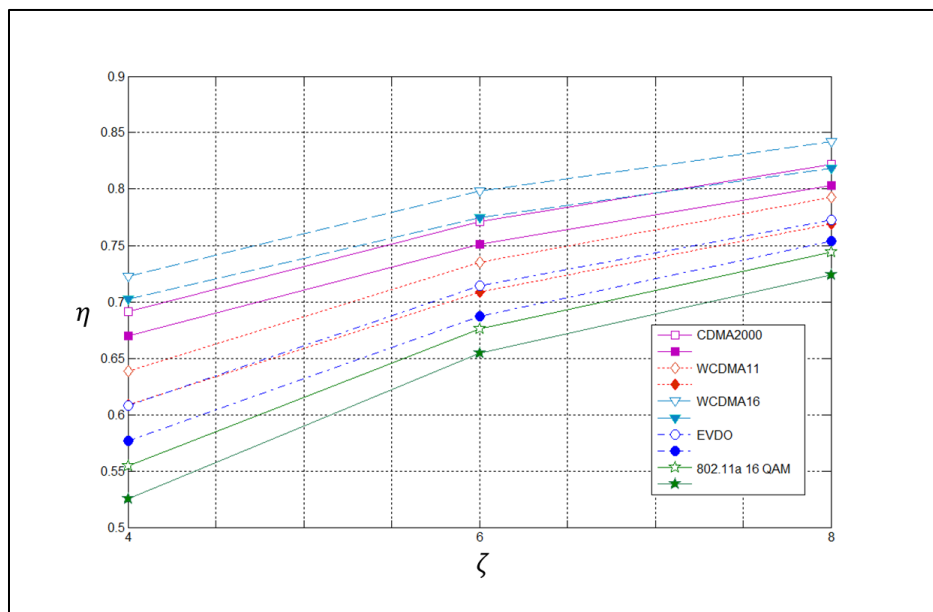


Figure 7-15 Thermodynamic efficiency for a given number of optimized domains

Each modulation type is indicated in the legend. Open symbols correspond to a theoretical optimal with $\eta_{diss} = 1$. Filled symbols correspond to measured values with $\eta_{diss} \cong .95$. The graphics in figure 7-15 ascend from the greatest signal *PAPR* to the least. Figure 7-16 illustrates the performance of the standards over the range of domains from 1 through 10.

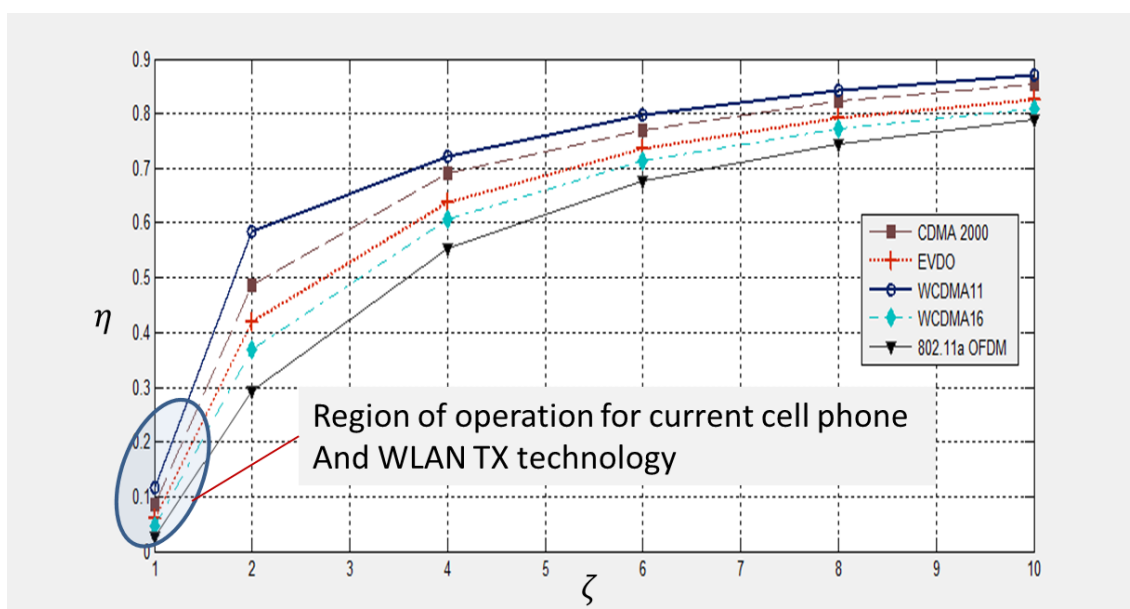


Figure 7-16 Optimized Efficiency Performance vs. ζ for (Standards Cases)

Appendix L provides an additional detailed example of an 802.11a waveform as a consolidation of the various calculations and quantities of interest. In addition, a schematic of the modulation test apparatus is included.

8. MISCELLANEOUS TOPICS

A variety of topics are presented in this chapter to illustrate an array of interesting interpretations related to the dissertation topic. The treatments are brief and include, some limits on performance for capacity, relation to Landauer's principle, time variant uncertainty, and Gabor's uncertainty. The diversity of subjects illustrates a wide range of applicability for the disclosed ideas.

8.1. Encoding Rate , Some Limits, and Relation to Landauer's Principle

The capacity rate equation was derived in chapter 4 for the D dimensional case ;

$$C \leq \sum_{\alpha=1}^D \frac{P_{m_\alpha}}{\langle \mathcal{E}_{k_\alpha} \rangle_s PAER_\alpha} \left(\ln \left[\frac{\left(\frac{m^2 P_{m_\alpha}}{PAER_\alpha} \right)}{\tilde{\sigma}_{p_{n,\alpha}}^2} + 1 \right] \right)$$

Consider the circumstance where $\frac{P_{m_\alpha}}{\langle \mathcal{E}_{k_\alpha} \rangle PAER_\alpha} \rightarrow \infty$

$$\lim_{\frac{P_{m_\alpha}}{\langle \mathcal{E}_{k_\alpha} \rangle PAER_\alpha} \rightarrow \infty} C = \frac{2D}{\ln(2)} \frac{P}{N_0} \equiv C_\infty$$

(8-1)

A limit of the following form is used to obtain the result of 8-1 [3, 63];

$$\lim_{x \rightarrow \infty} x \log_2 \left(\frac{x+1}{x} \right) = \log_2(e) = \frac{1}{\ln(2)}$$

The infinite slew rate capacity C_∞ is twice that for the comparative Shannon capacity because both momentum and configuration spaces are considered here. This is the capacity associated with instantaneous access to every unique coordinate of phase space. We may further rearrange the equation for C_∞ to obtain the minimum required energy per bit for finite non zero thermal noise where P is the average power per dimension;

$$\frac{P}{C_\infty} = \frac{N_o \ln(2)}{2D} \quad J/bit$$

(8-2)

N_o is an approximate equivalent noise power spectral density based on the thermal noise floor , $N_o = 2kT^\circ$, T° is a temperature in degrees Kelvin (K°) and Boltzman's constant $k = 1.38 \times 10^{-23} \text{ J/K}^\circ$. A factor of 2 is included to account for the independent influence of configuration noise and momentum noise. Therefore, the number of Joules per bit for $D=1$ is the familiar classical limit of $(.6931)kT^\circ/2$ and the energy per bit to noise density ratio is $E_b/N_o = \frac{\ln(2)}{2} \simeq -4.6 \text{ dB}$. This is 3dB lower than the classical results because we may encode one bit in momentum and one bit in configuration for a single energy investment [63].

Each message trajectory consisting of a sequence of samples would be infinitely long and therefore require an infinite duration of time to detect at a receiver to reach this performance limit. Also, the samples of the sequence must be Gaussian distributed.

Shannon also contemplated the error free data through put when the encoded values are other than Gaussian. In the case where the values are binary orthogonal encodings it can be shown that [63];

$$E_b/N_o \cong \frac{2 \ln \sqrt{2}}{2} = -1.6 \text{ dB}$$

We include both momentum and configuration to obtain the result per dimension. The encoded sequence must be comprised of an infinite sequence of binary orthogonal symbols to achieve this limit and we must use both configuration and momentum else the results increase by 3dB for the given E_b/N_o .

N_o as given is an approximation. Over its domain of accuracy the total noise variance may be approximated using [64];

$$\sigma_n^2 = \int_0^B N_o \, df$$

A difficulty with this approximation arises from the ultra-violet catastrophe when B approaches ultra-high frequencies [64]. Plank and Einstein resolved this inconsistency using a quantum correction which yields [11, 22, 30, 65];

$$P_n(f) = \frac{\hbar f}{e^{\hbar f/kT} - 1} \text{ W/Hz}, \quad h = 6.6254 \times 10^{-34} \text{ Js}$$

(8-3)

A plot of the result follows for room temperature and $2.9 K^\circ$. $\tilde{\sigma}_{p_{n,\alpha}}^2$ is composed of thermal and quantum terms which are plotted separately in the graph.

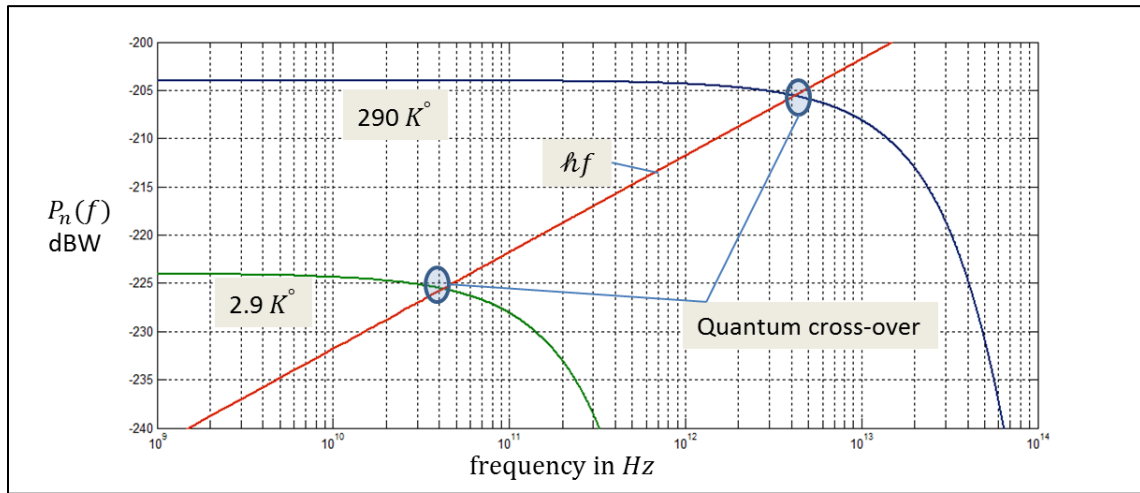


Figure 8-1 Noise Power vs. Frequency

The thermal noise with quantum correction has an approximate 3 dB bandwidth of $7.66e12$ Hz for the room temperature case and $7.66e10$ for the low temp case. The frequencies at which the quantum uncertainty variance competes with the thermal noise floor is approximately $4.26e12$ and $4.26e10$ Hz respectively. The corresponding adjusted values for $P_n(f) + hf$ are the suggested values to be used in the capacity equations to calculate noise powers at extreme bandwidths or low temperature. At the crossover points, the total value of $\tilde{\sigma}_{p_{n,\alpha}}^2$ is increased by 3dB. hf is apparently independent of temperature.

An equivalent noise bandwidth principle may be applied to accommodate the quantity $P_n(f) + hf$ and calculate an equivalent noise density \tilde{N}_0 over the information bandwidth B .

$$\tilde{N}_o = \frac{1}{B} \int_0^B \hbar f \frac{e^{\hbar f/kT^\circ}}{e^{\hbar f/kT^\circ} - 1} df$$

(8-4)

We may combine this density with the TE relation to obtain;

$$\frac{\langle \mathcal{E}_k \rangle_s}{\tilde{N}_o} \geq \frac{\max\{\dot{\vec{p}} \cdot \dot{\vec{q}}\}}{2 \int_0^B \hbar f \frac{e^{\hbar f/kT^\circ}}{e^{\hbar f/kT^\circ} - 1} df \text{ (PAER)}}$$

(8-5)

If we consider antipodal binary state encoding then the energy per sample correspond to one half the energy per bit. At frequencies where thermal noise is predominate we can calculate the required energy per bit to encode motion in a particle whilst overcoming the influence of noise such that over a suitably long interval of observation, a sequence of binary encodings may be correctly distinguished.

$$\frac{\langle \mathcal{E}_b \rangle}{\tilde{N}_o} \geq \frac{\max\{\dot{\vec{p}} \cdot \dot{\vec{q}}\}}{f_s kT^\circ \text{ (PAER)}}$$

(8-6)

The maximum work rate of the particle is therefore bounded by (for thermal noise only);

$$\max\{\dot{\vec{p}} \cdot \dot{\vec{q}}\} \leq f_s kT^\circ \text{ (PAER)} \ln(2)$$

(8-7)

According to chapter 5 a maximum theoretical efficiency to generate one bit is bounded by;

$$\eta \leq \frac{f_s k T^\circ \ln(2)}{P_m}$$

(8-8)

An example momentum space trajectory depicting, binary encoding, is illustrated in figure 8-2. Information is encoded in $\pm p_{max} = \pm 1$ the extremes of the momentum space for this example. This extreme trajectory is the quickest path between the two states. It is apparent that $|\langle v_p \rangle| \neq v_{max}$. Therefore $PAER \neq 1$. If we require $PAER = 1$ for maximum encoding efficiency, then Δt (the time span of the trajectory) must approach zero which requires the rate of work to approach infinity. Clearly, such a pathological case is also limited by relativistic considerations.

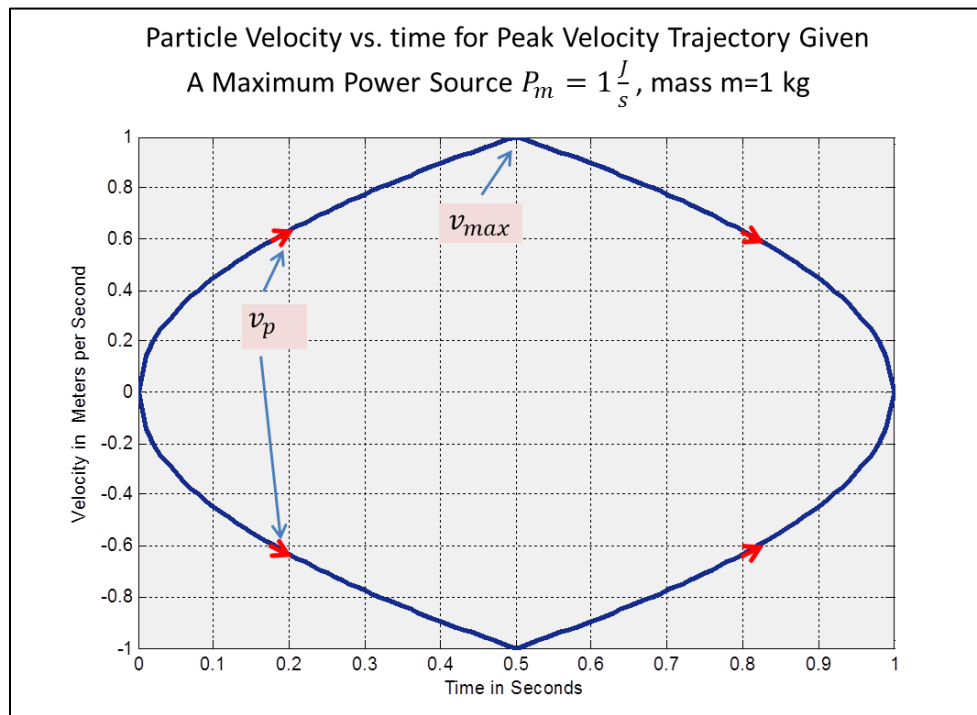


Figure 8-2 Binary Particle Encoding

Now suppose that we encode binary data in position rather than momentum. We illustrate this activity in the velocity vs. position plane for a single dimension for the position encoding of $\pm R_s$, the extremes of configuration space (ref. figure 8-3). The velocity trajectory as shown is the fastest between the extreme positions. In this view the particle momentum may be zero at the extremes $\pm R_s$ but not between. If we consider that information can be stored in the positions $\pm R_s$ then work is required to move the particle between these positions. Even when thermal noise is removed from the scenario we may calculate a finite maximum required work per bit because \tilde{N}_o possesses a residual quantum uncertainty variance which must be overcome to distinguish between the two antipodal states. This may be given approximately in equation 8-9 ;

$$\max\{\dot{p} \cdot \dot{q}\} \gtrsim f_s \hbar (PAER) \ln(2)$$

(8-9)

Note that *PAER* may only approach 1 as Δt approaches zero, requiring $f_s \rightarrow \infty$. No matter the encoding technique we cannot escape this requirement. If we construct a binary system which transfers distinguishable data in the presence of thermal noise or quantum noise, independent states require the indicated work rate per transition. From chapter 5 it is also known that since we cannot predict a future state of a particle, the delivery particle possesses an average recoil momentum during an exchange equal and opposite in a relative sense to the target particle encoding the state. This recoil momentum is waste, and ultimately dissipates in the environment according to the second law. According to equation 8.8 (the thermal noise regime) the theoretical efficiency of 1 is achieved when $P_m = f_s k T^\circ \ln \sqrt{2}$ which is equivalent to an energy per sample of

$$(\mathcal{E}_k)_s = kT^\circ \ln \sqrt{2}$$

(8-10)

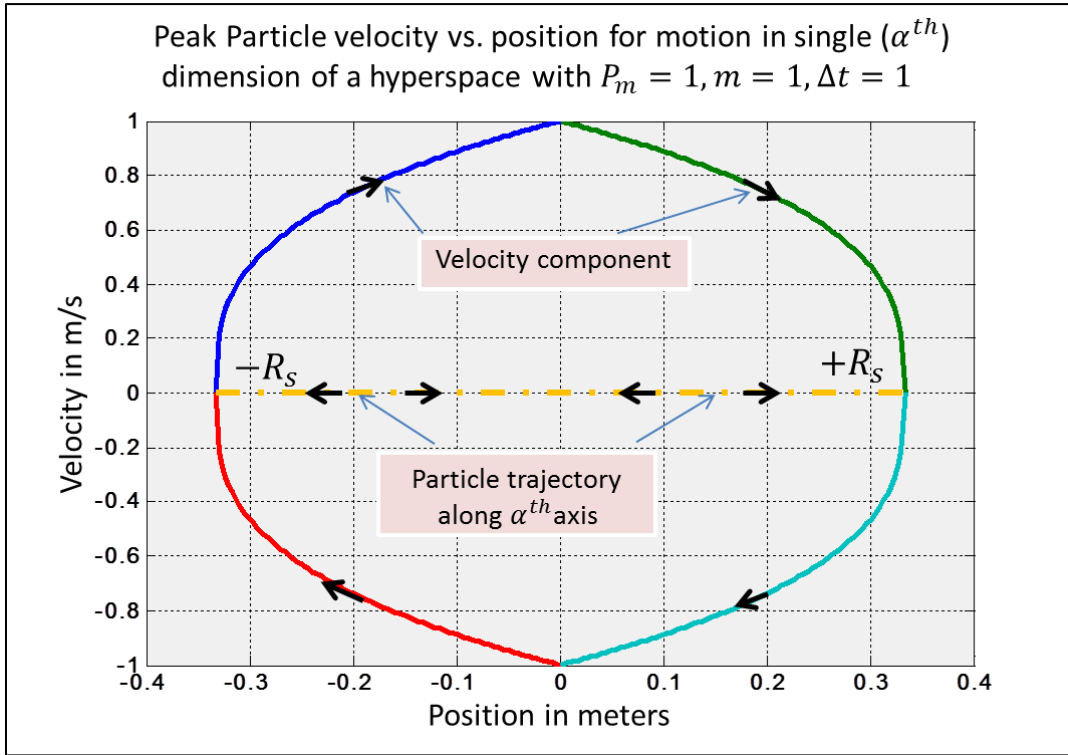


Figure 8-3 Peak Particle Velocity vs. Position for Motion

Likewise for the case where $T^\circ \rightarrow 0$ we have a minimum energy per sample limited by quantum effects.

$$\mathcal{E}_k \gtrsim hf_s \ln \sqrt{2}$$

(8-11)

In general we can calculate a minimum energy to unambiguously encode a bit of information using a binary antipodal encoding procedure as;

$$\varepsilon_b = \int_0^{2T_s} \max\{\dot{p} \cdot \dot{q}\} dt \geq f_s \tilde{N}_o \ln \sqrt{2}$$

(8-12)

If we remove the binary antipodal requirement in favor of maximum entropy encoding then we have;

$$\varepsilon_b \geq \frac{f_s \tilde{N}_o \ln(2)}{2}$$

(8-13)

, where \tilde{N}_o is given by equation 8-4.

However, this is for the circumstance of 100% efficiency, i. e. $PAER \rightarrow 1$

According to principles of chapter 3, if the information is encoded in the form of momentum, this information can only be removed by re-setting the momentum to zero. This means that at least the same energy investment is required to reverse an encoded momentum state. Likewise, if the information is recorded in position then a particle must possess momentum to traverse the distance between the positions. In one direction, for instance moving from $-R_s$ to R_s , a quantity of work is required. Reversing the direction requires at least the same energy. The foregoing discussion reveals a principle that at least $\tilde{N}_o \ln(2)$ is required to both encode or erase one bit of binary information. This resembles Landauer's principle which requires the environmental entropy to raise by the minimum of $kT^\circ \ln(2)$ when one bit of information is erased [7, 8, 66]. The important differences here are that the principle applies for the case of generating unique

data as well as annihilating data. In addition, the rate at which we require generation or erasure to occur, can affect the minimum requirement via the quantity $PAER$ (ref. eq. 8-7) since transitions are finite in time and energy. Finite transition times correspond to $PAER > 1$. This latter effect is not contemplated by Landauer. Thus efficiency considerations will necessarily raise the Landauer limit under all practical circumstances, because a power source with a maximum power of P_m is required corresponding to a $PAER > 1$. For the model of chapter 3 applied to binary encoding where transitions are defined using a maximum velocity profile such as indicated in figure 8-2, we can calculate $PAER = 2$ which at minimum doubles the power requirements to generate the antipodal bits of equation 8-12.

8.2. Time Variant Uncertainty

Time sampling of a particle trajectory in momentum space evolves independently from the allocation of dimensional occupation. The dimensional correlations for $\alpha \neq \beta$ will be zero for maximum uncertainty cases of interest. Likewise, the normalized auto-correlation is defined for $\alpha = \beta$. It is interesting to interject the dimension of time into the autocorrelation as suggested in eq. 3-26 through 3-28. In doing so we can derive a form of time variant uncertainty.

The density function of interest to be used for the uncertainty calculation may be written explicitly as;

$$\rho(\vec{p}_\Delta) = \frac{1}{\sqrt{2\pi(\sigma_\Delta^2)|\Lambda|}} e^{\left[-\frac{1}{2} \left(\frac{\vec{p}_\Delta}{\sigma_\Delta} \right)^T \Lambda^{-1} \left(\frac{\vec{p}_\Delta}{\sigma_\Delta} \right) \right]}$$

$$[\Lambda] = \begin{bmatrix} \sigma_{v_{11}}^2 & \Gamma_{12}\sigma_{v_1}\sigma_{v_2} \dots & \Gamma_{1D}\sigma_{v_1}\sigma_{v_D} \\ \Gamma_{21}\sigma_{v_2}\sigma_{v_1} & \sigma_{v_{22}}^2 \dots & \Gamma_{2D}\sigma_{v_2}\sigma_{v_D} \\ \Gamma_{D1}\sigma_{v_D}\sigma_{v_1} & \Gamma_{D2} \dots & \sigma_{v_{DD}}^2 \end{bmatrix}$$

$$\Gamma_{(\alpha,\beta)} = \frac{\sigma_{\alpha\beta}}{\sigma_\alpha\sigma_\beta}$$

(8-14)

The notation is organized to enumerate the dimensional correlations with α, β and the adjacent time interval correlations with $\ell, \hat{\ell}$. The time interval is given by;

$$t_\ell - t_{\ell+1} = T_s$$

$$(t_\ell - t_{\hat{\ell}}) \leq T_s$$

$$\vec{p}_\Delta = \vec{p}_{\hat{\ell}} - \vec{p}_\ell$$

$$\sigma_\Delta = \sqrt{\sigma_{\hat{\ell}}^2 + \sigma_\ell^2 - 2\gamma_{\ell,\hat{\ell}}\sigma_\ell\sigma_{\hat{\ell}}}$$

(8-15)

$\rho(\vec{p}_\Delta)$ represents the probability density for a transition between successive states where each state is represented by a vector. We can calculate the correlation coefficients for the time differential $(t_{\hat{\ell}} - t_\ell)$ recalling that the TE relation defines the sampling frequency f_s .

$$\gamma_{\ell,\hat{\ell}} = \frac{P_m}{f_s \langle \mathcal{E}_k \rangle_s \text{PAER} k_p} \frac{\sin \left[\frac{P_m}{\langle \mathcal{E}_k \rangle_s \text{PAER}} (t_{\hat{\ell}} - t_\ell) \right]}{\pi \frac{P_m}{\langle \mathcal{E}_k \rangle_s \text{PAER}} (t_{\hat{\ell}} - t_\ell)}$$

(8-16)

The uncertainty $H(\rho(\vec{p}_\Delta))$ is maximized whenever information distributed amongst the degrees of freedom are *iid* Gaussian . It is clear from the explicit form of $\rho(\vec{p}_\Delta)$ that the origin and the terminus of the velocity transition may be completely unique only under the condition that $\gamma_{\ell, \hat{\ell}} = 0$. This occurs at specific time intervals modulo T_s . Otherwise, there will be mutual information over the interval $\{\ell, \hat{\ell}\}$. Elimination of all forms of space-time cross-correlations maximizes $\rho(\vec{p}_\Delta)$. Given these considerations, the pdf for the state transitions may be factored to a product of terms.

$$\rho(\vec{p}_\Delta) = \prod_{\alpha=1}^D \frac{1}{\sqrt{(2\pi)(\sigma_{\hat{\ell}}^2 + \sigma_{\ell}^2)_\alpha}} e^{-\left(\frac{(\vec{v}_{\hat{\ell}})_\alpha^2}{2(\sigma_{\hat{\ell}}^2 + \sigma_{\ell}^2)_\alpha}\right)} \quad (8-17)$$

The origin and terminus coordinates are related statistically through the independent sum of their respective variances. An origin for a current trajectory is also a terminus for the prior trajectory.

The particle may therefore acquire any value within the momentum space and simultaneously occupy any conceivable location within the configuration space at the subsequent time offset of T_s . The case where the time differential $(t_{\hat{\ell}} - t_{\ell})$ is less than T_s carries corresponding temporal reduction of the phase space access, given knowledge of the prior sampling instant. If the phase space accessibility fluctuates as a function of time differential, then so too must the corresponding uncertainty for (\vec{p}_Δ) , at least over a short interval $0 \leq (t_{\ell} - t_{\hat{\ell}}) \leq T_s$. The corresponding differential entropy which incorporates a relative uncertainty metric over the trajectory evolution is governed by the correlation coefficient $\gamma_{\ell, \hat{\ell}}$. If the time difference $\Delta t = 0$

then by definition the differential entropy metric may be normalized to zero plus the quantum uncertainty variance on the order of \hbar . This means that if a current sample coordinate is known that for zero time lapse it is still known, at least to the quantum resolution. Adopting this convention, the relative entropy metric over the interval is defined as;

$$H_{\Delta} \equiv \ln \left(\sqrt{(\sigma_{\hat{p}}^2 + \sigma_{\ell}^2 - 2\gamma_{\ell, \hat{p}} \sigma_{\ell} \sigma_{\hat{p}}) 2\pi e + (1 + 2\pi e \hbar)} \right)$$

(8-18)

In this simple formula the origin state of the of the trajectory is considered as the average momentum state or zero.

When $T_s = 0$ then $\gamma_{\ell, \hat{p}} = 1$ and $H_{\Delta} \geq \ln(\sqrt{(1 + 2\pi e \hbar)})$. If $T_s = \frac{2\langle \mathcal{E}_k \rangle_s^{PAER}}{P_m}$ then $H_{\Delta} = \ln(\sqrt{(\sigma_{\hat{p}}^2 + \sigma_{\ell}^2) 2\pi e + (1 + 2\pi e \hbar)})$. The following graph records H_{Δ} for a normalized differential time ($T_s = 1$) into the future.

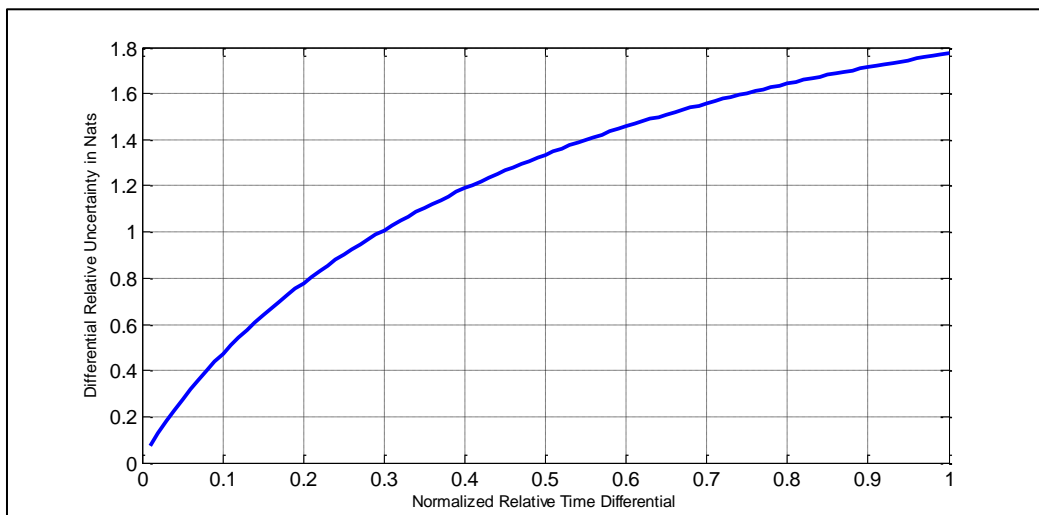


Figure 8-4 Between Sample Uncertainty For a Phase Space Reference Trajectory

At some increasing future time relative to a current known state, the particle entropy correspondingly increases up to the next sampling event. In this example P_m is limited to 10 Joules/second, the average kinetic energy is 1 Joule, the particle mass is 1kg, and the *PAER* is 10 dB. The relative uncertainty as plotted is strictly in momentum space and for a single dimension. This function is repetitive modulo T_s . The plotted uncertainty is proportional to the D^{th} root of an expanding hyper-sphere volume in which the particle exists.

At a future time differential of T_s the particle dynamic acquires full probable access to the phase space and entropy is maximized. Once the particle state is identified by some observation procedure then this uncertainty function resets. H_Δ is calculated based on an extreme where the origin of the example trajectory is at the center of the phase space. H_Δ may fluctuate depending on the origin of the sampled trajectory.

8.3. A Perspective of Gabor's Uncertainty

In Gabor's 1946 paper "Theory of Communication" He rigorously argued the notion that fundamental units, "logons", were a quantum of information based on the reciprocity of time and frequency. He commented that "This is a consequence of the fact that the frequency of a signal which is not of infinite duration can be defined only with a certain inaccuracy, which is inversely proportional to the duration in time, and vice versa." Gabor punctuated his paper with the time-frequency uncertainty relation for a complex pulse;

$$\Delta f \Delta t \geq \frac{1}{2}$$

(8-19)

This uncertainty is related to the ambiguity involved when observing and measuring a finite function of time such as a pulse. Gabor's pulse was defined over its rms extent corresponding more or less to energy metrics which may be considered as analogous to the baseband velocity pulse models of chapter 3. Gabor ingeniously expanded the finite duration pulse in a complex series of orthogonal functions and calculated the energy of the pulse in both the time and frequency domains. His tool was the Fourier integral. He was interested in complex band pass pulsed functions and determined that the envelope of such functions which is compliant with the minimum of the Gabor limit to be a probability amplitude commonly used in quantum mechanics. Gabor's paper was partially inspired by Pauli and reviewed by Max Born prior to publication.

Nyquist had reached a related conclusion in 1924 and 1928 with his now classic works, "*Certain Factors Affecting Telegraph Speed*" and "*Certain Topics in Telegraph Transmission Theory*". Nyquist expanded a "DC wave" into a series using Fourier analysis and determined the number of signal elements required to transmit a signal is twice the number of the sinusoidal components which must be preserved to determine the original DC wave formed by the signal element sequence. This was for the case of a sequence of telegraph pulses forming a message and repeated perpetually. This cyclic arrangement permitted Nyquist to obtain a proper complex Fourier representation without loss in generality since the message sequence duration could be made very long prior to repetition; an analysis technique later refined by Wiener [67]. Nyquist's

analysis concluded that the essential frequency span of the signal is half the rate of the signal elements and inversely related. The signal elements are fine structures in time or samples in a sense and his frequency span was determined by the largest frequency available in his Fourier expansion.

Gabor was addressing this wonder with his analysis and pointing out his apparent dissatisfaction with the lack of intuitive physical origin of the phenomena. He also regarded the analysis of Bennett in a similar manner concerning the time frequency reciprocity for communications, stating; *“Bennett has discussed it very thoroughly by an irreproachable method ,but, as is often the case with results obtained by Fourier analysis, the physical origin of the results remains somewhat obscure.”*. Gabor also comments; *“In spite of the extreme simplicity of this proof, it leaves a feeling of dissatisfaction. Though the proof (one forwarded in Gabor’s 1946 paper) shows clearly that the principle in question is based on a simple mathematics identity, it does not reveal this identity in tangible form [26].”*

We now present an explanation for the time-frequency uncertainty, using a time bandwidth product, based on physical principles expressed through the TE relation and the physical sampling theorem. An instantiation of Gabor’s In-phase or Quadrature phase pulse can be accomplished by using two distinct forces per in-phase and quadrature phase pulse according to the physical sampling theorem presented in chapter 3. The time span of such forces are separated in time by T_s . The characteristic duration of a pulse event is $\Delta t = 2T_s$.

From the TE relation we know;

$$\frac{f_{s_min}}{2} = \frac{P_m}{2\langle \mathcal{E}_k \rangle PAER} = B = \Delta t^{-1}$$

$$\frac{f_s}{2} \geq \frac{P_m}{2\langle \mathcal{E}_k \rangle PAER}$$

(8-20)

\tilde{B} the bandwidth available due to the sample frequency f_s is always greater than or equal to B the bandwidth available due to an absolute minimum sample frequency f_{s_min} so that;

$$\tilde{B} \geq \frac{f_{s_min}}{2}$$

Therefore,

$$\tilde{B} T_{s_max} \geq \frac{1}{2}$$

This is called a time bandwidth product. If one wishes to increase the observable bandwidth \tilde{B} then T_{s_max} may be lowered. If a lower bandwidth is required then T_{s_max} may be increased where T_{s_max} is an interval of time required between forces such that the forces may be uncorrelated given some finite P_m .

An example provides a connection between the TE relation, physical sampling theorem and Gabor's uncertainty. Figure 8-5 illustrates the sampling (depicted by vertically punctuated lines) of two sine waves of differing frequency. The frequency of the slower sine function is one fifth that of the greater and assigned a frequency $B_2 = f_c/5$. The sampling rate is set to capture the greater frequency sine function with bandwidth $B_1 = f_c$. In the first frame of fig. 8-5 the sample

rate $f_s \approx 2f_c$ with samples generated for both functions slightly skewed in time for convenience of representation.

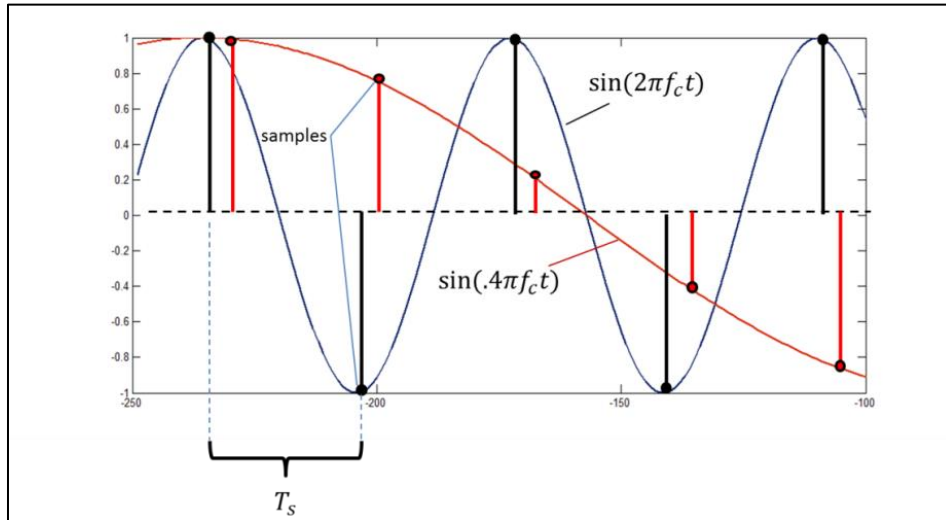


Figure 8-5 Sampling of Two Sine Waves at Different Frequencies

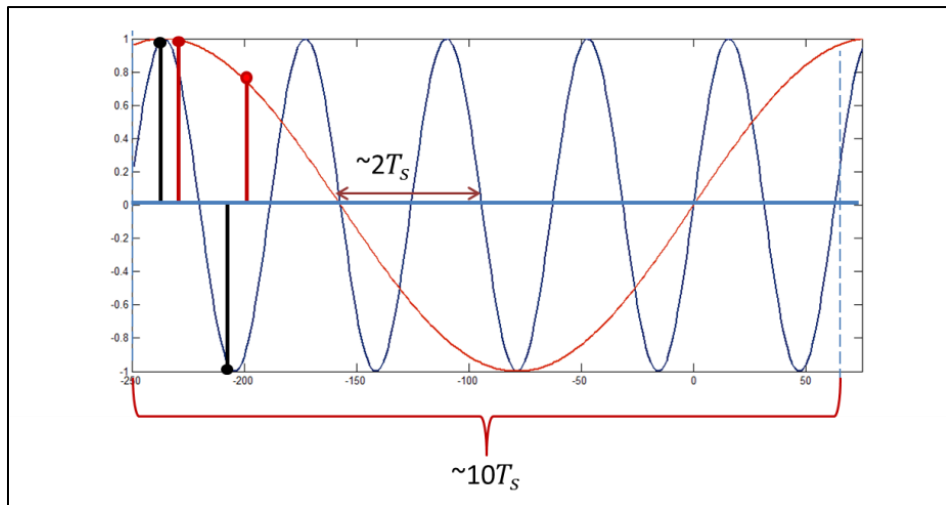


Figure 8-6 Sampling of Two Sine Waves at Different Frequencies

Only two samples are required to create or capture one cycle of the higher frequency sine wave.

However, two samples separated in time by T_s cannot create the trajectory of the slower sine

wave over its full interval $10T_s$. That trajectory is ambiguous without the additional 8 samples, as is evident by comparing frame 2 with frame 1 of the figure. The sampling frequency of $f_s \approx 2f_c$ is adequate for both sine waves but in order to resolve the slower sine wave and reconstruct it, the samples must be deployed over the full interval $10T_s$. The prior equation may capture this by accounting for the extended interval using a multiplicity of samples.

$$\frac{B_1}{5} (5 T_{s1}) \geq \frac{1}{2}$$

$$B_2 \geq \frac{1}{2(5 T_{s1})}$$

The slow sine wave case is significantly oversampled so that all frequencies below B_1 are accommodated but ambiguities may only be resolved if the sample record is long enough. This is consistent with Gabor's uncertainty relation as well as Nyquist's analysis.

We can address the requirement for an extended time record of samples by returning to the physical sampling theorem and a comparative form of the TE relation. The next equation calculates the time required between independently acting forces for a particle along the trajectory of the slow sine wave;

$$T_{s2} = T_{s1} \frac{PAER_2}{PAER_1} = T_{s1} \frac{\max\{\dot{\mathcal{E}}_k\}_1}{\max\{\dot{\mathcal{E}}_k\}_2} = 5T_{s1}$$

The result means that effective forces must be deployed with a separation of $5T_{s1}$ to create independent motion for the slower trajectory. Adjacent samples separated by $T_s = T_{s1}$ cannot produce independent samples for the slower waveform because they are significantly correlated.

Hence the effective change in momentum \dot{p} per sample is lower for the over sampled slow waveform. As a general result, the corresponding work rate is lower for the lower frequency sine wave so that;

$$T_{s2} = T_{s1} \frac{\max\{\dot{p} \cdot \dot{q}\}_1}{\max\{\dot{p} \cdot \dot{q}\}_2} \quad (8-21)$$

Even though 10 forces must be deployed to capture the entire slower sine wave trajectory over its cycle, only pairs taken from subsets of every 5th force may be jointly decoupled.

Gabor's analysis considered the complex envelope modulated onto orthogonal sinusoids. A complex carrier consisting of a cosine and sine has a corresponding TE equation;

$$f_{sI} + f_{sQ} \geq \frac{2P_m}{\langle \mathcal{E}_k \rangle PAER} \quad (8-22)$$

The effective samples for in phase and quadrature components occur over a common interval so that the sample frequency doubles yet so does the peak power excursion P_m for the complex signal. This is analogous to the case $D=2$. Gabor's modulation corresponds to a double side band suppressed carrier scenario. This is the same as specifying pulse functions $a_I(t)$, $a_Q(t)$ in the complex envelope as zero offset unbiased RV's, where the envelope takes the form ;

$$x(t) = a(t)e^{j\omega_c t + \varphi(t)} = a_I(t) \cos(\omega_c t + \varphi(t)) - a_Q(t) \sin(\omega_c t + \varphi(t))$$

To obtain Gabor's result, we now realize that the peak power in the baseband pulses expressed by $a_I(t)$, $a_Q(t)$ will be twice that of the unmodulated carrier. Therefore the TE relation for the complex envelope of $x(t)$ is given by;

$$f_{sI_BB} + f_{sQ_BB} \geq \frac{2(2P_m)}{\langle \mathcal{E}_k \rangle_s PAER}$$

This reduces to;

$$\frac{f_{s_BB}}{2} \geq \frac{P_{m_BB}}{\langle \mathcal{E}_k \rangle PAER}$$

(8-23)

The time bandwidth product now becomes;

$$B_{BB} \Delta t_{max} \geq \frac{1}{2}$$

$$\frac{P_{m_BB}}{2\langle \mathcal{E}_k \rangle_s PAER} \Delta t_{max} \geq \frac{1}{2}$$

(8-24)

A variation in the sample interval for independent forces which create a signal must be countered by an inverse variation in the apparatus bandwidth or correspondingly the work rate. $2NT_s = \Delta t_{max}$ for a sequence of deployed forces creating a signal trajectory, always extends to a time interval accommodating at least two independent forces for the slowest frequency component of the message. The minimum number of deployed forces occurs for $N = 1$, a single pulse event.

This result is also equivalent to Shannon's number which is given by $N = 2BT$, where $2B = f_{s_{min}}$ and $T = \Delta t_{max}$ [6]. Care must be exercised using Shannon's number to account for I and Q components.

9. SUMMARY

Communications is the transfer of information through space and time via the encoded motions of particles and corresponding fields. Information is determined by the uncertainty of momentum and position for the dynamic particles over their domain. The rate of encoding information is determined by the available energy per unit time required to accelerate and decelerate the particles over this domain. Only two statistical parameters are required to determine the efficiency of encoding; the average work per deployed force and the maximum required *PAPR* for the trajectory. This is an extraordinary result applicable for any momentum pdf.

Bandwidth in the Shannon-Hartley capacity equation is a parameter which limits the rate at which the continuous signal of the AWGN channel can slew. This in turn limits the rate at which information may be encoded. The physical sampling theorem determined from the laws of motion and suitable boundary conditions requires that the number of forces per second to encode a particle be given by;

$$f_s \geq \frac{P_m}{\langle \mathcal{E}_k \rangle_s PAER}$$

This frequency also limits the slew rate of the encoded particle along its trajectory and determines its bandwidth in a manner analogous to the bandwidth of Shannon according to;

$$B = \frac{P_m}{2\langle \mathcal{E}_k \rangle_s PAER}$$

The calculated capacity rate for the joint encoding of momentum and position in D independent dimensions was calculated as;

$$C \leq \sum_{\alpha=1}^D \frac{P_{m_\alpha}}{\langle \mathcal{E}_{k_\alpha} \rangle_s PAER_\alpha} \left(\ln \left[\frac{\left(\frac{2 P_{m_\alpha}}{PAER_\alpha} \right)}{\tilde{\sigma}_{p_{n,\alpha}}^2} + 1 \right] \right)$$

As this capacity rate increases, the required power source, P_{src} , for the encoding apparatus also increases as is evident from the companion equation;

$$C \leq \sum_{\alpha=1}^D \frac{P_{m_\alpha}}{\langle \mathcal{E}_{k_\alpha} \rangle_s PAER_\alpha} \left(\ln \left[\frac{\eta_{mod} \eta_{diss} P_{src}}{\tilde{\sigma}_n^2} + 1 \right] \right)$$

Therefore, increases in the modulation encoding efficiency η_{mod} can be quite valuable. For instance, in the case of mobile communications platform performance, data rates can be increased, time of operation extended, battery size and cost reduced or some preferred blend of these enhancements. In addition, the thermal footprint of the modulator apparatus may be significantly reduced.

Efficiency of the encoding process is inversely dependent on the dot product extreme, $\max\{\dot{\vec{p}} \cdot \dot{\vec{q}}\} = P_m$ divided by an average, $\langle \dot{\vec{p}} \cdot \dot{\vec{q}} \rangle = \sigma^2$, also known as *PAPR* or *PAER*. The fluctuations about the average represent changes in inertia which require work. Since these fluctuations are random, momentum exchanges required to encode particle motion (and therefore information) produce particle recoils which are inefficient. The difference between the instantaneous energy requirement and the maximum resource availability is proportional to the wasted energy of encoding. On the average, the wasted energy of recoil grows for large *PAPR*. This generally results in an encoding efficiency of the form;

$$\eta_{enc} = \frac{\sigma^2}{k_{enc}P_m + k_\sigma\sigma^2} = \frac{1}{k_{enc}PAPR + k_\sigma}$$

Coefficients k_{enc} and k_σ depend on apparatus implementation. Several cases were analyzed for an electronic modulator using the theory developed in this work, then tested in experiments.

Experiments included theoretical waveforms as well as 3G and 4G standards based waveforms.

The theory was verified to be accurate within the degree of measurement resolution, in this case $\sim .7\%$.

The inefficiency of encoding is regarded as a necessary inefficiency juxtaposed to dissipative inefficiencies such as friction, drag, resistance, etc. Capacity for the AWGN channel is achieved for very large $PAPR$, resulting in low efficiencies. However, if the encoded particle phase space is divided into multiple domains, then each domain may possess a lower individual $PAPR$ statistic than the case of a single domain phase space with equivalent capacity. The implication is that separate resources can be more efficiently allocated in a distributed manner throughout the phase space. Resources are accessed as the encoded particle traverses a domain boundary. Domain boundaries which are optimized in terms of overall thermodynamic efficiency are not arbitrary. The optimization in the case of a Gaussian information pdf takes the form of a ratio of composited gamma densities;

$$\eta_{enc} = \max \left\{ \frac{\sum_i \lambda_i k_{inorm} \int_{f\{V_T\}_{i-1}}^{f\{V_T\}_i} \mathcal{X}_e \rho(\mathcal{X}_e) d\mathcal{X}_e}{\sum_i \lambda_i k_{inorm} \int_{f\{V_T\}_{i-1}}^{f\{V_T\}_i} \mathcal{X}_{in} \rho(\mathcal{X}_{in}) d\mathcal{X}_{in}} \right\}$$

There is no known closed form solutions to this pdf ratio. A numerical calculus of variations technique was developed to solve for the optimal thresholds $\{V_T\}_i$ and $\{V_T\}_{i-1}$, defining domain

boundaries. The i^{th} domain weighting factor λ_i is a probability of domain occupation where a domain is defined between thresholds $\{V_T\}_i$ and $\{V_T\}_{i-1}$. In general, the numerator term corresponding to effective signal energy is based on a central gamma RV and the denominator term corresponding to apparatus input energy, is based on either a non-central or central gamma RV. Another optimization technique was also developed which reduces to an alternate form;

$$\max\{\check{\eta}_{tot}\} = \max\left\{\sum_i \lambda_i k_{i_{norm}} \int_{\eta_{\{i-1,i\}}}^{\eta_i} \check{\eta}_i p_i(\check{\eta}_i) d\check{\eta}_i\right\}$$

In this case, thresholds are determined in terms of the optimized threshold values for $\eta_{\{i-1\}}$, η_i . Although this optimization is in terms of an instantaneous efficiency it was shown to relate to the thermodynamic efficiency optimum.

Modulation efficiency enhancements were theoretically predicted. Several cases were tested which corroborate the accuracy of the theory. Efficiencies may be drastically improved by dividing a phase space into only a few domains. For instance, dividing the phase space into 8 optimized domains results in an efficiency of 75% and dividing it into 16 domains results in an efficiency of 86.5% for the case of a zero offset Gaussian signal. Excellent efficiencies were observed for experiments using various cell phone and wireless LAN standards as well.

A key principle of this work is that communication is accomplished through momentum exchange. Randomized momentum exchanges are always inefficient because the encoding particle and particle to be encoded are always in relative random motion resulting in wasted recoil momentum. Particle inertia which must be overcome prior to subsequent encodings which is not conveyed to the channel but rather absorbed by the environment. This raises the local

entropy in agreement with the second law of thermodynamics. It was also shown that information cannot be encoded without momentum exchange and information cannot be annihilated without momentum exchange, since communications is regarded as a physical process.

APPENDIX A:
PHASE SPACE UNCERTAINTY AND THE HYPER SPHERE

It is possible to identify the form of probability density function, $\rho(x)$, which maximizes Shannon's continuous uncertainty function for a given variance;

$$H[\rho(x)] = - \int_{-\infty}^{\infty} \rho(x) \ln \rho(x) \quad (\text{A1.1})$$

A formulation from the calculus of variations historically known as Dido's problem can be adapted for the required solution [69, 70]. The classical formulation was used to obtain the form of a fixed perimeter which maximizes the enclosed area. Thus the formulation is often referred to as an isoperimetric solution.

In the case of interest here it is desirable to find a solution given v , a single particle velocity in the D dimensional hyper space and a fixed kinetic energy as the resource which can move the particle. Specifically, we wish to obtain a probability density function, $(v_1, v_2 \dots v_D)$, which maximizes a D dimensional uncertainty hyperspace for momentum with fixed mass, given the variance of velocity v_α , where $\alpha = 1, 2, \dots D$.

This problem takes on the following character;

$$\max\{H[\rho(v_1, v_2 \dots v_D)]\} = \max \left\{ - \prod_{-\infty}^{\infty} \dots \int \rho(v_1, v_2 \dots v_D) \ln \rho(v_1, v_2 \dots v_D) dv_1, dv_2 \dots dv_D \right\} \quad (\text{A1.2})$$

The kernel of the integral in A1.2 shall be referred to as \mathfrak{F} on occasion in its various streamlined forms.

This D dimensional maximization can be partially resolved by recognizing two simple concepts. Firstly, In the absence of differing constraints for each of the D dimensions, a solution cannot bias the consideration of one dimension over the other. If all dimensions possess equivalent constraints then their physical metrics as well as any related probability distributions for v_α will be indistinguishable in form. A lack of dimensional constraints is in fact a *constraint by omission*.

Secondly, if the D dimensions are orthogonal, then variation in any one of the v_α variables is unique amongst all variable variations only if the v_α are mutually decoupled. It follows that the motions corresponding to v_α must be dimensionally decoupled to maximize A1.2. Maximizing the number of independent degrees of freedom for the particle is the underlying principle, similar to maximum entropy principles from statistical mechanics [14].

$\{v_1, v_2 \dots v_\alpha \dots v_D\}$ cannot be deterministic functions of one another else they share mutual information and the total number of independent degrees of freedom for the set is reduced.

Therefore,

$$\rho(v_1, v_2 \dots v_D) = \rho(v_1)\rho(v_2) \dots \rho(v_D) \tag{A1.3}$$

for a maximization. The v_α are orthogonal and statistically independent.

This reduces the maximization integral to a streamlined form over some interval a, b ;

$$\{J\} = \int_a^b \mathfrak{F}\{v_\alpha, \rho(v_\alpha), \dot{\rho}(v_\alpha)\} dv_\alpha$$

Or more explicitly,

$$\max\{J\} = \max\{H[\rho(v_1, v_2 \dots v_D)]\} = \max\left\{-\int \rho(v_\alpha)^D \ln(\rho(v_\alpha)^D) dv_\alpha\right\}$$

(A1.4)

We now define integral constraints. The first constraint is the probability measure.

$$\sum_{\alpha} J_{\alpha} = 1 = \sum_{\alpha} \int_{-\infty}^{\infty} \rho(v_{\alpha}) dv_{\alpha}$$

(A1.5)

Since no distinguishing feature has been introduced to differentiate $\rho(v_{\alpha})$ from any joint members of $\rho(v_1, v_2 \dots v_D)$, all the integrals of A1.5 are equivalent, which requires simply;

$$\sum_{\alpha} J_{\alpha} = 1 = D \int_{-\infty}^{\infty} \rho(v_{\alpha}) dv_{\alpha}$$

(A1.6)

A final constraint is introduced which limits the variance of each member function $\rho(v_{\alpha})$. This variance is proportional to an entropy power and can also be viewed as proportional to an average kinetic energy $\mathcal{E}_{k,\alpha} = \frac{1}{2}\sigma_{\alpha}^2$.

$$J_{\sigma} = D\sigma_{\alpha}^2 = D \int_{-\infty}^{\infty} v_{\alpha}^2 \rho(v_{\alpha}) d(v_{\alpha})$$

(A1.7)

Lagrange's method may be used to determine coefficients λ_α of the following formulation [21, 59].

$$\mathcal{I}_0 = \mathcal{I} + \mathcal{I}_\alpha + \mathcal{I}_\sigma$$

$$\mathcal{I}_0 = \int_a^b \dots \int \left(\mathfrak{F} + \sum_\alpha \lambda_\alpha \mathfrak{F}_\alpha + \sum_\alpha \lambda_{\sigma_\alpha} \mathfrak{F}_{\sigma_\alpha} \right) dv_1 \dots dv_D$$

(A1.8)

$$\mathfrak{F}_0 = \mathfrak{F} + D\lambda_\alpha \mathfrak{F}_\alpha + D\lambda_{\sigma_\alpha} \mathfrak{F}_{\sigma_\alpha}$$

Euler's equation of the following form must be solved;

$$\frac{d}{dv_\alpha} \frac{\partial \mathfrak{F}_0}{\partial \dot{\rho}_\alpha} - \frac{\partial \mathfrak{F}_0}{\partial \rho_\alpha} = 0$$

(A1.9)

Since derivative $\dot{\rho}$ constraints are absent;

$$-\frac{\partial \mathfrak{F}_0}{\partial \rho_\alpha} = 0$$

(A1.10)

And,

$$\mathfrak{F}_0 = \rho(v_\alpha)^D \ln \rho(v_\alpha)^D + D\lambda_\alpha \rho(v_\alpha) + D\lambda_{\sigma_\alpha} v_\alpha^2$$

(A1.11)

From A1.10;

$$\frac{\partial \mathfrak{F}_0}{\partial \rho(v_\alpha)} = D\rho(v_\alpha)^{D-1} + D\rho(v_\alpha)^{D-1} \ell n \rho(v_\alpha)^D + D\lambda_\alpha + D\lambda_{\sigma_\alpha} v_\alpha^2 = 0$$

(A1. 12)

Since all of the D dimensions are orthogonal with identically applied constraints, $D = 1$ is a suitable solution subset of A1.12. The problem therefore is reduced to solving;

$$1 + \ell n \rho_\alpha + \lambda_\alpha + \lambda_{\sigma_\alpha} v_\alpha^2 = 0$$

$$\rho_\alpha = e^{-\lambda_\alpha} e^{-\lambda_{\sigma_\alpha} v_\alpha^2} e^{-1}$$

(A1. 13)

A1.13 can be substituted into A1.7 to obtain;

$$\sigma_\alpha^2 = \int_{-\infty}^{\infty} (e^{-\lambda_\alpha} e^{-1}) v^2 e^{-\lambda_{\sigma_\alpha} v_\alpha^2} dv_\alpha$$

(A1. 14)

$$\sigma_\alpha^2 = \frac{1}{2} e^{(-\lambda_\alpha+1)} v_\alpha^2 e^{-\lambda_{\sigma_\alpha} v_\alpha^2} \Big|_{-\infty}^{\infty} - \int_{-\infty}^{\infty} e^{(-\lambda_\alpha+1)} v_\alpha e^{-\lambda_{\sigma_\alpha} v_\alpha^2} dv_\alpha$$

$$\therefore \sigma_\alpha^2 = \frac{e^{(-\lambda_\alpha+1)}}{2\lambda_{\sigma_\alpha}} \int_{-\infty}^{\infty} e^{-\lambda_{\sigma_\alpha} v_\alpha^2} dv_\alpha$$

(A1. 15)

Rearranging A1.15 gives;

$$\sigma_\alpha^2 = \frac{1}{2\lambda_{\sigma_\alpha}} \int_{-\infty}^{\infty} e^{(-\lambda_\alpha+1)} e^{-\lambda_{\sigma_\alpha} v_\alpha^2} dv_\alpha$$

$$\sigma_\alpha^2 = \frac{1}{2\lambda_{\sigma_\alpha}} \int_{-\infty}^{\infty} \rho_\alpha(v_\alpha) dv_\alpha = \frac{1}{2\lambda_{\sigma_\alpha}}$$

$$\therefore \lambda_{\sigma_\alpha} = \frac{1}{2\sigma_\alpha^2} = 1$$

This requires;

$$e^{(\lambda_\alpha+1)} = \int_{-\infty}^{\infty} e^{-\lambda_{\sigma_\alpha} v_\alpha^2} dv_\alpha = \int_{-\infty}^{\infty} e^{-\frac{v_\alpha^2}{2\sigma_\alpha^2}} dv_\alpha$$

(A1. 16)

$$e^{(\lambda_\alpha+1)} = \sqrt{2\pi\sigma_\alpha^2}$$

(A1. 17)

And;

$$\rho(v_\alpha) = e^{-(\lambda_\alpha+1)} e^{-\frac{v_\alpha^2}{2\sigma_\alpha^2}} = \frac{1}{\sqrt{2\pi}\sigma_\alpha} e^{-\frac{v_\alpha^2}{2\sigma_\alpha^2}}$$

(A1. 18)

It follows from A1.3 that the density function for the D dimensional case is simply;

$$(\rho(v_\alpha))^D = \frac{1}{(2\pi)^{D/2} \sigma_\alpha^D} \prod_{\alpha} e^{-\frac{v_\alpha^2}{2\sigma_\alpha^2}}$$

(A1. 19)

This is the density which maximizes A1.2 subject to a fixed total energy $\sigma^2 = \sum_{\alpha} \sigma_\alpha^2$ where the D dimensions are indistinguishable from one another.

v is Gaussian distributed in a D -dimensional space. This velocity has a maximum uncertainty for a given variance σ_α^2 .

Now if the particle is confined to some hyper volume it is useful to know the character of the volume. It was previously deduced that the dimensions are orthogonal. Thus we may represent the velocity as a vector sum of orthogonal velocities.

$$\vec{v} = \sum_{\alpha=1}^D \vec{v}_\alpha \hat{a}_\alpha$$

(A1. 20)

It was also determined that the $\rho(v_\alpha)$ have identical forms, i.e. they are *iid* Gaussian. Now let the maximum velocity v_{\max_α} in each dimension be determined as some multiple $k\sigma_\alpha$ on the probability tail of the Gaussian pdf, ignoring the asymptotic portions greater than that peak. Then A1.21 may be written in an alternate form;

$$v_{\max}^2 - \sum_{\alpha=1}^D (v_\alpha)^2 \geq 0; \quad v_\alpha \leq v_{\max}$$

(A1. 21)

$$v_{\max}^2 = \sum_{\alpha} \vec{v}_{\max_\alpha}^2 = \sum_{\alpha} k^2 \sigma_\alpha^2$$

(A1. 22)

A1.21 together with A1.22 define a hyper sphere volume with radius.

$$\sqrt{\mathcal{E}_{max}} = \sqrt{\sum_{\alpha} \frac{m}{2} k^2 \sigma_{\alpha}^2} = \sqrt{\sum_{\alpha} \frac{PAER}{2m} \sigma_{p_{\alpha}}^2}$$

(A1. 23)

k^2 is the *PAER* and $\sigma_{p_{\alpha}}^2$ is the momentum variance in the α^{th} dimension. The hyper sphere has an origin of zero with a zero mean Gaussian velocity pdf characterizing the particle motion in each dimension.

The form of the momentum space is a hyper sphere and therefore the physical coordinate space is also a hyper sphere. This follows since position is an integral of velocity. The mean velocity is zero and therefore the average position of the space may be normalized to zero. The position coordinates within the space are Gaussian distributed since the linear function of a Gaussian RV remains Gaussian. Just as the velocity may be truncated to a statistically significant but finite value so too the physical volume containing the particle can be limited to a radius R_s . Truncation of the hyper sphere necessarily comes at the price of reducing the uncertainty of the Gaussian distribution pdf in each dimension. Therefore, *PAER* should be selected to moderate this entropy reduction for this approximation given the application requirements.

The preceding argument justifying the hyper sphere may also be solved using the calculus of variations. The well-known solution in two dimensions is a circle. The perimeter of the circle is the shortest perimeter enclosing the largest area [70]. Since a hyper sphere may be synthesized as a volume of revolution based on the circle, it possesses the greatest enclosed volume for a given surface. The implication is that a particle may move in the largest possible volume given fixed energy resources when the volume is a hyper sphere. The greater the volume of the space which

contains the particle, the more uncertain its random location and if the particle is in motion the more uncertain its velocity. Joint representation of the momentum and position is a hyper spherical phase space.

APPENDIX B:
DERIVATION FOR MAXIMUM VELOCITY PROFILE

This Appendix derives the maximum velocity profile subject to a limit of P_m joules/second available to accelerate a particle from one end of a spherical space to the other where the sphere radius is R_s . Furthermore, it is assumed that the particle can execute the maneuver in Δt seconds but no faster. There is an additional constraint of zero velocity (momentum) at the sphere boundary. The maximum kinetic energy expenditure per unit time is given by;

$$\max\{\dot{\mathcal{E}}_k\} = P_m \quad (\text{B1.1})$$

The particle's kinetic energy and rate of work is given by;

$$\mathcal{E}_k = 1/2 mv^2 \quad (\text{B1.2})$$

$$\dot{\mathcal{E}}_k = m\vec{v} \cdot \frac{d\vec{v}}{dt} = \dot{\vec{p}} \cdot \vec{v} \quad (\text{B1.3})$$

$$m \equiv \text{mass}, \quad \vec{p} \equiv \text{momentum}, \quad \vec{v} \equiv \text{velocity}$$

Since the volume is symmetrical and boundary conditions require $|v| = 0$ at a distance $\pm R_s$ from the sphere center;

$$\mathcal{E}_{k_{max}} = \int_0^{\Delta t/2} \max\{\dot{\mathcal{E}}_k\} dt = \frac{\Delta t}{2} P_m \quad (\text{B1.4})$$

$$\epsilon_{k_{peak}} = tP_m \quad 0 \leq t \leq \frac{\Delta t}{2}$$

(B1.5)

$$\epsilon_{k_{peak}} = (\Delta t - t) P_m \quad \frac{\Delta t}{2} \leq t \leq \Delta t$$

(B1.6)

Under conditions of maximum acceleration and deceleration the kinetic energy vs. time is a ramp, illustrated in the following figure;

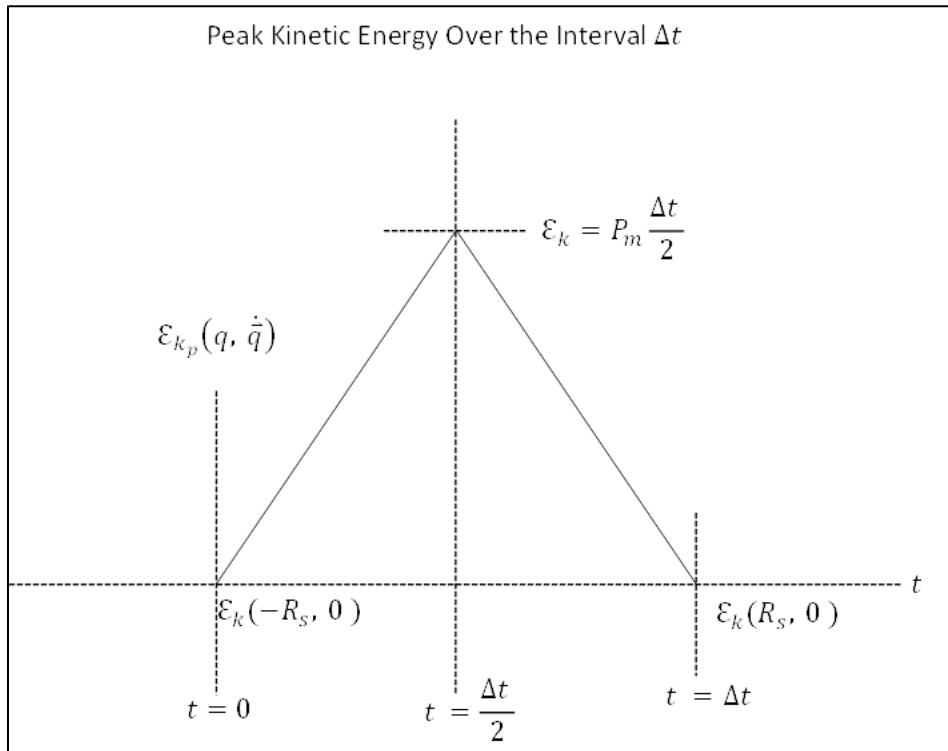


Figure B-1 Kinetic Energy vs. Time for Maximum Acceleration

\vec{q} and $\dot{\vec{q}}$ are position and velocity respectively ($\dot{\vec{q}} = \vec{v}$). B1.5 and B1.6 can be used to obtain peak velocity over the interval Δt .

$$\frac{1}{2} m v_p^2 = t P_m \quad 0 \leq t \leq \frac{\Delta t}{2}$$

$$R_s \leq q \leq 0$$

$$\pm \vec{v}_p = \sqrt{\frac{2P_m t}{m}} \hat{a}_r$$

(B1.7)

$$\frac{1}{2} m v_p^2 = (\Delta t - t) P_m \quad t/2 \leq t \leq \Delta t$$

$$0 \leq q \leq R_s$$

$$\mp \vec{v}_p = \sqrt{\frac{2P_m(\Delta t - t)}{m}} \hat{a}_r$$

(B1.8)

B1.7 and B1.8 are defined as the peak velocity profile.

Positive and negative velocities may also be defined as those velocities which are associated with motion of the particle in the $\pm \hat{a}_r$ direction with respect to the sphere center.

It should be clear that it is possible to have $\pm v_p$ over the entire domain since $\pm v_p$ is rectified in the calculation of \mathcal{E}_k and boundary constraints do not preclude such motions.

Position q may be calculated from these quantities through an integral of motion

$$\vec{q} = \int \vec{v}_p dt$$

(B1.9)

$$\vec{q} = \int -\sqrt{\frac{2P_m t}{m}} \hat{a}_r dt = \left(R_s - 2/3 v_{max} \sqrt{\frac{2}{\Delta t}} t^{3/2} \right) \hat{a}_r \quad 0 \leq t \leq \frac{\Delta t}{2}$$

$$R_s \geq q \geq 0$$

(B1.10)

Integration of the opposite velocity yields;

$$\vec{q} = \int -\sqrt{\frac{2P_m t}{m}} \hat{a}_r dt = \left(2/3 v_{max} \sqrt{\frac{2}{\Delta t}} t^{3/2} - R_s \right) \hat{a}_r \quad 0 \leq t \leq \frac{\Delta t}{2}$$

$$0 \geq q \geq R_s$$

(B1.11)

$\pm R_s$ is the constant of integration in both cases which may be deduced from boundary conditions, or initial and final conditions.

The other peak velocity profile trajectories (from B1.8) yield similar relationships;

$$\vec{q} = \int \pm \sqrt{\frac{2P_m(\Delta t - t)}{m}} \hat{a}_r dt = \pm \left(2/3 v_{max} \sqrt{\frac{2}{\Delta t}} (\Delta t - t)^{3/2} - R_s \right) \hat{a}_r$$

(B1.12)

where;

$$v_{max} = \sqrt{\frac{P_m \Delta t}{m}}$$

(B1. 13)

The result of B1.10 may be solved for the characteristic radius of the sphere, R_s ;

$$R_s = v_m \sqrt{\frac{2}{\Delta t} \left(\frac{\Delta t}{2}\right)^{3/2}} = \sqrt{\frac{2P_m}{m}} \left(\frac{\Delta t}{2}\right)$$

(B1. 14)

At this point it is possible to parametrically relate velocity and position. This can be accomplished by solving for time in equations B1.10, B1.11 and B1.12 then eliminating the time variable in the q and \dot{q} equations.

$$t = \left(\frac{3}{2} \sqrt{\frac{\Delta t}{2}} \frac{R_s - q}{v_m} \right)^{2/3} \quad R_s \geq q \geq 0$$

(B1. 15)

$$t = \Delta t - \left(\frac{3}{2} \sqrt{\frac{\Delta t}{2}} \frac{q + R_s}{v_m} \right)^{2/3} \quad 0 \geq q \geq -R_s$$

(B1. 16)

B1.15 and B1.16 may be substituted into the peak velocity equations B1.7 and B1.8.

$$\vec{v}_p = \sqrt{\frac{2P_m}{m}} \sqrt{t} \hat{a}_r = \left(\frac{3P_m}{m} (q + R_s) \right)^{1/3} \hat{a}_r \quad -R_s \leq q \leq 0$$

$$\vec{v}_p = - \left(\frac{3P_m}{m} (q + R_s) \right)^{1/3} \hat{a}_r \quad -R_s \leq q \leq 0$$

Similarly

$$\vec{v}_p = \sqrt{\frac{2P_m}{m}} \sqrt{\Delta t - t} = \left(\frac{3P_m}{m} (q - R_s) \right)^{1/3} \hat{a}_r \quad 0 \leq q \leq R_s$$

$$-\vec{v}_p = - \left(\frac{3P_m}{m} (q - R_s) \right)^{1/3} \hat{a}_r \quad 0 \leq q \leq R_s$$

APPENDIX C:
MAXIMUM VELOCITY PULSE AUTO CORRELATION

Consider the piece wise pulse specification;

$$\vec{v}_\alpha = \sqrt{\frac{2P_m t}{m}} \hat{a}_\alpha \quad 0 \leq t \leq \frac{\Delta t}{2}$$

(C1. 1)

$$\vec{v}_\alpha = \sqrt{\frac{2P_m (\Delta t - t)}{m}} \hat{a}_\alpha \quad \frac{\Delta t}{2} \leq t \leq \Delta t$$

(C1. 2)

The auto correlation of this pulse is given by (where we drop vector notations);

$$\Re_{v,v} = \int_{-\infty}^{\infty} v_\alpha(t) v_\alpha(t + \tau) dt$$

(C1. 3)

The auto correlation must be solved in segments. Since it is symmetric in time the result for the first half of the correlation response may simply be mirrored for the second half of the solution.

Figure C-1 illustrates the reference pulse described by equations C1.1, C1.2, along with the replicated convolving pulse. As the convolving pulse migrates through its various variable time domain positions equation C1.3 is recursively applied. The shaded area in the figure illustrates the evolving functional overlap in the domains of the two pulses. This is the domain of calculation.

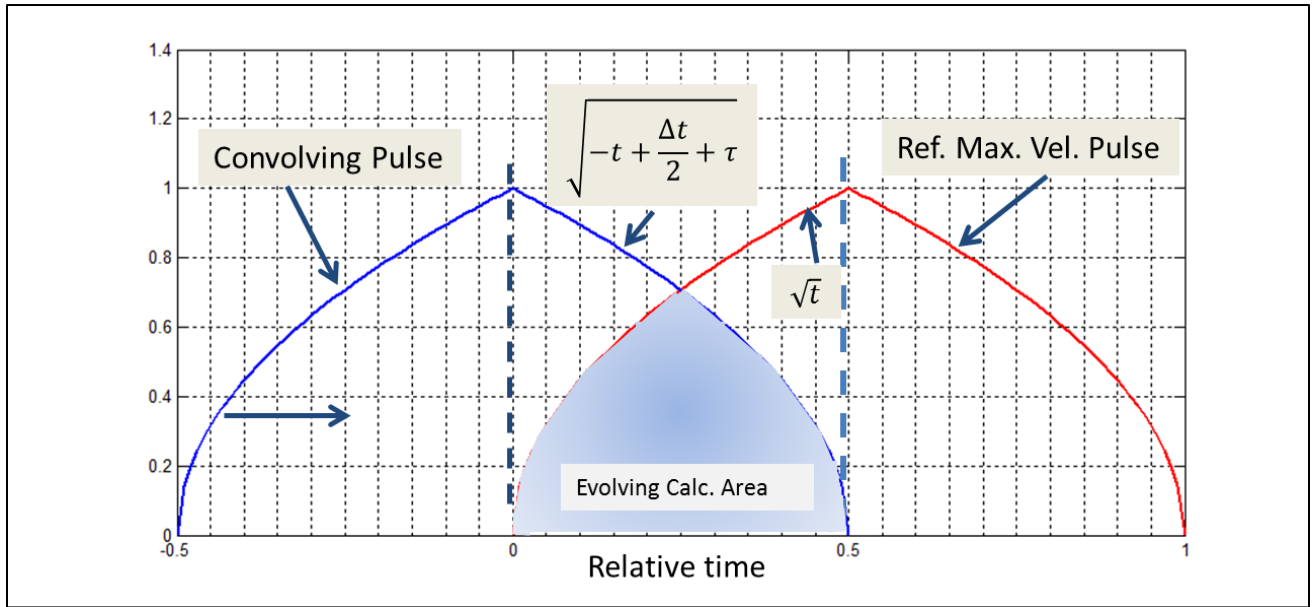


Figure C-1 Convolution Calculation Domain

For the first segment of the solution the two pulses overlap with their specific functional domains determined according to their relative variable time offsets. The reference pulse functional description of course does not change but the convolving pulse domain is dynamic.

The first solution then involves solving;

$$\mathfrak{R}_{v_a.v_a} = \int_0^{\frac{\Delta t}{2} + \tau} \sqrt{t} \sqrt{-t + \frac{\Delta t}{2} + \tau} dt = \int_0^{\frac{\Delta t}{2} + \tau} \left(-t^2 + t \left(\frac{\Delta t}{2} + \tau \right) \right)^{1/2} dt$$

(C1.4)

$$\Re_{v_a, v_a} = \left(\frac{t}{2} - \frac{\Delta t}{8} - \frac{\tau}{4} \right) \sqrt{-t^2 + t \left(\frac{\Delta t}{2} + \tau \right)} \Bigg|_0^{\frac{\Delta t}{2} + \tau} + \frac{\left(\frac{\Delta t}{2} + \tau \right)^2}{8} \left(-\sin \left(\frac{\frac{\Delta t}{2} + \tau - 2t}{\frac{\Delta t}{2} + \tau} \right) \right) \Bigg|_0^{\frac{\Delta t}{2} + \tau} \quad (C1.5)$$

$$\Re_{v_a, v_a} = \frac{\pi}{8} \left(\frac{\Delta t}{2} + \tau \right)^2 \quad -\Delta t \leq \tau \leq -\frac{\Delta t}{2} \quad (C1.6)$$

The next segment for evaluation corresponds with the pulse overlap illustrated in figure C-2.

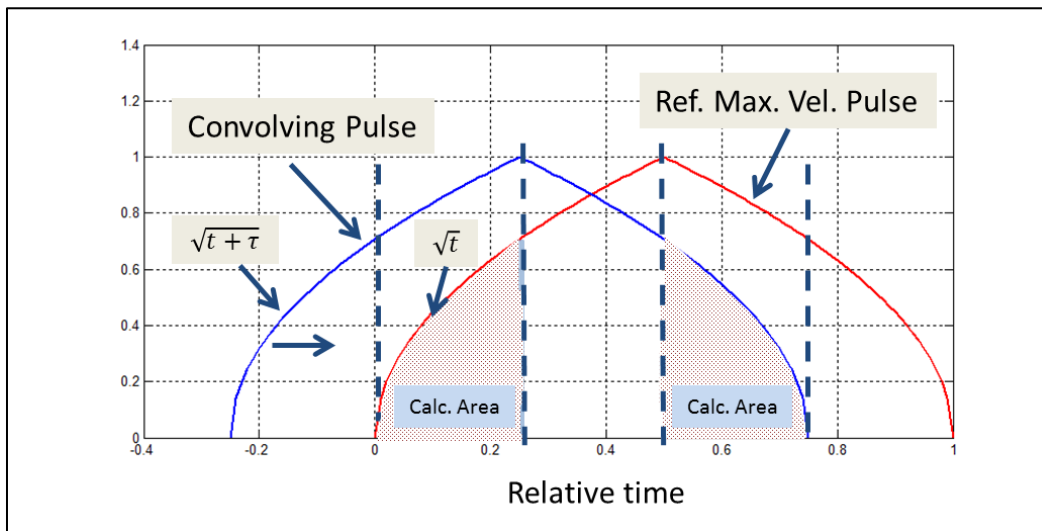


Figure C-2 Convolution Calculation Domain

The applicable equation to be solved is;

$$\int_0^{\frac{\Delta t}{2} + \tau} \sqrt{t} \sqrt{t - \tau} dt = \int_0^{\frac{\Delta t}{2} + \tau} \sqrt{t^2 - \tau t} dt \quad -\frac{\Delta t}{2} \leq \tau \leq 0$$

$$= \frac{2t - \tau}{4} \sqrt{t(t - \tau)} \Big|_0^{\frac{\Delta t}{2} + \tau} - \frac{\tau^2}{8} \left[\ln(2\sqrt{t(t - \tau)} + 2t - \tau) \right]_0^{\frac{\Delta t}{2} + \tau} \quad (\text{C1.7})$$

$$\mathfrak{R}_{v_b, v_b} = \left(\frac{\Delta t + \tau}{4} \sqrt{\left(\frac{\Delta t}{2} + \tau \right) \frac{\Delta t}{2}} \right) \times 2 \quad -\frac{\Delta t}{2} \leq \tau \leq 0 \quad (\text{C1.8})$$

$$\mathfrak{R}_{v_c, v_c} = \left(\frac{\tau^2}{8} \left[\ln \left(2 \sqrt{\left(\frac{\Delta t}{2} + \tau \right) \left(\frac{\Delta t}{2} \right) + \Delta t - \tau} \right) - \ln(-\tau) \right] \right) \times 2 \quad -\frac{\Delta t}{2} \leq \tau \leq 0 \quad (\text{C1.9})$$

C1.8 and C1.9 have been multiplied by 2 to account for both regions of overlap in figure C-2.

The last segment of solution also yields two results. The overlap region is indicated in figure 12-3.

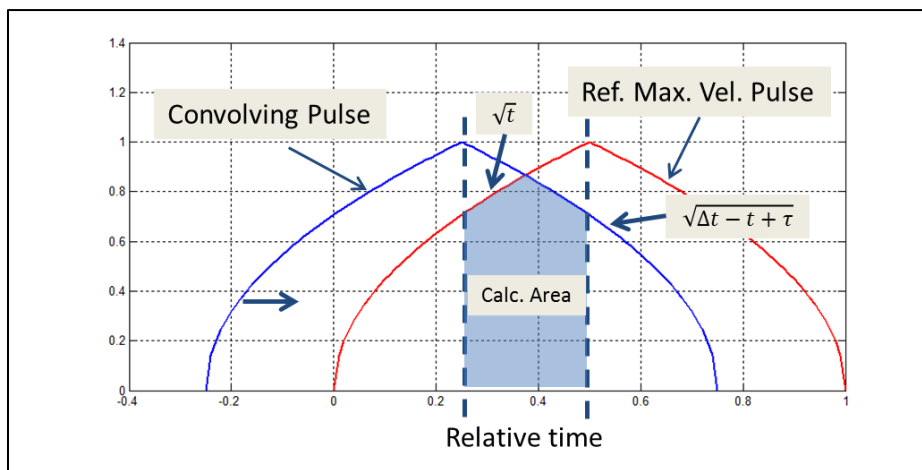


Figure C-3 Convolution Calculation Domain

The applicable integral is;

$$\int_{\frac{\Delta t}{2} + \tau}^{\frac{\Delta t}{2}} \sqrt{t} \sqrt{\Delta t - t + \tau} dt = \int_{\frac{\Delta t}{2}}^{\frac{\Delta t}{2} + \tau} \sqrt{t(\Delta t + \tau)} dt \quad -\frac{\Delta t}{2} \leq \tau \leq 0$$

(C1.10)

$$\begin{aligned} \mathfrak{R}_{v_d, v_d} &= \left(\frac{t}{2} + \frac{\Delta t + \tau}{-4} \right) \sqrt{t(\Delta t + \tau) - t^2} \Big|_{\frac{\Delta t}{2}}^{\frac{\Delta t}{2} + \tau} \\ &= \frac{\tau}{4} \sqrt{\frac{\Delta t}{2} (\Delta t + \tau) - \left(\frac{\Delta t}{2}\right)^2} - \frac{\tau}{4} \sqrt{\left(\frac{\Delta t}{2} + \tau\right) (\Delta t + \tau) - \left(\frac{\Delta t}{2} + \tau\right)^2} \quad -\frac{\Delta t}{2} \leq \tau \leq 0 \end{aligned}$$

(C1.11)

$$\mathfrak{R}_{v_e, v_e} = \frac{(\Delta t + \tau)^2}{8} \left[-\sin^{-1} \left(\frac{-2t + \Delta t + \tau}{\Delta t + \tau} \right) \right] \Big|_{\frac{\Delta t}{2}}^{\frac{\Delta t}{2} + \tau}$$

(C1.12)

$$\mathfrak{R}_{v_e, v_e} = \frac{(\Delta t + \tau)^2}{8} \left[-\sin^{-1} \left(\frac{\tau}{\Delta t + \tau} \right) + \sin^{-1} \left(-\frac{\tau}{\Delta t + \tau} \right) \right] \quad -\frac{\Delta t}{2} \leq \tau \leq 0$$

(C1.13)

The total solution is found from the sum of segmented solutions, C1.6, C1.8, C1.9, C1.11, C1.13 combined with its mirror image in time, symmetric about the peak of the autocorrelation.

$$\mathfrak{R}_{v, v} = \mathfrak{R}_{v_a, v_a} + \mathfrak{R}_{v_b, v_b} + \mathfrak{R}_{v_c, v_c} + \mathfrak{R}_{v_d, v_d} + \mathfrak{R}_{v_e, v_e}$$

(C1.14)

The terms in C1.14 may therefore be scaled as required to normalize the peak of the auto correlation corresponding to the mean of the square for the pulse. For instance, the peak energy of the maximum velocity pulse corresponds to a value of P_m/m . The following plot illustrates the result for $P_m/m = 1$.

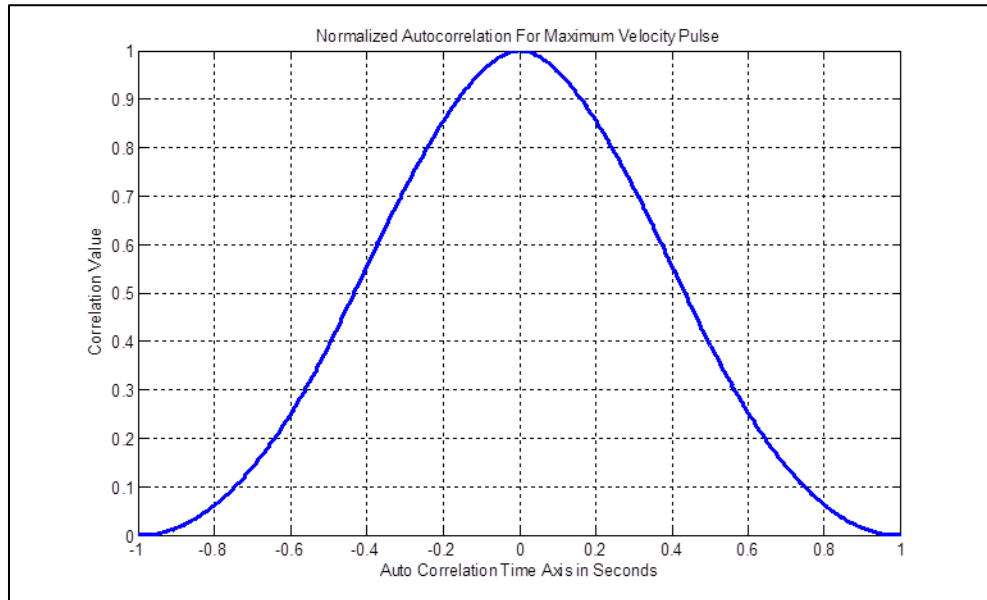


Figure C-4 Normalized Autocorrelation for Maximum Velocity Pulse

APPENDIX D:
DIFFERENTIAL ENTROPY CALCULATION

Shannon's continuous entropy also known as differential entropy may be calculated for the Gaussian multi-variate. The Gaussian multi-variate for the velocity random variable is given as;

$$\rho(v) = \frac{1}{\sqrt{(2\pi)^D [\Lambda]}} e^{-\frac{1}{2}(v_\alpha - \bar{v}_\alpha)^t \Lambda^{-1} (v_\beta - \bar{v}_\beta)}$$

(D1. 1)

D is the dimension of the multi-variate. α, β are enumerated from 1 to D and Λ is a covariance matrix and $(v_\alpha - \bar{v}_\alpha)^t$ is the transpose of $(v_\beta - \bar{v}_\beta)$.

From Shannon's definition;

$$H[\rho(v)] = - \int_{-\infty}^{\infty} \rho(v) \ln(\rho(v)) d(v)$$

(D1. 2)

We note that,

$$\ln \rho(v_\alpha) = -\frac{1}{2} (v_\alpha - \bar{v}_\alpha)^t \Lambda^{-1} (v_\beta - \bar{v}_\beta) \ln(e) - \ln(2\pi)^{D/2} |\Lambda|^{1/2}, \quad \alpha = 1, 2, \dots D$$

(D1. 3)

Since there are D variables the entropy must be calculated with a D -tuple integral of the form;

$$H[\rho(v)] = - \int_{-\infty}^{\infty} \dots \int_{-\infty}^{\infty} \rho(v) \ln(\rho(v)) d(\rho(v))$$

$$\rho(v) = \rho(v_1, v_2, \dots v_D)$$

(D1. 4)

The $D = 1$ case is obtained in Appendix J. Using the same approach we may extend the result over D dimensions ;

$$\begin{aligned}
 H[\rho(v)] &= \frac{1}{2} \int_{-\infty}^{\infty} \dots \int_{-\infty}^{\infty} \ln((2\pi e)^D |\Lambda|) \rho(v) dv \\
 &\quad + \frac{1}{2} \int_{-\infty}^{\infty} \dots \int_{-\infty}^{\infty} \rho(v_\alpha) (v_\alpha - \bar{v}_\alpha) \Lambda^{-1}(v_\beta - \bar{v}_\beta) dv
 \end{aligned}
 \tag{D1.5}$$

We may rewrite D1.5 with a change of variables for the second integral;

$$\begin{aligned}
 H[\rho(v)] &= \frac{1}{2} \int_{-\infty}^{\infty} \dots \int_{-\infty}^{\infty} \ln((2\pi e)^D |\Lambda|) \rho(v) dv + \int_{-\infty}^{\infty} \dots \int_{-\infty}^{\infty} z f(z) dz \\
 z_\alpha &= \frac{1}{2} (v_\alpha - \bar{v}_\alpha) \Lambda^{-1}(v_\beta - \bar{v}_\beta)
 \end{aligned}
 \tag{D1.6}$$

The second integral then is simply the expected value for z_α over the D-tuple which is equal to the dimension D divided by 2 for uncorrelated RVs;

$$E\{z_\alpha\} = E\left\{\frac{1}{2} (v_\alpha - \bar{v}_\alpha) \Lambda^{-1}(v_\beta - \bar{v}_\beta)\right\} = \frac{D}{2}
 \tag{D1.7}$$

The covariance matrix is given by;

$$[\Lambda] = \begin{bmatrix} \sigma_{v_1}^2 & \sigma_{12} & \dots & \sigma_{1D} \\ \sigma_{21} & \sigma_{v_2}^2 & & \vdots \\ \vdots & & \ddots & \\ \sigma_{D1} & \dots & & \sigma_{v_D}^2 \end{bmatrix}$$

(D1.8)

$$\sigma_{\alpha,\beta} = \sigma_\alpha \sigma_\beta \Gamma_{\alpha,\beta}$$

(D1.9)

σ^2 is a variance of the random variable. $\Gamma_{\alpha,\beta}$ is a correlation coefficient. The covariance is defined by

$$\begin{aligned} \sigma_{\alpha,\beta} &= E\{(v_\alpha - \bar{v}_\alpha)(v_\beta - \bar{v}_\beta)\} = \text{cov}\{v_\alpha, v_\beta\} \\ &= \iint_{-\infty}^{\infty} (v_\alpha - \bar{v}_\alpha)(v_\beta - \bar{v}_\beta)\rho(v_\alpha, v_\beta) dv_\alpha dv_\beta \end{aligned}$$

(D1.10)

In the case of uncorrelated zero mean Gaussian random variables $\sigma_{\alpha,\beta} = 0$ for $\alpha \neq \beta$ and 1 otherwise. Thus only the diagonal of D1.8 survives in such a circumstance. The entropy may be streamlined in this particular case to;

$$H[\rho(v)] = \ln \left[e^{\frac{D}{2}} \right] + \frac{1}{2} \ln((2\pi e)^D |\Lambda|)$$

(D1.11)

$$H[\rho(v)] = \frac{1}{2} \ln((2\pi e)^D |\Lambda|)$$

(D1.12)

Equation D1.12 is the maximum entropy case for the Gaussian multi-variate.

In the case where v_α and v_β are complex quantities then D1.10 will also spawn a complex covariance. In this case the elements of the covariance matrix become [25];

$$\begin{aligned} \tilde{\Lambda} = & E \left\{ (v_\alpha - \bar{v}_\alpha) (v_\beta - \bar{v}_\beta)^T \right\} + E \left\{ (\tilde{v}_\alpha - \tilde{v}_\alpha) (\tilde{v}_\beta - \tilde{v}_\beta)^T \right\} \\ & + jE \left\{ (\tilde{v}_\alpha - \tilde{v}_\alpha) (v_\beta - \bar{v}_\beta)^T \right\} - jE \left\{ (v_\alpha - \bar{v}_\alpha) (\tilde{v}_\beta - \tilde{v}_\beta)^T \right\} \end{aligned}$$

The complex covariance matrix can be used to double the dimensionality of the space because complex components of this vector representation are orthogonal. This form can be useful in the representation of band pass processes where a modulated carrier may be decomposed into $\sin(x)$ and $\cos(x)$ components.

Hence the uncertainty space can increase by a factor of 2 for the complex process if the variance in real and imaginary components are equal.

APPENDIX E

MINIMUM MEAN SQUARE ERROR (MMSE) AND CORRELATION

FUNCTION FOR VELOCITY BASED ON SAMPLED AND

INTERPOLATED VALUES

Let $\tilde{v}_\alpha(t) = v_\alpha(t)\delta(t - nT_s) * h_t$ be a discretely encoded approximation of a desired velocity for a dynamic particle. The input samples are zero mean Gaussian distributed and the input process possesses finite power. This is consistent with a maximum uncertainty signal. We are mainly concerned with obtaining an expression for the MMSE associated with the reconstitution of $v_\alpha(t)$ from a discrete representation. From the MMSE expression we may also imply the form of an correlation function for the velocity. When $\tilde{v}_\alpha(t)$ is compared to $v_\alpha(t)$ the comparison metric is cross correlation and becomes autocorrelation for $\tilde{v}_\alpha(t) = v_\alpha(t)$. The inter sample interpolation trajectories will spawn from a linear time invariant (LTI) operator $* h_t$. With this background, a familiar error metric can be minimized to optimize the interpolation, where the energy of each sample is conserved [23];

$$\langle v_\epsilon^2 \rangle = \sigma_\epsilon^2 = \left[\sum_n v_\alpha(t) - v_\alpha(t)\delta(t - nT_s) * h_t \right]^2 \quad (\text{E1.1})$$

Minimizing the error variance σ_ϵ^2 requires solution of;

$$v_\alpha(t) - v_\alpha(t)\delta(t - nT_s) * h_t = 0 \quad (\text{E1.2})$$

Impulsive forces $\delta(t - nT_s)$ are naturally integrated through Newton's laws to obtain velocity pulses. That analysis may easily be extended to tailor the forces delivered to the particle via an LTI mechanism where h_t disperses a sequence of forces in the preferable continuous manner. h_t

may be regarded as a filter impulse response where the integral of the time domain convolution operator is inherent in the laws of motion.

A schematic is a convenient way to capture the concept at a high level of abstraction.

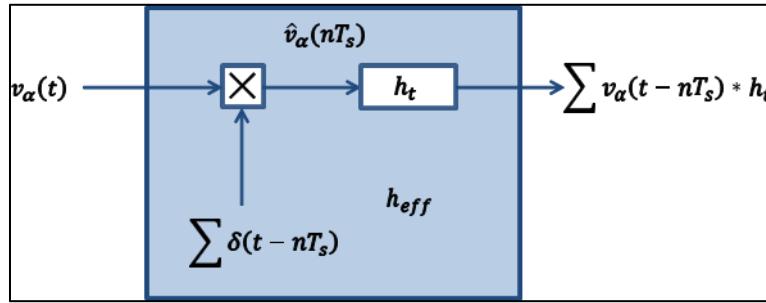


Figure E-1

The schematic illustrates the α^{th} dimension sampled velocity and its interpolation. Extension to D dimensions is straightforward.

It is evident that an effective LTI or linear shift invariant (LSI) impulse response $h_{eff} = 1$ provides the solution which minimizes σ_ϵ^2 .

The expanded error kernel may be compared to a cross correlation where h_t is a portion of the correlation operation . The cross correlation characteristics are gleaned from the expanded error kernel and cross correlation definition;

$$\sigma_\epsilon(\tau, nT_s)^2 = \langle v_\alpha(t + \tau)^2 - 2v_\alpha(t + \tau)v_\alpha(t - nT_s) * h_t + (v_\alpha(t - nT_s) * h_t)^2 \rangle \quad (E1.3)$$

$$\sigma_\epsilon(\tau, nT_s)^2 = \langle v_\tau^2 \rangle - 2|\gamma_{\tau, nT_s}| \langle v_\tau v_{nT_s} \rangle + (\gamma_{\tau, nT_s} \langle v_{nT_s} \rangle)^2 \quad (E1.4)$$

The notation has been streamlined, dropping the α subscript and adopting a two dimensional variation to allow for sample number and continuously variable time offset. The reference function $v_\alpha(t + \tau)$ is continuously variable over the domain while $v_\alpha(t - nT_s) * h_t$ is fixed. γ_{τ, nT_s} are cross correlation coefficients. These coefficients essentially reflect how well the operator $* h_t$ accomplishes the reconstruction of particle velocity while simultaneously providing a means to analyze the dependence between input stimulus and output response at prescribed intervals of T_s . $|\gamma_{\tau, nT_s}|_{norm} \leq 1$ under all circumstances.

The power cross correlation function (m=1) is defined in the usual manner;

$$\mathfrak{R}_{\tau, nT_s} = \frac{1}{2} \langle v_\tau v_{nT_s} \rangle \quad (E1.5)$$

Then

$$\tilde{\sigma}_\epsilon^2 = 2 \left[v_\tau^2 - 2|\gamma_{\tau, nT_s}| \mathfrak{R}_{\tau, nT_s} + (\gamma_{\tau, nT_s} \sigma_{nT_s})^2 \right] \quad (E1.6)$$

The extremes may be obtained by solving;

$$\frac{\partial \sigma_\epsilon^2}{\partial \gamma_{\tau, nT_s}} = -\mathfrak{R}_{\tau, nT_s} + |\gamma_{\tau, nT_s}| (\sigma_{nT_s})^2 = 0 \quad (E1.7)$$

$$\Re_{\tau, nT_s} = |\gamma_{\tau, nT_s}|(\sigma_{nT_s})^2 \quad (\text{E1. 8})$$

If the particle velocity is random and zero mean Gaussian and of finite power then it is known that \Re_{τ, nT_s} cannot take the form of a delta function [12]. Furthermore the correlation may possess only one maximum which occurs for $\Re_{\tau=0, nT_s=0}$. Whenever $\tau = nT_s \neq 0$ then the magnitude of the correlation cannot be gleaned by E1-7 unless the correlation coefficients may be obtained by some other means. They however cannot be 1 or -1, yet they can be zero.

Also, the correlation function may vary in the following manner;

$$\frac{\partial \Re_{\tau, nT_s}}{\partial \gamma_{\tau, nT_s}} = \pm \sigma_{nT_s}^2, @ \tau = nT_s \neq 0 \quad (\text{E1. 9})$$

Now this implies that the autocorrelation is zero for $\tau = nT_s \neq 0$ because E1-7 permits only a max. or min. value for the magnitude of correlation coefficients. A local maximum would reflect a slope of zero not $\pm \sigma_{nT_s}^2$ as obtained in E-9. Thus, if the slope is either positive or negative at modulo T_s offsets, the correlation is zero at those points and will oscillate between positive and negative values away from those points whenever the velocity variance is nonzero at $\tau = \pm nT_s$. This further implies that the correlation possesses crests and valleys between those correlation zeros. In addition, the correlation function must converge to zero at large offsets for $\tau = \pm nT_s$. This is consistent with a bandwidth limited process which insures finite power for the signal, a presumption of the analysis since the maximum power is specified as P_m . It is logical to suppose

that a finite input power process to a passive LTI network, h_t , must also produce a finite output power. It is known that the input process is Gaussian so that the output process must also be Gaussian. For a MMSE condition, it follows that each sample on the input must equal each sample at the output, regardless of the sample time. The only solution possible is that $h_{eff} = 1$.

We cannot further resolve the form of the correlation function which minimizes the MMSE without explicitly solving for h_t or injecting additional criteria. This can be accomplished by setting $h_{eff} = 1$ in figure E-1 and solving for h_t . When this additional step is accomplished the correlation function corresponding to the optimal impulse response LTI operator then takes on the form of the *sinc* function (reference chapter 3).

APPENDIX F:

MAX CARDINAL VS. MAX NL. VELOCITY PULSE

This appendix provides some support calculations for the comparison of maximum nonlinear and cardinal pulse types. The following figure illustrates the characteristic profiles.

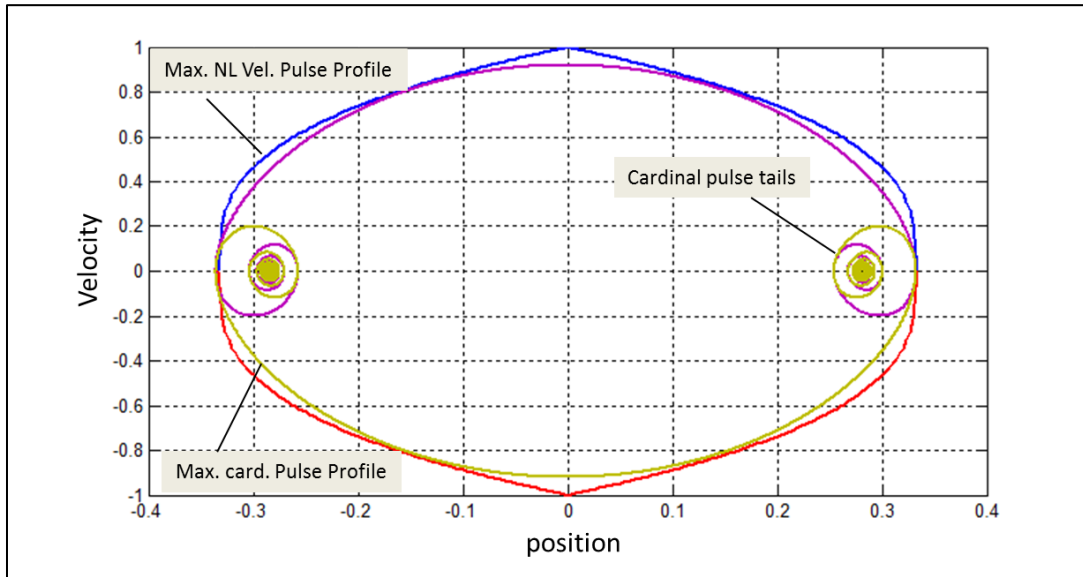


Figure F-1 Maximum Non-Linear and Cardinal Velocity Pulse Profiles

In this view the maximum cardinal profile is subordinate to the maximum nonlinear velocity pulse profile boundary. This is a reference view which implies that the configuration space is preserved. The time to traverse this space for both cases cannot be discerned without further specification of the resources required in both cases. Notice the precursor and post cursor tails of the cardinal pulse. They exist because the extended cardinal pulse persists over the interval $-\infty \leq t \leq \infty$. The tails possess ~9.3% of the pulse energy.

Let the fundamental cardinal pulse be given by;

$$v_{p_card} = v_{m_card} \frac{\sin(\pi f_s t)}{\pi f_s t}$$

The energy of the pulse is proportional to (m=1 unless otherwise indicated);

$$\mathcal{E}_{k_card} = \frac{v_{m_card}^2 \sin^2(\pi f_s t)}{2 (\pi f_s t)^2}$$

Then (for $v_{m_card}=1$) ;

$$\frac{d\mathcal{E}_{k_card}}{dt} = \frac{1 \sin(\pi f_s t)}{2 (\pi f_s t)^3} [2\pi f_s (\pi f_s t \cos(\pi f_s t)) - \sin(\pi f_s t)]$$

P_{m_card} is calculated from;

$$\max \left\{ \frac{d\mathcal{E}_{k_card}}{dt} \right\} = 0$$

The following graphic illustrates the solution for P_{m_card} .

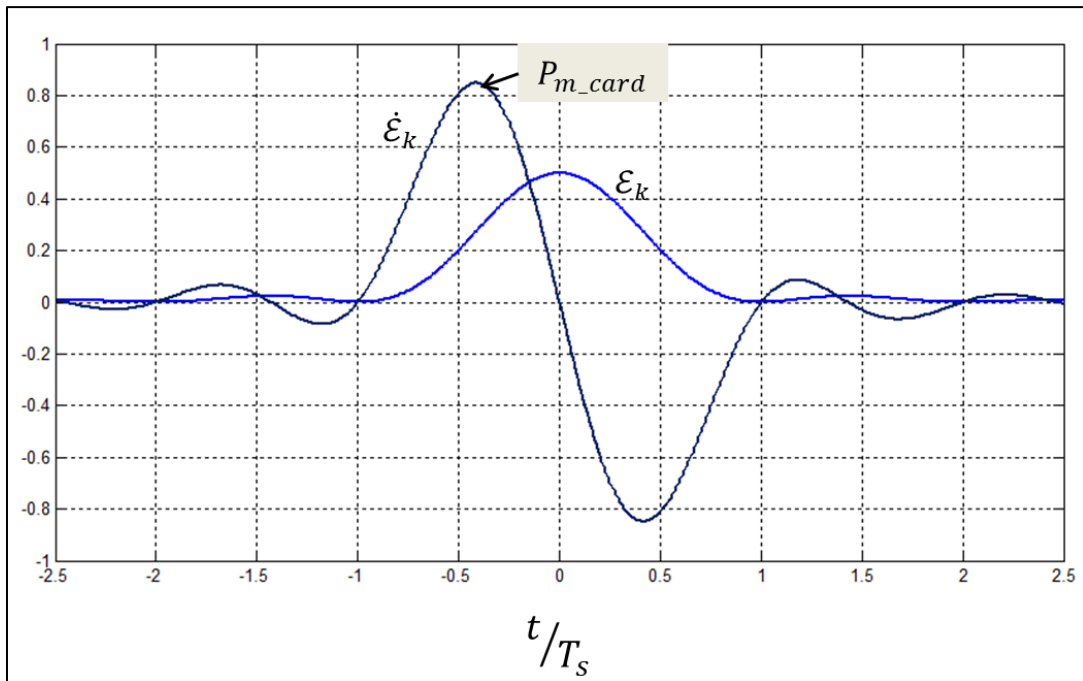


Figure F-2 Solution for P_{m_card} is approx. .843 @ $(t/T_s) \approx -0.42$. v_{max_card} is unity for this case.

Now suppose that the prior case is compared to the maximum nonlinear velocity pulse case where $v_m = 1$ and $T_s = 1$. Then $P_{max} = .5$ (reference Appendix B).

The ratio of the maximum power requirements is;

$$\frac{P_{m_card}}{P_{max}} = 1.686$$

This is the ratio when the pulse amplitudes are identical for both cases at the time $t/T_s = 0$. The total energy of the pulses are not equal and the distance a particle travels over a characteristic interval Δt is not the same for both cases. The information at the peak velocity is however equivalent. This circumstance may serve as a reference condition for other comparisons.

We may also calculate the required velocity in both cases for which the particle traverses the same distance in the same length of time $\Delta t = 2T_s$. This is a conservation of configuration space comparison. We equate the two distances by;

$$2 \int_0^{T_s} v_p dt = 2 \int_0^{T_s} v_{p_card} dt$$

The integral on the left is the distance for a nonlinear maximum velocity pulse case and the integral on the right is the maximum cardinal pulse case. Explicitly;

$$\int_0^{T_s} \sqrt{\frac{2P_m t}{m}} dt = \int_0^{T_s} v_{m_card} \frac{\sin(\pi f_s t)}{\pi f_s t} dt$$

v_{m_card} is to be calculated.

$$\frac{2}{3} \sqrt{\frac{2P_m}{m}} T_s^{3/2} = v_{m_card} \tilde{Si}(T_s)$$

$\tilde{Si}(T_s)$ is a function of the sine integral, integrated over the range $0 \leq t \leq T_s$, where $T_s = 1$ [68].

$$Si(z) = \int_0^z \frac{\sin(t)}{t} dt$$

$$\tilde{Si}(T_s) = \frac{T_s}{\pi} \int_0^{T_s} \frac{\sin(\dot{t})}{\dot{t}} d\dot{t}$$

$$\therefore v_{m_card} = \frac{2\pi}{3} \sqrt{\frac{2P_m}{m}} \sum_{n=0}^{\infty} \frac{(2n+1)(2n+1)!}{(-1)^n T_s^{(2n+1/2)}}$$

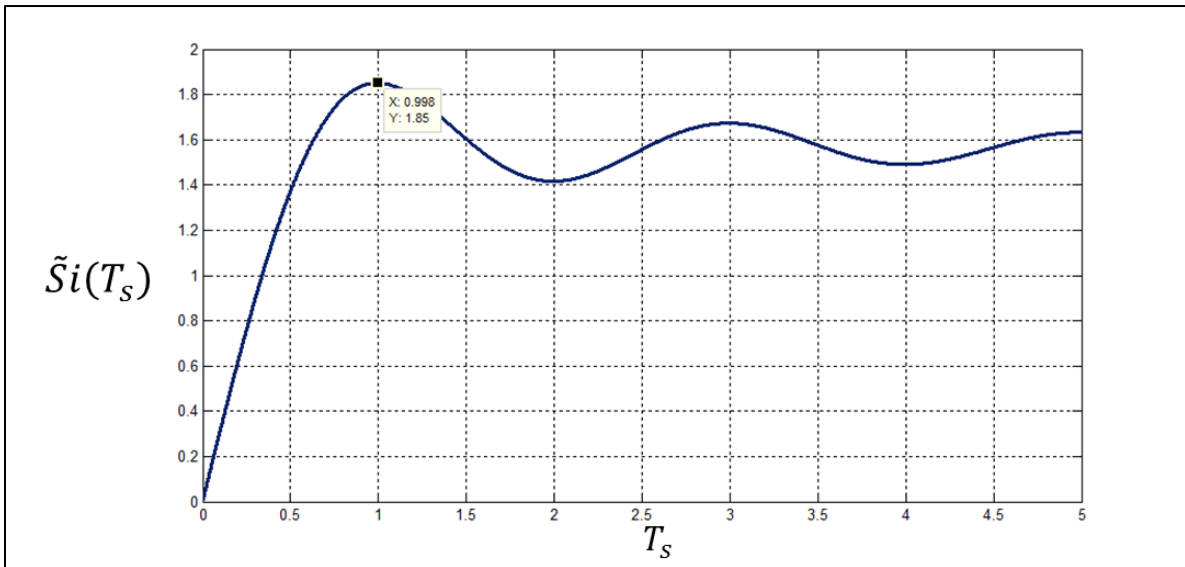


Figure F-3 Sine Integral Response

$$v_{m_card} \cong \frac{2\pi}{3} \sqrt{\frac{2P_m}{m}} \frac{1}{1.85} \approx 1.6\sqrt{P_m}; \quad \text{for } T_s = 1$$

In terms of v_{max} ;

$$1.6\sqrt{P_m} = 1.6 v_{max} \sqrt{\frac{m}{2T_s}} = 1.13 v_{max}$$

The power increase at peak velocity for the cardinal pulse compared to the nonlinear maximum velocity pulse is;

$$\left(\frac{v_{m_card}}{v_{max}}\right)^2 = 1.28$$

This represents an increase of ~ 1.07 dB at peak velocity.

The P_m increase however is noticeably greater and may be calculated using ratios normalized to the reference case;

$$\frac{\mathcal{E}_{max_card}}{\mathcal{E}_{max_card_ref}} = \frac{P_{max_card}}{P_{max_card_ref}}$$

Therefore;

$$P_{max_card} = \frac{\left(\frac{v_{m_card}}{2}\right)^2}{\left(\frac{v_{max_ref}}{2}\right)^2} (P_m)(P_{max_card_ref}) = \frac{(1.28)(.843)}{.5} P_m$$

And;

$$\frac{P_{max_card}}{P_m} \cong 2.158$$

This represents an increase of approximately 3.34 dB required for the peak power source enhancement relative to the maximum nonlinear velocity pulse case, to permit a maximum

cardinal pulse to span the same physical space in an equivalent time period Δt . The following figure illustrates the required rescaling for this case.

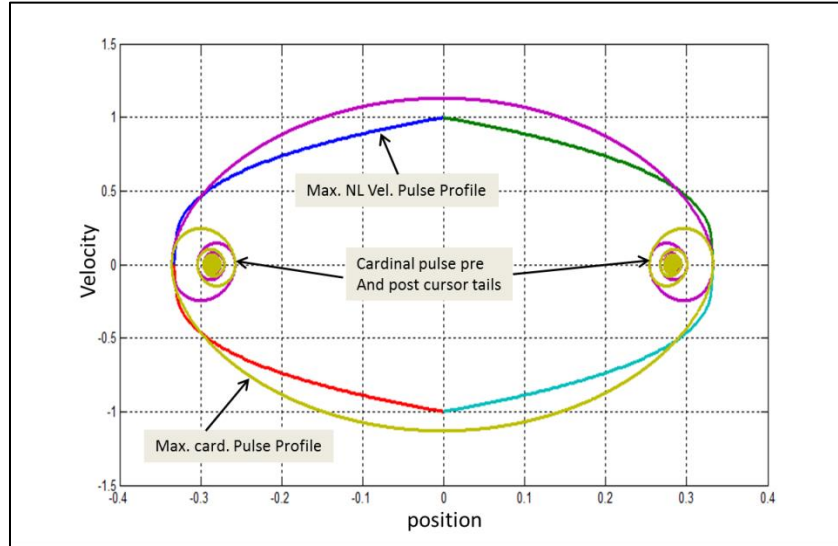


Figure F-4 Maximum Non-Linear and Cardinal Pulse Profiles

It is possible to calculate the required sampled time T_s for both pulse types in the case where the phase space is conserved for both scenarios and $P_{\max_card} = P_m = 1$. We shall assign the sample time the variable T_{ref} for the maximum nonlinear pulse type.

$$\frac{2}{3} \sqrt{\frac{2P_m}{m}} T_{ref}^{3/2} = v_{m_card} \tilde{S}i(T_s)$$

v_{m_card} is first calculated from (refer to reference case);

$$P_{\max_card} \approx 1.28 \mathcal{E}_{\max_card}$$

$$v_{m_card} = \sqrt{2 \frac{(P_{\max_card})}{1.28}} \approx 1.25$$

Therefore;

$$\left(\frac{T_s}{T_{ref}}\right)^{3/2} = \frac{2\pi}{3} \frac{1}{v_{m_card} \tilde{S}i(T_s)} \sqrt{\frac{2P_m}{m}} \cong 1.289; \quad \text{for } T_{ref} = 1$$

$$\therefore T_s = 1.179 T_{ref}$$

This corresponds to a bandwidth which is T_s^{-1} or $\approx .848$ of the reference BW. Therefore, a lower instantaneous power can be considered as a trade for a reduction in bandwidth.

The characteristic radius of the cardinal pulse case is calculated from the integration of velocity over the interval T_s ;

$$R_s = \frac{\pi}{T_s} \int_0^{T_s} (v_{max_card}) \frac{\sin(t)}{t} dt$$

For the normalized case of $T_s = \pi$ we obtain

$$R_s = (1.85)(v_{max_card})$$

APPENDIX G:
CARDINAL TE RELATION

The TE relation is examined as it relates to a maximum cardinal pulse. Also, the two pulse energies are compared. Although the two structures are referred to as pulses, they are applied as profiles or boundaries in chapter 3, restricting the trajectory of dynamic particles.

The general TE relation is given by;

$$\frac{1}{T_s} \geq \frac{\max\left\{\frac{d\mathcal{E}_k}{dt}\right\}}{k_p \langle \mathcal{E}_k \rangle (PAER)}$$

In the case of the most expedient velocity trajectory to span a space $k_p = 1$. This bound results in a nonlinear equation of motion. Therefore, a physically analytic design will constrain motions to avoid the most extreme trajectory associated with a $k_p = 1$ case or modify k_p .

The nature of the TE relation can be revealed in an alternate form;

$$P_{max} = \frac{k_p \mathcal{E}_{k_{max}}}{T_s}$$

P_{max} is defined as the maximum instantaneous power of a pulse $\max\left\{\frac{d\mathcal{E}_k}{dt}\right\}$ over the interval T_s .

$\mathcal{E}_{k_{max}}$ is the maximum kinetic energy over that same span of time. Then from appendix F the cardinal pulse will have the following values for k_p .

Case 1: $(\mathcal{E}_{k_{max_card}}/\mathcal{E}_{k_{max}}) = 1$, $(T_{s_max_card}/T_{s_max}) = 1$, $(R_{s_max_card}/R_{s_max}) = 1$

$$k_p = \frac{P_{max_card} T_s}{\mathcal{E}_{k_{max_card}}} = 1.28$$

Case 2: $(P_{max_card}/P_{max}) = 1$, $(R_{s_max_card}/R_{s_max}) = 1$

$$k_p = \frac{P_{\max_card} T_s}{\mathcal{E}_{k_{\max_card}}} = 1.179 \quad (\text{see Appendix F})$$

The subscript “max_card” refers to the maximum cardinal pulse type and the subscript “max” references the maximum nonlinear pulse type.

The total pulse energies for the 2 cases above are not equivalent. It should be noted that the energy average for the cardinal pulse is per unit time T_s . The total energy for both pulse types are given by;

$$\mathcal{E}_{k_{\max_tot}} = T_s P_{\max}$$

$$\mathcal{E}_{k_{\max_card_tot}} = \frac{m}{2} \int_{-\infty}^{+\infty} \left(v_{m_card} \frac{\sin(\pi f_s t)}{\pi f_s t} \right)^2 dt = (\mathcal{E}_{k_{\max_card}}) \frac{T_s}{\pi}$$

If both energies are equated then;

$$\frac{\mathcal{E}_{k_{\max_card_tot}}}{\mathcal{E}_{k_{\max_tot}}} = \frac{\mathcal{E}_{k_{\max_card}}}{\pi P_{\max}} = 1$$

This reveals a static relation between the two pulse types whenever total energies are equal, which can be restated simply as;

$$\frac{P_{\max_card}}{P_{\max}} = \pi(.843) \cong 2.648$$

APPENDIX H:
RELATION BETWEEN INSTANTANEOUS EFFICIENCY AND
THERMODYNAMIC EFFICIENCY

In this appendix two approaches for efficiency calculations are compared to provide alternatives in algorithm development. Optimization procedures may favor an indirect approach to the maximization of thermodynamic efficiency. In such cases, an instantaneous efficiency metric may provide significant utility. This appendix does not address those optimization algorithms. Thermodynamic Efficiency possesses a very particular meaning. It is determined from the ratio of two random variable mean values.

$$\eta \equiv \frac{\langle P_{out} \rangle}{\langle P_{in} \rangle}$$

Calculation of this efficiency precludes reduction of the power ratio prior to calculating the average. This fact can complicate the calculations in some circumstances. In contrast, consider the case where the ratio of powers is given by;

$$\langle \eta_{inst} \rangle = \left\langle \frac{P_{out_inst}}{P_{in_inst}} \right\rangle$$

η and η_{inst} do not possess the same meaning yet are correlated. It is often useful to reduce $\langle \eta_{inst} \rangle$ rather than η to obtain an optimization, the former implying the latter.

The proper thermodynamic calculation begins with the ratio of two differing RV's. The numerator is a non-central gamma or chi squared RV for the canonical case, which is obtained from;

$$\rho(\mathcal{X}) = \frac{dV_L}{d\mathcal{X}} \rho(V_L)$$

\mathcal{X} is the variable $(\tilde{V}_L - \langle V_L \rangle)^2$ where \tilde{V}_L is approximately Gaussian for $\sigma \ll V_s$. The completed transformation is given by;

$$\rho(\mathcal{X}) = \frac{1}{2\sqrt{\mathcal{X}}} \frac{1}{\sqrt{2\pi}\sigma} e^{-\frac{(\sqrt{\mathcal{X}} - \langle V_L \rangle)^2}{2\sigma^2}}$$

This can also be obtained from the more general non-central Gamma multivariable sum [25, 32];

$$\rho(\mathcal{X}) = \frac{1}{2} \left(\frac{\mathcal{X}}{\sum_i^N \langle V_{L_i} \rangle} \right)^{[(N-2)/4]} e^{-\frac{(x - \sum_i^N \langle V_{L_i} \rangle)}{2\sigma^2}} I_{[(N-2)/2]} \left(\frac{1}{2\sigma^2} \sqrt{\mathcal{X} \sum_i^N \langle V_{L_i} \rangle} \right); \quad \mathcal{X} \geq 0$$

, where $N=1$ in the reduced form, $I_{[(N-2)/2]}$ is a modified Bessel function of the first kind, and σ^2 is the variance of the Gaussian RV. The more general result applies to an arbitrary sum of N Gaussian signals with corresponding non-zero means.

The denominator of the thermodynamic efficiency is obtained from the sum of two RV's. One is positive non central Gaussian and the other is identical to $\rho(\mathcal{X})$.

Hence, the proper thermodynamic waveform efficiency is obtained from (where statistical and time averages are equated);

$$\eta = \frac{\int_{-\infty}^{\infty} \mathcal{X} \rho(\mathcal{X}) d\mathcal{X}}{\int_{-\infty}^{\infty} P_{in} \rho(P_{in}) dP_{in}}$$

We may work directly with this ratio or time averaged equivalents whenever the process is stationary in the wide sense. Sometimes the statistical ratio presents a formidable numerical challenge, particularly in cases of optimization where calculations must be obtained “on the fly”.

On the other hand, the averaged instantaneous power ratio is (where statistical and time averages are equated);

$$\langle (\eta_{inst_WF}) \rangle = \int_{-\infty}^{\infty} \eta_{inst_WF} \left[\frac{dV_L}{d\eta_{inst_WF}} \rho(V_L) \right] d\eta_{inst_WF}$$

$$\langle \eta_{inst_WF} \rangle = \int_{-\infty}^{\infty} \eta_{inst_WF} \left[\frac{V_s}{(1+\eta)^2} \frac{1}{\sqrt{2\pi\sigma^2}} e^{-\frac{\left(\eta \frac{V_s}{(1+\eta)} - \frac{V_s}{4}\right)^2}{2\sigma^2}} \right] d\eta_{inst_WF}$$

Now η and η_{inst_WF} are always obtained from the same fundamental quantities P_{out} and P_{in} with similar ratios and therefore are correlated. In fact they are exactly equivalent prior to averaging.

The instantaneous waveform power ratio for a type one electronic information encoder or modulator is given by;

$$\eta_{inst_WF} = Re \left\{ \frac{V_L^2}{(V_L V_s) - Z_r (V_L^2)} \right\}$$

, where Z_r is the ratio of power source impedance to load impedance. The meaning of this power ratio is an instantaneous measure of work rate at the system load vs. the instantaneous work rate referred to the modulator input. It is evident that the right hand side may reduce whenever the numerator and denominator terms are correlated. This reduction generally affords some numerical processing advantages.

We can verify that the thermodynamic waveform efficiency is always greater than or equal to the instantaneous waveform efficiency for the type 1 modulator.

$$\langle \eta_{inst_WF} \rangle = \left\langle \frac{V_L^2}{V_s V_L - V_L^2} \right\rangle = \frac{1}{\frac{V_s}{\langle V_L \rangle} - 1}$$

Likewise;

$$\eta = \frac{\langle V_L^2 \rangle}{\langle V_s V_L - V_L^2 \rangle}$$

The numerator and denominator may be divided by the same constant.

$$\eta = \frac{\frac{\langle V_L^2 \rangle}{\langle V_L \rangle^2}}{\frac{\langle V_s V_L - V_L^2 \rangle}{\langle V_L \rangle^2}} = \frac{\frac{\sigma^2 + \langle V_L \rangle^2}{\langle V_L \rangle^2}}{\frac{V_s}{\langle V_L \rangle} - \left(\frac{\sigma^2 + \langle V_L \rangle^2}{\langle V_L \rangle^2} \right)}$$

This result implies that;

$$\eta \geq \langle \eta_{inst_WF} \rangle$$

always, because;

$$\frac{\sigma^2 + \langle V_L \rangle^2}{\langle V_L \rangle^2} \geq 1$$

Whenever the signal component $\langle \tilde{V}_L^2 \rangle > 0$ then $\sigma^2 > 0$ and the thermodynamic efficiency is the greater of the two quantities.

Optimizing η_{inst_WF} always optimizes η for a given finite value of σ in the Gaussian case. That is,

in both circumstances an optimum depends on minimizing $\frac{V_s}{\langle V_L \rangle}$. This optimization is not arbitrary

however and must consider the uncertainty required for a prescribed information throughput

which is determined by the uncertainty associated with the random signal. $\frac{V_s}{\langle V_L \rangle}$ is therefore

moderated by the quantity σ^2 . As σ^2 , the information signal variance, increases, the quantity $\frac{V_s}{\langle V_L \rangle}$ must adjust such that the dynamic range of available power resources is not depleted or characteristic pdf for the information otherwise altered. In all cases of interest the maximum dynamic range of available modulation change is allocated to the signal. For symmetric signals this implies that $\frac{V_s}{\langle V_L \rangle} = 2$ for maximum dynamic range and that the power source impedance is zero. Whenever the source impedance is not zero then the available signal dynamic range reduces along with efficiency.

An example illustrates the two efficiency calculations. A series type one modulator is depicted in the following block diagram;

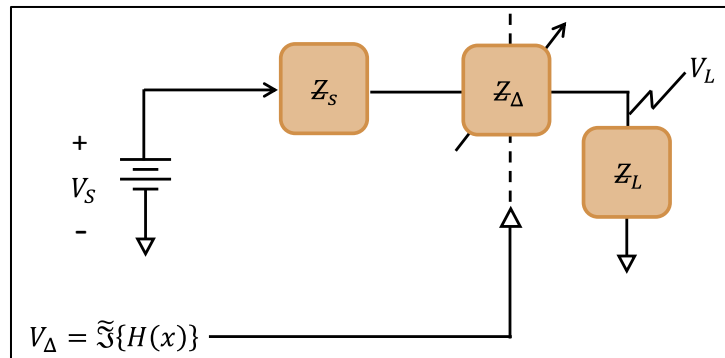


Figure H-1 Type 1 Encoder/Modulator

If the source and load impedances are real and equated then the instantaneous efficiency is given by;

$$\eta_{inst_WF} = \check{\eta} = \left\{ \frac{V_L^2}{(V_L V_s) - (V_L^2)} \right\}$$

The apparatus consists of the variable impedance, or in this case resistance, $Re\{Z_{\Delta}\}$, and the load Z_L . We are concerned with the efficiency of this arrangement when the modulation is approximately Gaussian. Z_s impacts the efficiency because it reduces the available input power to the modulator at Z_{Δ} . V_s is a measurable quantity whenever the apparatus is disconnected. Likewise, $Re\{Z_{\Delta}\}$ can be deduced from measurements in static conditions before and after the circuit is connected, provided Z_L, Z_{Δ} , are known. The desired output voltage across the load is obtained by modulating Z_{Δ} with some function of the desired uncertainty $H(x)$. The output V_L is offset Gaussian for the case of interest and is given by;

$$\rho(V_L) = \frac{1}{\sqrt{2\pi}\sigma} e^{-\frac{(V_L - \langle V_s/4 \rangle)^2}{2\sigma^2}}$$

The following graphic illustrates the modulated information pdf at an offset where $V_s = 2 \text{ vlt}$ s and $\sigma = .15$.

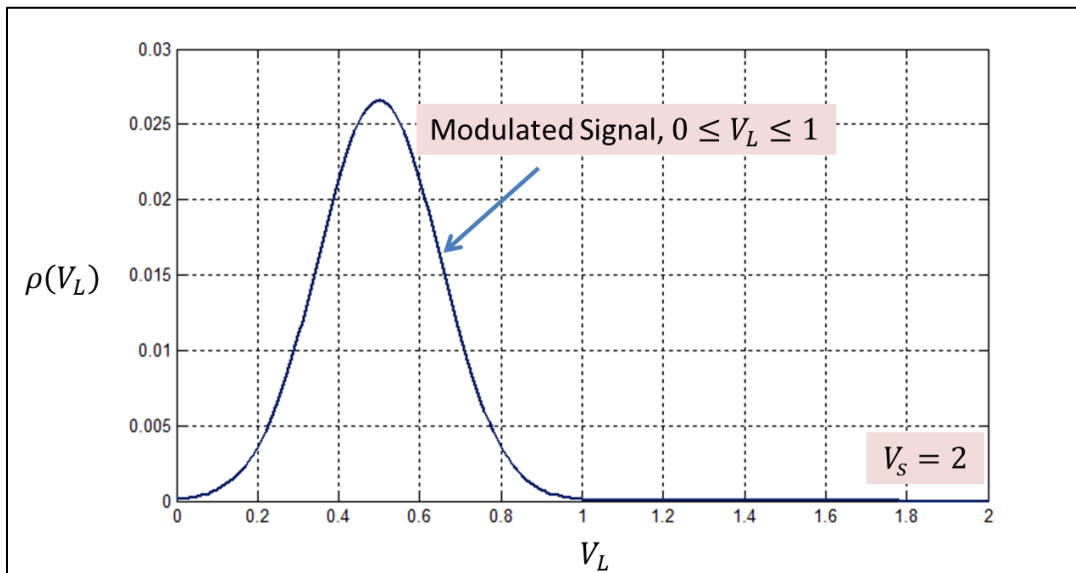


Figure H-2 Modulated Information pdf

Using the method of instantaneous efficiency we obtain a continuous pdf for η_{inst_WF} .

$$\rho(\check{\eta}) = \frac{V_s}{(1 + \check{\eta})^2} \frac{1}{\sqrt{2\pi\sigma^2}} e^{-\frac{\left(\eta - \frac{V_s}{(1+\check{\eta})} - \frac{V_s}{4}\right)^2}{2\sigma^2}}$$

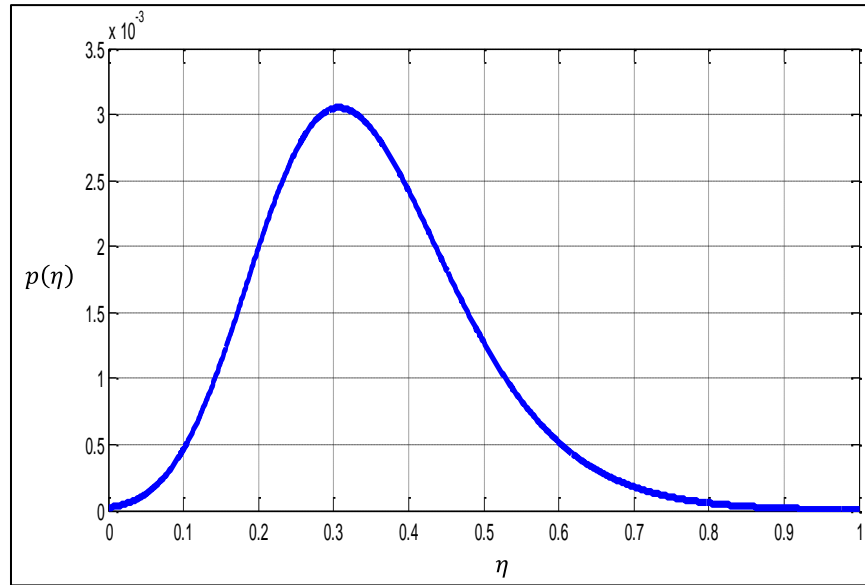


Figure H-3 pdf of Instantaneous Efficiency

The utility of this statistical form is primarily due to the reduction of the ratio to a single continuous RV rather than the ratio of two which must be separately analyzed prior to reduction.

The average of the instantaneous efficiency is then calculated from;

$$\langle(\eta_{inst_WF})\rangle = \int_{-\infty}^{\infty} \check{\eta} [\rho(\check{\eta})] d\check{\eta}$$

, or;

$$\langle\check{\eta}\rangle = \frac{1}{\frac{V_s}{\langle V_L \rangle} - 1} \approx .33$$

The thermodynamic waveform efficiency is found from;

$$\eta_{WF} = \frac{\sigma^2 + \langle V_L \rangle^2}{V_s \langle V_L \rangle - (\sigma^2 + \langle V_L \rangle^2)} = .375$$

Thus we see that the thermodynamic waveform efficiency is greater than the averaged instantaneous waveform efficiency in this example.

η may also be obtained from the statistical ratio;

$$\eta = \frac{\int_{-\infty}^{\infty} x \rho(x) dx}{\int_{-\infty}^{\infty} P_{in} \rho(P_{in}) dP_{in}}$$

$\rho(x)$ is illustrated in the following graphic;

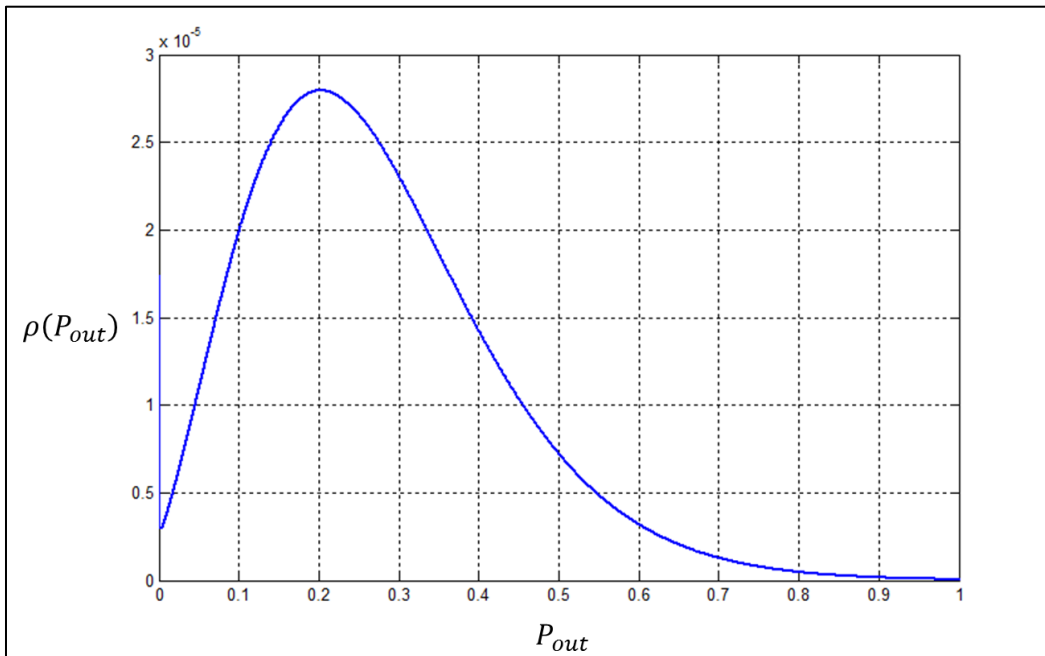


Figure H-4 Non Central Gamma pdf

This is a non-central gamma distribution with non-centrality parameter of $.25=\langle V_L \rangle^2$ and $\sigma^2 = .0225$. This pdf was verified by circuit simulation using a histogram to record the relative occurrence of output power values;

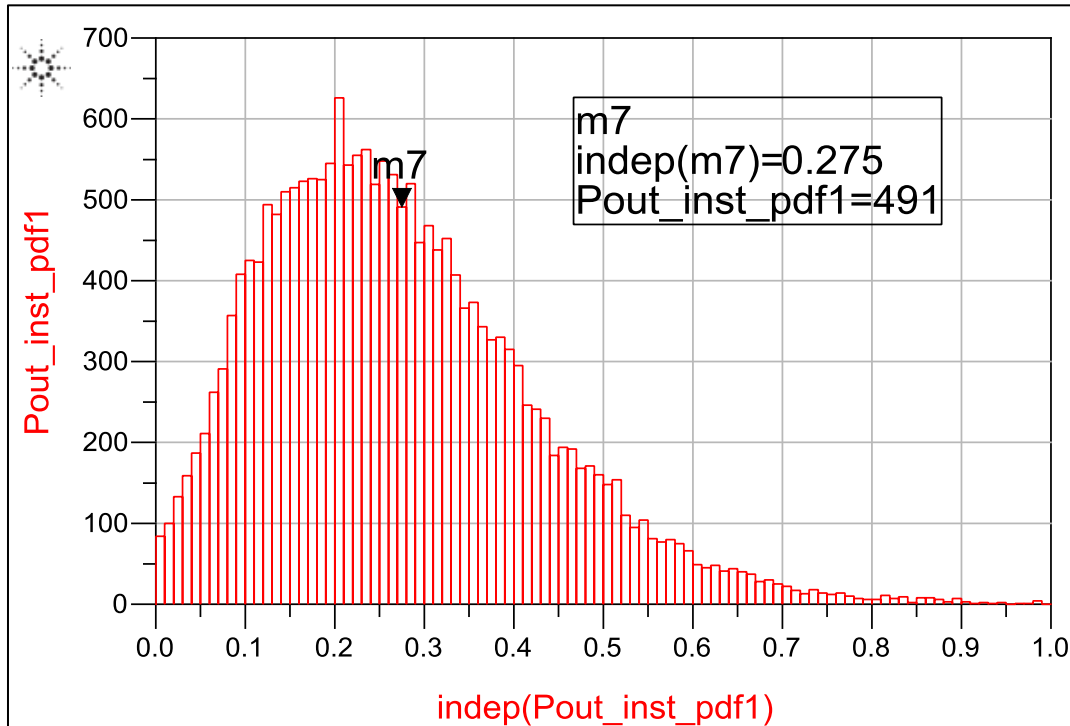


Figure H-5 Simulation of type 1 Modulator Output Power Histogram

The marker, m7 is near the theoretical mean of $.2725$.

The denominator pdf for Pin is the difference of the RV for Pout and the RV formed by the multiplication of $V_S V_L$ where V_L is non-central Gaussian. The marker is near the theoretical mean of $.2725$. The relative histogram for this RV is given in the following graphic;

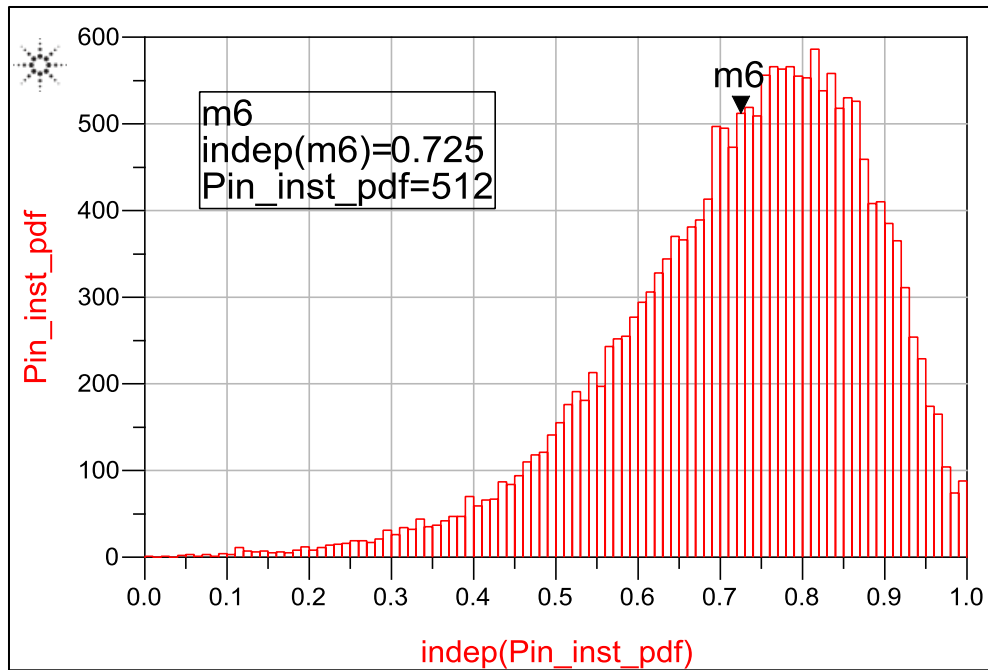


Figure H-6 Histogram for Pont $V_S V_L$

The marker $m6$ is near the theoretical mean of .7275. Calculating the means of these two distributions and taking their ratios yields the thermodynamic waveform efficiency. Proper thermodynamic efficiency must remove the effect of the offset term of the numerator, leaving a numerator dependent on the information bearing portion of the waveform only. Appendix I further explores the relationship between η and $\check{\eta}$.

Certain procedures of optimization involving time averages may favor working with thermodynamic efficiency directly. However, if an optimization is based on statistical analysis then instantaneous efficiency may be a preferable variable which in turn implies an optimized thermodynamic efficiency under certain conditions.

APPENDIX I:
WAVEFORM, THERMODYNAMIC, AND INSTANTANEOUS
EFFICIENCY RELATIONSHIPS

This appendix provides several comparisons of waveform and signal efficiencies. The comparisons provide a means of conversion between the various forms which can provide some analysis utility.

First, the proper thermodynamic waveform and thermodynamic signal efficiencies are compared for a type one modulator where $Z_r = 1$.

$$\eta_{WF} = \frac{\sigma^2 + \langle V_L \rangle^2}{V_s \langle V_L \rangle - (\sigma^2 + \langle V_L \rangle^2)}$$

$$\eta_{sig} = \tilde{\eta} = \frac{\sigma^2}{V_s \langle V_L \rangle - (\sigma^2 + \langle V_L \rangle^2)}$$

η_{sig} considers only the signal power as a valid output. This is as it should be since DC offsets and other anomalies do not encode information and therefore do not contribute positively to the apparatus deliverable. However, η_{WF} is related to η_{sig} and therefore is useful even though it retains the offset. If the maximum available modulation dynamic range is used then maximization of η_{WF} implies maximization of η_{sig} .

η_{WF}, η_{sig} may also be expressed in terms of the *PAPR* metric.

$$\eta_{WF} = \frac{\sigma^2 + \frac{V_s^2}{16}}{\frac{V_s^2}{4} - \left(\sigma^2 + \frac{V_s^2}{16} \right)} = \frac{\sigma^2 + \frac{P_{m_wf}}{4}}{P_{m_wf} - \left(\sigma^2 + \frac{P_{m_wf}}{4} \right)} = \frac{PAPR_{wf/sig} + 4}{3PAPR_{wf/sig} - 1}$$

$$\eta_{WF} = \frac{\sigma^2 + \frac{V_s^2}{16}}{\frac{V_s^2}{4} - \left(\sigma^2 + \frac{V_s^2}{16} \right)} = \frac{\langle P_{out_wf} \rangle}{P_{m_wf} - \langle P_{out_wf} \rangle} = \frac{1}{PAPR_{wf} - 1}; \quad \langle P_{out_wf} \rangle \leq P_{m_wf}/2$$

In the above equations $PAPR_{wf/sig}$ refers to the peak waveform to average signal power ratio and $PAPR_{wf}$ refers to the peak waveform to average waveform power ratio. These equations apply for $PAPR_{wf} > 4$ when the peak to peak signal dynamic range spans the available modulation range between 0 volts and $V_s/2$ volts at the load, and $Z_r = 1$. The dynamic range is determined by Z_r , the ratio of source to load impedance.

Signal based thermodynamic efficiency can be written as;

$$\tilde{\eta} = \frac{\sigma^2}{\frac{V_s^2}{4} - \left(\sigma^2 + \frac{V_s^2}{16}\right)} = \frac{1}{3PAPR_{sig} - 1} = \eta_{wf} - \frac{PAPR_{wf}}{6PAPR_{wf} - 4}$$

$$\tilde{\eta} \approx \eta_{wf} - \frac{1}{2}; \gg 1 \text{ for } PAPR_{wf} = 1$$

Therefore, if η_{WF} , and $PAPR_{wf}$ are known then $\tilde{\eta}$ may be calculated. Also it is apparent that increasing η_{WF} , increases $\tilde{\eta}$. Under these circumstances $\tilde{\eta} \leq 1/2$.

Now suppose that $Z_r \approx 0$, corresponding to the most efficient canonical case for a type 1 modulator. In this case, the maximum waveform voltage equals the open circuit source voltage, V_s . The following graphic illustrates the associated signal and waveform statistics. Notice that the dynamic portion of the waveform spans the maximum possible modulation range, given V_s .

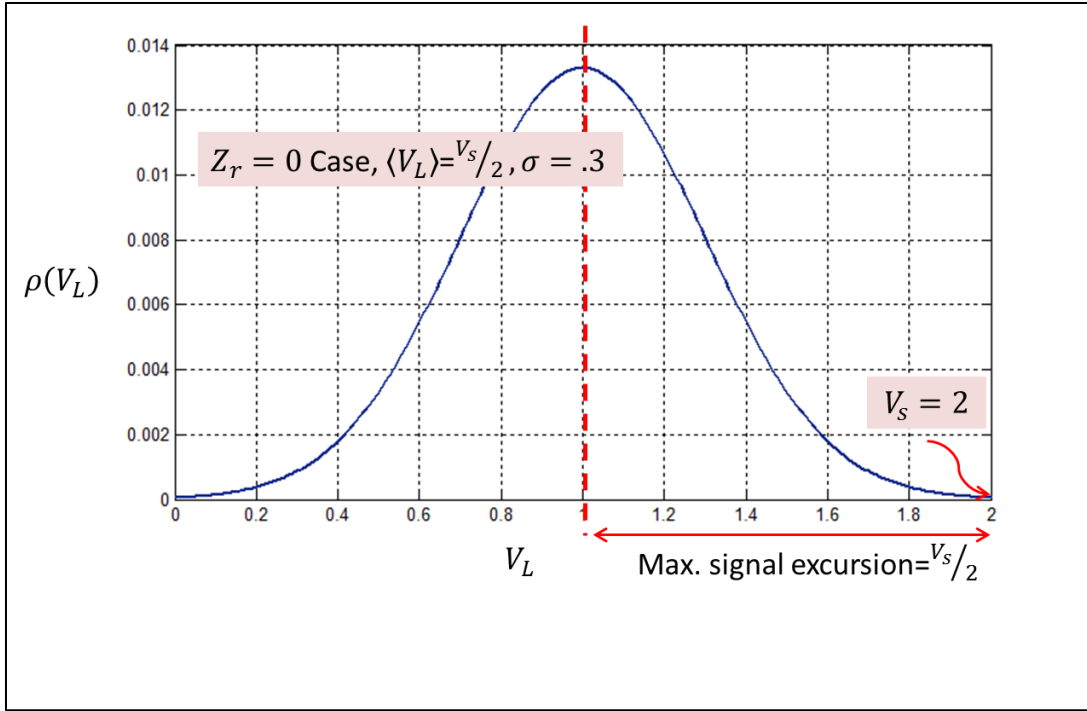


Figure I-1 pdf for Offset Canonical Case

The relevant relationships follow;

$$\eta_{WF} = \frac{\sigma^2 + \frac{V_s^2}{4}}{\frac{V_s^2}{2}} = \frac{2}{PAPR_{wf}}$$

$$\tilde{\eta} = \frac{\sigma^2}{\frac{V_s^2}{2}} = \frac{1}{2 PAPR_{sig}}$$

$$\frac{\eta_{WF}}{\tilde{\eta}} = 1 + PAPR_{sig} = 1 + \frac{PAPR_{wf}/sig}{4}$$

$\tilde{\eta}$ above is considered as a canonical case.

General cases where $Z_r \neq 0$ can be solved using the following equations;

$$Z_r = \frac{Z_s}{Z_L}$$

$$\eta_{WF} = \frac{\langle (\tilde{V}_L + \langle V_L \rangle)^2 \rangle}{\langle V_s(\tilde{V}_L + \langle V_L \rangle) - \text{Re}\{Z_r\}(\tilde{V}_L + \langle V_L \rangle)^2 \rangle} = \frac{1}{\frac{\langle V_s(\tilde{V}_L + \langle V_L \rangle) \rangle}{\langle (\tilde{V}_L + \langle V_L \rangle)^2 \rangle} - \text{Re}\{Z_r\}}$$

$$\langle V_L \rangle = \frac{Z_L V_s}{\langle Z_L + Z_s + Z_\Delta \rangle} = \frac{Z_L V_s}{2(Z_L + Z_s)} = (2 + 2Z_r)^{-1} V_s$$

$$V_{L_{max}} = \frac{Z_L V_s}{Z_L + Z_s} = 2\langle V_L \rangle = \frac{V_s}{1 + Z_r}$$

$$\therefore \eta_{WF} = \frac{1}{\frac{V_s \langle V_L \rangle}{(1 + \text{Re}\{Z_r\}) \langle (\tilde{V}_L + \langle V_L \rangle)^2 \rangle} - \text{Re}\{Z_r\}}$$

When $Z_r = 1$ then,

$$\eta_{WF} = \frac{1}{\frac{PAPR_{WF}}{4} - 1}$$

When $Z_r = 0$;

$$\eta_{WF} = \frac{2}{PAPR_{WF}}$$

Z_Δ is a variable impedance which implements the modulation. Its function is illustrated in Appendix H.

Thermodynamic signal efficiency is similarly determined;

$$\eta_{sig} = \tilde{\eta} = \frac{\langle (\tilde{V}_L)^2 \rangle}{\langle V_s(\tilde{V}_L + \langle V_L \rangle) - Re\{Z_r\}(\tilde{V}_L + \langle V_L \rangle)^2 \rangle} = \frac{1}{\langle \frac{V_s \langle V_L \rangle}{\sigma^2} - Re\{Z_r\} \left(1 + \frac{\langle V_L \rangle^2}{\sigma^2}\right) \rangle}$$

$$\tilde{\eta} = \frac{1}{\frac{V_s}{\langle V_L \rangle} PAPR_{sig} - Re\{Z_r\}(1 + PAPR_{sig})}$$

We can confirm the result by testing the cases $Z_r = 0, 1$.

$$\tilde{\eta} = \frac{1}{\langle \frac{V_s \langle V_L \rangle}{\sigma^2} \rangle} = \frac{1}{2 PAPR_{sig}}; \quad Z_r = 0$$

$$\tilde{\eta} = \frac{1}{\langle \frac{V_s \langle V_L \rangle}{\sigma^2} - \left(1 + \frac{\langle V_L \rangle^2}{\sigma^2}\right) \rangle} = \frac{1}{3 PAPR_{sig} - 1}; \quad Z_r = 1$$

Instantaneous Efficiency

In addition to proper thermodynamic efficiencies, it is possible to compare instantaneous waveform and thermodynamic signal efficiencies discussed in Appendix H. The most general form of the instantaneous power ratio $\eta_{inst_WF/\sigma^2} = \langle \frac{P_{out}}{P_{in}} \rangle$ is;

$$\eta_{inst_WF/\sigma^2} = \check{\eta} = \left\langle \frac{(\tilde{V}_L + \langle V_L \rangle)^2}{V_s(\tilde{V}_L + \langle V_L \rangle) - Re\{Z_r\}(\tilde{V}_L + \langle V_L \rangle)^2} \right\rangle = \frac{1}{\frac{V_s}{\langle V_L \rangle} - Re\{Z_r\}} = \lim_{\sigma \rightarrow 0} \eta_{WF}$$

This is the instantaneous waveform efficiency given a required signal variance. We have reduced η_{inst_WF/σ^2} taking advantage of the correlations between numerator and denominator terms where possible.

Although the calculation, η_{inst_WF/σ^2} , is not directly affected by average signal power, we stipulate that in any optimization procedure, the maximum dynamic range is preserved for and consumed by the signal. This requires a specific average value $\langle V_L \rangle$ and maximizes the uncertainty for a particular signal distribution. η_{inst_WF/σ^2} is dependent on $\langle V_L \rangle$. The maximum dynamic range caveat therefore limits a critical ratio as follows;

$$\langle V_L \rangle = \frac{V_s}{2(1 + Z_r)}$$

It is desirable to minimize Z_r to maximize efficiency. For the case of a single potential V_s , i.e. the case of a type one modulator, the maximum symmetric signal swing about the average output potential is always $\tilde{V}_m = V_{L_max}/2 = \langle V_L \rangle$. Increasing Z_r above zero diminishes the signal dynamic range converting this loss to heat in the power source. The quantity $V_s/[2(1 + Z_r)]$ is always considered as a necessary modulation overhead for a type 1 modulator.

Increasing $\langle V_L \rangle$ increases the peak signal swing \tilde{V}_m and therefore always increases the signal variance for a specified $PAPR$. Hence, increasing η_{inst_WF/σ^2} also increases the thermodynamic efficiency. A more explicit illustration of this dependency is given in the following equation obtained from the prior $\tilde{\eta}, \check{\eta} = \eta_{inst_WF/\sigma^2}$ derivations and their relationship to $\langle V_L \rangle$;

$$\tilde{\eta} = \frac{1}{\frac{V_s}{\langle V_L \rangle} PAPR_{sig} + \left(\frac{1}{\check{\eta}} - \frac{V_s}{\langle V_L \rangle} \right) (PAPR_{sig} + 1)}$$

$\langle V_L \rangle$ is defined in terms of impedances and V_s above. From the definition $0 \leq \check{\eta}/\sigma^2 \leq 1/2$. When $\check{\eta}/\sigma^2=1/2$, $\check{\eta}$ is maximized. At the other extreme, when $\check{\eta}$ tends to zero, $\frac{V_s}{\langle V_L \rangle}$ tends to infinity and $\check{\eta}$ also tends to zero.

Although the prior discussions focus on symmetric signal distributions (for instance Gaussian-like), arbitrary distributions may be accommodated by suitable adjustment of the optimal operating mean $\langle V_L \rangle$. In all circumstances however, the available signal dynamic range must contemplate maximum use of the span $\{V_s, 0\}$.

Source Potential Offset Considerations

The prior equations are based on circuits which return currents to a zero voltage ground potential. If this return potential is not zero then the formulas should be adjusted. In all prior equations, we may substitute $V_s = V_{s1} - V_{s2}$ where V_{s1}, V_{s2} are the upper and return supply potentials, respectively. In such cases, the optimal $\langle V_L \rangle$ is the average of those supplies when the pdf of the signal is symmetric within the span $\{V_{s1}, V_{s2}\}$. Otherwise, the optimal operational $\langle V_L \rangle$ is dependent on the mean of the signal pdf over the span $\{V_{s1}, V_{s2}\}$. The offset does not affect the maximum waveform power, P_{m_wf} . However, the maximum signal power is dependent on the span $\{V_{s1}, V_{s2}\}$ and the average $\langle V_L \rangle$. The signal power is dependent only on σ and any additional requirement to preserve the integrity of the signal pdf.

APPENDIX J:
COMPARISON OF GAUSSIAN AND CONTINUOUS UNIFORM
DENSITIES

This appendix provides a comparison of the differential entropies for the Gaussian and Uniform pdf's. The calculations reinforce the results from Appendix A where it is shown that the Gaussian pdf maximizes Shannon's entropy for a given variance σ_G^2 . Also this appendix confirms appendix D calculations for the case $D=1$. There is a particular variance ratio σ_u^2/σ_G^2 for which, when exceeded, the uniform density possesses an entropy greater than that of the Gaussian. This ratio is calculated. Finally the *PAPR* is compared for both cases.

First we begin with a calculation of the Gaussian density in a single dimension $D=1$.

$$H_G = - \int_{-\infty}^{\infty} \frac{1}{\sqrt{2\pi\sigma_G}} e^{-\frac{x^2}{2\sigma_G^2}} \ln \left[\frac{1}{\sqrt{2\pi\sigma_G}} e^{-\frac{x^2}{2\sigma_G^2}} \right] dx$$

$$H_G = - \frac{1}{\sqrt{2\pi\sigma}} \left[\ln(e) \int_{-\infty}^{\infty} \frac{-x^2}{2\sigma_G^2} e^{-\frac{x^2}{2\sigma_G^2}} dx + \int_{-\infty}^{\infty} -\ln(\sqrt{2\pi\sigma_G}) e^{-\frac{x^2}{2\sigma_G^2}} dx \right]$$

We now apply the following two definite integral formulas obtained from a CRC table of integrals [71].

$$\int_{-\infty}^{\infty} x^{2n} e^{-ax^2} dx = \frac{1 \cdot 3 \cdot 5 \cdots (2n-1)}{2^{n+1} a^n} \sqrt{\frac{\pi}{a}}$$

$$\int_{-\infty}^{\infty} e^{-a^2 x^2} dx = \frac{1}{2a} \Gamma\left(\frac{1}{2}\right) = \sqrt{\frac{\pi}{2a}}, \quad a > 0$$

The final result is

$$H_G = \frac{1}{2} \ln(e) + \ln(\sqrt{2\pi} \sigma_G) = \ln(\sqrt{2\pi e} \sigma_G)$$

Now the entropy H_u is obtained.

$$H_u = - \int_{-ul}^{ul} \frac{1}{ul - ll} \ln \left[\frac{1}{u - ll} \right] dx$$

Let the uniform density possess symmetry with respect to $x = 0$, the same axis of symmetry for a zero offset (zero mean) Gaussian density.

$$\therefore H_u = - \int_{-ul}^{ul} \frac{1}{2ul} \ln[2ul] dx = \ln[2ul]$$

The variance is obtained from;

$$\sigma_u^2 = \int_{-ul}^{ul} x^2 \frac{1}{2ul} dx = \frac{1}{3} x^3 \frac{1}{2ul} \Big|_{-ul}^{+ul} = 1/3 ul^2$$

Now we may begin the direct comparison between H_G and H_u .

Let $\sigma_G^2 = \sigma_u^2$. Then;

$$ul = \sqrt{3\sigma_G} \text{ for } \sigma_G^2 = \sigma_u^2$$

Therefore;

$$H_G = \ln(\sqrt{2\pi e} \sigma_G) \cong \ln(4.1327\sigma_G)$$

$$H_u = \ln(2\sqrt{3} \sigma_G) \simeq \ln(3.4641)$$

H_G is always greater than H_u for a given equivalent variance for the two respective densities.

Suppose we examine the circumstance where $H_u \geq H_G$ and $\sigma_u^2 \neq \sigma_G^2$.

Then,

$$\ln[2ul] \geq \ln[\sqrt{2\pi e} \sigma_G]$$

$$2ul \geq \sqrt{2\pi e} \sigma_G$$

$$ul \geq \frac{1}{2} \sqrt{2\pi e} \sigma_G$$

$$\frac{ul^2}{3} \geq \frac{\pi e \sigma_G^2}{6}$$

$$\frac{\sigma_u^2}{\sigma_G^2} \geq 1.423289$$

Therefore, the entropy of a uniformly distributed RV must possess a noticeable increase in variance over that of the Gaussian RV to encode an equivalent amount of information.

It is also instructive to obtain some estimate of the required *PAPR* for conveying the information in each case. In a strict sense, the Gaussian RV requires an infinite *PAPR*. However it is also known that a *PAPR* ≥ 16 is sufficient for all practical communications applications. In the case of a continuously uniformly distributed RV we have

$$PAPR_u = \frac{ul^2}{1/3 ul^2} = 3$$

Suppose we calculate *ul* for the case where $H_u = H_G$. We let $\sigma_G^2 = 1$ for the comparison

$$ul \cong 2.066$$

To obtain the entropy H_G the upper limit, ul_G , for the Gaussian RV must be at least 4. This means that roughly 4 times the peak power is required to encode information in the Gaussian RV compared to the uniform RV, whenever $H_u = H_G$. Likewise we may calculate

$$PAPR_G/PAPR_u \cong 5.\bar{3}.$$

The following graphic assists with the prior discussion.

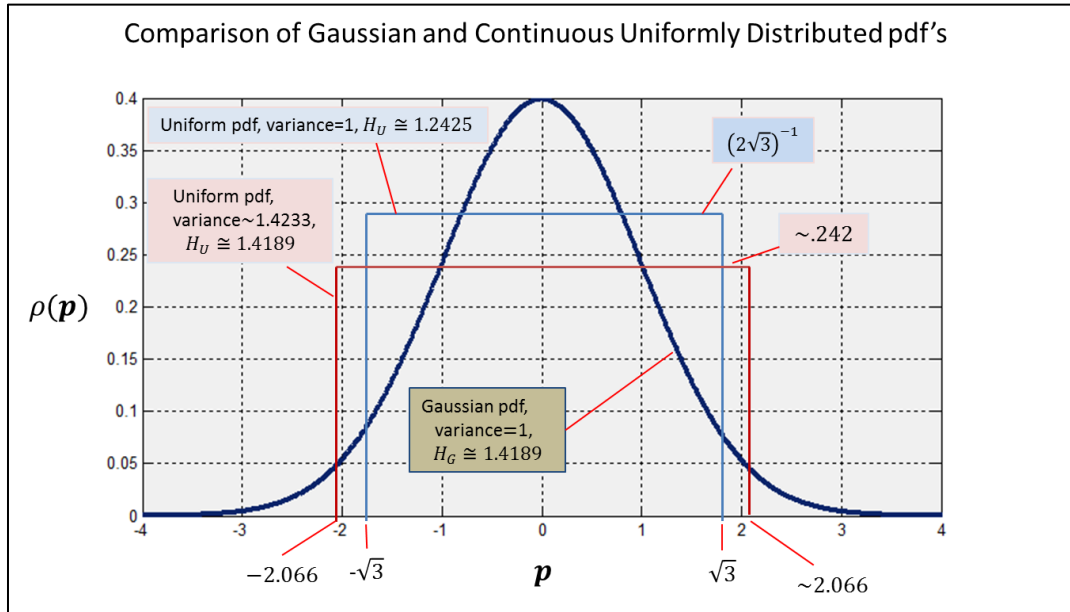


Figure J-1 Comparison of Gaussian and Continuous Uniformly Distributed pdf's

APPENDIX K:
ENTROPY RATE AND WORK RATE

The reader is referred to prior appendices, A, D, as well as chapter 4 to supplement the following analysis. Maximizing the transfer of physical forms of information Entropy per unit time requires maximization of work. This may be demonstrated for a joint configuration and momentum phase space. The joint entropy is;

$$H = -\frac{1}{\hbar^D} \int_{-p}^p \dots \int_{-R_s}^{R_s} \dots \rho(q, p)_\Omega \ln[\rho(q, p)_\Omega] dq_1 dp_1 \dots dq_D dp_D$$

Maximum entropy occurs when configuration and momentum are decoupled based on the joint pdf;

$$\rho(q, p) = \left(\frac{1}{\sqrt{(2\pi)^D [\Lambda_q]}} e^{-\frac{1}{2}(q_\alpha - \bar{q}_\alpha)^t \Lambda_q (q_\beta - \bar{q}_\beta)} \right) \left(\frac{1}{\sqrt{(2\pi)^D [\Lambda_p]}} e^{-\frac{1}{2}(p_\alpha - \bar{p}_\alpha)^t \Lambda_p^{-1} (p_\beta - \bar{p}_\beta)} \right) \quad (\text{K1.1})$$

It is apparent that the joint entropy is that of a scaled Gaussian multivariate and;

$$H = H_q + H_p \quad (\text{K1.2})$$

H_q, H_p are the uncertainties due to independent configuration position and momentum respectively. If we wish to maximize the information transfer per unit time we then need to ensure the maximum rate of change in the information bearing coordinates $\{q, p\}$. When the particle possesses the greatest average kinetic energy it will traverse greater distances per unit time. Hence we need only consider the momentum entropy to obtain the maximization we seek.

$$H_p = \ln(\sqrt{2\pi e})^{2D} + \ln(|\Lambda_p|^D) \quad (\text{K1.3})$$

$$[\Lambda_p] = \begin{bmatrix} \sigma_{p_1}^2 & 0 \dots & 0 \\ 0 & \sigma_{p_2}^2 \dots & 0 \\ 0 & 0 \dots & \sigma_{p_D}^2 \end{bmatrix} \quad (\text{K1.4})$$

Therefore maximizing K1.3 we may write;

$$\max\{e^{H_p}\} = \max\{(\sqrt{2\pi e})^{2D} + (|\Lambda_p|^D)\} \quad (\text{K1.5})$$

Recognizing that $(\sqrt{2\pi e})^{2D}$ is constant and that D is represented exponentially in the second term of K1.5, permits a simplification;

$$\max\{e^{H_p}\} = \max\{(|\Lambda_p|^D)\} \quad (\text{K1.6})$$

Suppose that we represent the covariance in terms of the time variant vector \vec{p} . K1.6 is further simplified;

$$\max\{|\langle \vec{p} \cdot \vec{p} \rangle|\} = \max\{(|\Lambda_p|^D)\} \quad (\text{K1.7})$$

We now take the maximization with respect to the equivalent energy and work form where mass is a constant;

$$\max\{\langle \dot{\vec{q}} \cdot \dot{\vec{p}} \rangle\} = \max\{\langle \dot{\mathcal{E}}_k \rangle\} \quad (\text{K1.8})$$

K1.8 and K1.7 are equivalent maximizations when time averages are considered. K1.8 essentially converts the kinetic energy inherent in the covariance definition of Λ_p to a power. It defines a rate of work which maximizes the rate of change of the information variables $\{\vec{q}, \vec{p}\}$. This is confirmed by comparison with a form of the capacity equation given in chapter 5;

$$C_\alpha = C_{q_\alpha} + C_{p_\alpha}$$

$$C_\alpha = \frac{P_{m_\alpha}}{2\langle \mathcal{E}_{k_\alpha} \rangle PAER_\alpha} \left(\ln \left[\frac{([\langle q_{x_\alpha}^2 \rangle + \tilde{\sigma}_{q_{n_\alpha}}^2])}{\tilde{\sigma}_{q_{n_\alpha}}^2} \right] + \ln \left[\frac{([\langle (p_{x_\alpha})^2 \rangle + \tilde{\sigma}_{p_{n_\alpha}}^2])}{\tilde{\sigma}_{p_{n_\alpha}}^2} \right] \right) \quad (\text{K1.9})$$

$$C \leq \sum_{\alpha=1}^D f_{s_\alpha} \left(\ln \left[\frac{(m^2 \langle \dot{\vec{p}}_\alpha \cdot \dot{\vec{q}}_\alpha \rangle_{eff_\alpha})}{\tilde{\sigma}_{p_{n_\alpha}}^2} + 1 \right] \right) \quad (\text{K1.10})$$

The variances of K1.9 are per unit time and $\langle \dot{\vec{p}}_\alpha \cdot \dot{\vec{q}}_\alpha \rangle_{eff_\alpha}$ in K1.10, define an effective work rate in the α^{th} dimension for the encoded particle. Increasing $\langle \dot{\vec{p}}_\alpha \cdot \dot{\vec{q}}_\alpha \rangle_{eff_\alpha}$ increases capacity.

Although this argument is specific to the Gaussian RV case, it extends to any RV due to the arguments of chapter 5 which establish pseudo capacity as a function of *PAPR* and entropy ratios

compared to the Gaussian case. If we wish to increase the entropy of any RV we must increase P_{max} for a given $\langle \dot{p}_\alpha \cdot \dot{q}_\alpha \rangle_{eff_\alpha}$. Conversely, if a fixed *PAPR* is specified, increasing $\langle \dot{p}_\alpha \cdot \dot{q}_\alpha \rangle_{eff_\alpha}$ increases P_{max} by definition and phase space volume increases with a corresponding increase in uncertainty.

APPENDIX L:
OPTIMIZED EFFICIENCY FOR AN 802.11a 16 QAM CASE

This appendix highlights aspects of the calculations and measurements involved with the optimization of a zero offset implementation of an 802.11a signal possessing a $PAPR \sim 12dB$.

The testing apparatus schematic is illustrated in the following figure .

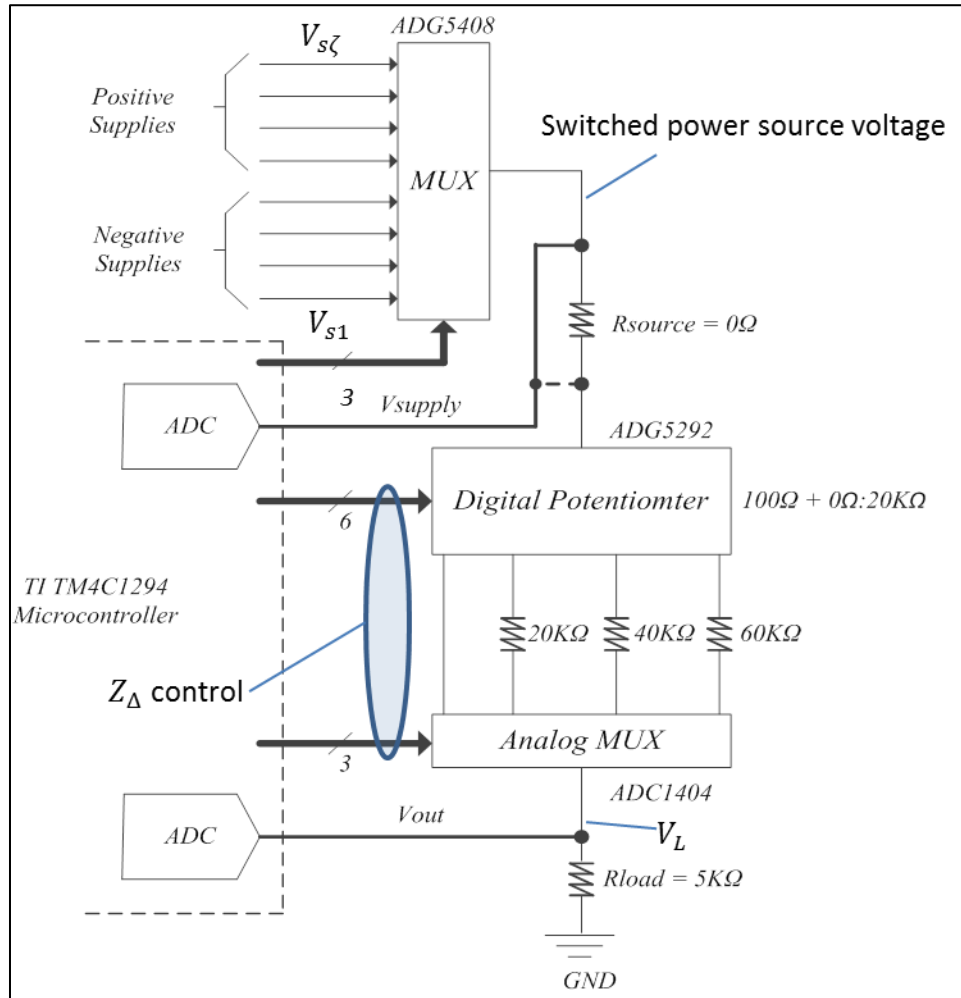


Figure L-1 Testing Apparatus Schematic

An analog multiplexer selects up to $= 8$ domains using a 3 bit domain control. Half of the domains are positive and half are negative for zero offset cases. A 9 bit modulation control maps the information into a resistance via the Z_{Δ} control. A variable voltage divider is formed using the

source resistance, effective Z_{Δ} value and the load resistance. The 9 bit control Z_{Δ} interpolates desired modulation trajectories over a domain determined by the i^{th} switched power source. The controller is an ARM based processor from Texas Instruments and the other analog integrated circuits can be obtained from Analog Devices. A C++ program and MATLAB were used to calculate the important quantities and evaluate measurements.

A custom C++ GUI indicates many of the metrics discussed in the main text and a table records efficiencies as well as weighting factors. Results of calculations and measurements for 4,6,8 domain optimizations follow.

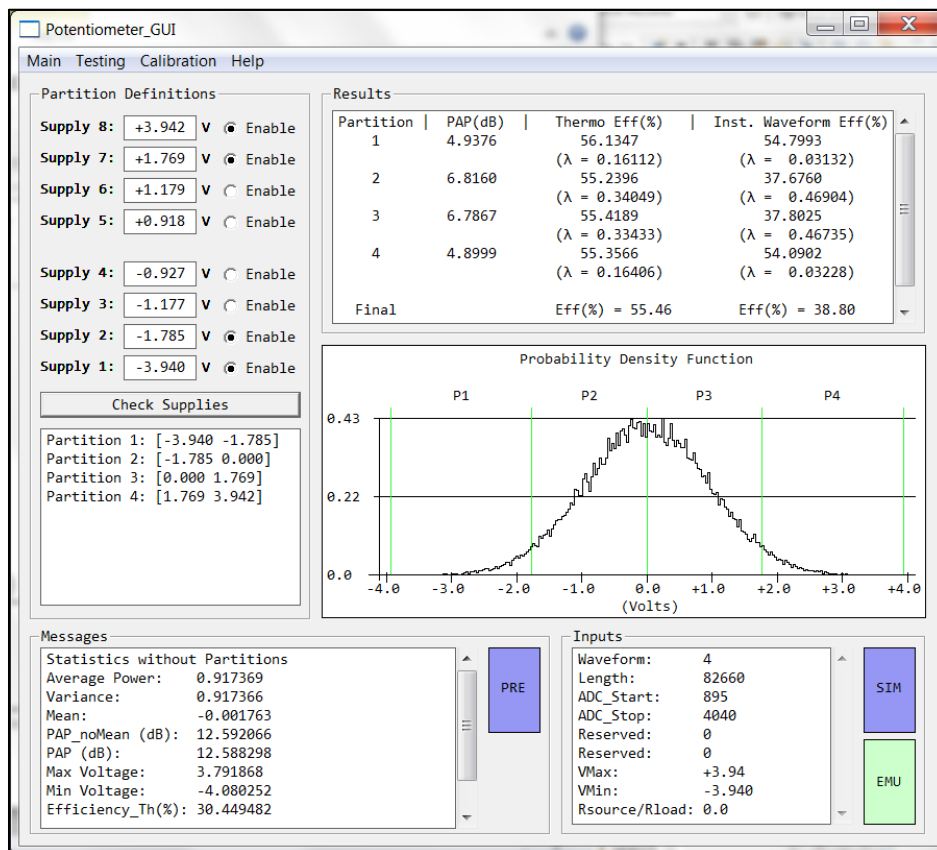


Figure L-2 Potentiometer GUI 1

Table L-1 Thermodynamic Efficiency and λ per Domain (4 Domains)

<i>Domain</i>	<i>Optimized Efficiency</i>	λ <i>(optimized)</i>		<i>Measured Efficiency</i>	λ <i>(effective)</i>
Domain 1	56.13%	0.161		53.4%	0.130
Domain 2	55.23%	0.340		50.78%	0.373
Domain 3	55.41%	0.334		53.6%	0.352
Domain 4	55.35%	0.164		53.63%	0.143
	55.46% (total)			52.53% (total)	

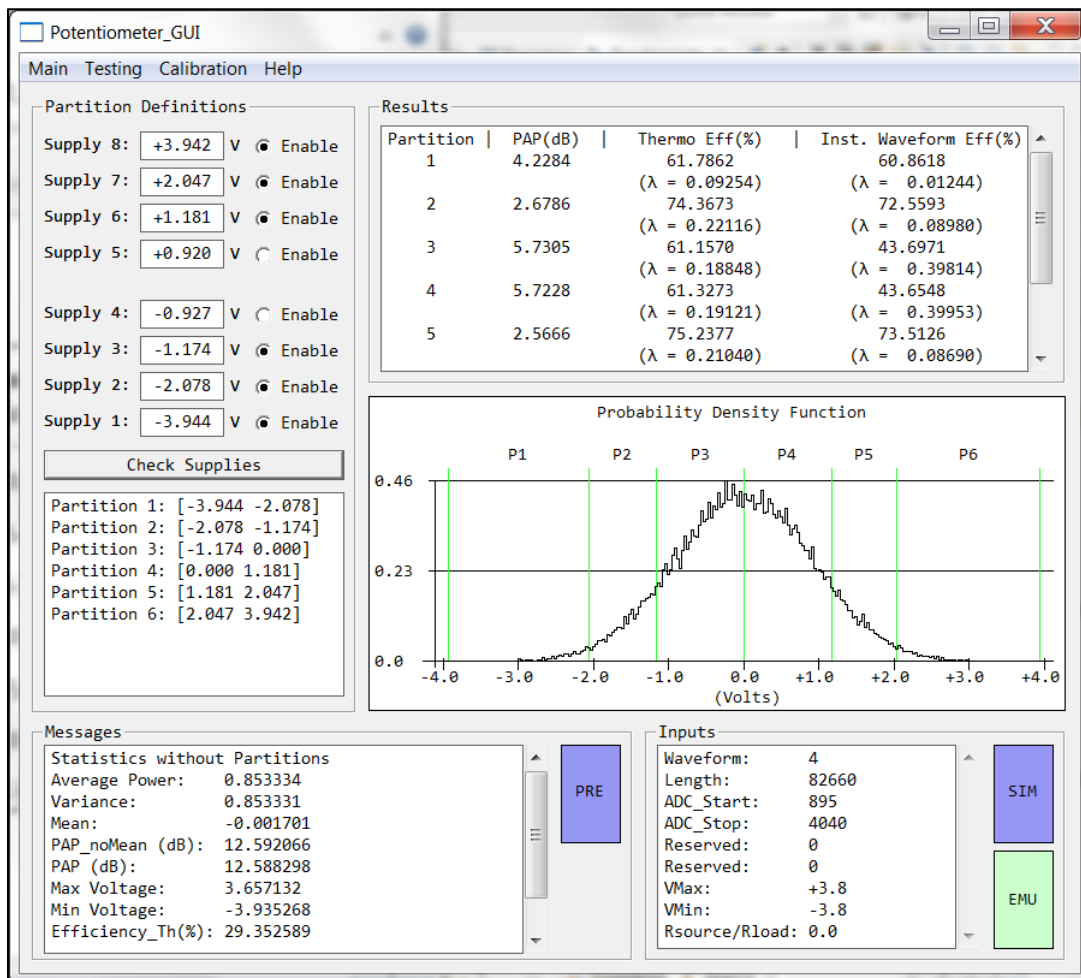


Figure L-3 Potentiometer GUI 2

Table L-2 Thermodynamic Efficiency and λ per Domain (6 Domains)

<i>Domain</i>	<i>Optimized Efficiency</i>	λ <i>(optimized)</i>			<i>Measured Efficiency</i>	λ <i>(effective)</i>
Domain 1	62.53%	0.104			59.9%	0.077
Domain 2	74.88%	0.222			73.2%	0.210
Domain 3	61.50%	0.174			59.0%	0.207
Domain 4	61.72%	0.177			60.1%	0.196
Domain 5	75.70%	0.211			73.5%	0.212
Domain 6	61.30%	0.109			59.4%	0.096
	67.6% (total)				65.42% (total)	

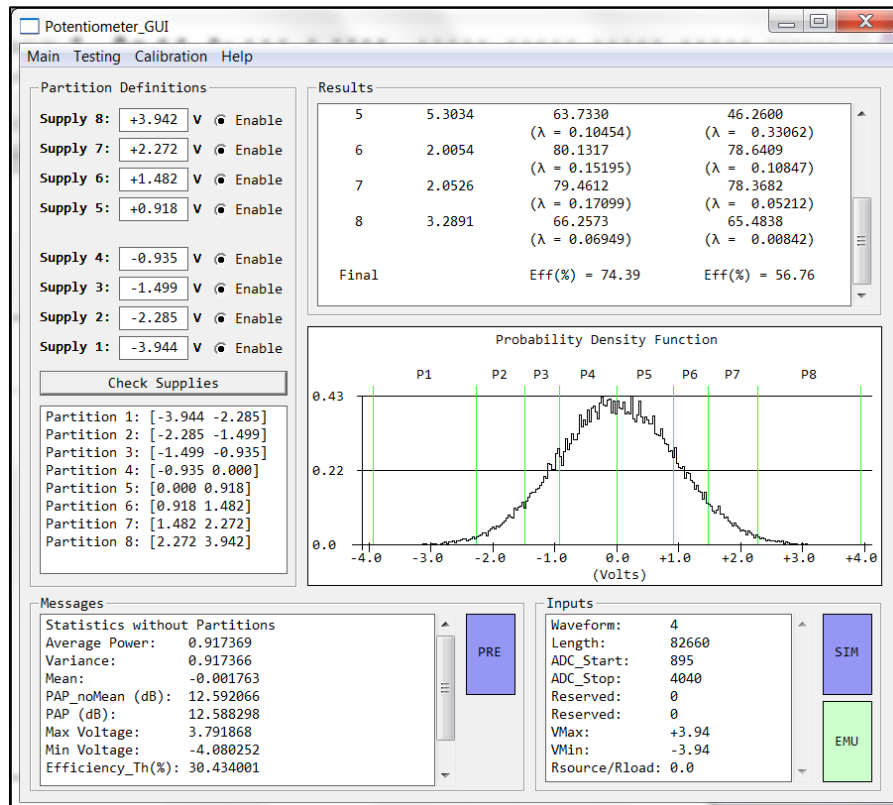


Figure L-4 Potentiometer GUI 3

Table L - 3 Thermodynamic Efficiency and λ per Domain (8 Domains)

<i>Domain</i>	<i>Optimized Efficiency</i>	λ <i>(optimized)</i>			<i>Measured Efficiency</i>	λ <i>(effective)</i>
Domain 1	66.93%	0.072			64.5%	0.047
Domain 2	79.37%	0.169			77.5%	0.157
Domain 3	80.10%	0.152			79.1%	0.153
Domain 4	62.97%	0.108			61.5%	0.133
Domain 5	63.73%	0.104			61.38%	0.116
Domain 6	80.13%	0.151			78.1%	0.167
Domain 7	79.46%	0.170			77.2%	0.165
Domain 8	66.25%	0.069			64.5%	0.058
	74.39%				72.4% (total)	

LIST OF REFERENCES

- [1] C. E. Shannon, "A Mathematical Theory of Communication," *The Bell System Technical Journal*, vol. 27, pp. 379-343, 623-656, 1948.
- [2] C. E. Shannon, "Communication in the Presence of Noise," *Proceedings of the IEEE*, vol. 86, no. 2, pp. 447-457, 1998.
- [3] B. P. Lathi and Z. Ding, *Modern Digital and Analog Communication Systems*, 4th ed. New York: Oxford UP, 2009.
- [4] H. Nyquist, "Certain Factors Affecting Telegraph Speed," *Bell System Technical Journal*, vol. 3, no. 2, pp. 324-346, 1924.
- [5] H. Nyquist, "Certain Topics in Telegraph Transmission Theory," *Transactions of the American Institute of Electrical Engineers*, vol. 47, no. 2, pp 617-644, 1928.
- [6] R. J. Marks II, *Introduction to Shannon Sampling and Interpolation Theory*. New York: Springer-Verlag, 1991.
- [7] R. Landauer, "Information Is Physical," *Physics and Computation*, 1992.
- [8] C. H. Bennett, "Notes on Landauer's Principle, Reversible Computation, and Maxwell's Demon," *Studies In History and Philosophy of Modern Physics*, vol. 34, no.3, pp. 501-510, 2003.
- [9] M. Karnani, *et al.*, "The Physical Character of Information." *Proceedings of the Royal Society A: Mathematical, Physical and Engineering Sciences*, vol. 465, pp. 2155-2175, 2009.

- [10] E. T. Whittaker, "On the Functions Which Are Represented by the Expansion of the Interpolation Theory," *Proceedings of the Royal Society of Edinburgh*, vol. 35, pp. 181-194, 1915.
- [11] R. E. Ziemer and W. H. Tranter, *Principles of Communications: Systems, Modulation, and Noise*, 6th ed., Hoboken, NJ: John Wiley & Sons, 2009.
- [12] D. Middleton, *An Introduction to Statistical Communication Theory*. Piscataway, NJ: IEEE, 1996.
- [13] W. Greiner *et al.*, *Thermodynamics and Statistical Mechanics*. New York: Springer, 2004.
- [14] E. T. Jaynes, "Information Theory and Statistical Mechanics," *Brandeis University Summer Institute Lectures in Theoretical Physics*, vol. 3, pp. 181-218, 1962.
- [15] C. E. Shannon and Warren Weaver, *The Mathematical Theory of Communication*. Urbana: University of Illinois, 1998.
- [16] A. Ben-Naim, *A Farewell to Entropy: Statistical Thermodynamics Based on Information: $S = \log W$* . Hackensack, NJ: World Scientific, 2008.
- [17] L. D. Landau and E. M. Lifchitz, *Mechanics*. 3rd ed. Oxford: Butterworth-Heinemann, 1976.
- [18] T. W. Kibble and F. H. Berkshire, *Classical Mechanics*, 5th ed. London: Imperial College, 2004.
- [19] J. V. José and E. J. Saletan. *Classical Dynamics: A Contemporary Approach*. Cambridge: Cambridge UP, 1998.
- [20] R. Weinstock, *Calculus of Variations, with Applications to Physics and Engineering*. New

York: Dover Publications, 1974.

- [21] J. B. Thomas, *An Introduction to Statistical Communication Theory*. New York: John Wiley & Sons, 1969.
- [22] D. V. Schroeder, *An Introduction to Thermal Physics*. San Francisco, CA: Addison Wesley, 2000.
- [23] G. R. Cooper and C. D. McGillem, *Probabilistic Methods of Signal and System Analysis*. New York: Holt, Rinehart, and Winston, 1971.
- [24] W. B. Davenport and W. L. Root, *An Introduction to the Theory of Random Signals and Noise*. New York: IEEE, 1987.
- [25] H. Urkowitz, *Signal Theory and Random Processes*. Norwood, MA: Artech House, 1983.
- [26] D. Gabor, "Theory of Communication," *The Journal of the Institution of Electrical Engineers - Part III: Radio and Communication Engineering*, vol. 93, no. 26, pp. 429-457, 1946.
- [27] L. E. Franks, "Further Results on Nyquist's Problem in Pulse Transmission," *IEEE Transactions on Communication Technology*, vol. 16, no.2, pp. 337-340, 1968.
- [28] G. S. Rawlins, "Quotation taken from course notes", *EEL 6537 Detection and Estimation Theory*, Professor Emeritus Dr. Nicolaos Tzannes, Definition attributed to Kolmogorov. UCF, Dept. of Electrical Engineering, Orlando.
- [29] J. L. Doob, *Stochastic Processes*. New York: Wiley, 1953.
- [30] W. Greiner, *Quantum Mechanics: An Introduction*. 3rd ed., Berlin: Springer, 1994.

- [31] H. Van Trees, *Detection, Estimation, and Modulation Theory*. New York: Wiley, 1968.
- [32] A. D. Whalen, *Detection of Signals in Noise*. San Diego, Ca: Academic, 1971.
- [33] C. W. Helstrom, *Statistical Theory of Signal Detection*. Oxford: Pergamon, 1960.
- [34] R. S. Kennedy, *Fading Dispersive Communication Channels*. New York: Wiley-Interscience, 1969.
- [35] S. Shibuya, *A Basic Atlas of Radio-Wave Propagation*. New York: Wiley, 1987.
- [36] K. Brayer, *Data Communications Via Fading Channels*. New York: IEEE, 1975.
- [37] D. J. Griffiths, *Introduction to Electrodynamics*. 3rd ed., Upper Saddle River, NJ: Prentice Hall, 1999.
- [38] J. D. Jackson, *Classical Electrodynamics*, 2nd ed. New York: John Wiley & Sons, 1975.
- [39] L. D. Landau and E. M. Lifshits, *The Classical Theory of Fields*. 4th ed. Oxford: Elsevier Butterworth-Heinemann, 1975.
- [40] D. Slater, *Near-Field Antenna Measurements*. Boston: Artech House, 1991.
- [41] M. E. Van Valkenburg, *Network Analysis*. Englewood Cliffs, NJ: Prentice-Hall, 1974.
- [42] E. N. Skomal and A. A. Smith, *Measuring the Radio Frequency Environment*. New York: Van Nostrand Reinhold, 1985.
- [43] L. D. Landau and E. M. Lifshitz, *Statistical Physics*. 3rd ed., Part 1., Oxford England: Butterworth-Heinemann, 1980.
- [44] C. Arndt, *Information Measures: Information and Its Description in Science and*

- Engineering*. Berlin: Springer, 2001.
- [45] B. R. Frieden, *Science from Fisher Information: A Unification*. Cambridge, UK: Cambridge UP, 2004.
- [46] I. I. Hirschman, "A Note on Entropy," *American Journal of Mathematics*, vol. 79, no.1, pp. 152-156, 1957.
- [47] W. Beckner, "Inequalities in Fourier Analysis," *The Annals of Mathematics*, vol. 102, no. 1, pp. 159-82, 1975.
- [48] D. J. MacKay, *Information Theory, Inference, and Learning Algorithms*. Cambridge, UK: Cambridge UP, 2004.
- [49] R. P. Feynman *et al.*, *The Feynman Lectures on Physics*, vol. 1, 2, 3, Reading, MA: Addison-Wesley Pub., 1963.
- [50] E. Fermi, *Thermo-Dynamics*. New York: Dover Publications, 1936.
- [51] K. Wark, *Thermodynamics*. New York: McGraw-Hill, 1977.
- [52] D. Halliday and R. Resnick. *Fundamentals of Physics*. New York: John Wiley & Sons, 1970.
- [53] R. Balian, *From Microphysics to Macrophysics: Methods and Applications of Statistical Physics*. Study ed. Vol. 1, 2. Berlin: Springer, 2007.
- [54] Y. L. Klimontovich, *Statistical Physics*. Chur, Switzerland: Harwood Academic, 1986.
- [55] G. S. Schott, *Electromagnetic Radiation and the Mechanical Reactions Arising from It*,

- Being an Adams Prize Essay in the University of Cambridge.* Cambridge, UK: Cambridge UP, 2012.
- [56] G. N. Plass, "Classical Electrodynamical Equations of Motion with Radiative Reaction," *Reviews of Modern Physics*, vol. 33, no. 1, pp. 37-62, 1961.
- [57] H. A. Lorentz, *The Theory of Electrons: And Its Applications to the Phenomena of Light and Radiant Heat*, 2nd ed. New York: Dover Publication, 1952.
- [58] M. Schwartz, *Principles of Electrodynamics*. New York: Dover Publications, 1972.
- [59] H. Goldstein *et al.*, *Classical Mechanics*. San Francisco: Addison Wesley, 2002.
- [60] M. N. Sadiku, *Elements of Electromagnetics*. New York: Oxford UP, 2015.
- [61] W. H. Hayt, *Engineering Electromagnetics*. New York: McGraw-Hill Book, 1981.
- [62] P. Y. Yu and M. Cardona, *Fundamentals of Semiconductors: Physics and Materials Properties*. Berlin: Springer, 2010.
- [63] M. K. Simon *et al.*, *Digital Communication Techniques: Signal Design and Detection*. New Jersey: PTR Prentice Hall, 1995.
- [64] R. Pettai, *Noise in Receiving Systems*. New York: Wiley, 1984.
- [65] P. A. Tipler, *Modern Physics*. New York: Worth, 1978.
- [66] C. H. Bennett, "Demons, Engines and the Second Law," *Scientific American*, vol. 257, no. 5, pp.108-16, 1987.
- [67] N. Wiener, "Generalized Harmonic Analysis," *Acta Mathematica*, vol. 55, no. 1, pp. 117-

258, 1930.

- [68] M. Abramowitz and I. A. Stegun, *Handbook of Mathematical Functions: With Formulas, Graphs, and Mathematical Tables*. New York: Dover Publications, 1964.
- [69] C. Lanczos, *The Variational Principles of Mechanics*, 4th ed. New York: Dover Pub., 1970.
- [70] B. Van Brunt, *The Calculus of Variations*. New York: Springer, 2010.
- [71] D. Zwillinger, *CRC - Standard Mathematical Tables and Formulae*, 30th ed. Boca Raton, FL: CRC, 1996.
- [72] S. Amari and H. Nagaoka, *Translations of Mathematical Monographs: Methods of Information Geometry*. Vol. 191. Providence, RI: American Mathematical Society, 2000.
- [73] K. A. Arwini and C. T. J. Dodson, *Information Geometry: Near Randomness and Near Independence*. Berlin: Springer, 2008.
- [74] R. B. Ash, *Information Theory*. New York: Dover Publications, 1965.
- [75] A. O. Barut, *Electrodynamics and Classical Theory of Fields and Particles*. New York: Dover Publications, 1980.
- [76] W. E. Baylis, "Understanding Electromagnetic Radiation from an Accelerated Charge," *University of Windsor*, [Online document], 2013 Aug. 7, Available: <http://web4.uwindsor.ca>
- [77] N. C. Beaulieu, "Introduction to Certain Topics in Telegraph Transmission Theory," *Proceedings of the IEEE*, vol. 90, no. 2, pp. 276-279, 2002.

- [78] I. Bialynicki-Birula and J. Mycielski, "Uncertainty Relations for Information Entropy in Wave Mechanics," *Communications in Mathematical Physics*, vol. 44, no. 2, pp. 129-132, 1975.
- [79] T. M. Cover, and J. A. Thomas, *Elements of Information Theory*. Hoboken, New Jersey: Wiley-Interscience, 2006.
- [80] S. R. De Groot, *The Maxwell Equations. Non-Relativistic and Relativistic Derivations from Electron Theory*, vol. 4, Amsterdam: North-Holland, 1969.
- [81] C. Fox, *An Introduction to the Calculus of Variations*. New York: Dover Publications, 1950.
- [82] I. M. Gelfand and S. V. Fomin. *Calculus of Variations*. Mineola, NY: Dover Publications, 1963.
- [83] I. S. Gradshteyn *et al.*, *Table of Integrals, Series, and Products*. New York: Academic, 1980.
- [84] W. Greiner, *Classical Electrodynamics*. New York: Springer, 1998.
- [85] E. T. Jaynes, *Probability Theory: The Logic of Science*. Cambridge, UK: Cambridge UP, 2003.
- [86] R. F. O'Connell, "The Equation of Motion of an Electron," *Physics Letters A*, vol. 313, no. 5-6, pp. 491-497, 2003.
- [87] R. K. Pathria, *Statistical Mechanics*, 2nd ed. Oxford: Elsevier Butterworth-Heinemann, 1996.
- [88] C. E. Pearson, *Handbook of Applied Mathematics: Selected Results and Methods*, 2nd ed.,

New York: Van Nostrand Reinhold, 1983.

- [89] M. B. Plenio and V. Vitelli, "The Physics of Forgetting: Landauer's Erasure Principle and Information Theory," *Contemporary Physics*, vol. 42, no. 1, pp. 25-60, 2001.
- [90] G. S. Rawlins, "Nonlinear Feed Forward Universal RF Power Modulator," *Proc. of The 13 International Symposium of Microwave and Optic Technology*, Prague, Czech Republic, 2011.
- [91] F. Rohrlich, *Classical Charged Particles: Foundations of Their Theory*. Reading, MA: Addison-Wesley, 1965.
- [92] S. R. Salinas, *Introduction to Statistical Physics*. New York: Springer, 2001.
- [93] G. A. Schott, "The Mechanical Forces Acting on Electric Charges in Motion," *Electromagnetic Radiation*, Cambridge, UK: Cambridge UP, pp. 173-184, 1912.
- [94] G. A. Schott, "On the Motion of a Lorentz Electron," *Phil. Mag.*, vol. 29, pp. 49-62, 1915.
- [95] G. A. Schott, *Electromagnetic Radiation*. Cambridge, UK: Cambridge UP, 1912, pp. 174-184.
- [96] G. Smith and J. A. Smolin, "An Exactly Solvable Model for Quantum Communications," *Nature*, vol. 504, pp. 263-267, 2013.
- [97] A. Sommerfeld, "Simplified Deduction of the Field and Forces of an Electron Moving in Any Given Way," *Zur Electronentheory*, pp. 346-367, 1904.
- [98] S. M. Wentworth, *Fundamentals of Electromagnetics with Engineering Applications*. Hoboken, NJ: John Wiley, 2005.

[99] E. T. Whittaker and K. Ogura, "Interpolation and Sampling," *Journal of Fourier Analysis and Applications*, vol. 17, no. 2, pp. 320-354, 2011.